School of Chemical and Petroleum Engineering

The Synthesis and Application of Novel Nanostructured Carbon Materials

Chen Wang

This thesis is presented for the Degree of
Doctor of Philosophy
of
Curtin University

December 2017

Declaration

To the best of my knowledge and belief this thesis contains no material previously published by any other person except where due acknowledgment has been made. This thesis contains no material which has been accepted for the award of any other degree or diploma in any university.

Signature: Chen Wang (Chen Wang)

Date: 25/10/2017

Acknowledgements

I would like to express my sincerest gratefulness to my principal supervisor, Prof Shaobin Wang for his guidance, patience and encouragement in my research. Prof Wang is a knowledgeable and humble scholar who always encourages me and inspires me in my PhD study. Especially when I felt depressed, he comforted and helped me patiently overcome difficulties encountered in study and life. Without his help and encouragement, I cannot complete my academic research smoothly.

My thanks also give to my co-supervisor Professor Hongqi Sun for his guidance in problem solving and paper writing. He gave me innovative ideas to design experiment, helped me solve academic problems and guided me to write good-quality paper. His selfless input contributes to my publications and thesis.

I would also like to thank Professor Shaomin Liu as the chairperson of the thesis committee for his encouragement and suggestions during my project. Also gratefulness gives to Professor Zongping Shao for his support and guidance in my research.

I also want to give my gratitude to the technicians, Yu, Jimmy, Andrew, Guanliang, Ann, Jason, Araya, Melina, Dipok and Karen for helping me prepare the chemicals and training me on the use of equipment and software. Special thanks give to Roshanak and Anja for their constant help, understanding and encouragement to facilitate my experiment.

I also appreciate the support, help and love from my friends and colleagues, Ting Gao, Wei Wang, Ping Liang, Yuxian Wang, Jian Kang, Xiaochen Guo, Huayang Zhang, Wenjie Tian, Qi Yang, Stacey, Li Zhou, Zana, Jijiang He, Yilin Liu, Qiaoran Liu, Leon Liu, Yazi Liu, Fern, and Heng Ye.

In addition, I would like to express my thanks to Cooperative Research Centre for Contamination Assessment and Remediation of the Environment (CRC CARE) for supporting my PhD scholarship.

Last but not least, I would like to express my deepest love and gratitude to my family. I truly thank you for your unconditional love and tremendous supports. Thank you for the support and love from my parents. Thank you for the understanding, love and encouragement from my husband. It is you that urges me to go through some depressing time in the PhD study and complete it smoothly and successfully. I love you all.

Abstract

One of public concerns nowadays has been the decomposition of recalcitrant organic pollutants into harmless substances in the environment. Advanced oxidation processes (AOPs) are favorable technologies that can generate both hydroxyl and sulfate radicals for toxicants degradation in water. In recent years, much attention has been paid to producing sulfate radicals through PMS activation by transition metals, carbon catalysts and so on. Carbon materials are green catalysts with large surface area, excellent catalytic performance and good stability. This study presents several novel carbon materials such as nitrogen-doped graphene, nitrogen-doped carbon nanotubes with encapsulated iron carbide, nitrogen-doped mesoporous carbon nanostructures with different morphologies and cobalt-based nanospheres supported by carbon sphere with a tunable oxidation layer for heterogeneous activation of peroxymonosulfate (PMS). Various characterization techniques were utilized to investigate the structures and morphologies of these nanomaterials as well as their intrinsic active sites. The synthesized carbon materials were applied in the catalytic oxidation of phenol solution by activating PMS. Varying reaction temperature, catalyst loading, and properties of catalysts play significant roles in catalytic oxidation of phenol. The generation of reactive radicals (sulfate and hydroxyl radicals) were investigated by electronic paramagnetic resonance. In addition, different quenching experiments were carried out to probe the mechanism of phenol degradation by the prepared carbocatalysts. These findings in this study would open a new avenue for the development of green catalysts in environmental remediation.

Publications by the Author

Published and Accepted:

1. **Wang C**, Kang J, Sun HQ, Wang SB. One-pot synthesis of N-doped graphene for metal-free advanced oxidation processes. Carbon. 2016, 102: 279-287.
2. **Wang C**, Kang J, Liang P, Zhang HY, Sun HQ, Wang SB. Ferric carbide nanocrystals encapsulated in nitrogen-doped carbon nanotubes as an outstanding environmental catalyst. Environ. Sci.: Nano. 2017, 4, 170-179.
3. Kang J, Duan XG, **Wang C**, Sun HQ, Wang SB. Facile synthesis of nitrogen-doped bamboo-like carbon nanotubes with Ni encapsulation for removal of emerging contaminants with excellent catalytic stability. Chem.Eng.J. 2018, 332, 398-408.

Manuscripts submitted or in preparation:

4. Kang J, **Wang C**, Zhang HY, Duan XG, Sun HQ, Tan XY, Wang SB. 3D hierarchical porous nitrogen-doped graphene with nickel encapsulation for oxidative degradation of antibiotics. (**Submitted**)
5. Liu Y, **Wang C**, Shao ZP, Wang SB. Co-based nanospheres supported by carbon sphere with a tunable oxidation layer in the application of lithium ion battery and wastewater treatment. (**To be submitted**)

Referred Conference

Wang C, Wang SB. Ferric carbide nanocrystals encapsulated in nitrogen-doped carbon nanotubes as an outstanding environmental catalyst. RACI CENTENARY CONGRESS 2017. July 23-28, 2017, Melbourne, Australia. (**Oral Presentation**)

Contents

Chapter 1 Introduction

1.1 Background

Water, an alternative name of life, is one of necessities to maintain human life.[1] An excessive growing of human society and rapid urbanization and industrialization have caused a range of environmental problems, which have exerted a heavy burden on the ecosystem, especially the negative impact on the safe and secured water for lives on the earth. Water pollution has become a public concern that requires ongoing evaluation and revision.[2, 3]

Many challenges, regardless of old and new, are faced by our current water supply systems. In both developing and developed countries, greater impacts are imposed by human activities on the exacerbation of water scarcity through polluting natural water sources.[4-7] In developing countries such as China, more than 90% of cities are threatened by water and approximately 500-million people barely have access to safe and clean drinking water. In United Sates, it is reported that 45% streams, 47% lakes and 32% bays and estuaries were regarded as contaminated. Worldwide, ameliorative drinking water systems are still a luxury to some 780-million people (WHO, 2012).[2, 8, 9] Contaminants, diverse in nature, were released to the surface water and groundwater randomly by agricultural irrigation and industrial activities and are detrimental to both human health and ecological environment because the majority of them are toxic, mutagenic or carcinogenic and can disrupt endocrine to humans, animals and aquatic life.[10] Even at low concentrations, some organic substances are still toxic and fatal.

Furthermore, global climate change exacerbates the already uneven distribution of fresh water by the destabilization of the supply. Therefore, global efforts are imperatively required to develop robust technologies for contaminants removal from water to ensure life safety and quality of human beings and animals in the world.[2]

Various contaminants, including heavy metals, inorganic pollutants, organic compounds as well as some other complex composites, are presented solely or coexist in wastewater.[10-12] Among various pollutants, phenolic compounds constitute a typical environmental hazard in both surface and ground waters due to their wide applications in different industries such as petroleum and petrochemical, textile industries, paper and pulp, pesticide, food-processing industries, pharmaceutical and resin manufacturing, etc.[13]

Photocatalytic oxidation, adsorption/separation processing, bioremediation, flocculation/coagulation and chemical oxidation are common wastewater treatment methods to overcome water pollution.[14] Conventional treatment methods are usually not effective because some contaminants are recalcitrant to be removed. Chemical oxidation, due to its rapid decomposition of organics into less harmful substances, is thus one of the most cost-effective and environmentally friendly techniques.[15, 16]

In the past few decades, advanced oxidation processes (AOPs) have gained extensive attention for the removal of a wide range of organic pollutants from wastewater. Particularly, AOPs that employ a combination of oxidants, UV radiation, catalysts, and ultrasound were recently received greater attention.[17, 18] In a typical AOPs system,

reactive oxygen species, including hydroxyl radical (·OH), sulfate radical ($SO_4^{\bullet-}$) or superoxide radical ($O_2^{\bullet-}$) are generated by hydrogen peroxide (H_2O_2), peroxymonosulfate (PMS) or persulfate (PS, also known as peroxydisulfate or PDS) and ozone (O_3) to attack the target compounds. Nowadays, the investigations of many AOPs have focused on the catalytic oxidation of phenol in aqueous solution, such as typical Fenton's reagents, Fenton-like reactions, ozonation, photodegradation, photo-Fenton, and heterogeneous photocatalysis.[19]

However, expensive chemical precursors, unstable agents, parasite reactions, rigid operation conditions (pH~3), generation of sludge to separate and/or moderate mineralization efficiency lead to a great increase in storage, transportation, reaction and post-treatment, thus limiting most of the AOPs, especially the traditional Fenton reactions based on hydroxyl radicals.[20] Recently, sulfate radical-based AOPs (SR-AOPs) have attracted much more attentions for wastewater treatment because they can overcome the shortages brought by hydroxyl radical-based systems through activation of PMS and PS. Normally, sulfate radicals have a stronger oxidative capacity, a better selectivity to target organics, a relatively short lifespan but unique reaction mechanism different from that of hydroxyl radicals. For instance, a facile oxidation of ammonia nitrogen in wastewater can be performed by SR-AOPs, which is barely decomposed by hydroxyl radical-based AOPs. Generally, PMS and PS can be activated by many methods to produce sulfate radicals for contaminants removal, such as homogeneous transition metals, heterogeneous transition metals and metal oxides, metal-free carbon catalysts, ozonation, ultraviolet irradiation, etc.[21] Reportedly, metal-free carbon catalysts are promising alternatives to transition metals because they have better stability and can avoid metal

leaching to prevent secondary contamination and therefore are widely applied in heterogeneous activation of PMS to produce sulfate radicals to decompose recalcitrant organics in wastewater.[22]

Due to their nanoscale dimensions, nanomaterials possess unique properties and multiple applications in water treatment, energy production, and contaminant sensing.[23] Graphene, a two-dimensional layer of carbon atoms arranged in a hexagonal crystalline structure, possesses unique physicochemical properties, notably the exceptionally high surface area, electron and thermal mobility, and mechanical strength.[24] Carbon nanotubes (CNTs), discovered several years earlier than graphene, is a term to describe a range of tubular nanostructures with similar structures and shapes.[25] Different synthesis methods have been developed to obtain graphene and CNTs. Recently, graphene and CNTs have been discovered to be able to effectively activate PMS to produce free radicals in green remediation technologies, completely avoiding the problem of metal ion leaching. Meanwhile, doping with heteroatoms can further enhance the catalytic performance of these nanomaterials.[26-30]

1.2 Objectives

The research is mainly aiming to synthesize several types of highly efficient and robust metal-free nitrogen-doped graphene and carbon nanotubes. Meanwhile, some carbon materials encapsulated with metal compounds are also discussed. These novel nanomaterials will be employed as heterogeneous catalysts for peroxymonosulfate (PMS) activation to produce reactive species for oxidative degradation of phenol in aqueous solution. In addition, perspectives about the intrinsic

mechanism of PMS activation as well as radical and non-radical mechanisms were investigated in this study.

The specific objectives of this research include：

a. To synthesize high-quality nitrogen-doped graphene in a large scale via one-pot green synthesis method.
b. To prepare nitrogen-doped carbon nanotubes with encapsulated iron carbide
c. To obtain nitrogen-doped mesoporous carbon nanostructures with different morphologies from graphene to carbon nanotubes
d. To synthesize a pomegranate-like structural Co sphere @ carbon sphere composite materials by a one-step hydrothermal method.
e. To utilize various characterization techniques to get a better understanding of the prepared catalysts
f. To investigate the catalytic performance and stability of the prepared catalysts for activation of PMS to degrade organic contaminants - phenol.
g. To study the reaction kinetics and activation energy of each catalyst.
h. To determine the effects of reaction parameters, such as catalyst loading, and reaction temperature on the efficiency of degradation.
i. To probe PMS activation mechanism during the catalytic degradation processes and to identify the active sites for degradation.

1.3 Thesis Organisation

Seven chapters, including introduction, literature review, results and discussions (four chapters), conclusions and perspectives for future studies, are included in this thesis.

Chapter 1: Introduction

This chapter outlines current waste water issues and associated solutions and carbon nanomaterials to alleviate these problems. Objectives and thesis organization are also presented in this chapter.

Chapter 2: Literature review

This chapter exhibits a detailed introduction of a popular water purification technology-advanced oxidation processes based on hydroxyl radicals and sulfate radicals for removal of organic contaminants. PMS activation methods and development of carbon nanomaterials for phenol removal are also discussed in this chapter.

Chapter 3: One pot synthesis of N-doped graphene for metal-free advanced oxidation processes (*Carbon, 102 (2016): 279-287*)

This chapter describes a facile one-pot pyrolysis of glucose, urea and ferric chloride to generate high-quality nitrogen-doped graphene in a large scale. The as-obtained graphene materials had be used as an excellent metal-free catalyst for PMS activation to catalytically degrade phenolic solutions, offering a promising material for environmental remediation.

Chapter 4: Ferric carbide nanocrystals encapsulated in nitrogen-doped carbon nanotubes as an outstanding environmental catalyst (*Environ. Sci.: Nano, 2017, 4, 170*)

This chapter reports the synthesis of nitrogen-doped carbon nanotubes with Fe_3C encapsulation by an easy one-pot strategy of iron chloride and melamine at different pyrolysis temperatures. Various characterization techniques were employed to investigate their morphologies, compositions, active sites and reactive mechanism of phenol degradation.

Chapter 5: Morphological control of nitrogen-doped carbon nanostructures and their environmental application

This chapter describes a one-step synchronous carbonization and nitridation approach of nitrogen-doped mesoporous carbon nanostructures with different morphologies via direct pyrolysis of a hybrid of precursors (glucose, melamine and iron chloride). Morphologies and compositions were systematically characterized. Quenching experiments were conducted to probe the generated reactive radicals to further understand the involved mechanism of catalytic oxidation of phenol solutions.

Chapter 6: Co-based nanospheres supported on carbon sphere with a tunable oxidation layer in the applications of lithium ion battery and wastewater treatment

This chapter describes pomegranate-like structural Co sphere @ carbon sphere composite materials by a one-step hydrothermal method. The partially oxidized sample and fully oxidized samples with different degrees of oxidation treatment were used in the application of water treatment and anode of lithium ion battery.

Chapter 7: Conclusion

This chapter gives a summary of the research results and provides some perspectives for research in the future.

References

[1] D.L. Danielopol, C. Griebler, A. Gunatilaka, J. Notenboom, Present state and future prospects for groundwater ecosystems, Environmental Conservation 30(2) (2003) 104-130.

[2] X. Qu, J. Brame, Q. Li, P.J.J. Alvarez, Nanotechnology for a Safe and Sustainable Water Supply: Enabling Integrated Water Treatment and Reuse, Accounts of Chemical Research 46(3) (2013) 834-843.

[3] A.B. Bhuiyan, M.B. Mokhtar, M.E. Toriman, M.B. Gasim, G.C. Ta, R. Elfithri, M.R. Razman, The environmental risk and water pollution: A review from the river basins around the world, American-Eurasian Journal of Sustainable Agriculture 7(2) (2013) 126-136.

[4] K. Zhang, Y.-L. Wei, E.Y. Zeng, A review of environmental and human exposure to persistent organic pollutants in the Pearl River Delta, South China, Science of The Total Environment 463 (2013) 1093-1110.

[5] A. Sepúlveda, M. Schluep, F.G. Renaud, M. Streicher, R. Kuehr, C. Hagelüken, A.C. Gerecke, A review of the environmental fate and effects of hazardous substances released from electrical and electronic equipments during recycling: Examples from China and India, Environmental Impact Assessment Review 30(1) (2010) 28-41.

[6] Y. Jiang, China's water security: Current status, emerging challenges and future prospects, Environmental Science & Policy 54 (2015) 106-125.

[7] Y. Jiang, China's water scarcity, Journal of Environmental Management 90(11) (2009) 3185-3196.

[8] S. Zaidi, Human health effects of oil development in the Ecuadorian Amazon: A challenge to legal thinking, Environmental Impact Assessment Review 14(5) (1994) 337-348.
[9] Z. Zhang, F. Tao, J. Du, P. Shi, D. Yu, Y. Meng, Y. Sun, Surface water quality and its control in a river with intensive human impacts–a case study of the Xiangjiang River, China, Journal of Environmental Management 91(12) (2010) 2483-2490.
[10] X. Gao, F. Zhou, C.-T.A. Chen, Pollution status of the Bohai Sea: An overview of the environmental quality assessment related trace metals, Environment International 62 (2014) 12-30.
[11] K. Pan, W.-X. Wang, Trace metal contamination in estuarine and coastal environments in China, Science of The Total Environment 421 (2012) 3-16.
[12] G. Lofrano, M. Carotenuto, G. Libralato, R.F. Domingos, A. Markus, L. Dini, R.K. Gautam, D. Baldantoni, M. Rossi, S.K. Sharma, M.C. Chattopadhyaya, M. Giugni, S. Meric, Polymer functionalized nanocomposites for metals removal from water and wastewater: An overview, Water Research 92 (2016) 22-37.
[13] A.K. Jain, V.K. Gupta, S. Jain, Suhas, Removal of Chlorophenols Using Industrial Wastes, Environmental Science & Technology 38(4) (2004) 1195-1200.
[14] C.A. Martínez-Huitle, E. Brillas, Decontamination of wastewaters containing synthetic organic dyes by electrochemical methods: A general review, Applied Catalysis B: Environmental 87(3) (2009) 105-145.
[15] A. Garg, I.M. Mishra, S. Chand, Oxidative phenol degradation using non-noble metal based catalysts, Clean - Soil, Air, Water 38(1) (2010) 27-34.
[16] L.A. Bernal-Martínez, C. Barrera-Díaz, C. Solís-Morelos, R. Natividad, Synergy of electrochemical and ozonation processes in

industrial wastewater treatment, Chemical Engineering Journal 165(1) (2010) 71-77.
[17] A. Babuponnusami, K. Muthukumar, A review on Fenton and improvements to the Fenton process for wastewater treatment, Journal of Environmental Chemical Engineering 2(1) (2014) 557-572.
[18] W.H. Glaze, J.-W. Kang, D.H. Chapin, The Chemistry of Water Treatment Processes Involving Ozone, Hydrogen Peroxide and Ultraviolet Radiation, Ozone: Science & Engineering 9(4) (1987) 335-352.
[19] A. Babuponnusami, K. Muthukumar, Degradation of Phenol in Aqueous Solution by Fenton, Sono-Fenton and Sono-photo-Fenton Methods, CLEAN – Soil, Air, Water 39(2) (2011) 142-147.
[20] J.J. Pignatello, E. Oliveros, A. MacKay, Advanced Oxidation Processes for Organic Contaminant Destruction Based on the Fenton Reaction and Related Chemistry, Critical Reviews in Environmental Science and Technology 36(1) (2006) 1-84.
[21] W.-D. Oh, Z. Dong, T.-T. Lim, Generation of sulfate radical through heterogeneous catalysis for organic contaminants removal: Current development, challenges and prospects, Applied Catalysis B: Environmental 194 (2016) 169-201.
[22] F. Rodríguez-reinoso, The role of carbon materials in heterogeneous catalysis, Carbon 36(3) (1998) 159-175.
[23] A. Kunhikrishnan, H.K. Shon, N.S. Bolan, I. El Saliby, S. Vigneswaran, Sources, Distribution, Environmental Fate, and Ecological Effects of Nanomaterials in Wastewater Streams, Critical Reviews in Environmental Science and Technology 45(4) (2015) 277-318.
[24] F. Perreault, A. Fonseca de Faria, M. Elimelech, Environmental applications of graphene-based nanomaterials, Chemical Society Reviews 44(16) (2015) 5861-5896.

[25] P. Serp, M. Corrias, P. Kalck, Carbon nanotubes and nanofibers in catalysis, Applied Catalysis A: General 253(2) (2003) 337-358.
[26] X. Duan, Z. Ao, H. Sun, S. Indrawirawan, Y. Wang, J. Kang, F. Liang, Z.H. Zhu, S. Wang, Nitrogen-Doped Graphene for Generation and Evolution of Reactive Radicals by Metal-Free Catalysis, ACS Applied Materials & Interfaces 7(7) (2015) 4169-4178.
[27] X. Duan, K. O'Donnell, H. Sun, Y. Wang, S. Wang, Sulfur and Nitrogen Co-Doped Graphene for Metal-Free Catalytic Oxidation Reactions, Small 11(25) (2015) 3036-3044.
[28] X. Duan, H. Sun, Y. Wang, J. Kang, S. Wang, N-Doping-Induced Nonradical Reaction on Single-Walled Carbon Nanotubes for Catalytic Phenol Oxidation, ACS Catalysis 5(2) (2015) 553-559.
[29] S. Indrawirawan, H. Sun, X. Duan, S. Wang, Low temperature combustion synthesis of nitrogen-doped graphene for metal-free catalytic oxidation, Journal of Materials Chemistry A 3(7) (2015) 3432-3440.
[30] H. Sun, S. Liu, G. Zhou, H.M. Ang, M.O. Tadé, S. Wang, Reduced Graphene Oxide for Catalytic Oxidation of Aqueous Organic Pollutants, ACS Applied Materials & Interfaces 4(10) (2012) 5466-5471.

Chapter 2 Literature Review

2.1 Introduction

As the most essential substance for life on the earth, water is a precious resource for human civilization. One of the most basic humanitarian goals is to have reliable access to clean and affordable water, which is also regarded as a major global challenge for the 21st century. Worldwide, water supply, exacerbated by rapid population growth, changeable global climate, and deteriorated water quality, struggles to keep up with the fast growing demand. Generally speaking, toxic chemicals and biological agents exceed what is naturally found in water body itself will be defined as water pollutants.[1]

Many organic contaminants present in wastewater, surface water and ground water are resulted from polluted soil, agricultural runoff, discharge of industrial wastewater and leakage of hazardous compounds storage, which pose severe threats to public health due to their poisonousness, endocrine disruption, mutagenic or carcinogenic ability to humans and animals even at very low concentrations.[2]

As one of common pollutants, metals can undesirably enter into aquatic environments and drinking water supplies through human activities, such as mining and industrial wastes, the corrosion of pipes, soldered joints, and plumbing materials. Therefore, an increasing interest has been aroused in the concentration control of toxic metals in water. For instance, in the light of the United States Environmental Protection Agency (EPA), the concentrations of copper (Cu) and lead (Pb) permitted in drinking water are 1.3 ppm and 15 ppb, respectively.[3, 4]

Phenol is also one of the major contaminants in surface and ground water. As a basic structural unit, it can be applied to synthesize a range of organic compounds that are widely used in various industries, such as chemical plants, pesticide and dye manufacturing industries, paper and pulp plants, resin manufacturing, coke manufacturing, tanning, textile, plastic, rubber, pharmaceutical plants, and petroleum industries.[5] Hence, wastewater discharged from these industries contains different types of phenols. It is an environmental hazard and toxic to human beings as well as aquatic fauna and flora. It is considered that phenol can be lethal to most of aquatic organisms when they are exposed to a concentration of 10-100 ppm.[6] Consequently, with respect to the wide prevalence of phenols in wastewaters and their poisonousness to human and animal life even at very low concentration, it is of high priority to remove them from wastewater, thus making it necessary to find efficient treatment methods.[7-9]

In an effort to cope with water pollution, rapid and significant advances in wastewater treatment methods have been gained, such as photocatalysis, adsorption, separation processes and biodegradation. However, many factors, including processing efficiency, operational approaches, energy requirements, and economic outcomes, limit their applications. With respect to phenol removal, a number of methods have been applied, such as ozonization, hydrogen peroxide oxidation, bioremediation, ion exchange, membrane filtration, electrochemical oxidation, photocatalytic degradation, reverse osmosis, and adsorption.[10, 11]

Adsorption, a facile operational method to effectively remove various organic and inorganic toxicants, has aroused great interests for

researchers in the past decades. It is a combination of purification and separation processes occurring between the adsorbent phase and target pollutants. When a substance is isolated from one phase on the surface of another substance, adsorption process thus happens, either in solid-liquid or solid-gas systems.[12] Adsorption process is generally derived from the electrostatic or non-electrostatic interactions between the adsorbent surface and the adsorbate. In comparison with the rest environmental remediation technologies, no residues are generated by adsorption and secondary pollution brought by harmful and toxic substances can therefore be prevented. Decisive factors of adsorption capabilities of adsorbents are pore volume, surface area, surface charge and surface functionalities.[13] Over the past decades, various categories of porous materials have been developed and their adsorption abilities have been investigated. Porous materials like activated carbon,[14] zeolites,[15] clay minerals,[16] biological materials,[17] industrial solid wastes[18] and some novel carbon-based materials such as graphene, graphene oxide and carbon nanotubes[13, 19] have been extensively applied in the high-efficiency adsorptive elimination of dye products, heavy metals and organic pollutants released from wastewater.[17] However, organic pollutants presented in the wastewater are only adsorbed in the adsorption process rather than destructed, and further treatment is still essential for destroy of the contaminants as well as collection and separation of adsorbents.[20] Accordingly, other effective treatment technologies are still needed for the effective decomposition of aqueous organic contaminants.

Biological treatment, also known as biodegradation or bioremediation, is the prominent pathway to degrade organic pollutants in natural systems. Without great amounts of chemicals and energy, the biological

remediation processes can degrade polluted compounds into harmless ones effectively in a relatively mild condition. Although polycyclic aromatic hydrocarbons (PAHs) may experience adsorption, photolysis or chemical degradation in nature, biodegradation, as reported, is still regarded as the major pathway for PAHs removal.[21] The catabolic activity of microbes plays a leading role in biodegradation. Algae, bacteria and fungi are microorganism for bioremediation.[22] Via biotransformation, they can mineralize the organic compounds into smaller metabolites, which will subsequently be decomposed into inorganic substances, carbon dioxide and water (aerobic), or methane (anaerobic). Many factors affect its degradation efficiency, such as the environment (pH, temperature, oxygen supply), population of microbes, acclimation degree, nutrient contents, organic structure, and cellular transport properties.[23, 24]

However, phenol is soluble and stable and its recalcitrant property makes it impossible to be removed by conventional physicochemical and biological treatment methods.[5] Therefore, advanced techniques, such as wet air oxidation, super critical oxidation and advanced oxidation processes (AOPs) are favorable to remove phenol in wastewater, either used individually or in combination.

Advanced oxidation processes are emerged as a promising alternative because of its capability to degrade recalcitrant substances and less energy requirement. Operated in ambient temperature and pressure, AOP generate a large quantity of reactive species, hydroxyl radicals ($^{\bullet}OH$) to attack organic contaminants in wastewater. To be mentioned, $^{\bullet}OH$ can be produced by different possible ways to comply with specific treatment requirements.[1]

Recently, sulfate radical ($SO_4^{\bullet-}$) based advanced oxidative processes (SR-AOPs), a promising alternative to hydroxyl radical-based AOPs, have gained intensive attentions. $SO_4^{\bullet-}$ has a higher oxidation potential (2.5 - 3.1 V) than $^{\bullet}OH$ (1.8 - 2.7 V) and is thus highly desirable for refractory products destruction. Sulfate radicals are usually generated by either persulfate (PS) or peroxymonosulfate (PMS), which are less expensive and environmentally friendly and can be activated homogeneously and heterogeneously by transition metals, metal oxides or metal-free carbon materials, minimizing secondary pollution resulted from metal leaching. In addition, $SO_4^{\bullet-}$ presents a better selectivity to pollutants and can be applied in a wider range of pH.[25-27]

Catalysts based on transition metals, Co, Mn and Fe, have been widely applied in the PMS activation to generate $SO_4^{\bullet-}$.[28-30] Nevertheless, transition metal-based catalysts are expensive and the associated problem of metal leaching can trigger secondary pollution. Of late, nanocarbon materials, such as graphene, graphene oxide, reduced graphene oxide and carbon nanotubes (CNTs) have developed into promising alternatives to metal-based catalysts to completely avoid the leaching problem of metal ions. A wide range of researches have demonstrated that these carbon nanomaterials enjoy the favorable catalytic ability for applications in energy and environmental fields owing to distinct electronic properties, relatively large theoretical surface area, superb thermal conductivity as well as sp^2-hybridized carbon framework. To be mentioned, PMS can be effectively activated by fullerene, graphene oxides, graphene nanoplates, single-walled carbon nanotubes (SWCNTs) and multi-walled carbon nanotubes (MWCNTs).[31-36]

2.2 Advanced oxidation processes

Firstly proposed in the 1980s for the treatment of potable water, advanced oxidation processes (AOPs) have strong and powerful hydroxyl or sulfate radicals to be dominant oxidizing agents. Afterwards, they were extensively utilized in the treatment of wastewaters containing a wide range of toxic, refractory and persistent organic contaminants.
The recalcitrant property of pollutants presented in wastewater makes conventional chemical and biological treatment methods not effective.[37, 38] Meanwhile, direct oxidation processes, though effective in degradation, often require special operating conditions in the removal of target compounds which will consequently increase operation cost.[39, 40] Therefore, AOPs are favorable alternative treatment methods to degrade refractory organic pollutants that are operated near ambient temperature and pressure.

In wastewater treatment utilizing AOPs, sufficient strong oxidants ($^{\bullet}OH$ or $SO_4^{\bullet-}$) are generated to easily destruct recalcitrant organic substances and certain inorganic pollutants and completely mineralize them into CO_2 and water, completely distinct from common oxidants like chlorine and ozone that have a combined role of decontamination and disinfection.

Different AOPs can treat different types of contaminants accordingly. Normally, the treatment efficiencies have a great dependence on the chosen AOP type, physical and chemical features of target pollutants, and operating conditions. Noticeably, other mechanisms, in addition to hydroxyl radical or sulfate radical-based oxidation processes, may

happen during the AOP treatment and eventually lead to the reduction of target contaminants.

2.2.1 Hydroxyl radical-based AOPs

Hydroxyl radical (•OH), with an oxidation potential of 2.8 V at pH = 0 and 1.95 V at pH = 14), is formerly regarded as the most reactive oxidizing agent in water treatment. Due to its non-selectivity, •OH can react with a large number of organic and inorganic compounds in wastewaters rapidly and readily with the rate constants in the order of 10^8-10^{10} M^{-1} s^{-1}.[41] It is normally thought that the following four basic pathways occurred in the attack of organic contaminants by •OH, that is, radical addition, hydrogen abstraction, electron transfer, as well as radical combination. Carbon-centred radicals (R• or R•-OH) are generated during these processes and they are likely to be converted into organic peroxyl radicals (ROO•) under O_2. The as-obtained radicals react further to produce much more active species like hydrogen peroxide (H_2O_2) and super oxide ($O_2^{\bullet-}$), which degrade and mineralize organic pollutants to harmless substances. Due to their very short lifetime, hydroxyl radicals can only be in situ produced via various approaches. Combined oxidizing agents (such as H_2O_2 and O_3), irradiation (such as ultraviolet light or ultrasound), and catalysts (such as Fe^{2+}) are common methods to produce hydroxyl radicals. Below is the summary of major AOPs for wastewater treatment based on the mechanisms of hydroxyl radical generation.

2.2.2.1 Ozone-based AOPs

Ozone (O_3) is a powerful oxidant and its oxidation potential is 2.07 V.[42] Two possible ways of oxidation are to be considered in an ozonation process. The first is the direct way of the reaction occurring between the ozone and the dissolved compounds. Oxidation by O_3 directly is prone to be selective in the reaction rate constants of 1.0×10^0-10^3 M^{-1} s^{-1}. During this process, O_3 is more likely to react with organic compounds in ionized and dissociated forms than those in neutral forms. The second is the radical way of the reaction between the radicals, i.e. hydroxyl radicals, produced by the break-down of ozone and the dissolved substances.[43, 44] The complicated ˙OH generation can be illustrated by different mechanisms and the overall reaction demonstrating the generation of OH· is presented as follow:[45]

$$3O_3 + H_2O \rightarrow 2OH^{\bullet} + 4O_2 \qquad \text{(Eq. 2.1)}$$

The yield of OH· can be greatly enhanced with the presence of other oxidants or irradiation. In the peroxone (O_3 / H_2O_2) system, for example, H_2O_2 decompose into hydroperoxide (HO_2^-), which will significantly stimulate O_3 decomposition and improve the production of ˙OH .

$$H_2O_2 \rightarrow HO_2^- + H^+ \qquad \text{(Eq. 2.2)}$$

$$HO_2^- + O_3 \rightarrow OH^{\bullet} + O_2^- + O_2 \qquad \text{(Eq. 2.3)}$$

By the irradiation of ultraviolet (UV), H_2O_2 can be produced as an extra oxidant mainly from the photolysis of O_3 (Eq. 4).

$$O_3 + H_2O + hv \rightarrow H_2O_2 + O_2 \qquad \text{(Eq. 2.4)}$$

Therefore, at least three pathways contribute to the generation of ·OH: (1) ozonation (Eq. 2.1); (2) O_3/H_2O_2 (Eq. 2.2 and Eq. 2.3); and (3) photolysis of H_2O_2, as shown in Eq. 2.5.

$$H_2O_2 + hv \rightarrow 2OH^{\bullet} \quad \text{(Eq. 2.5)}$$

2.2.2.2 UV-based AOPs

With catalysts or oxidants, ·OH can also be generated by photons. The most common catalyst used in photocatalysis tends to be titanium dioxide (TiO_2), a RO-type semiconductor with good stability, excellent performance and low cost. Combined with UV irradiation, the interaction between catalyst (a semiconductor) and oxidizing agent (oxygen) produces electron-hole pairs on the surface of the semiconductor. Generally, TiO_2 particles are initiated to generate positive holes in the valence band (hv^{+}_{vb}) with an oxidative capacity, and negative electrons at the conduction band (e^{-}_{cb}) with a reductive capacity, illustrated in Eq. 2.6.[46]

$$TiO_2 + hv \rightarrow e^-_{cb} + hv^+_{vb} \quad \text{(Eq. 2.6)}$$

These charged points react with organic compounds and water.[47] The as-formed holes and electrons are able to generate ·OH in the reactions with OH^-, H_2O, and $O_2^{\bullet-}$ occurring at TiO_2 surface.

$$hv^+_{vb} + OH^-_{(surface)} \rightarrow OH^{\bullet} \quad \text{(Eq. 2.7)}$$

$$hv^+_{vb} + OH^-_{(surface)} \rightarrow OH^{\bullet} + H^+ \quad \text{(Eq. 2.8)}$$

$$e^-_{cb} + O_{2(absorbed)} \rightarrow O_2^{\bullet-} \quad \text{(Eq. 2.9)}$$

These reactions are vital in the oxidative degradation processes because of high concentrations of H_2O and HO^- adsorbed on the surface.

Excess $^{\bullet}OH$ is prone to be generated by UV irradiation with oxidants like H_2O_2 or O_3. For instance, a H_2O_2 molecule is decomposed by UV irradiation to yield two $^{\bullet}OH$.

$$H_2O_2 + hv \rightarrow 2OH^{\bullet} \quad \text{(Eq. 2.10)}$$

Additionally, $^{\bullet}OH$ is likely to be produced via H_2O photolysis when the wavelength is less than 242 nm.

$$H_2O + hv \rightarrow OH^{\bullet} + H^{\bullet} \quad \text{(Eq. 2.11)}$$

The majority of researches engaged in photocatalysis emphasize the possible exploitation of solar spectrum wavelengths. Nevertheless, this is only partially true due to the rather poor overlapping between the absorption spectrum of TiO_2 and that of the sun at ground. In spite of that, intensive researches are implemented globally to gain modified (doped) TiO_2 featured by higher quantum yield with a broader absorption spectrum.

2.2.2.3 Fenton-based AOPs

H.J.H Fenton, the first scholar to discover Fenton reaction in 1894, reported that H_2O_2 was able to be activated by ferrous salts for the oxidation of tartaric acid.[48] In Fenton and Fenton-related processes, peroxide (usually H_2O_2) reacts with iron ions to form strong and reactive species to destruct both organic and inorganic substances. Fenton reaction can be achieved at room temperature and ambient pressure.[49]

Besides, the involved chemical reagents can be stored and handled easily and do not cause environmental damages.[50] The radical mechanisms of classical Fenton reactions are primarily represented by the reactions below.[51]

$$Fe^{2+} + H_2O_2 \rightarrow Fe^{3+} + OH^{\bullet} + OH^{-} \quad \text{(Eq. 2.12)}$$

$$Fe^{3+} + H_2O_2 \rightarrow Fe^{2+} + HO_2^{\bullet} + H^{+} \quad \text{(Eq. 2.13)}$$

$$OH^{\bullet} + H_2O_2 \rightarrow HO_2^{\bullet} + H_2O \quad \text{(Eq. 2.14)}$$

$$OH^{\bullet} + Fe^{2+} \rightarrow Fe^{3+} + OH^{-} \quad \text{(Eq. 2.15)}$$

$$Fe^{3+} + HO_2^{\bullet} \rightarrow Fe^{2+} + O_2H^{+} \quad \text{(Eq. 2.16)}$$

$$Fe^{2+} + HO_2^{\bullet} + H^{+} \rightarrow Fe^{3+} + H_2O_2 \quad \text{(Eq. 2.17)}$$

$$2HO_2^{\bullet} \rightarrow H_2O_2 + O_2 \quad \text{(Eq. 2.18)}$$

Eq. 2.12 is the major reaction of Fenton reaction, demonstrating the generation of $^{\bullet}OH$ between H_2O_2 and ferrous iron (Fe^{2+}) salts. Excessive hydrogen peroxide can further reduce ferric ions to ferrous ions and other radicals, as shown in Eq. 2.13. The definition of this reaction is Fenton-like reaction which has a much slower reaction rate than Fenton reaction. In addition, ferric ions produce solid sludge that need to be treated separately at typical water and wastewater treatment conditions, which will consequently increase the treatment cost and difficulty. However, the generated $^{\bullet}OH$ can be consumed by either H_2O_2 or Fe^{2+}, represented in Eqs. 2.14 and 2.15, the molar ratio of Fe^{2+} to H_2O_2, therefore, requires optimization to avoid scavenging and wastage of oxidants. The equations mentioned above demonstrate that an intricate mechanism is encased in Fenton reaction.[2]

Although ferryl ions were also proposed as reactive species, hydroxyl radicals were generally regarded as the major reactive species. However, they become most active only at an acidic condition, that is, Fenton reaction relies heavily on the solution pH and it is proved that the optimal pH for Fenton process was around 3.[52, 53] This will accordingly and inevitably restrict the practical applications of Fenton reaction in wastewater treatment. Moreover, the type of buffer solution also affects the degradation process. It is observed that acetic acid/acetate buffer can have the greatest oxidation efficiency whereas phosphate and sulfate buffers have the least. However, operational costs will inevitably be enhanced with the use of buffering and whether to use it varies with situations.

Concentration of H_2O_2 plays an important role in the total efficiency of the degradation process. Generally speaking, the degradation efficiency will be enhanced with the quantity of hydrogen peroxide.[54, 55] However, excessive hydrogen peroxide will cause higher COD and are detrimental to many organisms;[56, 57] accordingly, will significantly decrease the overall degradation efficiency. Meanwhile, redundant hydrogen peroxide will lead to the scavenging effect of produced hydroxyl radicals.

Many researches have reported the Fenton-related reactions for wastewater treatment in details. In view of classical Fenton treatment mechanism, modified Fenton processes, such as Fenton-like reactions, electron Fenton, UV/Fe^{2+}/H_2O_2, ultrasound (US)/Fe^{2+}/H_2O_2, UV/US/Fe^{2+}/H_2O_2, are proposed and have been proved to be effective for the decomposition of a variety of harmful organics from contaminated waterbodies.[6, 52, 58-60]

Due to its rapid destruction of organic contaminants, the oxidation of organics by US has received considerable attention.[61] When US irradiation ranges from 16 kHz to 100 MHz, nucleation, growth, and implosive collapse of cavities (consisting of vapor and microbubble filled with gas) can happen with compression and rarefaction cycles of the sound waves in turn. It is reported that an extremely high temperature from 4200 to 5000 K and a great pressure from 20 to 500 atm could be generated instantly during the collapse of microbubble. Hydroxyl radicals are thus produced by the fragmentation and pyrolysis of water molecules in the form of gas within microbubbles in such extreme conditions. After that, the radicals can enter into various chemical reactions in a gas bubble and/or in the bulk solution.[62, 63]

$$H_2O \rightarrow OH^{\bullet} + H^{\bullet} \qquad \text{(Eq. 2.19)}$$

Fenton and sonolysis can be combined to increase the quantity of hydroxyl radicals in solutions to degrade organic compounds more efficiently by utilizing the merits of both ultrasound and chemical reagents in Fenton.[64]

Effective electrochemical treatments have aroused great interest for the decomposition of toxic and refractory organics, which can be achieved by the two most usual techniques - anodic oxidation and indirect electro-oxidation.[65] In anodic oxidation, pollutants can be directly decomposed by electron transfer reactions. Meanwhile, they can also be mineralized by ˙OH radicals formed on the electrode surface (Eq. 2.20).

$$H_2O \rightarrow OH^{\bullet} + H^{+} + e^{-} \qquad \text{(Eq. 2.20)}$$

Anodic oxidation is normally carried out in the anodic compartment of the divided cell, in which the polluted solution is coped with a combination of an anode of Pt, undoped and doped PbO_2 and SnO_2.[66, 67] In electro-Fenton (EF) reaction, pollutants are destructed by Fenton's chemicals and anodic oxidation occurred at the anode surface. The electro-Fenton process's efficiency relies on electrode and electrolytes property, solution pH, dissolved oxygen content, catalyst concentration, current density as well as temperature.[68]

With regard to photo-Fenton (PF) process, a combination of UV irradiation with conventional Fenton system can generate more hydroxyl radicals than traditional Fenton reactions, which consequently enhance the degradation efficiency.[69] In short, the major purpose of PF is to increase the reduction of ferric ions to ferrous ions, as shown in Eq. 2.21.[70] The newly produced ferrous ions are in reaction with H_2O_2 to yield hydroxyl radical and ferric ion again and thus the cycle continues.

$$Fe(OH)^{2+} + hv \rightarrow Fe^{2+} + OH^{\bullet} \qquad \text{(Eq. 2.21)}$$

The PF process exhibits more satisfactory performance at pH 3.0.[71] In some cases, the replacement of UV irradiation with sunlight reduced the costs, but the degradation rates are very low.[72]

Sono-photo-Fenton (SPF) process is a combination of ultrasound and ultraviolet with Fenton chemicals, in which hydroxyl radicals can be produced greatly in an aqueous environment. Water sonolysis generates hydroxyl radicals as well hydrogen atoms, but their recombination significantly reduces the quantity of $H^{\bullet}$ and $^{\bullet}OH$ species. On the other hand, the application of UV light was applied to convert the hydrogen

peroxide which is generated by hydroxyl radicals' recombination, which thus increased the amount of ·OH.[73] The intermediates, produced from the reaction between Fe^{3+} and H_2O_2 in Fenton process, could be subsequently reduced to Fe^{2+} by sonolysis and photolysis.[68, 74] Compared with traditional Fenton reaction, the amount of ferrous salt needed in SPF process is rather small. However, ferrous ions are required to be added at regular intervals to continue the reaction. If not, the reaction will stop after ferrous ions completely convert into ferric ions. From the viewpoint of industrial application, it is noticeable that SPF process decreases the amount of ferrous ions in the target water.[75] Segura et al. investigated the application of SPF process for the degradation of phenol using Fe_2O_3/SBA-15 as a heterogeneous catalyst.[76] Mendez-Arriaga et al. investigated the degradation of recalcitrant pharmaceutical micro-pollutant ibuprofen (IBP) by means of sono-photo-Fenton, sono-photo-catalysis and TiO_2/Fe^{2+}/sonolysis processes.[77]

The irradiation of UV light can enhance the catalytic effect of Fe^{2+} in the EF process. Thus, the combined treatment using electrochemistry and photochemistry along with Fenton reaction is defined as photo-electro-Fenton (PEF) process, in which much more free radicals can be generated owning to the combination effect.[78, 79]

The major drawback of homogeneous Fenton and its combined processes is that they require ferrous ions at 50-80 ppm, which is above the standard levels. Meanwhile, vast amount of sludge can be produced during the neutralization procedure in the end when treating large quantity of wastewater by homogeneous AOPs.[80] Therefore, nano-zero valent iron (NZVI) is likely to be employed as an alternative to

initiate Fenton process to avoid these disadvantages. Zero valent state metals (such as Fe^0, Zn^0, Sn^0 and Al^0) have been proved to be exceptionally effective in contaminated water remediation.[81, 82] Due to its larger specific surface area and more reactive sites, NZVI was successfully applied to generate hydroxyl radicals in AOP system and thus gained prominence in environmental remediation.[83-85]

In heterogeneous Fenton reaction, NZVI oxidation offers a promising alternative approach to induce oxidation in heterogeneous Fenton reaction, which is illustrated in Eq. 2.22:[86]

$$O_2 + Fe^0 + 2H^+ \rightarrow Fe^{2+} + H_2O_2 \quad \text{(Eq. 2.22)}$$

Compared with traditional Fe^{2+}/H_2O_2 system, Fenton oxidation induced by NZVI can be in attachment with or coating on large particles.[87] However, NZVI could aggregate and thus decrease the reactivity and filtration is needed to remove NZVI particles at the final stage of the treatment. Therefore, NZVI particles could be immobilized in or on appropriate solid supports, and is also able to expand the effective pH range of the Fenton reaction.[88-90]

2.2.3 Sulfate radical-based AOPs

$S_2O_8^{2-}$, also known as persulfate anions, is the newest and strong oxidant alternative employed in in-situ chemical oxidation for organic pollutants treatment in ground water and soil. It has a standard oxidation potential (E^0) of 2.01 V compared with O_3 (2.07 V).[91] Relatively low cost, excellent solubility, good stability in the subsurface, as well as benign final products make persulfate oxidation a favorable choice among AOPs

for treatment of polluted soil and ground water. For the past years, sulfate radical-based AOPs have attracted great scientific and technological attentions for the effective removal of aromatic components from wastewater in a wide pH range of 2-8. Sulfate radical-based AOPs can be initiated by powerful sulfate radicals ($SO_4^{\bullet-}$), which are formed by $S_2O_8^{2-}$ under radiolysis, photolysis, elevated pH or heat activation of persulfate.[92] In addition to these methods, sulfate radicals can be most effectively activated through electron transfer with persulfate (PS) or peroxymonosulfate (PMS) activation by transition metals.[93-95]

Thermal activation needs to heat the subsurface that increases cost and brings some engineering challenges. UV irradiation requires the elimination of subsurface water before treatment that are also cost intensive (Eq. 2.23). With respect to activation based on transition metals (Eq. 2.24), heating or pumping can be avoided with direct injection of solution into the subsurface.[96, 97] It is known that $SO_4^{\bullet-}$ (2.5-3.1 V) have a higher oxidation potential than the strong oxidant $S_2O_8^{2-}$ (2.01 V) and $^{\bullet}OH$ (2.7 V in acid solution and 1.8 V in neutral solution). At acidic pH, sulfate radicals and hydroxyl radicals display comparable reduction potentials, however, sulfate radicals generally enjoy more selectivity for oxidation than hydroxyl radicals. Due to this, $SO_4^{\bullet-}$ can react with a variety of organic pollutants with near diffusion-limited rate constants.[98]

$$S_2O_8^{2-} \xrightarrow{\Delta/UV} 2SO_4^{\bullet-} \qquad \text{(Eq. 2.23)}$$

$$S_2O_8^{2-} + M^{n+} \rightarrow SO_4^{\bullet-} + SO_4^{2-} + M^{n+1} \qquad \text{(Eq. 2.24)}$$

The temperature in a thermally activated persulfate method ranges from 35 to 130 ^{o}C.[99] Sulfate radicals generated by metals are twice lower than that by heat or UV with the same molar persulfate concentration, which is illustrated by Eqs. 2.23 and 2.24. It is thus concluded that metal activation method is not efficient from the theoretical point. Radiolysis, UV or thermal activation of peroxymonosulfate can form both sulfate and hydroxyl radicals, but sulfate radicals as the dominant oxidizing reactive species can only be generated by transition-metal catalysis. Although other metals like Cu(I) and Ag(I) are proved to have an activation capability, ferrous ions (Fe^{2+}) and ferric ions (Fe^{3+}) are two most frequently used metals. A sulfate radical mechanism is involved in the cobalt-mediated decomposition and the only intermediates are peroxymonosulfate radicals. The same conditions were applied to iron (II), titanium (III), as well as oxovanadium (IV). However, hydroxyl radicals were regarded as the major oxidizing species when copper (I) is used. Other transition metals, including manganese, ruthenium, tungsten, nickel, iridium, molybdenum and cerium, have been demonstrated to have the ability to activate PMS.[30] The equations demonstrating the generation of sulfate radicals from peroxymonosulfate (PMS) activated by transition metals such as Co (II) are shown as follows.[100]

$$Co^{2+} + H_2O \overset{yield}{\longleftrightarrow} CoOH^+ + H^+ \quad \text{(Eq. 2.25)}$$

$$CoOH^+ + HSO_5^- \rightarrow CoO^+ + SO_4^{\bullet -} + H_2O \quad \text{(Eq. 2.26)}$$

$$CoO^+ + 2H^+ \overset{yield}{\longleftrightarrow} Co^{3+} + H_2O \quad \text{(Eq. 2.27)}$$

$$Co^{2+} + SO_4^{\bullet -} \rightarrow Co^{3+} + SO_4^{2-} \quad \text{(Eq. 2.28)}$$

$$Co^{3+} + HSO_5^- \rightarrow Co^{2+} + SO_5^{\bullet -} + H^+ \quad \text{(Eq. 2.29)}$$

$$2SO_5^{\bullet -} \overset{yield}{\longleftrightarrow} {}^{-}_{3}OSOOOOSO_3^{-} \rightarrow \{SO_4^{\bullet -}O_2SO_4^{\bullet -}\} \quad \text{(Eq. 2.30)}$$

$$\{SO_4^{\bullet -}O_2SO_4^{\bullet -}\} \rightarrow O_2 + S_2O_8^{2-} \quad \text{(Eq. 2.31)}$$

$$\{SO_4^{\bullet -}O_2SO_4^{\bullet -}\} \rightarrow O_2 + 2SO_4^{\bullet -} \quad \text{(Eq. 2.32)}$$

In spite of the different reaction patterns, sulfate radicals and hydroxyl radicals are highly active with a relatively short lifespan. Sulfate radicals, in similarity with hydroxyl radicals, may react with organic compounds through electron transfer, hydrogen abstraction, or addition mechanisms. However, hydroxyl radicals are prone to link to C=C bonds or to remove H from C-H bonds in contact with organic molecules.[101] On the contrary, sulfate radicals are strongly electrophilic and more likely to extract electrons from organic compounds which are then converted to organic radical cations, expanding the categories of pollutant transformation pathways, for instance, $SO_4^{\bullet -}$ accelerates the decarboxylation of carboxylic acids. Three possible reaction routes may be engaged in the reaction of sulfate radicals as a one electron transfer oxidant: (a) sulfate adduct was formed at the unsaturated double bond in accompany with the generation of active carbocation to react further; (b) electron abstraction was occurred at the carboxylate anion in combination with CO_2 loss, and (c) relatively weak hydrogen abstraction, that is abstraction of H, also happened. Although sulfate radicals have more selectivity toward oxidation, hydroxylation products, also intermediates of hydroxyl radical attack, are the major products generated by sulfate radical when it attacks on aromatics. Meanwhile, sulfate radicals may generate other intermediates, which are highly reactive oxygen species like hydroxyl through Eqs. 2.33 and 2.34 as well,[102] especially in alkaline environment as shown in Eq. 2.34.

$$SO_4^{\bullet -} + H_2O \rightarrow OH^{\bullet} + SO_4^{2-} + H^+ \quad \text{(Eq. 2.33)}$$

$$SO_4^{\bullet -} + OH^- \rightarrow OH^{\bullet} + SO_4^{2-} \quad \text{(Eq. 2.34)}$$

These reactive oxygen species are able to trigger various radical propagation and termination chain reactions to partially or fully decompose organic compounds. Recently, several researches have shown that surface radicals were able to degrade a series of organic contaminants quickly, such as 1,1,1-trichloroethane (TCE), trichloroethane (TCA), MTBE, and diphenylamine.

2.3 Peroxymonosulfate activation methods

One of the primary concerns of environmentalists is to decompose recalcitrant organic pollutants into harmless matters. AOPs have been developed as promising technologies to produce hydroxyl and sulfate radicals for the removal of organic contaminants for decades. Various methods, including chemical, photochemical, sonochemical and electrochemical processes, have been utilised to produce hydroxyl radicals directly or indirectly to react with organic pollutants.[103] In recent years, sulfate radicals generated from peroxymonosulfate activation have aroused great attention among researchers.

Peroxymonosulfate (PMS), is regarded as a strong oxidant to produce the powerful oxidant HSO_5^-. Oxone is the trade name of potassium peroxymonosulfate ($2KHSO_5 \cdot KHSO_4 \cdot K_2SO_4$). As a versatile and environmental friendly oxidant, it has been extensively used in bleaching, cleaning and disinfection areas. To be mentioned, it is a favourable provider of PMS.[104, 105]

PMS could be utilized as an oxidant for the syntheses of diverse organics. Compared with radical-based oxidation, PMS is not favorable in kinetics with respect to organic pollutants oxidation. Except that -SO_3 group substitute for one of H atoms, other parts of PMS structure is in similarity to that of H_2O_2.[106] The distance of peroxide bond (O-O) in PMS is 1.460 Å, similar to that of solid state H_2O_2 (1.453 Å), but inferior to that of $S_2O_8^{2-}$ (1.497 Å).[107, 108] It is anticipated that O-O bond energy involved in PMS, as estimated, is between that of H_2O_2 (213 kJ mol^{-1})[109] and PS (140 kJ mol^{-1}).[110]

Recently, due to its high reactivity and high potential in the generation of powerful sulfate radicals, PMS has become a promising alternative to hydrogen peroxide and persulfate and its activation has acquired increasing popularity in the degradation of a wide range of organic pollutants in wastewater treatment. Once activated, the generated sulfate radicals played a pivotal role in pollutants degradation.[111]

The oxidation rate of PMS is faster than that of H_2O_2 and as an oxidant, PMS is more powerful ($E^0_{HSO_5^-/HSO_4^-}$ = +1.82 V; $E^0_{H_2O_2/H_2O}$ = +1.76 V). By the production of protons, PMS can adjust the pH of solution in an automatic manner. PMS exhibits more efficiency as an oxidant in organic synthesis than H_2O_2 or PS. In addition, due to its good stability and relatively high oxidation potential, PMS is able to oxidize organic pollutants even though at a much slower rate in kinetics than degradation based on radicals.[112]

Peroxydisulfuric acid ($H_2S_2O_8$) and peroxymonosulfuric acid (H_2SO_5, also called Caro's acid) were discovered more than a century ago. Peroxymonosulfate anion (HSO_5^-), first described by Heinrich Caro, is

derived from Caro's acid to be highly reactive.[113] It can decompose very quickly in aqueous solution at neutral condition. In spite of being a strong oxidant in thermodynamics, PMS cannot directly react with a large quantity of pollutants very fast. In this sense, activation is compulsory, that is to say, an activator is needed to decompose PMS. It is reported that PMS activators can be classified as follows: transition metals (homogeneous and heterogeneous), ultraviolet, ultrasound, heat, electron conduction, carbon catalysts, etc.[103] In this part, we put emphasis on the transition metals and carbon catalysts.

2.3.1 Homogeneous transition metals for PMS activation

It was discovered that PMS activation by transition metals is more effective than activation by ultraviolet or visible light.[114] In 1958, a wide range of metal ions were utilized to decompose Caro's acid.[115] Since then, transition metals have been extremely applied in PMS activation. In 1981, Thompson[116] observed that oxovanadium (IV), VO^{2+}, was able to react with HSO_5^- to produce free radicals - sulfate radicals. The proposed equation that describes the PMS activation by VO^{2+} is as follows:

$$HSO_5^- + VO^{2+} \rightarrow SO_4^{\bullet -} + VO_2^+ + H^+ \qquad \text{(Eq. 2.35)}$$

In 1987, Manivannan and Maruthamuthu[117] described the kinetics involved in the aqueous polymerization of acrylonitrile activated by Co(II)/PMS system. Excellent work has been done by Anipsitakis and Dionysiou in the field of toxicants removal by PMS.[118, 119] They reported a highly efficient PMS activation method by Co^{2+} to produce sulfate radicals for the degradation of organics. Compared with the

classic Fenton reagent (H_2O_2/Fe^{2+}), Co^{2+}/PMS system exhibited excellent performance in the degradation of 2,4-dichlorophenol (2,4-DCP), atrazine and naphthalence. It is known that Ball and Edwards, for the first time, reported that cobalt ions could decompose peroxymonosulfate ion (Eq. 2.36).

$$Co^{2+} + HSO_5^- \rightarrow Co^{3+} + SO_4^{\bullet -} + OH^- \quad \text{(Eq. 2.36)}$$

In addition, Anipsitakis and Dionysiou[30] have also reported that different tranisiton metals can activate PMS to degrade 2,4-DCP. The capability of various transition metals in the removal of 2,4-DCP were in the following sequence : $Ni^{2+} < Fe^{3+} < Mn^{2+} < V^{3+} < Ce^{3+} < Fe^{2+} < Ru^{3+} < Co^{2+}$. It is concluded that Co^{2+} and Ru^{3+} exhibited the best performance to generate sulfate radicals and thus were regarded as the major reactive species. The Co^{2+}/PMS mechanism is illustrated in the equations from Eqs. 2.25 to Eqs. 2.32.

Ferrous ions are also found to activate PMS to produce free radicals. It should be noted that Co^{2+} and Fe^{2+} are considered as the most common catalysts for PMS activation. The following equations show the reactions occurred in PMS activation by Fe^{2+}.[120, 121]

$$Fe^{2+} + HSO_5^- \rightarrow Fe^{3+} + SO_4^{\bullet -} + OH^- \quad \text{(Eq. 2.37)}$$

$$Fe^{3+} + HSO_5^- \rightarrow SO_5^{\bullet -} + Fe^{2+} + H^+ \quad \text{(Eq. 2.38)}$$

$$Fe^{2+} + SO_4^{\bullet -} \rightarrow Fe^{3+} + SO_4^{2-} \quad \text{(Eq. 2.39)}$$

$$HSO_5^- + SO_4^{\bullet -} \rightarrow SO_4^{2-} + SO_5^{\bullet -} + H^+ \quad \text{(Eq. 2.40)}$$

$$HSO_5^- + H_2O \rightarrow SO_4^{2-} + 2HO^{\bullet} + H^+ \quad \text{(Eq. 2.41)}$$

$$SO_5^{\bullet -} + 2H_2O \rightarrow SO_4^{2-} + 3HO^{\bullet} + H^+ \quad \text{(Eq. 2.42)}$$

With regard to PMS activation, Co^{2+} and Fe^{2+} exhibit superior performance than Co^{3+} and Fe^{3+} to produce strong and powerful reactive species. Figure 2.1 illustrated the mechanism of PMS activation by homogeneous transition metals catalysts.[103]

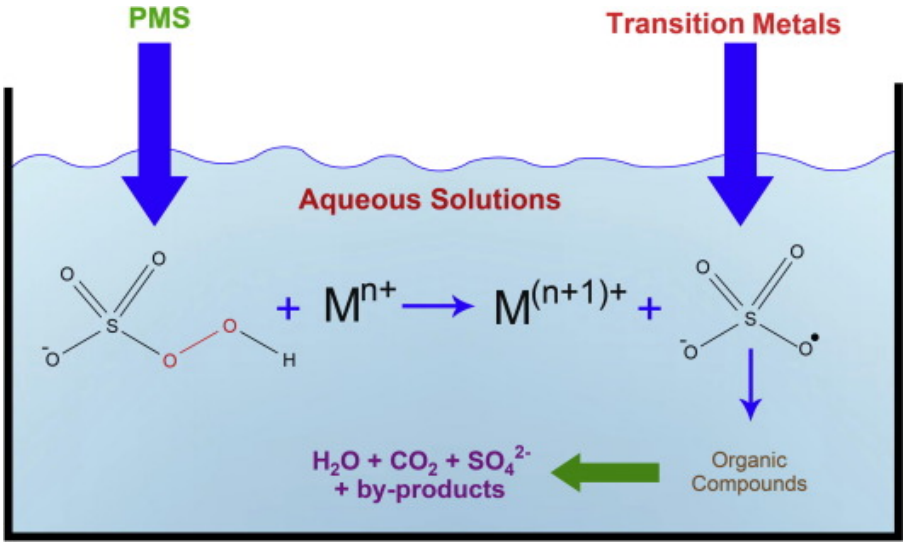

Figure 2.1 The scheme of PMS activation by transition metals as homogeneous catalyst.

The following parameters were compared in the consideration of the likelihood of Fenton reagent (Fe^{2+}/H_2O_2) replaced by Co^{2+}/PMS: (1) solution pH - Fenton chemicals is only effective at pH 3-4, but Co^{2+}/PMS can be efficient at a wide range of pH 2-8; (2) redox potential - the redox potential for $SO_5^{\bullet -}$ is 1.1 V, for $SO_4^{\bullet -}$ 2.5-3.1 V, and for $^{\bullet}OH$ 1.8-2.7 V; (3) final product - $SO_4^{\bullet -}$ can degrade a wide variety of organic compounds, but $^{\bullet}OH$ cannot decompose some refractory organics; (4)secondary contamination - H_2O_2 tends to be more environmentally friendly than peroxymonosulfate because only H_2O, OH^- and O_2 were produced by H_2O_2, but PMS produced SO_4^{2-}. However, SO_4^{2-} can be

easily handled due to its aqueous phase and also has low toxicity; (5) cost - Although H_2O_2 is cheaper than PMS, the use of iron and hydrogen peroxide, combined with pH adjustment and sludge disposal should also be included in the cost.[122] On the other hand, the cost of Co^{2+}/PMS is mainly the cost of PMS because only a small amount of cobalt is required to be a catalyst and pH adjustment as well as sludge treatment is not needed. The above comparison fully suggested that Co^{2+}/PMS can be acted as a promising alternative to Fenton reaction in the treatment of organic pollutants in wastewater.

However, some factors limit the applications of homogeneous catalysts. (a) It is difficult to recover homogeneous catalysts and thus intricate technical or economical separation techniques are needed; (b) To activate PMS in high concentration, high stoichiometric amounts of catalysts are required, particularly when treating high strength wastewaters, which will eventually generate more residuals in effluents as another problem; (c) Transition metal species have a great dependence on pH because hydroxide precipitates could be formed in alkaline pH and hydrated species could be produced in acidic pH, both of which will decrease catalysts availability.[103, 123]

2.3.2 Heterogeneous transition metals for PMS activation

In order to generate $SO_4^{\bullet-}$ from PMS by heterogeneous catalysis, it is necessary for PMS to be in close contact with the redox active surface of the catalyst to occur a wide range of surface PMS-catalyst interactions. Due to the short lifetime of $SO_4^{\bullet-}$, target compounds must be in the range of the diffusion limit of $SO_4^{\bullet-}$ to ensure the effective occurrence of oxidation reaction.[30]

More reactive than molecular oxygen, peroxymonosulfate radical is able to reduce some transition metals as well.[124] At the same time, the oxidized transition metal ions could be reproduced by direct oxidation of organic compounds via disproportionation reactions. Figure 2.2 demonstrated the working mechanism involved in the electron transfer reaction between PMS and heterogeneous transition metal catalysts.[125]

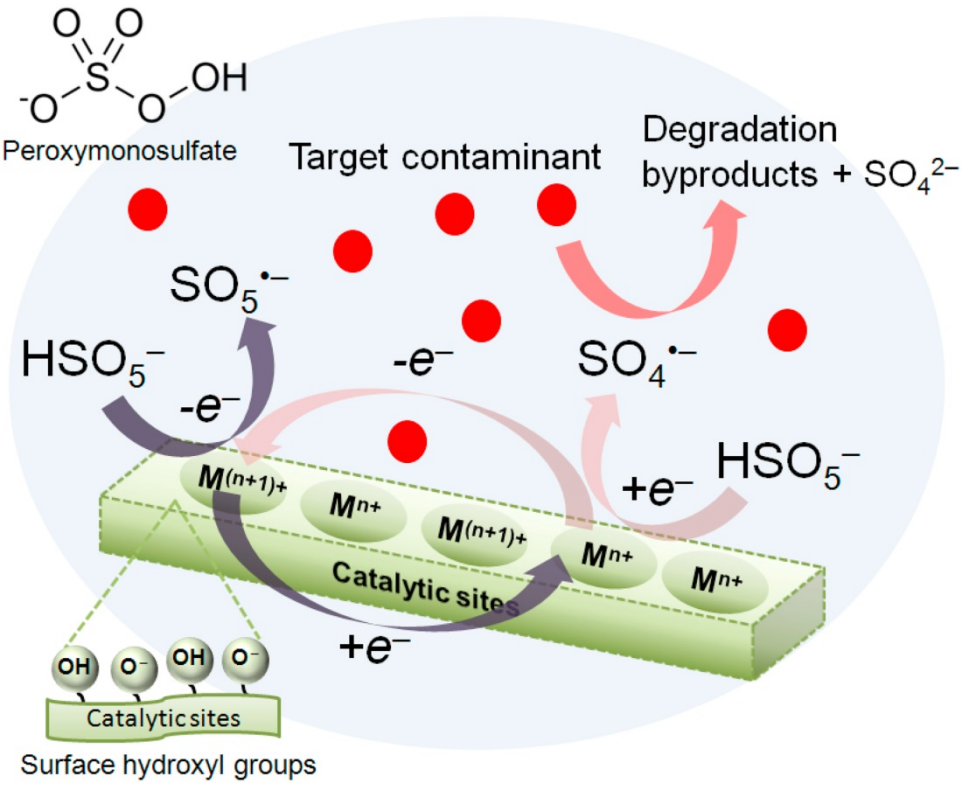

Figure 2.2 The redox reaction involved in PMS and heterogeneous transition metal catalyst.

The surface hydroxyl group, either on the surface of catalyst or that of support, gains prominence in the enhancement of PMS activation. The surface hydroxyl group in protonated form, as reported, is less effective in PMS activation.[27, 126, 127] Catalyst loading, pH as well as PMS

amount are common factors that affect the catalyst performance at the constant temperature, as illustrated by the following kinetics:[128]

$$C_t = C_0 e^{\frac{k_i \quad [Cat-OH]}{k_{PMS}(K_{eq}[H^+]+1)} C_{PMS_0}(e^{-k_{PMS}t}-1)} \quad \text{(Eq. 2.43)}$$

in which C_t and C_o represent pollutant concentrations at time t and initial concentration, respectively, K_{eq} stands for the catalyst equilibrium constant, k_i means the intrinsic rate constant, k_{PMS} is the first-order rate constant of PMS decomposition, [Cat–OH] symbolizes the catalyst loading and C_{PMS_0} represents PMS amount at the initial stage.

Even at a low concentration, it has proved that Co^{2+}/PMS were effective in the decomposition of organic pollutants. However, cobalt leaching is the biggest disadvantage of homogeneous catalysis. Being a primary metal pollutant in the environment, the discharged cobalt ions would lead to secondary environmental pollution. A series of health problems, for example, respiratory problems, allergies, cardiomyopathy, mutagenicity and carcinogenicity, etc. can be resulted from exposure to cobalt.[122, 129] Consequently, heterogeneous catalysis with solid catalysts has received great applause in the PMS activation in the realm of wastewater remediation technology.

Different heterogeneous catalysts have been utilized in the PMS activation based on various transition metals (or their combinations) and metal-free catalysts (green carbon-based catalysts). Fig. 2.3 schematically described the mechanism of PMS heterogeneous activation.[103]

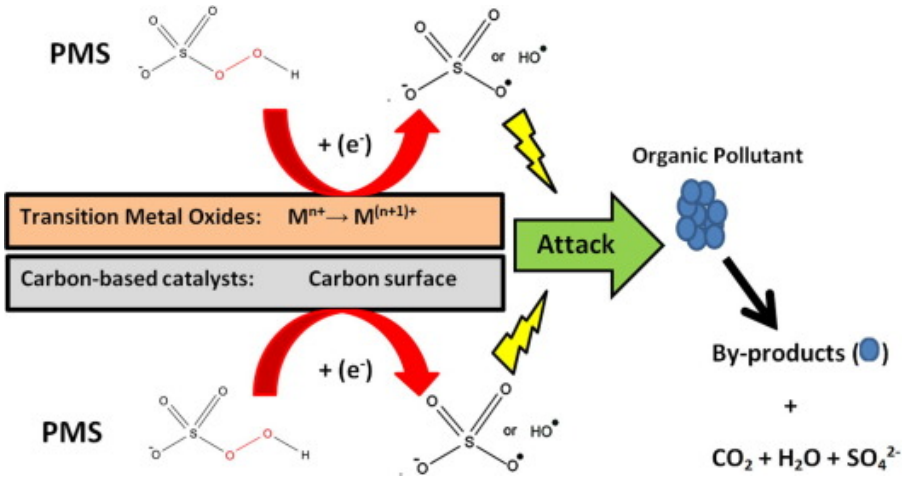

Fig. 2.3 The scheme of heterogeneous activation of PMS.

2.3.2.1 Cobalt oxides and supported cobalt heterogeneous catalysts

Cobalt oxides have been regarded as one of the most popular catalysts in PMS heterogeneous activation to catalytically oxidize organic pollutants. Five cobalt oxides, including CoO, CoO_2, CoO(OH), Co_2O_3 and Co_3O_4, have already been explored and identified.[122] Three of these oxides (CoO, Co_2O_3 and Co_3O_4) are able to activate PMS for degradation of many contaminants and can also be utilized attached to different supports like carbon-based materials or zeolites or, used only as nanoparticles.[103]

Anipsitakis et al.[130] were the first to explore the reactivity of CoO and Co_3O_4 in PMS activation for oxidation of 2,4-DCP to replace homogeneous Co^{2+}/PMS. In spite of catalytic performance of 2,4-DCP on both CoO and Co_3O_4, only Co_3O_4 was considered to stimulate heterogeneous catalysis and dissolved Co in the solution facilitate CoO catalysis. The stability of nano-Co_3O_4 was tested by Chen et al.[131] in decomposition of Acid Orange 7 by PMS activation. It has been acclaimed that due to rapid degradation and low leaching of Co, neutral

condition is more favorable for the heterogeneous property of nano-Co_3O_4, further leading to its long-term stability. Wang et al.[132] achieved phenol degradation by PMS activation with the application of Co_3O_4 nanorods. When used solely, PMS and Co_3O_4 nanorods were both not effective in phenol degradation. It was concluded that Co_3O_4 exhibit unfavorable performance when calcination temperature increased. The mechanism of Co_3O_4/PMS system was proposed by Yu et al.,[120] who asserted that generated Co^{2+} ions took part in the homogeneous redox reactions and Co^{3+} ions subsequently precipitated into the crystal lattice of Co_3O_4 in order to reduce cobalt loss.

Despite good catalytic performance, Co_3O_4 nanoparticles are prone to agglomerate to reduce the catalytic activity during the reaction.[133] Therefore, immobilization of Co and Co_3O_4 on various materials is a good idea to enhance the catalytic activity because it can reduce Co ion leaching, thus avoiding secondary contamination to the environment and highly improved the stability and reusability of catalysts.[134] In addition, introduction of supporting materials would be able to tune the surface characteristics (normally larger surface areas) and thus enhance the catalytic performance.[114] Up to now, several different support materials have been applied in the preparation of supported cobalt catalysts.

Metal oxides have recently been in the application of cobalt support to activate PMS. Degussa P-25 was firstly regarded as an excellent support material for supported cobalt catalyst - Co/TiO_2.[135] Compared with unsupported Co_3O_4, better efficiency was observed on Co/TiO_2 in PMS heterogeneous activation with little cobalt leaching at the molar ratio of Co : Ti = 0.1 and the calcination temperature of 500 ^oC. Further study

investigated the effects of support materials (Al_2O_3, SiO_2, TiO_2) as well as cobalt precursors ($Co(NO_3)_2$, $CoCl_2$, $CoSO_4$) on the interaction of cobalt and support materials, cobalt leaching, as well as catalysts reactivity.[136] It was concluded that Co/Al_2O_3 and Co/TiO_2 exhibited much less cobalt loss than Co/SiO_2, and Co/TiO_2 prepared by $Co(NO_3)_2$ demonstrated the best performance in 2,4-DCP degradation. Co_3O_4-Bi_2O_3 was developed by Ding et al.[137] to degrade different pollutants, such as methylene blue (MB), RhB, phenol and 2,4-DCP. With regard to MB degradation, Co_3O_4-Bi_2O_3/PMS system was 8.6 folds faster than that of Co_3O_4/PMS. The performances of different oxides as support materials for the preparation of cobalt catalysts were studied by Zhang et al.[126] in the decomposition of organic dyes by PMS activation. The catalyst of Co/MgO can completely degrade methylene blue (MB) in less than 7 min, showing the best reactivity. The result was exceptionally better than homogeneous cobalt ions and some heterogeneous Co_3O_4 catalysts. Another cobalt catalyst supported by MgO was prepared by Stoyanova et al.[127] and exhibited much higher efficiency than unsupported Co_3O_4. The reasons why MgO-supported cobalt catalysts showed better performance tends to be less cobalt leaching, better dispersion of cobalt oxide and higher production of Co-OH.

A series of competitive radical tests proved that the major species in the catalytic degradation of phenol by Co_3O_4 and supported Co_3O_4 was the sulfate radical. Liang et al.[138] discovered that mesoporous α-MnO_2 demonstrated to be a good supporting material for the synthesis of supported cobalt catalyst (Co_3O_4/MnO_2), which showed much higher performance with complete phenol degradation in just 20 min.

Carbon and nanocarbon materials, for instance, activated carbons (AC), graphite, carbon aerogels (CA) or xerogel (CX), graphene, graphene oxides (GO) and reduced graphene oxides (rGO), have been extensively used in the preparation of supported cobalt catalysts for PMS activation because they have high specific surface area to absorb organic pollutants, excellent porous structure as well as controlled functional groups.

Cobalt catalysts supported by AC were prepared to activate PMS and the primary Co species existed in the system was Co_2O_3 which was in the homogeneous distribution on the surface of AC. 35% and 30% phenol were respectively absorbed on AC and Co/AC in 1 h.[139] In the removal of phenol, only 48% phenol was degraded by AC/PMS, but for Co-AC/PMS system, complete phenol removal was achieved in just 30 min. In addition, compared with Co_3O_4, Co_3O_4/graphene greatly reduced Co^{2+} leaching. Expended graphite (EG) as a support for Co_3O_4 was applied to activate PMS.[140] Similar to activated carbon, CA or CX, a newly porous carbon material with high surface area, demonstrate good adsorption ability and have been applied for environmental catalysis. Carbon aerogel doped by Co oxide (Co/CA) was synthesized for PMS activation to oxidize phenol, in which CoO and Co_3O_4 were regarded as the major Co species.[141] 20% phenol was adsorbed in just 20 min and reached equilibrium in 90 min for Co/CA with no PMS and 100% phenol was decomposed in 120 min in the heterogeneous oxidation. GO, easily fabricated by chemical modification, is made up of a hexagonal ring carbon network with sp^2 and sp^3-hybridized carbon atoms. With a large surface area, the exfoliated GO sheets appear to be promising candidates as support materials. Co_3O_4 supported by GO was prepared by Shi et al.[142] to degrade 100% Orange II in water very quickly in just 7 min, exceptionally better than that of Co^{2+}/PMS system. Yao et

al.[143] investigated the preparation of cobalt catalysts supported by rGO via a hydrothermal approach. Complete removal of phenol was reached in 60 min for pure Co_3O_4, but for Co_3O_4/rGO, only 20 min.

A variety of materials, including zeolite, SBA-15, red mud, have been applied as supports for cobalt oxides and metallic cobalt due to their high specific surface area, excellent mechanical strength, superb chemical stability, as well as relatively low cost.[144] However, these solid wastes also have the possibility to introduce toxic substances to water. Zeolite with Y type was first reported by Chu et al.[145] to be used as a support for cobalt catalysts. Although 100% Monuron was degraded in just 10 min, this supported cobalt catalysts with zeolite showed poor stability which cannot be enhanced by various post-treatment methods. Shukla et al.[29] reported a relatively stable cobalt catalyst supported by zeolite (Co-ZSM-5). Co catalysts supported by ZSM-5, zeolite-A as well as zeolite-X prepared via an ion-exchange approach were applied in phenol decomposition by a variety of oxidants, such as H_2O_2, PS and PMS. A high activity in activating PMS but no performance in H_2O_2 and PS were demonstrated by Co-ZSM-5 in phenol oxidation. The rapid reaction rate exhibited by Co-zeolite-A and Co-zeolite-X were resulted from homogeneous activation along with significant cobalt leaching. In the synthesis of SBA-15, co-condensation approach were used to prepare cobalt catalysts supported by mesoporous silica SBA-15 with three cobalt salt precursors ($CoCl_2$, $CoAc_2$ and $Co(NO_3)_2$).[146] It was observed that the catalysts originated from $CoCl_2$ and $CoAc_2$ demonstrated similar activities with complete phenol removal in 200 min, while for catalysts from $Co(NO_3)_2$, it prolonged to 390 min. Co/SBA-15 was also prepared by Hu et al.[147] through an incipient wetness impregnation technique. The powder Co/SBA-15 covered by

polytetrafluoroethylene (PTFE) membrane maintained high catalytic activity with low cobalt leaching even in the 25 runs of recycling experiments.

Being a by-product derived from alumina refinery, red mud (RM) cannot be disposed easily because of its high alkalinity. Therefore, using RM to prepare catalysts can alleviate solid waste to contribute to environment protection. Two RM-supported catalysts, Co/RM-NT (raw red mud) and RM-T (washed red mud) were prepared with Co concentration from 1 to 5 wt%.[26] The former could degrade 100% phenol in 90 min, which the latter only 60 min. Comparative studies were carried out by Saputra et al.[148] on the performances of red mud and fly ash (FA) as support materials for cobalt catalysts. In the presence of PMS, phenol could be degraded by Co/FA and Co/RM. Co/RM, owing to high dispersion of Co oxide and surface alkalinity of RM, exhibited a much better activity than Co/FA.

2.3.2.2 Iron-based heterogeneous catalysts

Iron, the fourth most abundant element on earth, is benign and cheap and poses no severe threat to human health and the environment. The magnetic properties of zero valent iron (ZVI), magnetite (Fe_3O_4) and maghemite (γ-Fe_2O_3) have also aroused great attentions in terms of stability and reusability.[149, 150] Iron-based nanomaterials combined with some supports have been widely used by many researchers to activate PMS in catalysis due to their low cost and efficiency.[151] Meanwhile, iron is considered to be a desirable alternative to cobalt due to cobalt toxicity even at very low concentrations. PMS activators on the

basis of Fe are commonly ZVI, Fe_2O_3 and Fe_3O_4. The following equations illustrate the mechanism of PMS activated by ZVI:[152, 153]

$$Fe^0 + HSO_5^- + 2H^+ \rightarrow Fe^{2+} + HSO_4^- + H_2O \quad \text{(Eq. 2.44)}$$

$$Fe^{2+} + HSO_5^- \rightarrow Fe^{3+} + SO_4^{\bullet -} + OH^- \quad \text{(Eq. 2.45)}$$

$$Fe^{3+} + HSO_5^- \rightarrow Fe^{2+} + SO_5^{\bullet -} + H^+ \quad \text{(Eq. 2.46)}$$

ZVI encapsulated by carbon can cope with particle agglomeration and fast deposition rate brought by ZVI to enhance the hydrophilicity/hydrophobicity and adsorption ability of the catalysts.[154, 155] It has been reported that carbon encapsulated nano iron hybrids (nano Fe^0/Fe_3C@CS)[156] and carbon spheres encapsulated by nanoscaled ZVI (nano-Fe^0@CS)[157] with good stability and magnetic property were successfully prepared to activate PMS in wastewater remediation. 85% dichlorophenol was degraded by Fe_2O_3-montmorillonite in 2.5 h, but the result for H_2O_2 and acetic acid were 70% and 50% in 3.5 h, respectively.[158] Ji et al.[159] reported the decolorization of Rhodamine B(RhB) in porous Fe_2O_3 activation of PMS. The catalytic process required a relatively high loading of Fe_2O_3, which consists of a majority of Fe^{3+} species. The activation processes were proposed to be similar to those of CuO and Fe^{3+} on the surface must be reduced to Fe^{2+} before it can produce $SO_4^{\bullet -}$ from PMS. The hematite functionalized by dipicolinic acid has been employed as PMS activator to degrade BPA.[160] Magnetic Fe_3O_4, another form of iron oxides, can initiate PMS activation and doping with other transition metals such as Co, Mn, Ni and Cr can improve the catalytic performance of Fe_3O_4, which can also been enhanced when Fe_3O_4 was immobilized

on CuNiCr-LDH support. However, possible leaching of Cr from the support prevented its practical application in water remediation.[161] However, a disadvantage of iron-based catalysts is that SO_4^{2-} substituted for two hydroxyl groups on the surface to form a binuclear bridge complex made up of Fe-O-S(O_2)-O-Fe, which deactivated iron-based catalysts.[162]

2.3.2.3 Other transition metal heterogeneous catalysts

In addition to iron and cobalt, manganese and copper oxides also have the ability to activate PMS. Due to their good stability, low cost, excellent efficiency and no threat to the environment, various nanoscaled manganese oxides such as MnO, Mn_3O_4, MnO_2 and Mn_2O_3 have already received researchers concern.[163-165] Wang and co-workers have already synthesized a variety of nanosized Mn oxides, Mn oxides with various crystallographic phases and supported Mn oxides to oxidize PMS to remove phenol.[166-168] The mechanisms of PMS activation involved in heterogeneous Mn oxides are illustrated as follows:[169]

$$2MnO_2 + 2HSO_5^- \rightarrow Mn_2O_3 + 2SO_5^{\bullet -} + 2OH^- \quad \text{(Eq. 2.47)}$$

$$2Mn_3O_4 + 2HSO_5^- \rightarrow 3Mn_2O_3 + 2SO_4^{\bullet -} + 2H^+ \quad \text{(Eq. 2.48)}$$

$$Mn_2O_3 + 2HSO_5^- \rightarrow 2MnO_2 + 2SO_4^{\bullet -} + 2H^+ \quad \text{(Eq. 2.49)}$$

$$2MnO + 2HSO_5^- \rightarrow Mn_2O_3 + 2SO_4^{\bullet -} + 2H^+ \quad \text{(Eq. 2.50)}$$

$$3Mn_2O_3 + HSO_5^- \rightarrow 2Mn_3O_4 + SO_5^{\bullet -} + OH^- \quad \text{(Eq. 2.51)}$$

The ability of Mn to form various oxidation states determines the reactive capacity of Mn oxides. It was found that Mn_2O_3 was most

effective in PMS activation and 100%, 90%, 66.4% and 61.5% phenol was removed respectively by Mn_2O_3/PMS, MnO/PMS, Mn_3O_4/PMS and MnO_2/PMS.[169] Three different one-dimensional (1D) α -MnO_2 nanostructures (nanorods, nanotubes and nanowires) were fabricated by Wang et al.[170] to activate PMS and nanowires exhibited the best performance due to its largest surface area. They also studied the effects of diverse crystallographic dimensions of MnO_2 (α, β, γ-MnO_2) on the efficiency and stability and found that α -MnO_2 was the best catalyst.[171] It was found that crystallinity degree exerted a more important effect on catalytic activity of Mn oxides than the specific surface area.

Manganese oxide octahedral molecular sieves (OMS-2) have attracted the attentions of researchers due to its large specific surface area, high density of lattice oxygen and existence of Mn at various valence states.[172, 173] OMS-2 was prepared by Duan et al.[174] for AO7 removal with PMS. In this study, dissolved Mn^{2+} was demonstrated to be the non-responsible agent of degradation. Surface modification is necessary for OMS-2 to activate PMS because PMS is prone to be activated by basic surface, but OMS-2 has many acidic sites.[125] OMS-2 encapsulated by Fe_3O_4 can introduce ferromagnetism and yield a core shell structure but reduced catalytic performance.[175] However, the introduction of ferromagnetism into the catalyst with Fe_3O_4 to fabricate Fe_3O_4/Mn_3O_4/rGO[176] and Fe_3O_4/MnO_2[177] has proved to enhance the reactivity. In addition, Mn oxides could be applied as a support as well to enhance reactivity in catalysis of different transition metal oxides such as Co_3O_4 and CuO.

Different oxidation states limit Mn to maintain the chemical phases after PMS oxidations. A significant decrease from 100% phenol removal in the first run to 30% in the second run was observed on Mn_2O_3 catalysts because the chemical phase of Mn changed and intermediates formed were deposited on the surface of the catalysts.[169] Therefore, different post treatment methods, such as calcination, washing, chemical methods, are needed to recover its activity.[178]

Zero valent copper (ZVC) and cupric oxides (CuO and Cu_2O) were also regarded as PMS activators.[153, 179] It was found that CuO had a higher catalytic activity than Cu_2O, implying oxides with Cu^{2+} enjoyed more effectiveness for PMS activation.[180] Compared to CuO with surface area of 1.52 m^2/g, Cu/ZSM5 with surface area of 354 m^2/g exhibited better catalytic performance, demonstrating that physical property exerts a great influence on the PMS activation.[181] CuO was used to degrade phenol solutions by Ji et al. and 65% phenol was removed in 60 min, while for CuO/H_2O_2 system, only 12% phenol was degraded within the same time.[182]

2.3.2.4 Bimetal oxide heterogeneous catalysts

Introducing another metal into metal oxides enables the catalysts to be more controllable due to various advantages, such as increased stability, versatility, ability of magnetic separation, high redox activity and better catalytic performance.[183] A combination of metal oxides have widely been applied as heterogeneous catalysts for oxidant reactions with the chemical formula of $A_xB_{3-x}O_4$ in which A and B refer to metals such as Co, Fe, Cu, Mn, Zn and so on.[184] However, Co and Fe are the major transition metals to form these oxides. Magnetic nanomaterials, for

example, $CoFe_2O_4$, $CuFe_2O_4$, and $Co_xFe_{3-x}O_4$ have been extensively utilized as promising catalysts in PMS activation due to their excellent catalytic performance and ability of magnetic separation.[185, 186] Yang et al.[27] reported the synthesis of nanomaterial with mixed iron and cobalt oxides and applied it in the heterogeneous catalysis. Compared to Co_3O_4, $CoFe_2O_4$ showed high efficiency in PMS activation because of the existence of more Co^{2+}, less leaching of Co resulted from strong combination of Fe and Co, and easy recovery by magnetic separation. In addition, the number of hydroxyl groups on the catalyst surface can be increased by the existence of Fe and hydroxyl groups are perceived as the stimulator of heterogeneous PMS activation. Yao et al.[187] investigated the preparation of magnetic hybrids of $CoFe_2O_4$ and graphene. 100% phenol was removed on $CoFe_2O_4$-graphene in just 30 min with the addition of rGO into $CoFe_2O_4$, while only 51% phenol was degraded by pure $CoFe_2O_4$ in 60 min. Moreover, an external magnet could easily remove the hybrids from the reaction solution. Magnetic composites of Fe_3O_4/carbon-sphere/cobalt were fabricated by Wang et al.[188] to completely remove phenol in just 30 min by PMS activation and strong magnetism were still remained in the system after the reaction. Ding et al.[189] synthesized $CuFe_2O_4$ magnetic nanoparticles to oxidize PMS to decompose tetrabromobisphenol A (TBBPA). It was found that both Cu^{2+} and Fe^{3+} could improve the catalytic performance. Due to Fe^{3+} reduction, a synergistic effect was demonstrated by the existence of Cu^{+} and Fe^{3+}. $CuCo_2O_4$/PMS system was able to degrade 87.2% sulfamethazine (SMZ), while for Co_3O_4, $CuFe_2O_4$, CuO, and Fe_3O_4, the results were 51.1%, 11.3%, 12.5%, and 7.9%, respectively.[180] The major reactive species for the generation of sulfate radicals was demonstrated to be Co^{2+}. Different synthesis methods affect the efficiency of catalysts. Compared with preparation

method with no use of any organic precursors, solvothermal approach can decrease the efficiency of $CuFe_2O_4$, $CoFe_2O_4$ and $MnFe_2O_4$ with the increase in organic solvent and surfactant. RhB can be decolorized by nano-ferrite cobalt ($Co_xFe_{3-x}O_4$) in PMS heterogeneous activation and catalytic activity was found to rely on the content of cobalt.[186] In another study, Acid Orange II (AOII) can be degraded by $Fe_{3-x}M_xO_4$ (M = Cr, Mn, Co and Ni).[161] It was found that except that no change was seen for Cr, removal efficiency was enhanced with the growth in the amount of M. A mixed metal oxide spinel with no presence of Fe or Co was reported to degrade organic compounds with PMS. The catalytic performance of $CuBi_2O_4$ (CuB) attached on various metal oxides revealed that the best performance was shown by CoO-CuB compared with FeO-CuB and CuO-CuB. The degradation efficiency follows this order: CoO-CuB > Co_3O_4 > CuO-CuB > FeO-CuB > Fe_2O_3.[190]

2.3.2.5 Metal-free heterogeneous catalysts

PMS could be activated by carbon-based materials to produce radicals as well, such as activated carbon (AC), graphene, graphene oxide (GO), reduced graphene oxide (rGO), nanodiamond, carbon nanotubes (CNTs) and graphite. These materials are environmentally friendly and tend to be promising alternatives to poisonous and expensive metals to completely avoid metal leaching problem.[191, 192]

AC enjoys high surface areas and plentiful catalytic functional groups like quinone, ketone, carbonyl, as well as carboxyl groups. Due to these properties, AC has been regarded as a promising catalyst widely used in the catalytic redox reactions and as a support of adsorption for metal-based catalysts. The quantities of surface functional groups with

delocalized π electrons, together with AC specific surface areas, determine the performance of various ACs used as PMS activators.[125] Generally, the mechanism of PMS activated by AC, similar to that by H_2O_2, is mediated by the delocalized π electrons, which are illustrated as follows:[193]

$$C-\pi+\ HSO_5^-\ \rightarrow C-\pi^+ +\ OH^- +\ SO_4^{\bullet -} \quad \text{(Eq. 2.52)}$$

$$C-\pi^+ +\ HSO_5^-\ \rightarrow C-\pi +\ H^+ +\ SO_5^{\bullet -} \quad \text{(Eq. 2.53)}$$

Recently, PMS activation can be enhanced by AC modified with ammonia because the generated pyrrolic group facilitate electron transfer in the decomposition.[194] Nevertheless, AC is not likely to be a catalyst with long-term stability because repeated uses consume its adsorption ability and phenols and surface moieties are easily oxidized by PMS and produced radicals.[195] Studies have shown that powder activated carbon (PAC), granular activated carbon (GAC) as well as activated carbon fibre (ACF) can all activate PMS and the system of ACF/PMS exhibited higher degradation rate of dye than that of GAC/PMS.[196] Nevertheless, adsorption ability of ACF on pollutants could result in the improvement of degradation efficiency. Sun et al.[35] firstly adopted rGO to activate PMS for the degradation of phenol, chlorophenols and dyes and they considered that the major active sites to oxidize PMS are the zigzag edges as well as ketonic groups on the edges of rGO. Different dimensions of nanocarbon material, such as 1D single walled carbon nanotubes (SWCNTs), 2D graphene nanoplate (GNP), 3D hexagonally ordered mesoporous carbon (CMK-3) and cubically-ordered mesoporous carbon (CMK-8), were utilized to activate PMS for phenol degradation.[197] It was concluded that CMK-3, CMK-8 and SWCNTs

showed excellent catalytic performance in phenol removal due to their high surface area and edge defects featured by high density of electronic states which are vital to the reactions of electron transfer. Another study reported that catalytic activities of GO and nanodiamonds can be improved by heat treatment under N_2 atmosphere because at this condition, defective edges increased, surplus oxygen functional groups were removed and electrons moved more quickly in the redox reactions.

It is generally known that PMS are more likely to be activated on an alkaline surface. However, GO/rGO has an acid surface and thus chemical modification is necessary. Meanwhile, catalyst activity can be greatly improved by surface modification of carbon materials because alteration in surface affects the adsorption ability and catalytic capacity of materials.[126] The activated porous rGO was proved to be a highly effective catalyst in the adsorption and oxidation of phenol and methylene blue with a high specific surface area of 1200 m^2 g^{-1}.[198] Physical activation method can promote the catalytic performance of rGO compared with chemical and physiochemical activation methods.[199] The reason for this is that CO_2 facilitate the formation of a large quantity of oxygen functional groups and enhance porosity. The rGO with surface defectives and zigzag edges, as reported, possesses a large quantity of redox active moieties with electrons in mobility for PMS activation, implying that an increase in the defect density can promote PMS activation. The ketonic group on the surface of rGO can experience electron transfer reactions with PMS to generate $SO_4^{\bullet-}$and $SO_5^{\bullet-}$. The active sites of rGO are regarded as some oxygen functional goups like nucleophilic ketonic and quinoidic groups.[200] These groups are abundant in electrons and able to mediate redox reactions. The following equations demonstrate the processes of PMS heterogeneously activated by oxygen functional groups of rGO:[198]

$$C = C = O + HSO_5^- \rightarrow SO_4^{\bullet -} + C = C - O^+ + OH^- \quad \text{(Eq. 2.54)}$$

$$C = C - O^+ + HSO_5^- \rightarrow C = C = O + SO_5^{\bullet -} + H^+ \quad \text{(Eq. 2.55)}$$

Meanwhile, catalytic performance of catalysts can also be boosted by heteroatoms doping, such as N, P, S, or B.[31-34, 36, 201, 202] Carbon-based materials doped with heteroatoms can bring about many advantages, such as an increase in defective edges, surface hydrophilicity and electron mobility, a change in the electron density in the local carbon atom, an introduction of new electrocatalytic active sites and an acceleration of electron transfer reaction with PMS.[203, 204] Nitrogen-doped graphene and CNT co-doped by nitrogen and sulfur were employed as more efficient catalysts to activate PMS than rGO and carbon nanotubes.[31, 32] The rGO co-doped by B and N is twice more efficient than Co_3O_4 to activate PMS.[201] However, it is reported that doping excessively would trigger many problems such as zig-zag defects blockage brought by B_2O_3.[205] Future research of doped catalysts could be extended to materials doped with other electron donors like K and Rb and acceptors like Br_2 and I_2 to improve catalytic activity.[206, 207]

In spite of its high nitrogen content, graphitic-carbon nitride (g-C_3N_4) used alone cannot effectively activate PMS to degrade pollutants. However, when g-C_3N_4 was supported by AC[208] and MCM-41[209], a synergistic effect was observed between g-C_3N_4 and the support with O species presented in g-C_3N_4 as the main active site for PMS activation.

To be noted, carbon-based materials also have some shortcomings. (1) due to cannibalistic oxidation, carbon-based catalysts usually have poor stability that cannot be used for many times, for example, as to N-doped rGO,[31] the phenol degradation efficiency dropped from 100% to 31%

after the first use and for N,B co-doped rGO,[201] it decreased from 100% to 20%; (2) several carbon-based catalysts, such as CNTs and graphene, are expensive in comparison with some metal-based catalysts. Therefore, it is compulsory to improve the sustainability of carbon-based materials to enhance its overall removal efficiency.

The mechanism of PMS activated by carbon-based materials was formerly not clear. In addition to the popular radical-based mechanism with the generation of $^{\bullet}OH$ and $SO_4^{\bullet-}$, non-radical degradation mechanism of nanodiamond and nitrogen-doped single walled carbon nanotube have recently been proposed by some studies on the basis of direct electron extraction of organic pollutants.[210, 211] Usually, radical and nonradical processes coexist in the degradation of organic pollutants by N-doped single-walled CNT.

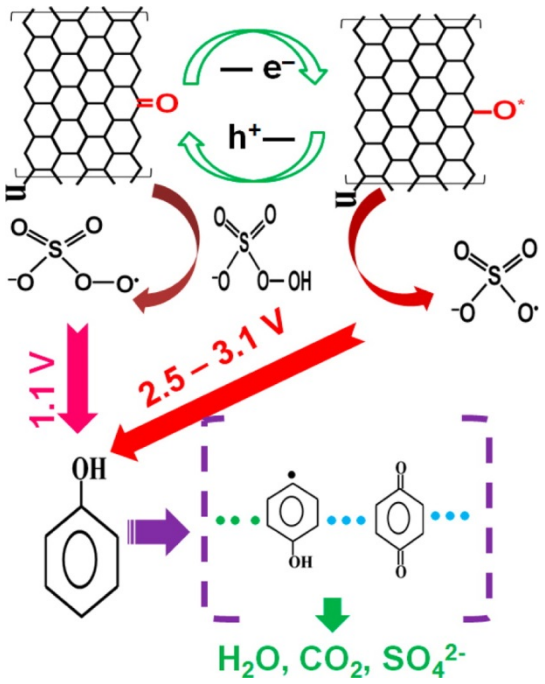

Figure 2.4 The mechanism of PMS activation by rGO for phenol degradation.

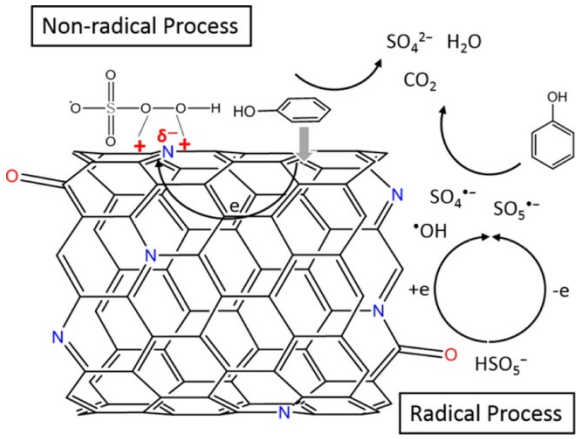

Figure 2.5 The non-radical and radical mechanism of PMS activation by N-doped CNTs.

As seen in Figure 2.5, the absorption of PMS and phenol were firstly occurred on the sp^2 sites rich in electron and subsequently, PMS was activated either by radical or non-radical routes and phenol was degraded on the surface of N-doped single-walled CNT. It is presumed that PMS symmetric structure, along with its weaker oxidation and adsorption ability on CNT contributes to the non-radical pathway.[212] It is noticeable that carbon structure determines whether radical and nonradical pathways will occur.[213] The sp^2 conjugation as well as ketonic groups facilitate the generation of $^{\bullet}OH$ and $SO_4^{\bullet-}$ from PMS dissociation. In addition, carbon networks equipped with defective edges are conducive to the emergence of nonradical process which has better selectivity to targeted organic pollutants, greater resistance to pH change and weaker influence by water matrix species. Moreover, single oxygen ($^1O_2$) has been identified as the major reactive species in the activation of PMS with quinones in another study.[214] The focus of future research is on the detection of generated radicals, their respective contributions to organics degradation and the impacts of various surface functional groups on the non-radical mechanism, which would be open a new avenue for the solution of cannibalistic oxidation.

2.4 Carbon nanomaterials and characterizations

Termed as the Century of the Environment, the 21st century has faced many issues such as explosive population, intensified industrialization and urbanization, worldwide climate change and contaminated water, air and soils.[215] Among these, environmental problems have become major public concerns that require global efforts to alleviate their implications on human health and ecosystems. Recently, nanomaterials have aroused great interests of researchers in the applications of wastewater remediation,[216] energy production[217] and contaminant sensing.[218] Meanwhile, nanomaterials can overcome the shortcomings of metal-based catalysts such as high cost, poor stability, bad selectivity, influence by gas poisoning and harmfulness to the environment.[216] Carbon nanomaterials are defined to describe a wide variety of carbon materials smaller than 100 nm in at least one dimension with unique properties derived from their nanoscale features, many of which have been employed in the applications of wastewater treatment. Figure 2.6 provides a schematic illustration of some nanocarbons.[219]

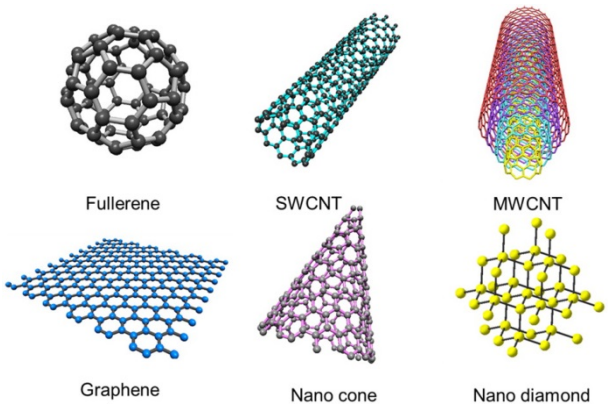

Figure 2.6 Schematic illustration of some nanocarbons.

Various methods can be utilized to characterize nanocarbon materials. Scanning electron microscopy (SEM) is regarded as the most standard tool that can have a general idea of the materials. TEM, X-ray diffraction, along with Raman spectroscopy are routine techniques to characterize the microstructural features of nanomaterials. High-resolution TEM (HRTEM) is considered as the only characterization technique to obtain a clear image of atoms arrangement of catalyst. Electron diffraction at selected area provides information on the graphene crystallinity from the microscopic level. Meanwhile, elemental analysis of certain areas can also be obtained from HRTEM. Raman spectroscopy, with monitoring the 2D, G and D bands, is considered as a very powerful tool for nanomaterials characterization. Generally, the positions of the three bands are approximately 2600, 1600, and 1350 cm^{-1}, respectively. The G-band stands for the presence of sp^2 -hybridized carbon atoms, and the D-band gives evidence for defects like disorders, edges and boundaries. The 2D-band renders information on the number of layers of the graphene material. The intensity ratio of G and D band is a good indicator of the quality of graphene. Graphene materials with high quality have a low I_D/I_G ratio and a high I_{2D}/I_G ratio and the existence of dopant will intensify the D band. For example, the Raman spectra of graphene produced from exfoliation of graphite or CVD method exhibit no or a very weak D band. On the contrary, those produced by reduction of graphene oxide with many defects and oxygen groups have a higher I_D/I_G. X-ray photoemission spectroscopy (XPS), Fourier Transform Infrared Spectroscopy (FTIR), and thermogravimetric and thermodesorption methods are the approaches to investigate the surface functionality and adsorption properties of nanomaterials. XPS is considered to obtain information on the nature of the active sites in graphene-based materials. After appropriate correction, XPS can

determine the existence, absence and quantity of element on the surface of the samples. In addition, the types of C, N, O and other elements and their relative contributions in the catalysts can also be obtained from XPS. FTIR has been widely applied in the characterization of graphene oxide, but it turns to be useless for reduced graphene oxide and other graphene-based materials because there are not intense adsorption vibrations in IR. Thermogravimetry is utilized to study the total weight loss of the materials when heated to 800 ^{o}C or above under air atmosphere. At 100 ^{o}C, the weight loss is attributed to the water desorption. After that, combustion begins at around 300 °C and the biggest slope in the weight loss occurs at around 500 °C. Brunauer-Emmett-Teller (BET) analysis determined by nitrogen adsorption-desorption technique can give an idea of surface area and pore size distribution of carbon materials. [220-223]

2.4.1 Graphene

Graphene is a 2D layer of carbon atoms in the arrangement of a sp^2-bonded hexagonal crystalline structure with distinct physicochemical characteristics, particularly high specific surface area, excellent electron and thermal mobility, as well as strong mechanical strength.[224] The theoretical value of the specific surface area of graphene is to be 2630 m^2 g^{-1}, the highest among all the materials, and this property enables it to be applied in adsorption or surface reactions.[225] Meanwhile, graphene can be used as a filler to enhance the mechanical strength of softer materials due to its remarkable mechanical properties.[226] Graphene is the building block of graphite, in which p-stacking of graphene sheets supports the lamellar graphite structure tightly in place and the interlayer spacing between sheets is 3.34 Å.[227] Graphene-based materials

include graphene, graphene doped by heteroatoms and other one-atom thick 2D layered materials composed of other elements besides carbon. Overview of structure and main characteristics of graphene-based nanomaterials are listed in Figure 2.7.[228]

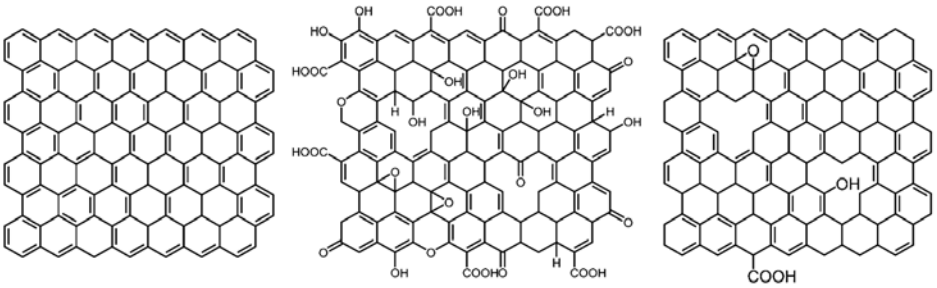

Properties	Graphene	Graphene Oxide	Reduced Graphene Oxide
Synthesis	-Chemical vapor deposition -Thermal decomposition of SiC -Graphite exfoliation	-Oxidation and exfoliation of graphite	-Reduction of graphene oxide
C:O ratio	No oxygen	2-4	8-246
Young's modulus (TPa)	1	0.2	0.25
Electron mobility ($cm^2\ V^{-1}\ s^{-1}$)	10 000–50 000	insulator	0.05–200
Production cost	High	Low	Low

Figure 2.7 Overview of structure and main properties of graphene-based nanomaterials relevant for environmental applications.

Meanwhile, exfoliation of graphite can generate single-layered graphene and micromechanical exfoliation, first developed by Geim and Novoselov, can produce graphene with high quality.[229] However, micromechanical exfoliation is labour-intensive and unsuitable for a large production of graphene. Graphite ultrasonication can also exfoliate graphene in organic solvents but with low yields.[230, 231] The most common approach for graphene production in large scale with high quality is decomposing SiC thermally or epitaxial growth of graphene on

the hot surfaces of transition metals through chemical vapour deposition (CVD) of precursors of hydrocarbons such as methane or alcohols.[232, 233] Copper and nickel are regarded as the preferred transition metals in CVD.[234, 235] It is reported that CVD method has been regarded as the most desirable strategy for the production of high quality graphene with very low, or even free of oxygen content. The mechanism tends to depend on the templating effect from metal atoms whose spherical shape and size is suitable for a six carbon ring and can play a role as dehydrogenating centres to generate hydrogen and carbon in the process of graphene sheet growth. These high-cost methods can produce small amount of high-quality graphene to be applied in electronic applications, but inappropriate for catalysis.[236]

Graphene oxide (GO), an oxidized form of graphene, is another graphene-based material with large quantities of oxygen functional groups such as carboxyl, hydroxyl, carbonyl, and epoxy in the carbon framework.[237] The generally accepted method for GO with many defects is on the basis of the traditional Hummers method initiated in 1958, in which graphite was treated and deeply oxidized by a mixture of concentrated sulfuric acid (H_2SO_4), sodium nitrate ($NaNO_3$), and oxidizing agent - potassium permanganate ($KMnO_4$).[238] Up to now, various approaches have been developed to improve the yield and decrease the production of harmful gases, but $KMnO_4$ is still kept as the major oxidant that frequently used in the production of GO.[239, 240] Due to the feasible preparation method in large quantities, GO has been considered as one of the most desirable graphene-based material as catalyst. Physicochemical properties have been greatly changed by the oxidation of graphene to GO. The excellent electronic and mechanical features of graphene were decreased by the introduction of many defects

into the carbon structure, making GO more hydrophilic.[241] Along with this property, high surface area as well as many oxygen functional groups on the surface enable GO to perform various chemical functionalizations, making GO a building block for graphene-based material.[237] Some variations of Hummers methods were conducted by the use of different oxidants and acids.[242] For example, as a good alternative to sulfuric acid, phosphoric acid can increase the viscosity of the mixture.[239] If the restoration of original carbon lattice can be achieved, GO can be regarded as a cheap and desirable material to produce graphene via ultrasound exfoliation and reduction with chemical reducing agents, thermal treatment, ultraviolet or microwave.[243, 244] However, complete reduction of GO cannot be achieved so far because oxygen groups cannot be completely removed by reduction and residual oxygenated functional groups and holes and defects are left in the material. Therefore, the quality of material is lower than that derived from CVD process. To be noted, reduced GO bring many new properties, such as carbon vacancies, residual oxygen content, and carbon structures with agglomerated pentagons and heptagons and these defects enable GO to partially restore the properties of pristine graphene.[245] Therefore, a new term, chemically converted graphene, reduced graphene or reduced GO (rGO) is created to describe this special chemical structure that different from graphene.

In doped graphene-based materials, carbon atoms, normally below a percentage of 10, are took place by nitrogen, boron, phosphorus or sulfur.[236] The widely accepted method for the preparation of doped graphene materials is to introduce dopant element in the synthetic process of carbon material.[246] In addition, other procedures of graphene doping rely on the high reactivity of GO that are able to

experience the replacement of oxygen by other elements, which may cause incorporation of these elements by adding appropriate chemical agents. After GO is reduced, a certain amount of heteroatom can be kept on the carbon layer. Recently, another doping approach was reported to use a biopolymer with doping element in the modified or non-modified form.[247] It was found that heteroatom can be easily introduced into the graphene layer during pyrolysis. When temperature increases from 600 to 1200 ^{o}C, doping percentage decreases. It was concluded that graphene quality can be enhanced by an increase in temperature due to the removal of defects at high temperature. Meanwhile, some natural polymers can serve as sources of both carbon and other elements, for example, chitosan consists of carbon and nitrogen and carragenate is made up of carbon sulfur. In addition, the modification of polymer can be achieved by the addition of another element not present in the polymer. For example, carbohydrates can be easily modified with phosphates[248] and borates[247] to obtain graphene-based materials with both phosphorus and boron elements. Figure 2.8 gives a summary of preparation methods most frequently used for graphene materials.

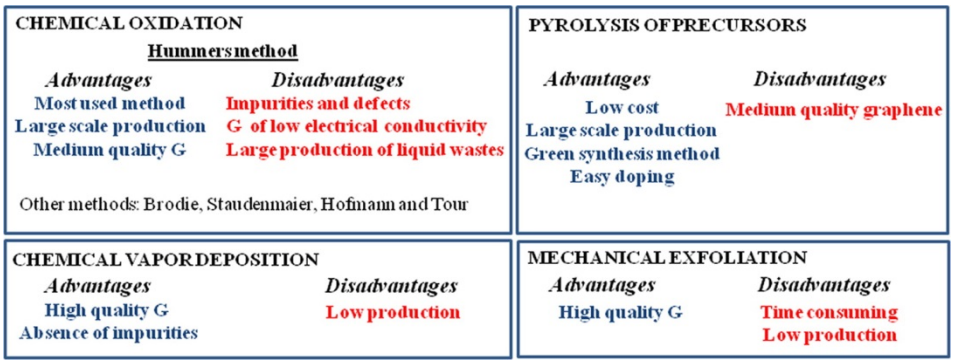

Figure 2.8 Overview of most-used preparation procedures for graphene materials

2.4.2 Carbon nanotubes

Discovered and characterized some years earlier than graphene, carbon nanotubes (CNTs) is a term to represent a variety of tubular carbon nanostructures equipped with similar structures and shapes.[249] The ideal CNTs are based on a hexagonal lattice made up of sp^2 carbon atoms like graphene. Nevertheless, the edges of graphene sheets in nanotubes are fused to generate a cylindrical tube with a relatively high aspect ratio. CNTs of the simplest form are equipped with a single graphenic wall and is capped at two ends. The diameters of single-walled carbon nanotubes (SWCNTs) are about 0.4-2 nm and lengths are several micrometers with an empty internal space. Different amount of graphenic layers in the walls of the cylindrical structure can generate double-walled and multi-walled CNTs. The aspect ratio, referring to the ratio of length to diameter, is often greater than 10000 for carbon nanotubes, and as a result, CNTs are considered as the most anisotropic materials that have ever been produced. Besides these parameters, chirality, that is the angle between the hexagons and the nanotube axis, can enable carbon atoms in the vicinity of nanotube circumference to be in an arrangement of several ways. The most common patterns are armchair, zigzag and chiral.[250]

In spite of the same basic structure, the synthesis methods of CNTs and graphene are completely different. Several methods have been well established on the preparation of CNTs.[251] The simplest preparation method depends on an arc discharge existed between two carbon electrodes in a chamber in an atmosphere of inert gas, the category and pressure of which determine the yield, purity and quality of resulting CNTs. He, CH_4 and H_2 are common gases used in this method.[252] Besides these gases, a range of volatile organic molecules can be added into the chamber to affect the characteristics of generated CNTs.[253]

Multi-walled CNTs, on the other hand, are formed by arc discharges without a catalyst. However, the preparation of single-walled CNTs can be achieved if the electrodes are derived from graphite with catalytic nanoparticles of metals like Ni, Fe, Co, Pt and Rh or their alloys. In an atmosphere of H_2 or Ar, double walled CNTs can also be generated by arc-discharge approach with the employment of Ni, Co, Fe and S mixture as the catalyst.[254] It can also be produced by pulsed arc discharges with the alloy of Y/Ni as the catalyst.[255] It has also been reported that CNTs can be produced by pulsed-laser ablation of a graphite target in a chamber with a controlled atmosphere. Catalytic nanoparticles of Ni or Co or the mixture are usually included in the graphite target and the ablation is carried out with either Nd : YAG or CO_2 lasers.[256]

CVD over a metal catalyst is regarded as the most powerful approach for CNTs preparation. The most widely used carbon vapor is methane, ethane, acetylene, ethylene, a mixture of H_2/CH_4, or ethanol. And the metal catalyst normally tends to be Fe, Co or Ni nanoparticles or some alloys of these elements. After the flowing of carbon vapor over the nanoparticles, they are broken down by heat or plasma irradiation, reconstructing CNTs after the catalytic nucleation.[257] Several parameters, such as nanoparticles composition and morphology, carbon source, substrate nature, decomposition temperature, are utilized to evaluate the quality, yield, purity and properties of the CNTs produced from CVD.[258, 259] Metallic and amorphous carbon impurities and deficiency in chirality control are the major difficulties in CNTs generation. Metal impurities derived from the catalyst, along with the by-product of amorphous carbon nanostructures are frequently occurred in the soot of CNTs.

Up to now, CNTs growth mechanism has been well understood. In summary, CNTs prepared from arc discharge or laser vaporization approaches are suitable for the investigation at a laboratory level, and CVD is prone to the mass production of multi-walled CNTs.[219] In a research conducted by Tessonnier et al.[260] 1 g cobalt-manganese-based catalyst in spinel type is able to generate approximately 180 g multi-walled CNTs under an atmosphere of a mixture of ethylene and hydrogen at 650 ^{o}C for 2 h, realizing an industrial yield of 70 kg·h^{-1} with very scarce impurities left in the catalyst. Multi-walled CNTs are still the major category of nanocarbon material applied in catalysis.

In spite of the preference for many applications, single-walled CNTs cannot be produced at a large quantity with a reasonable cost, which limit their practical uses. Compared with multi-walled CNTs, the industrial production of single-walled CNTs is still lack of development. High temperatures of CVD make hydrocarbon pyrolyze too fast and particles sinter together and thus CVD for the growth of single-walled CNTs cannot be obtained on an industrial scale.[219]

For the sustainable development, the employment of iron-based catalysts in CNTs growth has aroused great interest.[261, 262] Recently, the synthesis of CNTs in vertical alignment has become a progress in CNTs preparation.[263] Being catalyst support, aligned CNTs can be applied in the field of electrocatalysis[264] and microreactors.[265] However, this special CNTs can only be obtained in the laboratory.

Compared with undoped CNTs, CNTs doped by different heteroatoms like nitrogen or boron are regarded as different nanocarbons because of their diverse properties in different reactions as catalyst support.

Important progress has been achieved in the preparation of CNTs doped by nitrogen or boron with methods in similarity to those producing CNTs. During the process of CNTs preparation, doping carbons with nitrogen- or boron- precursors can homogeneously incorporate nitrogen or boron into the whole carbon structure.[266] Nitrogen-doped CNTs can be produced most effectively by CVD process in combination with nitrogen-containing precursors like melamine, benzylamine, acetonitrile, N-heterocycles, or ammonia, 1,2-ethylenediamine, and pyridine mixed with carbon sources. Nitrogen could be introduced into the CNTs via direct replacement of a carbon atom or a pyridinic bonding configuration. Without a hollow channel, nitrogen-doped CNTs usually exhibit bamboo-like structure. Strict control of many thermodynamic parameters is needed in the reaction of N incorporation in the CVD.[219] To be mentioned, there is a growing attention in the preparation of CNT-like materials. For instance, boron nitride nanotubes (BNNTs),[267] similar to CNTs in structure, are an electrical insulator with a band gap of 5 eV and independent of tube geometry. Beyond that, BNNTs are ideal catalysts due to their good stability, outstanding mechanical properties, and excellent thermal conductivity. Another material that receives research attention is carbon nitride nanotubes (CNNTs), which serve as a support for catalytic nanoparticles, as well as materials in photocatalysis and electrocatalysis.[268, 269]

2.5 Conclusion

Advanced oxidation processes are found to be an environmental friendly process for the degradation of refractory compounds. They are near ambient temperature and pressure water treatment processes which involve the generation of hydroxyl radicals and sulfate radicals in

sufficient quantity to affect water purification. Hydroxyl radicals-based AOPs are classified according to hydroxyl radical generation methods (chemical, eletro-chemical, sono-chemical and photochemical). The combination of conventional and nonconventional AOPs like photo-electro-Fenton and sono-electro-Fenton are also widely utilized in the processes of different contaminants removal.

AOPs are now shiting towards use of sulfate radical due to its unique characterisitics of high oxidation potential, applicability in a wide pH range, more stability than hydroxyl radicals and being more selective. PMS is an effective and promising oxidant for producing hydroxyl and sulfate radicals. PMS-based AOPs can open a new perspective of oxidative reactions to degrade the organic pollutants. Activation methods are comprehensively discussed amongst which heterogeneous catalysts have attracted much attention in case of PMS catalysing since no metals would be released into the aqueous solution.

Nanomaterials have recently aroused great interests of researchers in the applications of wastewater remediation, energy production and contaminants sensing. Nanomaterials can overcome the shortcomings of metal-based catalysts such as high cost, poor stability, bad selectivity, influence by gas poisoning and harmfulness to the environment. Graphene and carbon nanotubes are two most widely used carbon materials due to their unique characteristics such as large surface area, good thermal conductivity, and distinctive carbon configuration. Various methods, including SEM, TEM, XRD, XPS, etc. can be utilized to characterize nanocarbon materials. Meanwhile, they can be prepared by different synthesis methods. Doping graphene and carbon nanotubes

with heteroatom is an effective approach to improve their catalytic performance in phenol degradation.

References

[1] M.A. Oturan, J.-J. Aaron, Advanced oxidation processes in water/wastewater treatment: principles and applications. A review, Critical Reviews in Environmental Science and Technology 44(23) (2014) 2577-2641.

[2] A. Babuponnusami, K. Muthukumar, A review on Fenton and improvements to the Fenton process for wastewater treatment, Journal of Environmental Chemical Engineering 2(1) (2014) 557-572.

[3] X. Gao, F. Zhou, C.-T.A. Chen, Pollution status of the Bohai Sea: An overview of the environmental quality assessment related trace metals, Environment International 62 (2014) 12-30.

[4] K. Pan, W.-X. Wang, Trace metal contamination in estuarine and coastal environments in China, Science of The Total Environment 421 (2012) 3-16.

[5] A.K. Jain, V.K. Gupta, S. Jain, Suhas, Removal of Chlorophenols Using Industrial Wastes, Environmental Science & Technology 38(4) (2004) 1195-1200.

[6] M. Pimentel, N. Oturan, M. Dezotti, M.A. Oturan, Phenol degradation by advanced electrochemical oxidation process electro-Fenton using a carbon felt cathode, Applied Catalysis B: Environmental 83(1) (2008) 140-149.

[7] A. Babuponnusami, K. Muthukumar, Degradation of Phenol in Aqueous Solution by Fenton, Sono-Fenton and Sono-photo-Fenton Methods, CLEAN – Soil, Air, Water 39(2) (2011) 142-147.

[8] H. Kusić, N. Koprivanac, A.L. Bozić, I. Selanec, Photo-assisted Fenton type processes for the degradation of phenol: a kinetic study, J Hazard Mater 136(3) (2006) 632-644.
[9] E.M. Siedlecka, P. Stepnowski, Phenols Degradation by Fenton Reaction in the Presence of Chlorides and Sulfates, Polish Journal of Environmental Studies 14(6) (2005).
[10] D. Mantzavinos, E. Psillakis, Enhancement of biodegradability of industrial wastewaters by chemical oxidation pre-treatment, Journal of Chemical Technology and Biotechnology 79(5) (2004) 431-454.
[11] G.K. Nagda, A.M. Diwan, V.S. Ghole, Potential of tendu leaf refuse for phenol removal in aqueous systems, Applied Ecology and Environmental Research 5(2) (2007) 1-9.
[12] M.N. Rashed, Adsorption technique for the removal of organic pollutants from water and wastewater, Organic pollutants-monitoring, risk and treatment, InTech2013.
[13] K. Yang, B. Xing, Adsorption of organic compounds by carbon nanomaterials in aqueous phase: Polanyi theory and its application, Chemical reviews 110(10) (2010) 5989-6008.
[14] C.H. Tessmer, R.D. Vidic, L.J. Uranowski, Impact of Oxygen-Containing Surface Functional Groups on Activated Carbon Adsorption of Phenols, Environmental Science & Technology 31(7) (1997) 1872-1878.
[15] Z. Li, T. Burt, R.S. Bowman, Sorption of ionizable organic solutes by surfactant-modified zeolite, Environmental Science & Technology 34(17) (2000) 3756-3760.
[16] S.S. Tahir, N. Rauf, Removal of a cationic dye from aqueous solutions by adsorption onto bentonite clay, Chemosphere 63(11) (2006) 1842-1848.

[17] G. Crini, Non-conventional low-cost adsorbents for dye removal: a review, Bioresource technology 97(9) (2006) 1061-1085.
[18] S. Wang, Y. Boyjoo, A. Choueib, Z.H. Zhu, Removal of dyes from aqueous solution using fly ash and red mud, Water research 39(1) (2005) 129-138.
[19] J. Xu, L. Wang, Y. Zhu, Decontamination of bisphenol A from aqueous solution by graphene adsorption, Langmuir 28(22) (2012) 8418-8425.
[20] S. Wang, H. Sun, H.-M. Ang, M.O. Tadé, Adsorptive remediation of environmental pollutants using novel graphene-based nanomaterials, Chemical engineering journal 226 (2013) 336-347.
[21] C.E. Cerniglia, Biodegradation of polycyclic aromatic hydrocarbons, Biodegradation 3(2-3) (1992) 351-368.
[22] J.A. Field, E. De Jong, G.F. Costa, J.A. De Bont, Biodegradation of polycyclic aromatic hydrocarbons by new isolates of white rot fungi, Applied and environmental microbiology 58(7) (1992) 2219-2226.
[23] S.Y. Yuan, J.S. Chang, J.H. Yen, B.-V. Chang, Biodegradation of phenanthrene in river sediment, Chemosphere 43(3) (2001) 273-278.
[24] M. Dua, A. Singh, N. Sethunathan, A. Johri, Biotechnology and bioremediation: successes and limitations, Applied microbiology and biotechnology 59(2) (2002) 143-152.
[25] Q. Yang, H. Choi, Y. Chen, D.D. Dionysiou, Heterogeneous activation of peroxymonosulfate by supported cobalt catalysts for the degradation of 2,4-dichlorophenol in water: The effect of support, cobalt precursor, and UV radiation, Applied Catalysis B: Environmental 77(3) (2008) 300-307.
[26] S. Muhammad, E. Saputra, H. Sun, H.-M. Ang, M.O. Tadé, S. Wang, Heterogeneous catalytic oxidation of aqueous phenol on red mud-

supported cobalt catalysts, Industrial & Engineering Chemistry Research 51(47) (2012) 15351-15359.
[27] Q. Yang, H. Choi, S.R. Al-Abed, D.D. Dionysiou, Iron-cobalt mixed oxide nanocatalysts: heterogeneous peroxymonosulfate activation, cobalt leaching, and ferromagnetic properties for environmental applications, Applied Catalysis B: Environmental 88(3) (2009) 462-469.
[28] J. Zou, J. Ma, L. Chen, X. Li, Y. Guan, P. Xie, C. Pan, Rapid Acceleration of Ferrous Iron/Peroxymonosulfate Oxidation of Organic Pollutants by Promoting Fe(III)/Fe(II) Cycle with Hydroxylamine, Environmental Science & Technology 47(20) (2013) 11685-11691.
[29] P. Shukla, S. Wang, K. Singh, H.M. Ang, M.O. Tadé, Cobalt exchanged zeolites for heterogeneous catalytic oxidation of phenol in the presence of peroxymonosulphate, Applied Catalysis B: Environmental 99(1) (2010) 163-169.
[30] G.P. Anipsitakis, D.D. Dionysiou, Radical generation by the interaction of transition metals with common oxidants, Environmental science & technology 38(13) (2004) 3705-3712.
[31] X. Duan, Z. Ao, H. Sun, S. Indrawirawan, Y. Wang, J. Kang, F. Liang, Z.H. Zhu, S. Wang, Nitrogen-Doped Graphene for Generation and Evolution of Reactive Radicals by Metal-Free Catalysis, ACS Applied Materials & Interfaces 7(7) (2015) 4169-4178.
[32] X. Duan, K. O'Donnell, H. Sun, Y. Wang, S. Wang, Sulfur and Nitrogen Co-Doped Graphene for Metal-Free Catalytic Oxidation Reactions, Small 11(25) (2015) 3036-3044.
[33] X. Duan, H. Sun, Y. Wang, J. Kang, S. Wang, N-Doping-Induced Nonradical Reaction on Single-Walled Carbon Nanotubes for Catalytic Phenol Oxidation, ACS Catalysis 5(2) (2015) 553-559.

[34] S. Indrawirawan, H. Sun, X. Duan, S. Wang, Low temperature combustion synthesis of nitrogen-doped graphene for metal-free catalytic oxidation, Journal of Materials Chemistry A 3(7) (2015) 3432-3440.
[35] H. Sun, S. Liu, G. Zhou, H.M. Ang, M.O. Tadé, S. Wang, Reduced Graphene Oxide for Catalytic Oxidation of Aqueous Organic Pollutants, ACS Applied Materials & Interfaces 4(10) (2012) 5466-5471.
[36] H.Q. Sun, C. Kwan, A. Suvorova, H.M. Ang, M.O. Tade, S.B. Wang, Catalytic oxidation of organic pollutants on pristine and surface nitrogen-modified carbon nanotubes with sulfate radicals, Applied Catalysis B-Environmental 154 (2014) 134-141.
[37] A. Garg, I.M. Mishra, S. Chand, Oxidative Phenol Degradation Using Non-Noble Metal Based Catalysts, CLEAN - Soil, Air, Water 38(1) (2010) 27-34.
[38] L.A. Bernal-Martínez, C. Barrera-Díaz, C. Solís-Morelos, R. Natividad, Synergy of electrochemical and ozonation processes in industrial wastewater treatment, Chemical Engineering Journal 165(1) (2010) 71-77.
[39] P. Kritzer, E. Dinjus, An assessment of supercritical water oxidation (SCWO): existing problems, possible solutions and new reactor concepts, Chemical Engineering Journal 83(3) (2001) 207-214.
[40] J. Levec, A. Pintar, Catalytic wet-air oxidation processes: a review, Catalysis Today 124(3) (2007) 172-184.
[41] S. Esplugas, J. Gimenez, S. Contreras, E. Pascual, M. Rodríguez, Comparison of different advanced oxidation processes for phenol degradation, Water research 36(4) (2002) 1034-1042.
[42] A. Vogelpohl, S.-M. Kim, Advanced oxidation processes (AOPs) in wastewater treatment, Journal of Industrial and Engineering Chemistry 10(1) (2004) 33-40.

[43] J. Hoigné, H. Bader, Rate constants of reactions of ozone with organic and inorganic compounds in water-I: non-dissociating organic compounds, Water Research 17(2) (1983) 173-183.
[44] J. Hoigné, H. Bader, Rate constants of reactions of ozone with organic and inorganic compounds in water-II: dissociating organic compounds, Water research 17(2) (1983) 185-194.
[45] C. Gottschalk, J.A. Libra, A. Saupe, Reaction Mechanism, Ozonation of Water and Waste Water, Wiley-VCH Verlag GmbH & Co. KGaA2009, pp. 13-26.
[46] W.Z. Tang, Physicochemical treatment of hazardous wastes, CRC Press2016.
[47] J. Gimenez, D. Curco, P. Marco, Reactor modelling in the photocatalytic oxidation of wastewater, Water Science and Technology 35(4) (1997) 207-213.
[48] H.J.H. Fenton, LXXIII.-Oxidation of tartaric acid in presence of iron, Journal of the Chemical Society, Transactions 65 (1894) 899-910.
[49] W.H. Glaze, J.-W. Kang, D.H. Chapin, The chemistry of water treatment processes involving ozone, hydrogen peroxide and ultraviolet radiation, (1987).
[50] J.J. Pignatello, E. Oliveros, A. MacKay, Advanced oxidation processes for organic contaminant destruction based on the Fenton reaction and related chemistry, Critical reviews in environmental science and technology 36(1) (2006) 1-84.
[51] A.Y. Sychev, V.G. Isak, Iron compounds and the mechanisms of the homogeneous catalysis of the activation of O_2 and H_2O_2 and of the oxidation of organic substrates, Russian Chemical Reviews 64(12) (1995) 1105-1129.

[52] A. Babuponnusami, K. Muthukumar, Degradation of phenol in aqueous solution by fenton, sono-fenton and sono-photo-fenton methods, Clean–Soil, Air, Water 39(2) (2011) 142-147.
[53] F.J. Rivas, F.J. Beltran, J. Frades, P. Buxeda, Oxidation of p-hydroxybenzoic acid by Fenton's reagent, Water Research 35(2) (2001) 387-396.
[54] S.H. Lin, H.G. Leu, Operating characteristics and kinetic studies of surfactant wastewater treatment by Fenton oxidation, Water Research 33(7) (1999) 1735-1741.
[55] Y.W. Kang, K.-Y. Hwang, Effects of reaction conditions on the oxidation efficiency in the Fenton process, Water research 34(10) (2000) 2786-2790.
[56] S.H. Lin, C.C. Lo, Fenton process for treatment of desizing wastewater, Water research 31(8) (1997) 2050-2056.
[57] K. Ito, W. Jian, W. Nishijima, A.U. Baes, E. Shoto, M. Okada, Comparison of ozonation and AOPs combined with biodegradation for removal of THM precursors in treated sewage effluents, Water Science and Technology 38(7) (1998) 179-186.
[58] X.-R. Xu, X.-Y. Li, X.-Z. Li, H.-B. Li, Degradation of melatonin by UV, UV/H_2O_2, Fe^{2+}/H_2O_2 and UV/Fe^{2+}/H_2O_2 processes, Separation and Purification Technology 68(2) (2009) 261-266.
[59] C. Jiang, S. Pang, F. Ouyang, J. Ma, J. Jiang, A new insight into Fenton and Fenton-like processes for water treatment, J Hazard Mater 174(1) (2010) 813-817.
[60] D. Hermosilla, M. Cortijo, C.P. Huang, The role of iron on the degradation and mineralization of organic compounds using conventional Fenton and photo-Fenton processes, Chemical Engineering Journal 155(3) (2009) 637-646.

[61] A. Francony, C. Petrier, Sonochemical degradation of carbon tetrachloride in aqueous solution at two frequencies: 20 kHz and 500 kHz, Ultrasonics Sonochemistry 3(2) (1996) S77-S82.
[62] K.S. Suslick, S.J. Doktycz, E.B. Flint, On the origin of sonoluminescence and sonochemistry, Ultrasonics 28(5) (1990) 280-290.
[63] O. Dahlem, V. Demaiffe, V. Halloin, J. Reisse, Direct sonication system suitable for medium-scale sonochemical reactors, AIChE Journal 44(12) (1998) 2724-2730.
[64] J. Liang, S. Komarov, N. Hayashi, E. Kasai, Recent trends in the decomposition of chlorinated aromatic hydrocarbons by ultrasound irradiation and Fenton's reagent, Journal of material cycles and waste management 9(1) (2007) 47-55.
[65] C. Pulgarin, J. Kiwi, Overview on photocatalytic and electrocatalytic pretreatment of industrial non-biodegradable pollutants and pesticides, CHIMIA International Journal for Chemistry 50(3) (1996) 50-55.
[66] C. Comninellis, C. Pulgarin, Anodic oxidation of phenol for waste water treatment, Journal of applied electrochemistry 21(8) (1991) 703-708.
[67] C. Comninellis, C. Pulgarin, Electrochemical oxidation of phenol for wastewater treatment using SnO_2, anodes, Journal of Applied Electrochemistry 23(2) (1993) 108-112.
[68] W.-P. Ting, M.-C. Lu, Y.-H. Huang, The reactor design and comparison of Fenton, electro-Fenton and photoelectro-Fenton processes for mineralization of benzene sulfonic acid (BSA), J Hazard Mater 156(1) (2008) 421-427.
[69] G. Ruppert, R. Bauer, G. Heisler, The photo-Fenton reaction-an effective photochemical wastewater treatment process, Journal of Photochemistry and Photobiology A: Chemistry 73(1) (1993) 75-78.

[70] B.C. Faust, J. Hoigné, Photolysis of Fe (III)-hydroxy complexes as sources of OH radicals in clouds, fog and rain, Atmospheric Environment. Part A. General Topics 24(1) (1990) 79-89.
[71] S.-M. Kim, S.-U. Geissen, A. Vogelpohl, Landfill leachate treatment by a photoassisted Fenton reaction, Water Science and Technology 35(4) (1997) 239-248.
[72] O. Legrini, E. Oliveros, A.M. Braun, Photochemical processes for water treatment, Chemical reviews 93(2) (1993) 671-698.
[73] C. Wu, X. Liu, D. Wei, J. Fan, L. Wang, Photosonochemical degradation of Phenol in water, Water Research 35(16) (2001) 3927-3933.
[74] A.A. Pradhan, P.R. Gogate, Degradation of p-nitrophenol using acoustic cavitation and Fenton chemistry, J Hazard Mater 173(1) (2010) 517-522.
[75] P. Vaishnave, A. Kumar, R. Ameta, P.B. Punjabi, S.C. Ameta, Photo oxidative degradation of azure-B by sono-photo-Fenton and photo-Fenton reagents, Arabian Journal of Chemistry 7(6) (2014) 981-985.
[76] Y. Segura, R. Molina, F. Martinez, J.A. Melero, Integrated heterogeneous sono-photo Fenton processes for the degradation of phenolic aqueous solutions, Ultrasonics sonochemistry 16(3) (2009) 417-424.
[77] F. Mendez-Arriaga, R.A. Torres-Palma, C. Pétrier, S. Esplugas, J. Gimenez, C. Pulgarin, Mineralization enhancement of a recalcitrant pharmaceutical pollutant in water by advanced oxidation hybrid processes, water research 43(16) (2009) 3984-3991.
[78] B. Boye, M.M. Dieng, E. Brillas, Degradation of herbicide 4-chlorophenoxyacetic acid by advanced electrochemical oxidation

methods, Environmental Science & Technology 36(13) (2002) 3030-3035.
[79] A. Babuponnusami, K. Muthukumar, Advanced oxidation of phenol: a comparison between Fenton, electro-Fenton, sono-electro-Fenton and photo-electro-Fenton processes, Chemical Engineering Journal 183 (2012) 1-9.
[80] B. Iurascu, I. Siminiceanu, D. Vione, M.A. Vicente, A. Gil, Phenol degradation in water through a heterogeneous photo-Fenton process catalyzed by Fe-treated laponite, Water research 43(5) (2009) 1313-1322.
[81] R.M. Powell, R.W. Puls, S.K. Hightower, D.A. Sabatini, Coupled iron corrosion and chromate reduction: mechanisms for subsurface remediation, Environmental science & technology 29(8) (1995) 1913-1922.
[82] K.D. Warren, R.G. Arnold, T.L. Bishop, L.C. Lindholm, E.A. Betterton, Kinetics and mechanism of reductive dehalogenation of carbon tetrachloride using zero-valence metals, J Hazard Mater 41(2-3) (1995) 217-227.
[83] A. Babuponnusami, K. Muthukumar, Removal of phenol by heterogenous photo electro Fenton-like process using nano-zero valent iron, Separation and Purification Technology 98 (2012) 130-135.
[84] D.H. Bremner, A.E. Burgess, D. Houllemare, K.-C. Namkung, Phenol degradation using hydroxyl radicals generated from zero-valent iron and hydrogen peroxide, Applied Catalysis B: Environmental 63(1) (2006) 15-19.
[85] S.M. Ponder, J.G. Darab, T.E. Mallouk, Remediation of Cr (VI) and Pb (II) aqueous solutions using supported, nanoscale zero-valent iron, Environmental Science & Technology 34(12) (2000) 2564-2569.
[86] M.S. Yalfani, S. Contreras, F. Medina, J. Sueiras, Phenol degradation by Fenton's process using catalytic in situ generated

hydrogen peroxide, Applied Catalysis B: Environmental 89(3) (2009) 519-526.
[87] J.A. Bergendahl, T.P. Thies, Fenton's oxidation of MTBE with zero-valent iron, Water research 38(2) (2004) 327-334.
[88] M. Kallel, C. Belaid, R. Boussahel, M. Ksibi, A. Montiel, B. Elleuch, Olive mill wastewater degradation by Fenton oxidation with zero-valent iron and hydrogen peroxide, J Hazard Mater 163(2) (2009) 550-554.
[89] W.-x. Zhang, Nanoscale iron particles for environmental remediation: an overview, Journal of nanoparticle Research 5(3) (2003) 323-332.
[90] J.M. Rodríguez-Maroto, F. García-Herruzo, A. García-Rubio, C. Gómez-Lahoz, C. Vereda-Alonso, Kinetics of the chemical reduction of nitrate by zero-valent iron, Chemosphere 74(6) (2009) 804-809.
[91] S.G. Huling, B.E. Pivetz, In-situ chemical oxidation, ENVIRONMENTAL PROTECTION AGENCY WASHINGTON DC OFFICE OF WATER, 2006.
[92] Y. Deng, C.M. Ezyske, Sulfate radical-advanced oxidation process (SR-AOP) for simultaneous removal of refractory organic contaminants and ammonia in landfill leachate, Water Research 45(18) (2011) 6189-6194.
[93] M.G. Antoniou, A.A. de la Cruz, D.D. Dionysiou, Degradation of microcystin-LR using sulfate radicals generated through photolysis, thermolysis and e^- transfer mechanisms, Applied Catalysis B: Environmental 96(3) (2010) 290-298.
[94] Y. Yang, J.J. Pignatello, J. Ma, W.A. Mitch, Comparison of Halide Impacts on the Efficiency of Contaminant Degradation by Sulfate and Hydroxyl Radical-Based Advanced Oxidation Processes (AOPs), Environmental Science & Technology 48(4) (2014) 2344-2351.

[95] R. Yuan, S.N. Ramjaun, Z. Wang, J. Liu, Effects of chloride ion on degradation of Acid Orange 7 by sulfate radical-based advanced oxidation process: Implications for formation of chlorinated aromatic compounds, J Hazard Mater 196 (2011) 173-179.
[96] D.A. House, Kinetics and mechanism of oxidations by peroxydisulfate, Chemical reviews 62(3) (1962) 185-203.
[97] I.M. Kolthoff, I.K. Miller, The chemistry of persulfate. II. The reaction of persulfate with mercaptans solubilized in solutions of saturated fatty acid soaps, Journal of the American Chemical Society 73(11) (1951) 5118-5122.
[98] X. He, A. Armah, K.E. O'Shea, D.D. Dionysiou, Kinetics and mechanisms of cylindrospermopsin destruction by sulfate radical-based advanced oxidation processes, water research 63 (2014) 168-178.
[99] A. Tsitonaki, B. Petri, M. Crimi, H. Mosbæk, R.L. Siegrist, P.L. Bjerg, In situ chemical oxidation of contaminated soil and groundwater using persulfate: a review, Critical Reviews in Environmental Science and Technology 40(1) (2010) 55-91.
[100] Y. Ji, C. Dong, D. Kong, J. Lu, New insights into atrazine degradation by cobalt catalyzed peroxymonosulfate oxidation: kinetics, reaction products and transformation mechanisms, J Hazard Mater 285 (2015) 491-500.
[101] P. Neta, V. Madhavan, H. Zemel, R.W. Fessenden, Rate constants and mechanism of reaction of sulfate radical anion with aromatic compounds, Journal of the American Chemical Society 99(1) (1977) 163-164.
[102] R.H. Waldemer, P.G. Tratnyek, R.L. Johnson, J.T. Nurmi, Oxidation of chlorinated ethenes by heat-activated persulfate: kinetics and products, Environmental Science & Technology 41(3) (2007) 1010-1015.

[103] F. Ghanbari, M. Moradi, Application of peroxymonosulfate and its activation methods for degradation of environmental organic pollutants, Chemical Engineering Journal 310 (2017) 41-62.
[104] S. Wacławek, K. Grübel, M. Černík, Simple spectrophotometric determination of monopersulfate, Spectrochimica Acta Part A: Molecular and Biomolecular Spectroscopy 149 (2015) 928-933.
[105] J. Sun, X. Li, J. Feng, X. Tian, Oxone/Co^{2+} oxidation as an advanced oxidation process: comparison with traditional Fenton oxidation for treatment of landfill leachate, Water research 43(17) (2009) 4363-4369.
[106] M. Yu, A.L. Teel, R.J. Watts, Activation of Peroxymonosulfate by Subsurface Minerals, Journal of Contaminant Hydrology 191 (2016) 33-43.
[107] J. Flanagan, W.P. Griffith, A.C. Skapski, The active principle of Caro's acid, $HSO5^-$: X-ray crystal structure of $KHSO_5 \bullet H_2O$, Journal of the Chemical Society, Chemical Communications (23) (1984) 1574-1575.
[108] J. Flanagan, W.P. Griffith, A.C. Skapski, The active principle of Caro's acid, $HSO\ 5^-$: X-ray crystal structure of $KHSO_5 \cdot H_2O$, Journal of the Chemical Society, Chemical Communications (23) (1984) 1574-1575.
[109] W. Reints, D.A. Pratt, H.-G. Korth, P. Mulder, O-O Bond dissociation enthalpy in di (trifluoromethyl) peroxide (CF_3OOCF_3) as determined by very low pressure pyrolysis. density functional theory computations on O-O and O-H bonds in (fluorinated) derivatives, The Journal of Physical Chemistry A 104(46) (2000) 10713-10720.
[110] I.M. Kolthoff, I.K. Miller, The chemistry of persulfate. I. The kinetics and mechanism of the decomposition of the persulfate ion in

aqueous medium1, Journal of the American Chemical Society 73(7) (1951) 3055-3059.
[111] X. Pang, Y. Guo, Y. Zhang, B. Xu, F. Qi, $LaCoO_3$ perovskite oxide activation of peroxymonosulfate for aqueous 2-phenyl-5-sulfobenzimidazole degradation: effect of synthetic method and the reaction mechanism, Chemical Engineering Journal 304 (2016) 897-907.
[112] J.-y. Pu, J.-q. Wan, Y. Wang, Y.-w. Ma, Different Co-based MOFs templated synthesis of Co_3O_4 nanoparticles to degrade RhB by activation of oxone, RSC Advances 6(94) (2016) 91791-91797.
[113] L.A.C. Teixeira, J.P.M. Andia, L. Yokoyama, F.V. da Fonseca Araújo, C.M. Sarmiento, Oxidation of cyanide in effluents by Caro's Acid, Minerals Engineering 45 (2013) 81-87.
[114] H. Sun, S. Wang, Catalytic oxidation of organic pollutants in aqueous solution using sulfate radicals, Catalysis 27 (2015) 209-247.
[115] D.L. Ball, J.O. Edwards, The catalysis of the decomposition of Caro's acid, The Journal of Physical Chemistry 62(3) (1958) 343-345.
[116] R.C. Thompson, Reduction of peroxomonosulfate by oxovanadium (IV) in acidic solution. Role of the sulfate radical anion, Inorganic Chemistry 20(11) (1981) 3745-3748.
[117] G. Manivannan, P. Maruthamuthu, Peroxo salts as initiators of vinyl polymerization-III. Polymerization of acrylonitrile initiated by the peroxomonosulphate-Co (II) redox system, European polymer journal 23(4) (1987) 311-313.
[118] G.P. Anipsitakis, D.D. Dionysiou, Degradation of organic contaminants in water with sulfate radicals generated by the conjunction of peroxymonosulfate with cobalt, Environmental science & technology 37(20) (2003) 4790-4797.
[119] G.P. Anipsitakis, D.D. Dionysiou, M.A. Gonzalez, Cobalt-mediated activation of peroxymonosulfate and sulfate radical attack on

phenolic compounds. Implications of chloride ions, Environmental Science & Technology 40(3) (2006) 1000-1007.
[120] Y. Zhiyong, W. Wenhua, S. Lin, L. Liqin, W. Zhiyin, J. Xuanfeng, D. Chaonan, Q. Ruiying, Acceleration comparison between Fe^{2+}/H_2O_2 and Co^{2+}/oxone for decolouration of azo dyes in homogeneous systems, Chemical Engineering Journal 234 (2013) 475-483.
[121] A. Rastogi, S.R. Al-Abed, D.D. Dionysiou, Sulfate radical-based ferrous-peroxymonosulfate oxidative system for PCBs degradation in aqueous and sediment systems, Applied Catalysis B: Environmental 85(3) (2009) 171-179.
[122] P. Hu, M. Long, Cobalt-catalyzed sulfate radical-based advanced oxidation: a review on heterogeneous catalysts and applications, Applied Catalysis B: Environmental 181 (2016) 103-117.
[123] K. Pirkanniemi, M. Sillanpää, Heterogeneous water phase catalysis as an environmental application: a review, Chemosphere 48(10) (2002) 1047-1060.
[124] G. Duca, Homogeneous catalysis with metal complexes: fundamentals and applications, Springer Science & Business Media2012.
[125] W.-D. Oh, Z. Dong, T.-T. Lim, Generation of sulfate radical through heterogeneous catalysis for organic contaminants removal: current development, challenges and prospects, Applied Catalysis B: Environmental 194 (2016) 169-201.
[126] W. Zhang, H.L. Tay, S.S. Lim, Y. Wang, Z. Zhong, R. Xu, Supported cobalt oxide on MgO: highly efficient catalysts for degradation of organic dyes in dilute solutions, Applied Catalysis B: Environmental 95(1) (2010) 93-99.
[127] M. Stoyanova, I. Slavova, V. Ivanova, Catalytic performance of supported nanosized cobalt and iron-cobalt mixed oxides on MgO in

oxidative degradation of Acid Orange 7 azo dye with peroxymonosulfate, Applied Catalysis A: General 476 (2014) 121-132.
[128] W.-D. Oh, Z. Dong, Z.-T. Hu, T.-T. Lim, A novel quasi-cubic $CuFe_2O_4$-Fe_2O_3 catalyst prepared at low temperature for enhanced oxidation of bisphenol A via peroxymonosulfate activation, Journal of Materials Chemistry A 3(44) (2015) 22208-22217.
[129] R.R. Solís, F.J. Rivas, O. Gimeno, Removal of aqueous metazachlor, tembotrione, tritosulfuron and ethofumesate by heterogeneous monopersulfate decomposition on lanthanum-cobalt perovskites, Applied Catalysis B: Environmental 200 (2017) 83-92.
[130] G.P. Anipsitakis, E. Stathatos, D.D. Dionysiou, Heterogeneous activation of oxone using Co_3O_4, The Journal of Physical Chemistry B 109(27) (2005) 13052-13055.
[131] X. Chen, J. Chen, X. Qiao, D. Wang, X. Cai, Performance of nano-Co_3O_4/peroxymonosulfate system: kinetics and mechanism study using Acid Orange 7 as a model compound, Applied Catalysis B: Environmental 80(1) (2008) 116-121.
[132] Y. Wang, L. Zhou, X. Duan, H. Sun, E.L. Tin, W. Jin, S. Wang, Photochemical degradation of phenol solutions on Co 3 O 4 nanorods with sulfate radicals, Catalysis Today 258 (2015) 576-584.
[133] J. Deng, S. Feng, K. Zhang, J. Li, H. Wang, T. Zhang, X. Ma, Heterogeneous activation of peroxymonosulfate using ordered mesoporous Co_3O_4 for the degradation of chloramphenicol at neutral pH, Chemical Engineering Journal 308 (2017) 505-515.
[134] K.-Y.A. Lin, B.-J. Chen, Magnetic carbon-supported cobalt derived from a Prussian blue analogue as a heterogeneous catalyst to activate peroxymonosulfate for efficient degradation of caffeine in water, Journal of colloid and interface science 486 (2017) 255-264.

[135] Q. Yang, H. Choi, D.D. Dionysiou, Nanocrystalline cobalt oxide immobilized on titanium dioxide nanoparticles for the heterogeneous activation of peroxymonosulfate, Applied Catalysis B: Environmental 74(1) (2007) 170-178.
[136] Q. Yang, H. Choi, Y. Chen, D.D. Dionysiou, Heterogeneous activation of peroxymonosulfate by supported cobalt catalysts for the degradation of 2, 4-dichlorophenol in water: the effect of support, cobalt precursor, and UV radiation, Applied Catalysis B: Environmental 77(3) (2008) 300-307.
[137] Y. Ding, L. Zhu, A. Huang, X. Zhao, X. Zhang, H. Tang, A heterogeneous Co_3O_4-Bi_2O_3 composite catalyst for oxidative degradation of organic pollutants in the presence of peroxymonosulfate, Catalysis Science & Technology 2(9) (2012) 1977-1984.
[138] H. Liang, H. Sun, A. Patel, P. Shukla, Z.H. Zhu, S. Wang, Excellent performance of mesoporous Co_3O_4/MnO_2 nanoparticles in heterogeneous activation of peroxymonosulfate for phenol degradation in aqueous solutions, Applied Catalysis B: Environmental 127 (2012) 330-335.
[139] P.R. Shukla, S. Wang, H. Sun, H.M. Ang, M. Tadé, Activated carbon supported cobalt catalysts for advanced oxidation of organic contaminants in aqueous solution, Applied Catalysis B: Environmental 100(3) (2010) 529-534.
[140] P. Shi, X. Dai, H. Zheng, D. Li, W. Yao, C. Hu, Synergistic catalysis of Co_3O_4 and graphene oxide on Co_3O_4/GO catalysts for degradation of Orange II in water by advanced oxidation technology based on sulfate radicals, Chemical Engineering Journal 240 (2014) 264-270.
[141] Y. Hardjono, H. Sun, H. Tian, C.E. Buckley, S. Wang, Synthesis of Co oxide doped carbon aerogel catalyst and catalytic performance in

heterogeneous oxidation of phenol in water, Chemical engineering journal 174(1) (2011) 376-382.
[142] P. Shi, R. Su, F. Wan, M. Zhu, D. Li, S. Xu, Co_3O_4 nanocrystals on graphene oxide as a synergistic catalyst for degradation of Orange II in water by advanced oxidation technology based on sulfate radicals, Applied Catalysis B: Environmental 123 (2012) 265-272.
[143] Y. Yao, Z. Yang, H. Sun, S. Wang, Hydrothermal synthesis of Co_3O_4-graphene for heterogeneous activation of peroxymonosulfate for decomposition of phenol, Industrial & Engineering Chemistry Research 51(46) (2012) 14958-14965.
[144] M. Anbia, M. Rezaie, Synthesis of supported ruthenium catalyst for phenol degradation in the presence of peroxymonosulfate, Water, Air, & Soil Pollution 227(9) (2016) 349.
[145] W. Chu, W.K. Choy, C.Y. Kwan, Selection of supported cobalt substrates in the presence of oxone for the oxidation of monuron, Journal of agricultural and food chemistry 55(14) (2007) 5708-5713.
[146] P. Shukla, H. Sun, S. Wang, H.M. Ang, M.O. Tadé, Co-SBA-15 for heterogeneous oxidation of phenol with sulfate radical for wastewater treatment, Catalysis Today 175(1) (2011) 380-385.
[147] L. Hu, X. Yang, S. Dang, An easily recyclable Co/SBA-15 catalyst: heterogeneous activation of peroxymonosulfate for the degradation of phenol in water, Applied Catalysis B: Environmental 102(1) (2011) 19-26.
[148] E. Saputra, S. Muhammad, H. Sun, H.M. Ang, M.O. Tadé, S. Wang, Red mud and fly ash supported Co catalysts for phenol oxidation, Catalysis Today 190(1) (2012) 68-72.
[149] P. Xu, G.M. Zeng, D.L. Huang, C.L. Feng, S. Hu, M.H. Zhao, C. Lai, Z. Wei, C. Huang, G.X. Xie, Use of iron oxide nanomaterials in

wastewater treatment: a review, Science of the Total Environment 424 (2012) 1-10.
[150] A.B. Cundy, L. Hopkinson, R.L.D. Whitby, Use of iron-based technologies in contaminated land and groundwater remediation: a review, Science of the total environment 400(1) (2008) 42-51.
[151] J. Zhao, Y. Zhang, X. Quan, S. Chen, Enhanced oxidation of 4-chlorophenol using sulfate radicals generated from zero-valent iron and peroxydisulfate at ambient temperature, Separation and Purification Technology 71(3) (2010) 302-307.
[152] A. Volpe, M. Pagano, G. Mascolo, A. Lopez, R. Ciannarella, V. Locaputo, Simultaneous Cr (VI) reduction and non-ionic surfactant oxidation by peroxymonosulphate and iron powder, Chemosphere 91(9) (2013) 1250-1256.
[153] F. Ghanbari, M. Moradi, M. Manshouri, Textile wastewater decolorization by zero valent iron activated peroxymonosulfate: compared with zero valent copper, Journal of Environmental Chemical Engineering 2(3) (2014) 1846-1851.
[154] Y. Li, Y. Zhang, J. Li, X. Zheng, Enhanced removal of pentachlorophenol by a novel composite: nanoscale zero valent iron immobilized on organobentonite, Environmental pollution 159(12) (2011) 3744-3749.
[155] H.Q. Sun, G.L. Zhou, S.Z. Liu, H.M. Ang, M.O. Tadé, S.B. Wang, Nano-Fe0 encapsulated in carbon spheres for oxidation of aqueous phenol with sulphate radicals, ACS Appl. Mater. Interfaces 4 (2012) 6235-6241.
[156] Y. Wang, H. Sun, X. Duan, H.M. Ang, M.O. Tadé, S. Wang, A new magnetic nano zero-valent iron encapsulated in carbon spheres for oxidative degradation of phenol, Applied Catalysis B: Environmental 172 (2015) 73-81.

[157] H. Sun, G. Zhou, S. Liu, H.M. Ang, M.O. Tadé, S. Wang, Nano-Fe0 encapsulated in microcarbon spheres: synthesis, characterization, and environmental applications, ACS applied materials & interfaces 4(11) (2012) 6235-6241.
[158] J. Virkutyte, R.S. Varma, Eco-friendly magnetic iron oxide-pillared montmorillonite for advanced catalytic degradation of dichlorophenol, ACS Sustainable Chemistry & Engineering 2(7) (2014) 1545-1550.
[159] F. Ji, C. Li, X. Wei, J. Yu, Efficient performance of porous Fe 2 O 3 in heterogeneous activation of peroxymonosulfate for decolorization of Rhodamine B, Chemical engineering journal 231 (2013) 434-440.
[160] W.-D. Oh, S.-K. Lua, Z. Dong, T.-T. Lim, High surface area DPA-hematite for efficient detoxification of bisphenol A via peroxymonosulfate activation, Journal of Materials Chemistry A 2(38) (2014) 15836-15845.
[161] G. Wei, X. Liang, Z. He, Y. Liao, Z. Xie, P. Liu, S. Ji, H. He, D. Li, J. Zhang, Heterogeneous activation of Oxone by substituted magnetites Fe 3− x MxO 4 (Cr, Mn, Co, Ni) for degradation of Acid Orange II at neutral pH, Journal of Molecular Catalysis A: Chemical 398 (2015) 86-94.
[162] M.A. Al-Shamsi, N.R. Thomson, Treatment of organic compounds by activated persulfate using nanoscale zerovalent iron, Industrial & Engineering Chemistry Research 52(38) (2013) 13564-13571.
[163] L. Zhang, L. Zhao, J. Lian, Nanostructured Mn 3 O 4–reduced graphene oxide hybrid and its applications for efficient catalytic decomposition of Orange II and high lithium storage capacity, RSC Advances 4(79) (2014) 41838-41847.
[164] Y. Wang, Y. Xie, H. Sun, J. Xiao, H. Cao, S. Wang, 2D/2D nano-hybrids of γ-MnO 2 on reduced graphene oxide for catalytic ozonation

and coupling peroxymonosulfate activation, J Hazard Mater 301 (2016) 56-64.
[165] J. Du, J. Bao, Y. Liu, H. Ling, H. Zheng, S.H. Kim, D.D. Dionysiou, Efficient activation of peroxymonosulfate by magnetic Mn-MGO for degradation of bisphenol A, J Hazard Mater 320 (2016) 150-159.
[166] E. Saputra, S. Muhammad, H. Sun, A. Patel, P. Shukla, Z.H. Zhu, S. Wang, α-MnO 2 activation of peroxymonosulfate for catalytic phenol degradation in aqueous solutions, Catalysis Communications 26 (2012) 144-148.
[167] E. Saputra, H. Zhang, Q. Liu, H. Sun, S. Wang, Egg-shaped core/shell α-Mn_2O_3@ α-MnO_2 as heterogeneous catalysts for decomposition of phenolics in aqueous solutions, Chemosphere 159 (2016) 351-358.
[168] Q. Liu, X. Duan, H. Sun, Y. Wang, M.O. Tade, S. Wang, Size-tailored porous spheres of manganese oxides for catalytic oxidation via peroxymonosulfate activation, The Journal of Physical Chemistry C 120(30) (2016) 16871-16878.
[169] E. Saputra, S. Muhammad, H. Sun, H.-M. Ang, M.O. Tadé, S. Wang, Manganese oxides at different oxidation states for heterogeneous activation of peroxymonosulfate for phenol degradation in aqueous solutions, Applied Catalysis B: Environmental 142 (2013) 729-735.
[170] Y. Wang, S. Indrawirawan, X. Duan, H. Sun, H.M. Ang, M.O. Tadé, S. Wang, New insights into heterogeneous generation and evolution processes of sulfate radicals for phenol degradation over one-dimensional α-MnO_2 nanostructures, Chemical Engineering Journal 266 (2015) 12-20.
[171] E. Saputra, S. Muhammad, H. Sun, H.M. Ang, M.O. Tadé, S. Wang, Different crystallographic one-dimensional MnO_2 nanomaterials

and their superior performance in catalytic phenol degradation, Environmental science & technology 47(11) (2013) 5882-5887.
[172] S. Luo, L. Duan, B. Sun, M. Wei, X. Li, A. Xu, Manganese oxide octahedral molecular sieve (OMS-2) as an effective catalyst for degradation of organic dyes in aqueous solutions in the presence of peroxymonosulfate, Applied Catalysis B: Environmental 164 (2015) 92-99.
[173] Y.S. Ding, X.F. Shen, S. Sithambaram, S. Gomez, R. Kumar, V.M.B. Crisostomo, S.L. Suib, M. Aindow, Synthesis and catalytic activity of cryptomelane-type manganese dioxide nanomaterials produced by a novel solvent-free method, Chemistry of materials 17(21) (2005) 5382-5389.
[174] L. Duan, B. Sun, M. Wei, S. Luo, F. Pan, A. Xu, X. Li, Catalytic degradation of Acid Orange 7 by manganese oxide octahedral molecular sieves with peroxymonosulfate under visible light irradiation, J Hazard Mater 285 (2015) 356-365.
[175] M. Wei, Y. Ruan, S. Luo, X. Li, A. Xu, P. Zhang, The facile synthesis of a magnetic OMS-2 catalyst for decomposition of organic dyes in aqueous solution with peroxymonosulfate, New Journal of Chemistry 39(8) (2015) 6395-6403.
[176] B. Yang, Z. Tian, B. Wang, Z. Sun, L. Zhang, Y. Guo, H. Li, S. Yan, Facile synthesis of Fe_3O_4/hierarchical-Mn_3O_4/graphene oxide as a synergistic catalyst for activation of peroxymonosulfate for degradation of organic pollutants, RSC Advances 5(27) (2015) 20674-20683.
[177] S. Zhang, Q. Fan, H. Gao, Y. Huang, X. Liu, J. Li, X. Xu, X. Wang, Formation of Fe_3O_4@ MnO_2 ball-in-ball hollow spheres as a high performance catalyst with enhanced catalytic performances, Journal of Materials Chemistry A 4(4) (2016) 1414-1422.

[178] H. Sun, H. Liang, G. Zhou, S. Wang, Supported cobalt catalysts by one-pot aqueous combustion synthesis for catalytic phenol degradation, Journal of colloid and interface science 394 (2013) 394-400.
[179] P. Zhou, B. Liu, J. Zhang, Y. Zhang, G. Zhang, C. Wei, J. Liang, Y. Liu, W. Zhang, Radicals induced from peroxomonosulfate by nanoscale zero-valent copper in the acidic solution, Water Science and Technology 74(8) (2016) 1946-1952.
[180] Y. Feng, J. Liu, D. Wu, Z. Zhou, Y. Deng, T. Zhang, K. Shih, Efficient degradation of sulfamethazine with $CuCo_2O_4$ spinel nanocatalysts for peroxymonosulfate activation, Chemical Engineering Journal 280 (2015) 514-524.
[181] F. Ji, C. Li, Y. Liu, P. Liu, Heterogeneous activation of peroxymonosulfate by Cu/ZSM5 for decolorization of Rhodamine B, Separation and Purification Technology 135 (2014) 1-6.
[182] F. Ji, C. Li, L. Deng, Performance of CuO/Oxone system: Heterogeneous catalytic oxidation of phenol at ambient conditions, Chemical engineering journal 178 (2011) 239-243.
[183] W. Wu, Z.-H. Huang, T.-T. Lim, Recent development of mixed metal oxide anodes for electrochemical oxidation of organic pollutants in water, Applied Catalysis A: General 480 (2014) 58-78.
[184] D.S. Mathew, R.-S. Juang, An overview of the structure and magnetism of spinel ferrite nanoparticles and their synthesis in microemulsions, Chemical Engineering Journal 129(1) (2007) 51-65.
[185] J. Deng, Y. Shao, N. Gao, C. Tan, S. Zhou, X. Hu, $CoFe_2O_4$ magnetic nanoparticles as a highly active heterogeneous catalyst of oxone for the degradation of diclofenac in water, J Hazard Mater 262 (2013) 836-844.

[186] S. Su, W. Guo, Y. Leng, C. Yi, Z. Ma, Heterogeneous activation of Oxone by $Co_xFe_{3-x}O_4$ nanocatalysts for degradation of rhodamine B, J Hazard Mater 244 (2013) 736-742.
[187] Y. Yao, Z. Yang, D. Zhang, W. Peng, H. Sun, S. Wang, Magnetic $CoFe_2O_4$-graphene hybrids: facile synthesis, characterization, and catalytic properties, Industrial & Engineering Chemistry Research 51(17) (2012) 6044-6051.
[188] Y. Wang, H. Sun, H.M. Ang, M.O. Tadé, S. Wang, Magnetic Fe_3O_4/carbon sphere/cobalt composites for catalytic oxidation of phenol solutions with sulfate radicals, Chemical Engineering Journal 245 (2014) 1-9.
[189] Y. Ding, L. Zhu, N. Wang, H. Tang, Sulfate radicals induced degradation of tetrabromobisphenol A with nanoscaled magnetic $CuFe_2O_4$ as a heterogeneous catalyst of peroxymonosulfate, Applied Catalysis B: Environmental 129 (2013) 153-162.
[190] W.-D. Oh, S.-K. Lua, Z. Dong, T.-T. Lim, Rational design of hierarchically-structured $CuBi_2O_4$ composites by deliberate manipulation of the nucleation and growth kinetics of $CuBi_2O_4$ for environmental applications, Nanoscale 8(4) (2016) 2046-2054.
[191] K.-Y.A. Lin, Y.-C. Chen, Accelerated decomposition of Oxone using graphene-like carbon nitride with visible light irradiation for enhanced decolorization in water, Journal of the Taiwan Institute of Chemical Engineers 60 (2016) 423-429.
[192] X. Duan, Z. Ao, D. Li, H. Sun, L. Zhou, A. Suvorova, M. Saunders, G. Wang, S. Wang, Surface-tailored nanodiamonds as excellent metal-free catalysts for organic oxidation, Carbon 103 (2016) 404-411.
[193] C. Moreno-Castilla, M.A. Fontecha-Cámara, M.A. Álvarez-Merino, M.V. López-Ramón, F. Carrasco-Marín, Activated carbon cloth

as adsorbent and oxidation catalyst for the removal of amitrole from aqueous solution, Adsorption 17(3) (2011) 413-419.
[194] S. Yang, L. Li, T. Xiao, Y. Zhang, D. Zheng, Promoting effect of ammonia modification on activated carbon catalyzed peroxymonosulfate oxidation, Separation and Purification Technology 160 (2016) 81-88.
[195] J. Zhang, X. Shao, C. Shi, S. Yang, Decolorization of Acid Orange 7 with peroxymonosulfate oxidation catalyzed by granular activated carbon, Chemical engineering journal 232 (2013) 259-265.
[196] S. Yang, T. Xiao, J. Zhang, Y. Chen, L. Li, Activated carbon fiber as heterogeneous catalyst of peroxymonosulfate activation for efficient degradation of Acid Orange 7 in aqueous solution, Separation and Purification Technology 143 (2015) 19-26.
[197] S. Indrawirawan, H. Sun, X. Duan, S. Wang, Nanocarbons in different structural dimensions (0-3D) for phenol adsorption and metal-free catalytic oxidation, Applied Catalysis B: Environmental 179 (2015) 352-362.
[198] W. Peng, S. Liu, H. Sun, Y. Yao, L. Zhi, S. Wang, Synthesis of porous reduced graphene oxide as metal-free carbon for adsorption and catalytic oxidation of organics in water, Journal of Materials Chemistry A 1(19) (2013) 5854-5859.
[199] S. Liu, W. Peng, H. Sun, S. Wang, Physical and chemical activation of reduced graphene oxide for enhanced adsorption and catalytic oxidation, Nanoscale 6(2) (2014) 766-771.
[200] W. Qi, D. Su, Metal-free carbon catalysts for oxidative dehydrogenation reactions, Acs Catalysis 4(9) (2014) 3212-3218.
[201] H. Sun, Y. Wang, S. Liu, L. Ge, L. Wang, Z. Zhu, S. Wang, Facile synthesis of nitrogen doped reduced graphene oxide as a superior metal-free catalyst for oxidation, Chemical Communications 49(85) (2013) 9914-9916.

[202] C. Wang, J. Kang, H. Sun, H.M. Ang, M.O. Tadé, S. Wang, One-pot synthesis of N-doped graphene for metal-free advanced oxidation processes, Carbon 102 (2016) 279-287.
[203] Y. Gao, G. Hu, J. Zhong, Z. Shi, Y. Zhu, D.S. Su, J. Wang, X. Bao, D. Ma, Nitrogen-Doped sp2-Hybridized Carbon as a Superior Catalyst for Selective Oxidation, Angewandte Chemie International Edition 52(7) (2013) 2109-2113.
[204] D. Yu, K. Goh, L. Wei, H. Wang, Q. Zhang, W. Jiang, R. Si, Y. Chen, Multifunctional nitrogen-rich “brick-and-mortar” carbon as high performance supercapacitor electrodes and oxygen reduction electrocatalysts, Journal of Materials Chemistry A 1(36) (2013) 11061-11069.
[205] B. Frank, R. Blume, A. Rinaldi, A. Trunschke, R. Schlögl, Oxygen insertion catalysis by sp2 carbon, Angewandte Chemie International Edition 50(43) (2011) 10226-10230.
[206] A.M. Rao, P.C. Eklund, S. Bandow, A. Thess, R.E. Smalley, Evidence for charge transfer in doped carbon nanotube bundles from Raman scattering, Nature 388(6639) (1997) 257.
[207] L. Duclaux, Review of the doping of carbon nanotubes (multiwalled and single-walled), Carbon 40(10) (2002) 1751-1764.
[208] M. Wei, L. Gao, J. Li, J. Fang, W. Cai, X. Li, A. Xu, Activation of peroxymonosulfate by graphitic carbon nitride loaded on activated carbon for organic pollutants degradation, J Hazard Mater 316 (2016) 60-68.
[209] H. Dong, M. Wei, J. Li, J. Fang, L. Gao, X. Li, A. Xu, Catalytic performance of supported gC 3 N 4 on MCM-41 in organic dye degradation with peroxymonosulfate, RSC Advances 6(75) (2016) 70747-70755.

[210] X. Duan, H. Sun, Y. Wang, J. Kang, S. Wang, N-doping-induced nonradical reaction on single-walled carbon nanotubes for catalytic phenol oxidation, Acs Catalysis 5(2) (2014) 553-559.
[211] C. Wang, J. Kang, P. Liang, H. Zhang, H. Sun, M.O. Tadé, S. Wang, Ferric carbide nanocrystals encapsulated in nitrogen-doped carbon nanotubes as an outstanding environmental catalyst, Environmental Science: Nano 4(1) (2017) 170-179.
[212] X. Duan, Z. Ao, H. Sun, L. Zhou, G. Wang, S. Wang, Insights into N-doping in single-walled carbon nanotubes for enhanced activation of superoxides: a mechanistic study, Chemical Communications 51(83) (2015) 15249-15252.
[213] X. Duan, Z. Ao, L. Zhou, H. Sun, G. Wang, S. Wang, Occurrence of radical and nonradical pathways from carbocatalysts for aqueous and nonaqueous catalytic oxidation, Applied Catalysis B: Environmental 188 (2016) 98-105.
[214] Y. Zhou, J. Jiang, Y. Gao, J. Ma, S.-Y. Pang, J. Li, X.-T. Lu, L.-P. Yuan, Activation of peroxymonosulfate by benzoquinone: a novel nonradical oxidation process, Environmental science & technology 49(21) (2015) 12941-12950.
[215] J. Lubchenco, Entering the century of the environment: a new social contract for science, Science 279(5350) (1998) 491-497.
[216] X. Qu, P.J.J. Alvarez, Q. Li, Applications of nanotechnology in water and wastewater treatment, Water research 47(12) (2013) 3931-3946.
[217] Q. Zhang, E. Uchaker, S.L. Candelaria, G. Cao, Nanomaterials for energy conversion and storage, Chemical Society Reviews 42(7) (2013) 3127-3171.
[218] W. Yang, K.R. Ratinac, S.P. Ringer, P. Thordarson, J.J. Gooding, F. Braet, Carbon nanomaterials in biosensors: should you use nanotubes

or graphene?, Angewandte Chemie International Edition 49(12) (2010) 2114-2138.
[219] D.S. Su, S. Perathoner, G. Centi, Nanocarbons for the development of advanced catalysts, Chemical reviews 113(8) (2013) 5782-5816.
[220] C.e.N.e.R. Rao, A.e.K. Sood, K.e.S. Subrahmanyam, A. Govindaraj, Graphene: the new two-dimensional nanomaterial, Angewandte Chemie International Edition 48(42) (2009) 7752-7777.
[221] X. Jia, J. Campos-Delgado, M. Terrones, V. Meunier, M.S. Dresselhaus, Graphene edges: a review of their fabrication and characterization, Nanoscale 3(1) (2011) 86-95.
[222] C. Soldano, A. Mahmood, E. Dujardin, Production, properties and potential of graphene, Carbon 48(8) (2010) 2127-2150.
[223] V. Singh, D. Joung, L. Zhai, S. Das, S.I. Khondaker, S. Seal, Graphene based materials: past, present and future, Progress in materials science 56(8) (2011) 1178-1271.
[224] A.K. Geim, Graphene: status and prospects, science 324(5934) (2009) 1530-1534.
[225] V.C. Sanchez, A. Jachak, R.H. Hurt, A.B. Kane, Biological interactions of graphene-family nanomaterials: an interdisciplinary review, Chemical research in toxicology 25(1) (2011) 15-34.
[226] J.R. Potts, D.R. Dreyer, C.W. Bielawski, R.S. Ruoff, Graphene-based polymer nanocomposites, Polymer 52(1) (2011) 5-25.
[227] C. Hontoria-Lucas, A.J. López-Peinado, J.d.D. López-González, M.L. Rojas-Cervantes, R.M. Martin-Aranda, Study of oxygen-containing groups in a series of graphite oxides: physical and chemical characterization, Carbon 33(11) (1995) 1585-1592.
[228] F. Perreault, A.F. De Faria, M. Elimelech, Environmental applications of graphene-based nanomaterials, Chemical Society Reviews 44(16) (2015) 5861-5896.

[229] A.K. Geim, K.S. Novoselov, The rise of graphene, Nature materials 6(3) (2007) 183-191.
[230] Y. Zhu, S. Murali, W. Cai, X. Li, J.W. Suk, J.R. Potts, R.S. Ruoff, Graphene and graphene oxide: synthesis, properties, and applications, Advanced materials 22(35) (2010) 3906-3924.
[231] Y. Hernandez, V. Nicolosi, M. Lotya, F.M. Blighe, Z. Sun, S. De, I.T. McGovern, B. Holland, M. Byrne, Y.K. Gun'Ko, High-yield production of graphene by liquid-phase exfoliation of graphite, Nature nanotechnology 3(9) (2008) 563-568.
[232] W.A. De Heer, C. Berger, X. Wu, P.N. First, E.H. Conrad, X. Li, T. Li, M. Sprinkle, J. Hass, M.L. Sadowski, Epitaxial graphene, Solid State Communications 143(1) (2007) 92-100.
[233] X. Li, W. Cai, J. An, S. Kim, J. Nah, D. Yang, R. Piner, A. Velamakanni, I. Jung, E. Tutuc, Large-area synthesis of high-quality and uniform graphene films on copper foils, Science 324(5932) (2009) 1312-1314.
[234] Y.I. Zhang, L. Zhang, C. Zhou, Review of chemical vapor deposition of graphene and related applications, Accounts of chemical research 46(10) (2013) 2329-2339.
[235] A.T. Murdock, A. Koos, T.B. Britton, L. Houben, T. Batten, T. Zhang, A.J. Wilkinson, R.E. Dunin-Borkowski, C.E. Lekka, N. Grobert, Controlling the orientation, edge geometry, and thickness of chemical vapor deposition graphene, Acs Nano 7(2) (2013) 1351-1359.
[236] S. Navalon, A. Dhakshinamoorthy, M. Alvaro, H. Garcia, Carbocatalysis by graphene-based materials, Chemical reviews 114(12) (2014) 6179-6212.
[237] D.R. Dreyer, S. Park, C.W. Bielawski, R.S. Ruoff, The chemistry of graphene oxide, Chemical Society Reviews 39(1) (2010) 228-240.

[238] W.S. Hummers Jr, R.E. Offeman, Preparation of graphitic oxide, Journal of the American Chemical Society 80(6) (1958) 1339-1339.
[239] D.C. Marcano, D.V. Kosynkin, J.M. Berlin, A. Sinitskii, Z. Sun, A. Slesarev, L.B. Alemany, W. Lu, J.M. Tour, Improved synthesis of graphene oxide, (2010).
[240] V.C. Tung, M.J. Allen, Y. Yang, R.B. Kaner, High-throughput solution processing of large-scale graphene, Nature nanotechnology 4(1) (2009) 25-29.
[241] J.W. Suk, R.D. Piner, J. An, R.S. Ruoff, Mechanical properties of monolayer graphene oxide, ACS nano 4(11) (2010) 6557-6564.
[242] C.K. Chua, Z. Sofer, M. Pumera, Graphite oxides: effects of permanganate and chlorate oxidants on the oxygen composition, Chemistry-A European Journal 18(42) (2012) 13453-13459.
[243] C.K. Chua, M. Pumera, Chemical reduction of graphene oxide: a synthetic chemistry viewpoint, Chemical Society Reviews 43(1) (2014) 291-312.
[244] S. Pei, H.-M. Cheng, The reduction of graphene oxide, Carbon 50(9) (2012) 3210-3228.
[245] A. Bagri, C. Mattevi, M. Acik, Y.J. Chabal, M. Chhowalla, V.B. Shenoy, Structural evolution during the reduction of chemically derived graphene oxide, Nature chemistry 2(7) (2010) 581-587.
[246] H. Wang, T. Maiyalagan, X. Wang, Review on recent progress in nitrogen-doped graphene: synthesis, characterization, and its potential applications, Acs Catalysis 2(5) (2012) 781-794.
[247] A. Dhakshinamoorthy, A. Primo, P. Concepcion, M. Alvaro, H. Garcia, Doped Graphene as a Metal-Free Carbocatalyst for the Selective Aerobic Oxidation of Benzylic Hydrocarbons, Cyclooctane and Styrene, Chemistry-A European Journal 19(23) (2013) 7547-7554.

[248] P.M. Barna, Carbohydrate Phosphorylation with Phosphoric Acid, Polyphosphoric Acid, Pyrophosphoric Acid, and Anhydrous Phosphoric Acid, Synthetic Communications 1(3) (1971) 207-214.
[249] S. Iijima, T. Ichihashi, Single-shell carbon nanotubes of 1-nm diameter, nature 363(6430) (1993) 603-605.
[250] V. Georgakilas, J.A. Perman, J. Tucek, R. Zboril, Broad family of carbon nanoallotropes: classification, chemistry, and applications of fullerenes, carbon dots, nanotubes, graphene, nanodiamonds, and combined superstructures, Chemical reviews 115(11) (2015) 4744-4822.
[251] J. Prasek, J. Drbohlavova, J. Chomoucka, J. Hubalek, O. Jasek, V. Adam, R. Kizek, Methods for carbon nanotubes synthesis, Journal of Materials Chemistry 21(40) (2011) 15872-15884.
[252] C. Journet, W.K. Maser, P. Bernier, A. Loiseau, Large-scale production of single-walled carbon nanotubes by the electric-arc technique, Nature 388(6644) (1997) 756.
[253] T.W. Ebbesen, A. P M, Large-scale synthesis of carbon, Nature 358 (1992) 16.
[254] J.L. Hutchison, N.A. Kiselev, E.P. Krinichnaya, A.V. Krestinin, R.O. Loutfy, A.P. Morawsky, V.E. Muradyan, E.D. Obraztsova, J. Sloan, S.V. Terekhov, Double-walled carbon nanotubes fabricated by a hydrogen arc discharge method, Carbon 39(5) (2001) 761-770.
[255] T. Sugai, H. Yoshida, T. Shimada, T. Okazaki, H. Shinohara, S. Bandow, New synthesis of high-quality double-walled carbon nanotubes by high-temperature pulsed arc discharge, Nano letters 3(6) (2003) 769-773.
[256] T. Guo, P. Nikolaev, A. Thess, D.T. Colbert, R.E. Smalley, Catalytic growth of single-walled manotubes by laser vaporization, Chemical physics letters 243(1) (1995) 49-54.

[257] S.A. Steiner Iii, T.F. Baumann, B.C. Bayer, R. Blume, M.A. Worsley, W.J. MoberlyChan, E.L. Shaw, R. Schlögl, A.J. Hart, S. Hofmann, Nanoscale zirconia as a nonmetallic catalyst for graphitization of carbon and growth of single-and multiwall carbon nanotubes, Journal of the American Chemical Society 131(34) (2009) 12144-12154.
[258] A. Szabó, C. Perri, A. Csató, G. Giordano, D. Vuono, J.B. Nagy, Synthesis methods of carbon nanotubes and related materials, Materials 3(5) (2010) 3092-3140.
[259] Z. Liu, L. Jiao, Y. Yao, X. Xian, J. Zhang, Aligned, Ultralong Single-walled carbon nanotubes: from synthesis, sorting, to electronic devices, Advanced Materials 22(21) (2010) 2285-2310.
[260] J.P. Tessonnier, M. Becker, W. Xia, F. Girgsdies, R. Blume, L. Yao, D.S. Su, M. Muhler, R. Schlögl, Spinel-type cobalt-manganese-based mixed oxide as sacrificial catalyst for the high-yield production of homogeneous carbon nanotubes, ChemCatChem 2(12) (2010) 1559-1561.
[261] D.S. Su, X.W. Chen, Natural lavas as catalysts for efficient production of carbon nanotubes and nanofibers, Angewandte Chemie International Edition 46(11) (2007) 1823-1824.
[262] M. Endo, K. Takeuchi, Y.A. Kim, K.C. Park, T. Ichiki, T. Hayashi, T. Fukuyo, S. Iinou, D.S. Su, M. Terrones, Simple synthesis of multiwalled carbon nanotubes from natural resources, ChemSusChem 1(10) (2008) 820-822.
[263] Q. Zhang, J.Q. Huang, M.Q. Zhao, W.Z. Qian, F. Wei, Carbon nanotube mass production: principles and processes, ChemSusChem 4(7) (2011) 864-889.
[264] S. Wang, E. Iyyamperumal, A. Roy, Y. Xue, D. Yu, L. Dai, Vertically Aligned BCN Nanotubes as Efficient Metal-Free Electrocatalysts for the Oxygen Reduction Reaction: A Synergetic Effect

by Co-Doping with Boron and Nitrogen, Angewandte Chemie International Edition 50(49) (2011) 11756-11760.
[265] N. Ishigami, H. Ago, Y. Motoyama, M. Takasaki, M. Shinagawa, K. Takahashi, T. Ikuta, M. Tsuji, Microreactor utilizing a vertically-aligned carbon nanotube array grown inside the channels, Chemical Communications (16) (2007) 1626-1628.
[266] I. Florea, O. Ersen, R. Arenal, D. Ihiawakrim, C.d. Messaoudi, K. Chizari, I. Janowska, C. Pham-Huu, 3D analysis of the morphology and spatial distribution of nitrogen in nitrogen-doped carbon nanotubes by energy-filtered transmission electron microscopy tomography, Journal of the American Chemical Society 134(23) (2012) 9672-9680.
[267] D. Golberg, Y. Bando, Y. Huang, T. Terao, M. Mitome, C. Tang, C. Zhi, Boron nitride nanotubes and nanosheets, ACS nano 4(6) (2010) 2979-2993.
[268] S.-W. Bian, Z. Ma, W.-G. Song, Preparation and characterization of carbon nitride nanotubes and their applications as catalyst supporter, The Journal of Physical Chemistry C 113(20) (2009) 8668-8672.
[269] X. Zhou, B. Jin, L. Li, F. Peng, H. Wang, H. Yu, Y. Fang, A carbon nitride/TiO_2 nanotube array heterojunction visible-light photocatalyst: synthesis, characterization, and photoelectrochemical properties, Journal of Materials Chemistry 22(34) (2012) 17900-17905.

Chapter 3 One-pot synthesis of N-doped graphene for metal-free advanced oxidation processes

Abstract

Recently graphene and its derivatives as novel metal-free materials have attracted considerable attention in environmental remediation technologies. One of the barriers to practical applications is the mass production of high quality graphene-based catalysts. In this study, high-quality nitrogen-doped graphene (NG) nanomaterials were synthesized by controlled pyrolysis of a mixture of glucose, ferric chloride and urea. Glucose serves as a carbon precursor, urea as a nitrogen precursor, and hexahydrate ferric chloride as both a template and a catalyst. It was found that a low oxygen level of 2-4 at% and a nitrogen doping level of 0.5-1.8 at% were achieved at a moderate temperature. The obtained nitrogen-doped graphene was employed as a metal-free catalyst for efficient phenol degradation by peroxymonosulfate (PMS) activation. Kinetic studies showed that the phenol degradation facilitated by NG catalysis followed first-order reaction kinetics. Electron paramagnetic resonance (EPR) was performed to detect radical generation in order to reveal the mechanism of PMS activation processes and phenol degradation pathways on nanocarbons. It was found that both •OH and $SO_4^{\bullet -}$ *were produced in the catalytic oxidation processes and played significant roles in phenol oxidation.*

3.1 Introduction

Organic pollutants like phenolic compounds and dyes in wastewater, caused by alarmingly growth of population and rapid development of urbanization and industrialization, have received great public concerns due to their toxicity and resistance to natural degradation. Therefore, effective measures and technologies are required to be employed to completely remove such organics from the eco-system.[1-3] Among various water treatment technologies that can address this environmental challenge, advanced oxidation processes (AOPs) have been widely used because they can effectively and completely decompose different types of pollutants.[4] Fenton reaction is one of typical AOPs that have been demonstrated to be highly effective in complete removal of pollutants by producing hydroxyl radicals (•OH). Recently, sulfate radicals ($SO_4^{\bullet-}$) have been discovered as an excellent alternative to hydroxyl radicals (•OH) due to their higher oxidation potential and the flexible pH range.[5, 6] Cobalt-, manganese- and iron-based catalysts have been extensively applied for activation of PMS to produce sulfate radicals.[1, 7-9] However, metal-based catalysts are expensive and the associated metal leaching can lead to secondary contamination to water bodies, resulting in several health and environmental problems.[10, 11] Therefore, metal-free, green catalysts are highly desirable as promising alternatives to conventional metal-based catalysts for environmental remediation.[12]

Graphene, a two-dimensional structure of sp^2-hybridized carbon atoms arranged in a hexagonal crystalline ring, has demonstrated superior metal-free catalysis.[13] The interest in graphene and graphene-based materials stems from their distinctive physicochemical properties, particularly the exceptionally electron and thermal mobility, high surface

area, and mechanical strength.[14] These superb properties have triggered extensive applications in a variety of fields such as solar cells,[15] lithium ion batteries,[16] biosensors,[17] and supercapacitors.[18] Recent studies have demonstrated that chemically reduced graphene oxide (rGO) can be employed as a metal-free catalyst to activate PMS in water decontamination.[12]

Doping the carbon network of graphene with adventitious heteroatoms (e.g., N, B and P) introduces new active sites, increases the electrical conductivity as well as notably enhances catalytic activity of graphene.[19, 20] The doped graphene promises many fascinating properties.[21-23] Wei and co-workers synthesized N-doped graphene by a chemical vapor deposition (CVD) method and observed an n-type behavior indicating that substitutional doping can effectively modulate the electrical properties of graphene.[24] Yang et al. reported that N- and S-codoped graphene sheets via a thermal preparation method demonstrated a good electrocatalytic activity, long durability and high selectivity in metal-free oxygen reduction reactions.[25] In environmental remediation, the authors proved that modification of rGO [26] and pristine multi-walled carbon nanotubes (MWCNTs)[27] with nitrogen atoms using ammonium nitrate as the N precursor can dramatically boost the performance of PMS activation. N-doped graphene synthesized by directly annealing graphene oxide with a novel nitrogen precursor of melamine also showed an excellent efficiency in degradation of phenol solutions.[28]

A number of preparation methods, such as micromechanical exfoliation of graphite, CVD, oxidation-reduction method, pyrolysis or calcination methods, have been developed to produce graphene.[29, 30] The popular

Hummers' method has been restricted by the energy-intensive, complex procedures and the employment of strong acids and oxides.[31] Large scale fabrication of high-quality graphene products is still a challenging task. Meanwhile, nitrogen-doped nanoporous carbon can be achieved by treating the carbon materials either with ammonia gas/air or nitrogen-containing carbon precursors, such as melamine, polyacrylonitrile, polyvinylpyridine, and quinolone-containing pitch.[32] However, simultaneous carbonization and nitrogen doping for preparation of nitrogen-doped graphene has been less explored. Therefore, development of high-quality nitrogen-doped graphene sheets is tremendously desirable for metal-free remediation.

In this chapter, we report the scalable production of high-quality nitrogen-doped graphene sheets using one-pot pyrolysis of a mixture of glucose, ferric chloride and urea. The prepared graphene materials were able to serve as an excellent metal-free catalyst to activate PMS for catalytic oxidation of organic pollutants in water, providing a promising green material for environmental remediation.

3.2 Experimental

Materials and Chemicals. D-glucose, urea, hexahydrate ferric chloride ($FeCl_3 \cdot 6H_2O$) and potassium peroxymonosulfate ($2KHSO_5 \cdot 3KHSO_4 \cdot K_2SO_4$, Oxone) were purchased from Sigma-Aldrich. Acetone and hydrochloric acid (32%) were obtained from Chem-Supply. Phenol was obtained from Ajax Finechem. Ultrapure water was used in all of the experiments.

Synthesis of Nitrogen-doped Graphene (NG). In a typical procedure, 3 g glucose, 3 g $FeCl_3 \cdot 6H_2O$ and a certain amount of urea were dissolved in 10 mL water in a crucible. A yellow colored solution was vaporized at 80 ℃ in air and further dried in an oven for 24 h, and then a black solid was obtained. The solid was then calcined in a quartz tube furnace at 700 ℃ for 6 h under a nitrogen flow of 50 mL min^{-1}. After cooling down to room temperature, the sample was placed in a beaker containing 100 mL hydrochloric acid with magnetic stirring for 6 h to remove iron. The solid sample was washed in succession with ultrapure water and acetone for several times. Finally, the sample was dried in an oven at 60 ℃ overnight to obtain NG-10 (10% mass ratio of urea in the mixture) and NG-20 (20% mass ratio of urea in the mixture), respectively. NG was prepared with the same amount of $FeCl_3 \cdot 6H_2O$ and urea without any glucose while CG (C-graphene) was prepared with the same amount of $FeCl_3 \cdot 6H_2O$ and glucose but without any urea.

Characterization of Materials. X-ray diffraction (XRD) patterns were acquired on a Bruker D8-Advanced X-ray instrument using a Cu-Kα radiation with λ at 1.5418 Å. Nitrogen sorption isotherms were obtained on a Tristar II 3020 after degassing the samples at 110 ℃ for 4 h. The Brunauer-Emmett-Teller (BET) equation and the Barrett-Joyner-Halenda (BJH) method were utilized to evaluate the specific surface area and the pore size distribution of the samples, respectively. Fourier transform infrared (FTIR) spectra were obtained from a Bruker instrument with an ATR correction mode. X-ray photoelectron spectroscopy (XPS) was carried out to determine the chemical states of elements using a Thermo Escalab 250 with Al-Kα X-ray. Thermogravimetric-differential thermal analysis (TG-DTA) was carried out by heating the samples in an air flow at a rate of 100 mL min^{-1} using a Perkin-Elmer Diamond TGA/DTA

thermal analyzer with a heating rate of 10 ℃ min^{-1}. Scanning electron microscopy (SEM) was applied to investigate the morphology of the catalysts using a Zeiss Neon 40 EsB FIBSEM. Raman analysis was performed on an ISA dispersive Raman spectrometer using argon ion laser (514 nm). Electron paramagnetic resonance (EPR) spectra were obtained on a Bruker EMS-plus to detect the free radicals generated during activation of PMS and oxidation of phenol solutions.

Catalytic Oxidation of Phenol Solutions. The catalytic oxidation of phenol was carried out in a 500 mL conical flask with phenol solution (20 ppm), the catalyst (0.2 g L^{-1}) and PMS (2.0 g L^{-1}) in a constant-temperature controlled water bath for the kinetic studies. At each time interval, 1 mL solution was withdrawn by a syringe, filtered by a 0.45 mm Millipore film, and injected into a vial. Then 0.5 mL of methanol as a quenching reagent was immediately injected into the reaction solution. The mixed solution was analyzed by a high performance liquid chromatograph (HPLC, Varian) with a C-18 column and a UV detector set at 270 nm.

Mechanistic Studies of the Catalytic Processes. An EMS-plus EPR instrument from Bruker was employed to detect the free radicals captured by 5,5-dimethyl-1-pyrroline (DMPO, ＞ 99.0%) during PMS activation, operating under the following conditions: centre field, 3515 G; sweep width, 100 G; microwave frequency, 9.87 GHz; power setting, 18.75 mW; scan number, 3. The radical quantitative information was acquired from the Spin Fitting from Bruker Xenon Software Package.

3.3 Results and Discussion

The crystallographic structures of the samples were examined by XRD analysis. Figure 3.1 shows XRD patterns of the graphene-based materials. Strong and sharp peaks at around 26° and weak peaks at 43° emerged in all the four samples, corresponding to the (002) and (100) reflections of hexagonal graphitic carbon, respectively.[33] The pronounced (002) peak at 26° (2θ) for CG was also observed for nitrogen-doped graphene, confirming the formation of graphene structure. The broad background band centred at 26° can be attributed to the presence of intercalated "N defects" in the nitrogen-doped graphene structure.[34] The intensities of the peaks on CG and NG were much stronger than those of previous studies, demonstrating that this novel synthesis can produce high-quality graphene as well as its derivatives.

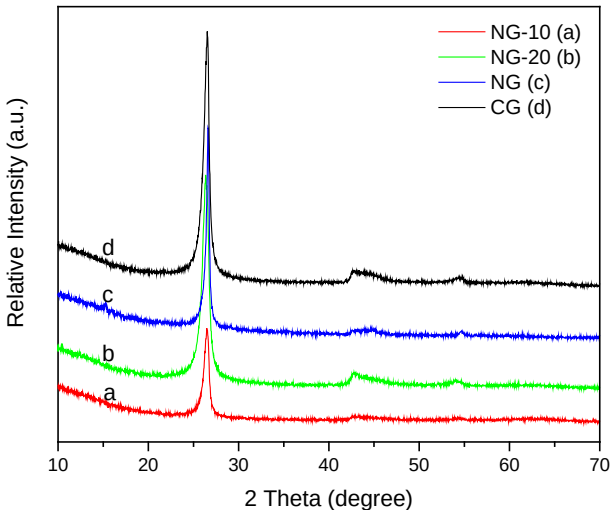

Figure 3.1 XRD patterns of NG-10, NG-20, NG and CG samples.

Raman spectroscopy is a powerful technique for the investigation of the degree of graphitization, number of layers and doping status of graphene.[35] The G-band gives the evidence for the existence of sp^2-

hybridized carbon atoms, while the D-band demonstrates defects such as disorders, edges and boundaries of the carbon framework. The 2D-band provides information on the number of layers of the graphene materials.[36] Raman spectra of CG and N-graphene are displayed in Figure 3.2. The characteristic D band (1319 cm^{-1}), G band (1570 cm^{-1}) and 2D band (2647 cm^{-1}) were observed. The intensity ratios of D band to G band (I_D/I_G) can be used to evaluate the structural disorder and defect of graphitic carbon materials. The I_D/I_G values of NG-10, NG-20, NG and CG were estimated to be 0.947, 1.332, 1.015 and 1.044, respectively. Based on Raman results, it could be concluded that the defective degree of NG-20 was higher than NG-10 and CG, possibly due to the great interruption caused by the incorporation of nitrogen atoms to the well-ordered sp^2-hybridized and curved honeycomb nanosheets.[37] The strong D band indicated that N-doping would

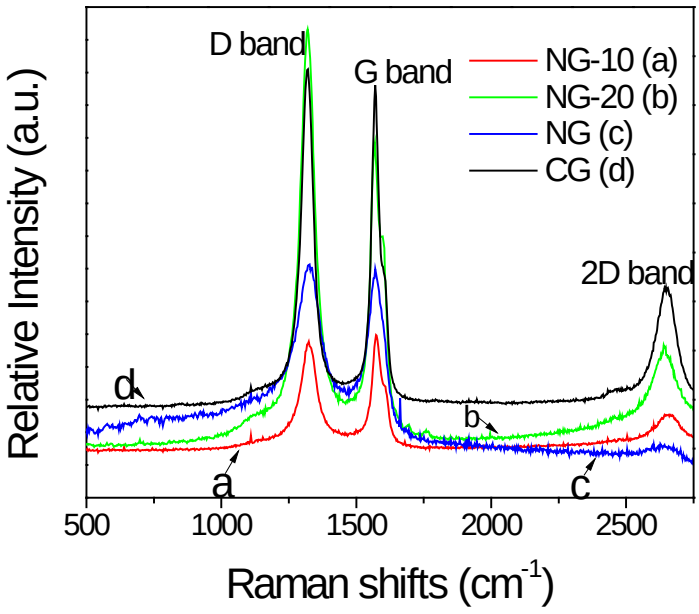

Figure 3.2 Raman spectra of NG-10, NG-20, NG and CG

significantly enhance the defect density. However, the I_D/I_G value of NG-10 was a bit lower than CG because of low nitrogen doping level of NG-10, indicating a minor effect of nitrogen doping on the defective degree and no significant change of sp^2 carbon network of the NG-10 by nitrogen modification. The I_D/I_G values of NG and CG are much lower than that of a typical rGO (1.48) [12] and nitrogen-doped graphene prepared by annealing GO with melamine (1.34) [28] or ammonium nitrate (1.41) [38], wherein GO was prepared by the Hummers' method. This indicated that the CG and NG prepared in this study are of a high quality with fewer defects.

Figure 3.3(a) shows N_2 adsorption/desorption isotherms and pore size distributions of NG-10, NG-20, NG and CG materials. According to the IUPAC classification, all of the samples presented type IV isotherms with a type III hysteresis loop, indicating the presence of typical mesoporous structures.[32] As seen, the samples displayed distinct hysteresis loops at the relative pressure range (P/P_0) of 0.45 to 0.95 and a moderate increase at low relative pressure. However, the hysteresis loop on NG was narrower than those of the other three samples, suggesting a less porous structure and thus lower surface area and pore volume.[39] The detailed textural properties can be seen in Table 3.1.

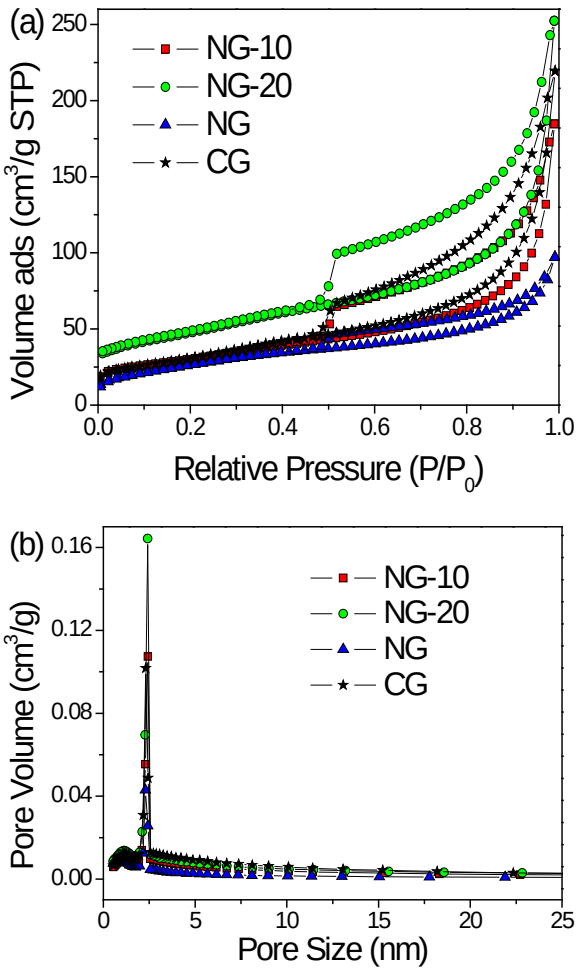

Figure 3.3 (a) N_2 adsorption/desorption isotherms and (b) pore size distributions of NG-10, NG-20, NG and CG.

The pore size distributions of the obtained materials are shown in Figure 3.3(b). All the four samples displayed a similar mesopore size distribution, i.e., a single modal pore diameter distribution centered at around at 2.3-2.4 nm was observed for each sample, demonstrating that urea or glucose was not the key parameter in determining the pore structure.

Table 3.1 summarizes the sorption results of NG-10, NG-20, NG and CG. The SSA of CG was 112.5 m^2/g, slightly higher than NG-10 of

106.4 m^2/g. After increasing urea content to 20%, the SSA value of NG-20 was enhanced to 165.8 m^2/g, higher than NG and CG. However, the SSA of NG decreased to some extent, which might be owing to (i) the less spaces between layered hierarchical structures grown on the surfaces, and (ii) lower exfoliation degree induced by the reduction/annealing processes with large amount of urea, in consistent with the highly disorientated and crinkled structure observed in the SEM (shown later).

Table 3.1 Textural properties of NG-10, NG-20, NG and CG samples

	BET surface area, m^2/g	Pore volume, cm^3/g	Average pore size, nm
NG-10	106.4	0.21	6.0
NG-20	165.8	0.28	5.7
NG	99.3	0.10	4.4
CG	112.5	0.26	6.1

Figure 3.4 demonstrates FTIR of the obtained four samples. None of them showed strong signals, indicating that no high level of oxygen containing species, such as carboxylic (COOH), carbonyl (C=O) and hydroxyl groups exist. This observation can be confirmed by XPS spectra. Meanwhile, no nitrogen related peaks were found in the FTIR spectra of NG, indicating that nitrogen has been incorporated into graphene.

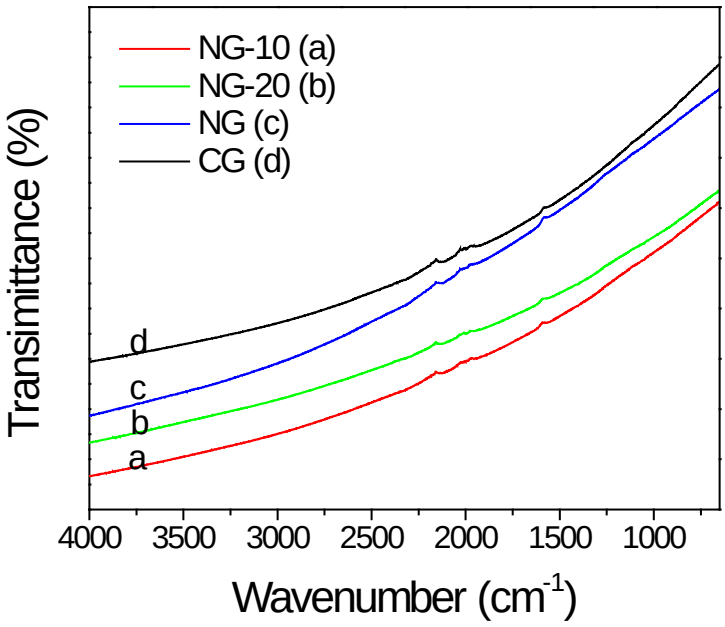

Figure 3.4 FTIR spectra of NG-10, NG-20, NG and CG.

The thermal behaviors of all the four samples were investigated by TGA-DSC. The curves are presented in Figure 3.5 (a) and (b), respectively. The analysis was performed in air at a heating rate of 10 ^{o}C min^{-1}. Figure 3.5 (a) indicates that there are three regions in the NG weight loss process. First, a minor weight loss occurs from room temperature to about 300 ^{o}C which may be due to the evaporation of adsorbed water molecules. Second, a minor weight loss occurs from 300 to 500 ^{o}C which can be attributed to the removal of residual oxygenated functional groups generating CO_2 and H_2O, and the DSC curve also shows a characteristic step or peak at 431 ^{o}C. Finally, a major weight loss can be observed between 500 and 680 ^{o}C. The TGA and DSC curves show a characteristic step or strong exothermal peak at 598 ^{o}C due to the carbon combustion and decomposition. No further weigh loss of NG can be observed after 680 ^{o}C. The weight loss was determined to be stabilized at 7% after 688 ^{o}C, indicating the complete combustion of carbon and

oxidation of iron with a final product of iron compound.[38] The iron compound was hard to be removed by hydrochloric acid, in good agreement with the XPS result.[40]

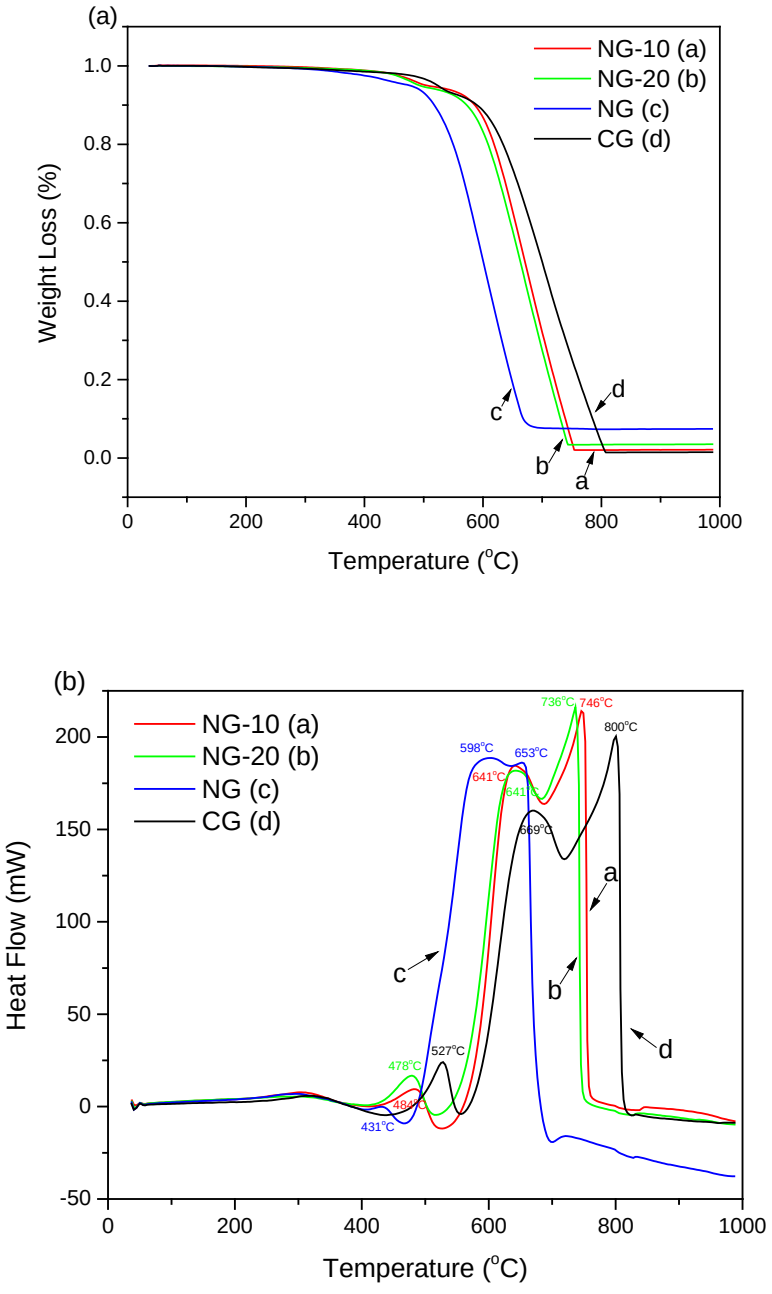

Figure 3.5 TGA (a) and DSC (b) curves of NG-10, NG-20, NG and CG.

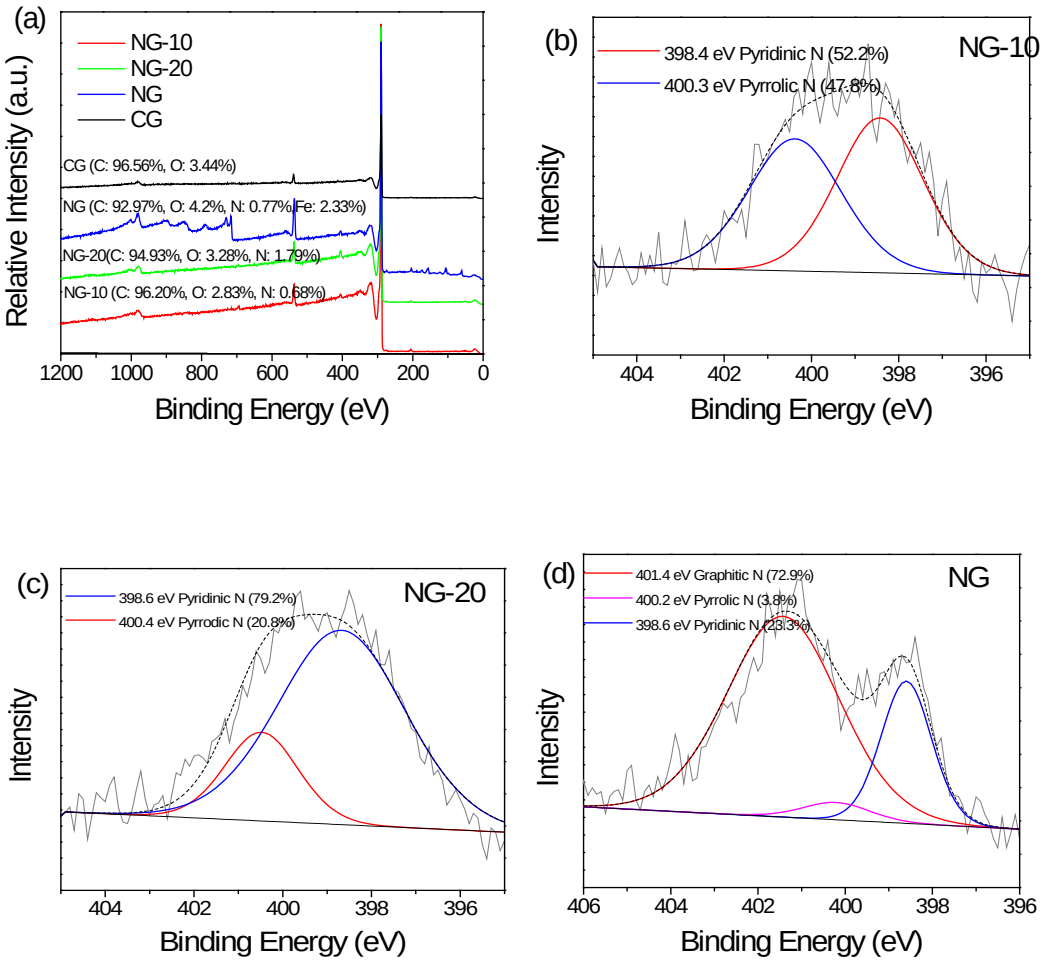

Figure 3.6 XPS surveys of NG-10, NG-20, NG and CG samples (a) and N 1s scan of NG-10 (b), NG-20 (c) and NG (d).

XPS studies were carried out to give insights into the composition and chemical states of the prepared graphene materials. Figure 3.6 (a) shows that on CG, only carbon and oxygen were detected, and oxygen exists at a very low ratio of 3.44 at%, which was consistent with the FTIR results in Figure 4. The oxygen levels were subsequently reduced to 2.83 and 3.28 at% after nitrogen doping but increased to 4.2 at% with the substitution of glucose by urea, partially due to the introduction of NO_x species. The oxygen contents in these four samples were much lower than those of rGO (14.44 at%)[12] and N-rGO (11.53 at%) derived from

reduction of graphite oxide,[26] suggesting that this novel method can generate high-quality graphene and graphene-based materials with low oxygen levels. NG-10 and NG-20 also demonstrate a low ratio of oxygen and increasing level of nitrogen. It was reported that carbocyclic and lactone groups begin to decompose into CO_2 at about 250 ^oC, whereas carbonyl and –COOH groups would turn into CO and CO_2 above 450 ^oC.[38] Thus, these surface oxygen groups would function as the active sites to react with urea to form C-N bond and dope nitrogen into graphene layers.

The nitrogen levels of NG-10, NG-20 and NG were determined to be 0.68, 1.79, and 0.77 at%, respectively. The doping level is similar to N-CNT[27] but not comparable to that of in-situ doping because the nitrogen doping levels will decrease significantly when the calcination temperature is above 500 ^oC, which will break C-N bonds and remove the nitrogen from NG. The relatively low doping levels in comparison with that of N-rGO (5.61 at%) were also ascribed to the highly stable structure of these graphene sheets, in consistent with the results of TGA in Figure 3.5.[26]

The high resolution XPS N 1s spectrum of NG was fitted into three peaks with binding energies at 401.4, 400.2 and 398.6 eV, corresponding to the graphitic (or quaternary) , pyrrolic, and pyridinic N, respectively.[41] Substitutional nitrogen doping was achieved at a portion of 72.9% in the overall nitrogen dopants, much higher than that in N-CNT (16.0%) and NG-700 (22.5%). On the other hand, only pyridinic and pyrrolic nitrogen species were found in NG-10 and NG-20 because low content of precursors might only lead to surface modification and thus nitrogen was not able to integrate into the interior

of graphene sheets and was only located at the defective sites. It was well established that greater nitrogen doping can produce more graphitic nitrogen in the carbon network.

It can be seen that graphitic N increases with the nitrogen precursor but pyrrolic N decreases, which may be attributed to that graphitic N is more stable than the pyrrolic N into the carbon lattice during the construction of graphene sheets under annealing. The high content of graphitic N in NG indicated that nitrogen was able to incorporate into the graphitic carbon framework, thus change the NG structure.

XPS also suggested that 2.33 at% Fe existed in NG, proving that some iron compound was not completely removed by acid, which was in good agreement with TGA results in Figure 3.5 (a). In addition, the detected Fe loading was lower than that from TGA, indicating that partial iron was encapsulated into carbon. Therefore, it is difficult to remove the Fe species encapsulated in carbon with the common way, such as ball-milling and leaching in hot acid solution because they are protected by clingy graphitic layers.[40]

Figure 3.7 shows SEM images of graphene and various N-graphene samples. It was found that many exfoliated layers and several stacked layers were observed in CG.[12] After the nitrogen doping process, graphene were broken down and the morphology was changed remarkably. Disordered exfoliated layers and partially aggregated and crinkled structures were obtained in NG. This further indicated that high content of nitrogen precursor is able to incorporate nitrogen into the graphitic carbon framework. The bulk structure of the NG was altered

because nitrogen atoms were located not only at the defective sites of the graphene sheets, but also integrated into the interior of graphene sheets.

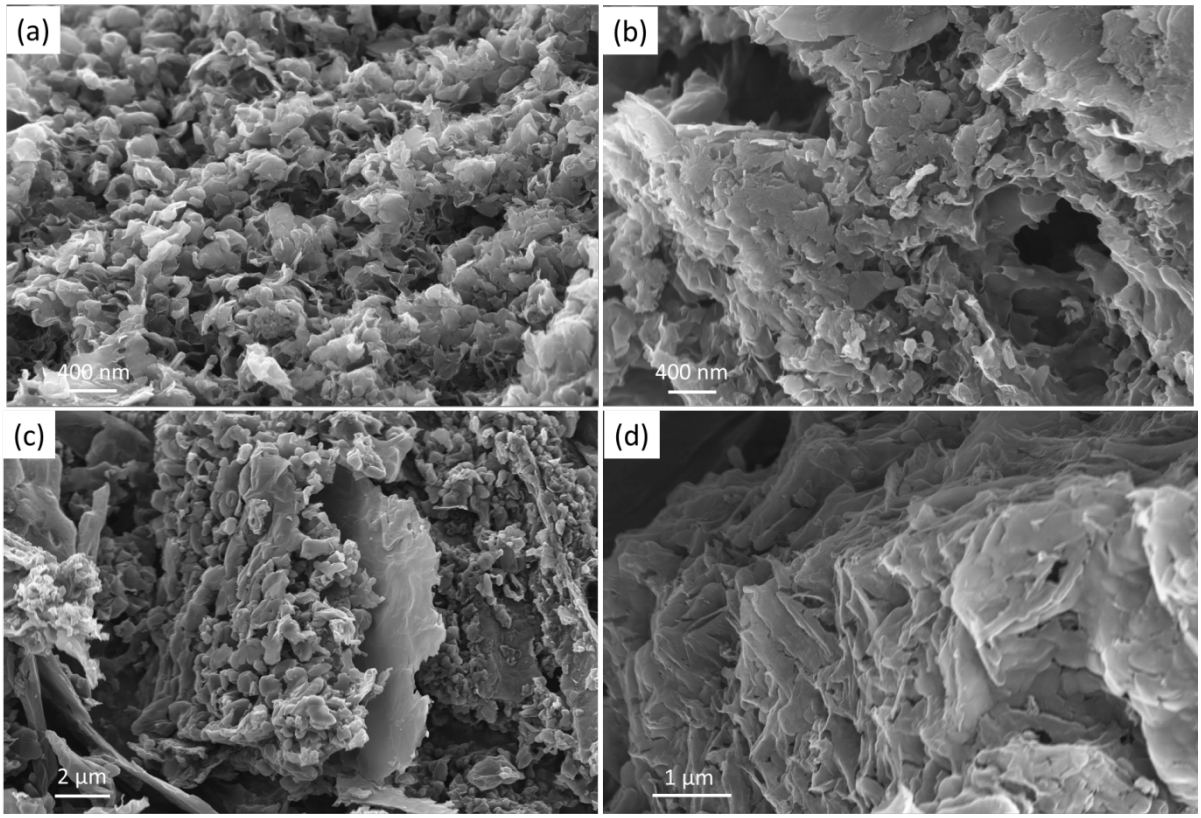

Figure 3.7 SEM images of (a) NG-10, (b) NG-20, (c) NG and (d) CG

The catalytic activities of various carbocatalysts were investigated in catalytic activation of PMS for phenol oxidation in aqueous solutions. Figure 3.8 (a) shows that PMS itself can hardly generate active radicals to degrade phenol without a solid catalyst and only 6% phenol was removed, indicating that PMS cannot be effectively activated by ambient temperature to produce sulfate radicals. Meanwhile, without the addition of PMS, only around 4% phenol was removed by the adsorption of NG. In addition, CG (undoped graphene) was not able to effectively activate PMS for the phenol oxidation reactions and only decomposed 56% phenol in 180 min. The performance of phenol degradation was

improved on NG-10 and NG-20, and 96% and 98% phenol removal efficiencies were achieved in 180 min, respectively. NG was able to completely degrade phenol in 90 min, exhibiting the best catalytic performance. NG was more efficient than the reduced graphene oxide (70.4%)[12] and multi-walled carbon nanotubes (76%)[27] respectively, within 180 min in previous studies, and comparable to sulfur and nitrogen co-doped graphene.[19]

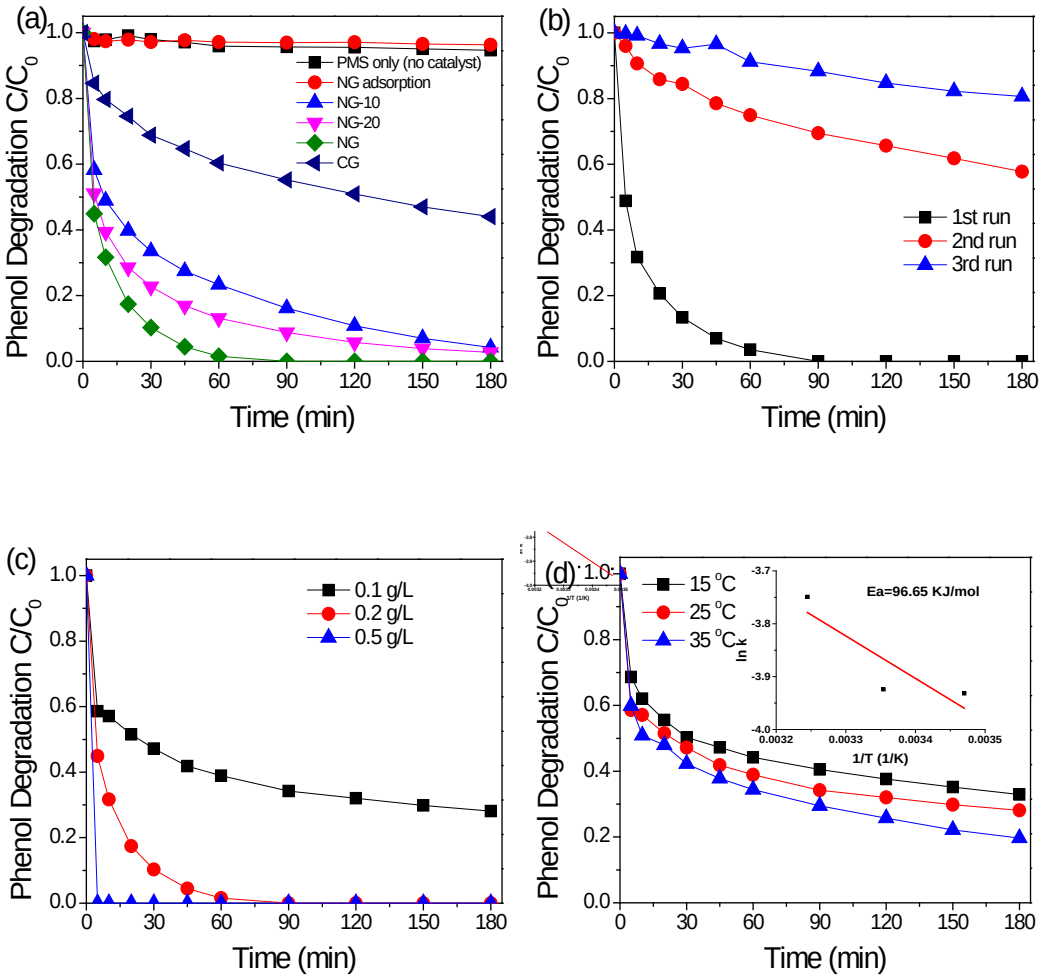

Figure 3.8 (a) Phenol degradation under various catalysts, (b) stability and recyclability studies of NG (catalyst: 0.2 g/L; PMS: 2 g/L; T: 25 °C), (c) effect of catalyst loading on phenol removal, and (d) effect of reaction temperature on phenol removal (catalyst = 0.1 g/L).

The results of all these four materials demonstrated that nitrogen doping exerts a more significant effect than SSA on the improved performance of phenol catalytic oxidation. NG has the lowest SSA (99.3 m^2 g^{-1}) but demonstrated a greater enhancement in catalytic performance. This strongly suggested that nitrogen doping may play a dominant role in the catalytic performance of nitrogen-doped materials prepared by this simple and green method. The doped nitrogen would change the electronic structure of carbon atoms nearby, and thus accelerate the electron transfer for the catalytic processes.

A pseudo-first-order reaction was applied for the estimation of the kinetic rates of graphene materials, as shown below:

$$\ln\left(\frac{C}{C0}\right) = -kt \qquad \text{(Eq. 3.1)}$$

The reaction rate constants (k) of phenol oxidation on NG-10, NG-20, NG and CG were estimated to be 0.032, 0.044, 0.071, and 0.011 min^{-1}, respectively. Upon nitrogen doping, NG-10, NG-20 and NG presented higher activities than CG without nitrogen doping. Meanwhile, NG showed the highest efficiency among all the materials, which were 2.2, 1.6 and 6.5 folds higher than that of NG-10, NG-20 and CG, respectively.

Stability and reusability tests were also carried out on NG and are shown in Figure 3.8 (b). The fresh sample (first run) was able to completely decompose phenol in 90 min, and phenol removals at 42% and 20% were achieved in 180 min for the second and third runs, respectively. In a similar study, N-doped CNT decomposed 100% phenol in 20 min in

the first run, but removed 100% and 89% phenol in 120 and 180 min for the second and third runs. [37] In another study, around 58% and 31% of phenol was removed after 180 min in the second and third runs, respectively, compared to 100% decomposition of phenol in 45 min for the fresh catalyst[26]. In addition, rGO achieved complete decomposition of phenol in 150 min in the first run, yet only 58% and 25% phenol removal was achieved in 180 min for the second and third runs, respectively.[12] The deactivation of the catalyst might be ascribed to intricate influence of surface chemistry and structural changes, including the adsorption of intermediates, coverage of surface active sites, change of pore structures, and dopants re-fabrication in graphene network.

Figure 3.8 (c) shows the effect of catalyst loading on phenol oxidation. 100% phenol removal was achieved at only 5 and 90 min for 0.5 and 0.2 g/L NG, respectively. Meanwhile, 0.1 g/L NG only degraded 72% phenol in 180 min. Because of the minor adsorption on NG, the significant enhancement in the efficiency of phenol removal was attributed to the more active sites brought in by the increase of catalyst dosage to activate PMS.

The effect of solution temperature on PMS activation of NG is shown in Figure 3.8 (d). Unlike cobalt catalysis, a slight increase in phenol degradation efficiency was observed at elevated temperatures. To be specific, 67, 72 and 80% phenol were removed in 180 min at 15, 25 and 35 ^{o}C (catalyst loading 0.1 g/L), respectively. Generally, elevated temperature stimulates phenol adsorption and electron transfer to create more reactive radicals. The weak temperature dependence of carrier mobility has been suggested to be the instinct feature of NG. This might

be part of the reason that temperature can only slightly affect the catalytic reaction. The activation energy of NG for catalytic oxidation of phenol, based on the first order kinetics and determined by the Arrhenius equation, was calculated to be 96.6 kJ/mol, higher than NG-700 (18.6 kJ/mol)[28], N-CNT (36.0 kJ/mol)[37], and graphene (84.0 kJ/mol). [12]

Both the intricate electronic states and the spin culture of covalent carbon have been demonstrated to have a close correlation to the catalytic properties of nanocarbon materials.[12] PMS activation indeed relies on the electron transfer from the catalyst to PMS to break up the O_3SO-OH bond and generate active radicals. The abundant free-flowing electrons in the sp^2-hybridized graphene shell could present great potential to facilitate electron transport to HSO_5^- (PMS) to generate sulfate ($SO_4^{\bullet-}$) and hydroxyl ($\bullet$OH) radicals. [37] It was proposed that the active sites of nanocarbon materials in PMS can be sp^2 carbon, zigzag edges with unconfined π electrons, and electron rich-containing oxides such as ketonic and quinone groups(C=O) at the defect edges.[42, 43] Although a high percentage of Fe/FeO_x existed after pyrolysis before acid treatment, the majority of them were removed by strong and concentrated acid for many hours and washed by ultrapure water and acetone for several times until the solution had no color. In addition, phenol was a weak acid to activate FeO_x into iron ions and it could be concluded that the catalytic activity of NG is not contributed by iron species. The promoted catalytic performance of NG was possibly due to the sp^2 carbon by graphitic N doping and N atoms at the defective sites. In this study, a large portion of substitutional N doping (graphitic N) with a smaller covalent radius and higher electronegativity than C atom was achieved by a simple and green doping strategy. The proposed mechanism of PMS activation on NG is illustrated in Scheme 3.1. The

graphitic N induced electron transfer from adjacent carbon atoms to nitrogen, thus breaking the chemical inertness of the sp^2 carbon layer and altering the catalytic activity of graphene. The positively charged adjacent carbon atoms have greater potential to absorb HSO_5^- and break the O-O bond ($HO—SO_4^-$) to generate •OH and $SO_4^{\bullet-}$, which further degrade phenol to CO_2 and H_2O. [28]

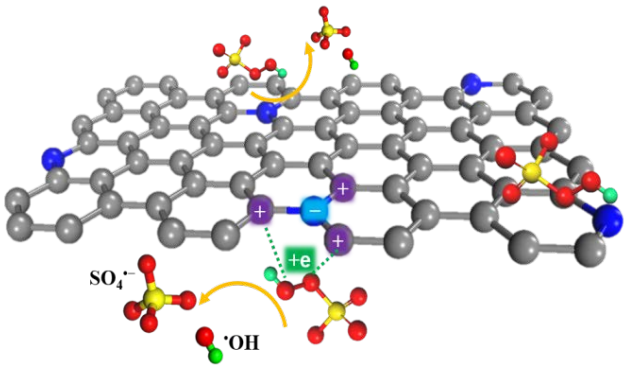

Scheme 3.1 Proposed mechanism of PMS activation on NG.

However, the much higher content of graphitic N in NG did not improve catalytic degradation greatly. It is reported that pyridinic and pyrrolic N dopants are much more active than oxygen-containing functional groups and they are the contributors to excellent catalytic activity of N-CNT.[27] The relatively good efficiency of NG-10 and NG-20 was attributed to the pyridinic and pyrrolic N atoms because no graphitic N was produced from XPS. NG, high in graphitic N but low in pyrrolic N, is not able to degrade phenol quickly, compared to NG-700 (100% degradation in 15 min) with 54.51% pyridinic N, 23.09% pyrrolic N and 22.49% graphitic N. [28] Therefore, it could be concluded that it may be the combined effect of graphitic N and pyrrolic N that determine the

efficiency of phenol degradation, with a dominant role of graphitic N because of its high charge density and asymmetric spin density.[44]

It was known that metal-based catalysts can activate PMS to generate both hydroxyl and sulfate radicals.[5] NG obtained a rapid phenol removal by PMS activation. Here, for better understanding the mechanism of PMS activation on NG, we employed electron paramagnetic resonance (EPR) to probe the generation and evolution of reactive radicals using DMPO as a radical spin trapping agent.

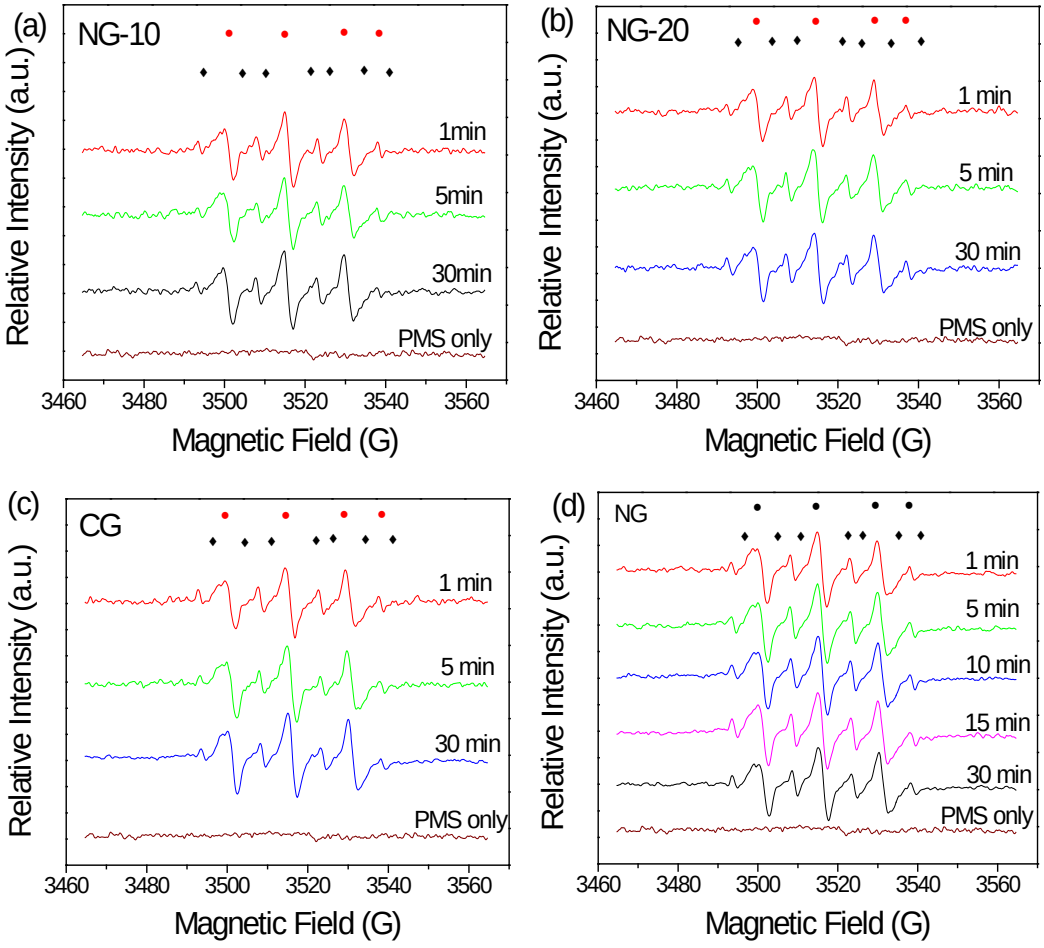

Figure 3.9 EPR spectra of DMPO adducts under different conditions (●: DMPO-OH;◆: DMPO-SO_4).

Radical generation is shown in Figures 3.9 at different reaction time (1, 5, and 30 min). It can be seen that very few active radicals were generated by PMS itself without a catalyst and NG had the ability to activate PMS effectively to generate both $SO_4^{\bullet-}$ and •OH all the time. At 1 min, •OH appeared as the major species, indicating that large quantity of •OH was produced initially and might play a critical role for phenol degradation in the first few minutes. Subsequently, phenol oxidation consumes •OH radicals and the amount decreased accordingly. A growth in •OH after 5 min was observed possibly because •OH generated by PMS accumulated. A similar trend was observed by $SO_4^{\bullet-}$ but with a relatively smaller scale. During the degradation reactions, $SO_4^{\bullet-}$ radicals were used for phenol oxidation. Figure 3.9 (d) shows more detailed evolution of reactive radicals on NG activation of PMS. From the EPR results, it can be proven that NG can effectively activate PMS to generate both sulfate and hydroxyl radicals, and the latter one plays a dominant role in catalytic phenol oxidation at the initial stage. It can be induced that both $SO_4^{\bullet-}$ and •OH function as reactive radicals to attack phenol during the oxidation processes. The reactions referring to the electron transfer processes facilitated by NG are shown below:

$$HSO_5^- + e^- \rightarrow OH^\bullet + SO_4^{2-} \quad \text{(Eq. 3.2)}$$

$$HSO_5^- + e^- \rightarrow OH^- + SO_4^{\bullet-} \quad \text{(Eq. 3.3)}$$

$$HSO_5^- - e^- \rightarrow H^+ + SO_5^{\bullet-} \quad \text{(Eq. 3.4)}$$

$$OH^\bullet + SO_4^{2-} \rightarrow SO_4^{\bullet-} + OH^- \quad \text{(Eq. 3.5)}$$

$$SO_4^{\bullet-} + OH^- \rightarrow SO_4^{2-} + OH^\bullet \quad \text{(Eq. 3.6)}$$

3.4 Conclusions

A green and feasible synthesis was developed to fabricate nitrogen-doped graphene with both structural and compositional modifications. This approach can produce both high-quality and a quantity of graphene without involving strong oxidants and acids. The prepared N-doped graphene has low oxygen content but relatively high nitrogen content. N-doped graphene presented an excellent performance in catalytic activation of PMS for phenol oxidation, and was superior to rGO from Hummers' method. Kinetic studies indicated that catalyst loading will influence the degradation efficiency, whereas the temperature showed a marginal effect. EPR spectra suggested that both $SO_4^{\bullet-}$ and •OH were generated during the activation and oxidation processes and played essential roles in phenol removal. This study offered an excellent metal-free catalyst for carbocatalysis and the induced energy and environmental applications. This green catalyst will contribute to the pursuit of an innovative remediation technology without secondary contamination, which will open a venue for the development of sustainable wastewater treatment.

References

[1] Y. Wang, H. Sun, H.M. Ang, M.O. Tadé, S. Wang, Synthesis of magnetic core/shell carbon nanosphere supported manganese catalysts for oxidation of organics in water by peroxymonosulfate, Journal of Colloid and Interface Science 433 (2014) 68-75.

[2] P. Shukla, H. Sun, S. Wang, H.M. Ang, M.O. Tadé, Co-SBA-15 for heterogeneous oxidation of phenol with sulfate radical for wastewater treatment, Catalysis Today 175(1) (2011) 380-385.

[3] X. Duan, H. Sun, J. Kang, Y. Wang, S. Indrawirawan, S. Wang, Insights into Heterogeneous Catalysis of Persulfate Activation on

Dimensional-Structured Nanocarbons, ACS Catalysis 5(8) (2015) 4629-4636.

[4] S. Wang, H. Sun, H.M. Ang, M.O. Tadé, Adsorptive remediation of environmental pollutants using novel graphene-based nanomaterials, Chemical Engineering Journal 226 (2013) 336-347.

[5] Y. Wang, H. Sun, X. Duan, H.M. Ang, M.O. Tadé, S. Wang, A new magnetic nano zero-valent iron encapsulated in carbon spheres for oxidative degradation of phenol, Applied Catalysis B: Environmental 172-173 (2015) 73-81.

[6] Y. Wang, H. Sun, H.M. Ang, M.O. Tadé, S. Wang, 3D-hierarchically structured MnO_2 for catalytic oxidation of phenol solutions by activation of peroxymonosulfate: Structure dependence and mechanism, Applied Catalysis B: Environmental 164 (2015) 159-167.

[7] Y. Yao, S. Miao, S. Liu, L.P. Ma, H. Sun, S. Wang, Synthesis, characterization, and adsorption properties of magnetic Fe_3O_4@graphene nanocomposite, Chemical Engineering Journal 184 (2012) 326-332.

[8] Y. Wang, S. Indrawirawan, X. Duan, H. Sun, H.M. Ang, M.O. Tadé, S. Wang, New insights into heterogeneous generation and evolution processes of sulfate radicals for phenol degradation over one-dimensional α-MnO_2 nanostructures, Chemical Engineering Journal 266 (2015) 12-20.

[9] Y. Wang, H. Sun, H.M. Ang, M.O. Tadé, S. Wang, Magnetic Fe_3O_4/carbon sphere/cobalt composites for catalytic oxidation of phenol solutions with sulfate radicals, Chemical Engineering Journal 245 (2014) 1-9.

[10] H. Sun, H. Liang, G. Zhou, S. Wang, Supported cobalt catalysts by one-pot aqueous combustion synthesis for catalytic phenol degradation, Journal of Colloid and Interface Science 394 (2013) 394-400.

[11] H. Sun, G. Zhou, S. Liu, H.M. Ang, M.O. Tadé, S. Wang, Nano-Fe^0 encapsulated in microcarbon spheres: synthesis, characterization, and environmental applications, ACS Applied Materials & Interfaces 4(11) (2012) 6235-6241.

[12] H. Sun, S. Liu, G. Zhou, H.M. Ang, M.O. Tadé, S. Wang, Reduced graphene oxide for catalytic oxidation of aqueous organic pollutants, ACS Applied Materials & Interfaces 4(10) (2012) 5466-5471.

[13] K.S. Novoselov, A.K. Geim, S.V. Morozov, D. Jiang, Y. Zhang, S.V. Dubonos, I.V. Grigorieva, A.A. Firsov, Electric field effect in atomically thin carbon films, Science 306(5696) (2004) 666-669.

[14] F. Perreault, A. Fonseca de Faria, M. Elimelech, Environmental applications of graphene-based nanomaterials, Chemical Society Reviews 44(16) (2015) 5861-5896.

[15] D.R. Kauffman, A. Star, Graphene versus carbon nanotubes for chemical sensor and fuel cell applications, Analyst 135(11) (2010) 2790-2797.

[16] E. Yoo, J. Kim, E. Hosono, H.-s. Zhou, T. Kudo, I. Honma, Large reversible Li storage of graphene Nanosheet Families for Use in Rechargeable Lithium Ion Batteries, Nano Letters 8(8) (2008) 2277-2282.

[17] Y. Wang, Y. Shao, D.W. Matson, J. Li, Y. Lin, Nitrogen-doped graphene and its application in electrochemical biosensing, ACS Nano 4(4) (2010) 1790-1798.

[18] L. Sun, L. Wang, C. Tian, T. Tan, Y. Xie, K. Shi, M. Li, H. Fu, Nitrogen-doped graphene with high nitrogen level via a one-step hydrothermal reaction of graphene oxide with urea for superior capacitive energy storage, RSC Advances 2(10) (2012) 4498-4506.

[19] X. Duan, K. O'Donnell, H. Sun, Y. Wang, S. Wang, Sulfur and nitrogen co-doped graphene for metal-Free catalytic oxidation reactions, Small 11(25) (2015) 3036-3044.
[20] D. Geng, S. Yang, Y. Zhang, J. Yang, J. Liu, R. Li, T.-K. Sham, X. Sun, S. Ye, S. Knights, Nitrogen doping effects on the structure of graphene, Applied Surface Science 257(21) (2011) 9193-9198.
[21] R.P. Rocha, J.P.S. Sousa, A.M.T. Silva, M.F.R. Pereira, J.L. Figueiredo, Catalytic activity and stability of multiwalled carbon nanotubes in catalytic wet air oxidation of oxalic acid: The role of the basic nature induced by the surface chemistry, Applied Catalysis B: Environmental 104(3–4) (2011) 330-336.
[22] Y. Zhou, K. Neyerlin, T.S. Olson, S. Pylypenko, J. Bult, H.N. Dinh, T. Gennett, Z. Shao, R. O'Hayre, Enhancement of Pt and Pt-alloy fuel cell catalyst activity and durability via nitrogen-modified carbon supports, Energy & Environmental Science 3(10) (2010) 1437-1446.
[23] S. Wang, L. Zhang, Z. Xia, A. Roy, D.W. Chang, J.-B. Baek, L. Dai, BCN graphene as efficient metal-free electrocatalyst for the oxygen reduction reaction, Angewandte Chemie International Edition 51(17) (2012) 4209-4212.
[24] D. Wei, Y. Liu, Y. Wang, H. Zhang, L. Huang, G. Yu, Synthesis of N-doped graphene by chemical vapor deposition and its electrical properties, Nano Letters 9(5) (2009) 1752-1758.
[25] S. Yang, L. Zhi, K. Tang, X. Feng, J. Maier, K. Müllen, Efficient synthesis of heteroatom (N or S)-Doped graphene based on ultrathin graphene oxide-porous silica sheets for oxygen reduction reactions, Advanced Functional Materials 22(17) (2012) 3634-3640.
[26] H. Sun, Y. Wang, S. Liu, L. Ge, L. Wang, Z. Zhu, S. Wang, Facile synthesis of nitrogen doped reduced graphene oxide as a superior metal-

free catalyst for oxidation, Chemical Communications 49(85) (2013) 9914-9916.

[27] H.Q. Sun, C. Kwan, A. Suvorova, H.M. Ang, M.O. Tade, S.B. Wang, Catalytic oxidation of organic pollutants on pristine and surface nitrogen-modified carbon nanotubes with sulfate radicals, Applied Catalysis B-Environmental 154 (2014) 134-141.

[28] X. Duan, Z. Ao, H. Sun, S. Indrawirawan, Y. Wang, J. Kang, F. Liang, Z.H. Zhu, S. Wang, Nitrogen-doped graphene for generation and evolution of reactive radicals by metal-free catalysis, ACS Applied Materials & Interfaces 7(7) (2015) 4169-4178.

[29] K.S. Novoselov, V.I. Falko, L. Colombo, P.R. Gellert, M.G. Schwab, K. Kim, A roadmap for graphene, Nature 490(7419) (2012) 192-200.

[30] S. Park, R.S. Ruoff, Chemical methods for the production of graphenes, Nat Nano 4(4) (2009) 217-224.

[31] W.S. Hummers, R.E. Offeman, Preparation of Graphitic Oxide, Journal of the American Chemical Society 80(6) (1958) 1339-1339.

[32] X. Huang, Q. Wang, X.Y. Chen, Z.J. Zhang, N-doped nanoporous carbons for the supercapacitor application by the template carbonization of glucose: The systematic comparison of different nitridation agents, Journal of Electroanalytical Chemistry 748 (2015) 23-33.

[33] K.F. Babu, B. Rajagopalan, J.S. Chung, W.M. Choi, Facile synthesis of graphene/N-doped carbon nanowire composites as an effective electrocatalyst for the oxygen reduction reaction, International Journal of Hydrogen Energy 40(21) (2015) 6827-6834.

[34] L. Qu, Y. Liu, J.-B. Baek, L. Dai, Nitrogen-doped graphene as efficient metal-free electrocatalyst for oxygen reduction in fuel cells, ACS Nano 4(3) (2010) 1321-1326.

[35] A.C. Ferrari, J.C. Meyer, V. Scardaci, C. Casiraghi, M. Lazzeri, F. Mauri, S. Piscanec, D. Jiang, K.S. Novoselov, S. Roth, A.K. Geim, Raman spectrum of graphene and graphene layers, Physical Review Letters 97(18) (2006) 187401.

[36] B. Zhang, J. Song, G. Yang, B. Han, Large-scale production of high-quality graphene using glucose and ferric chloride, Chemical Science 5(12) (2014) 4656-4660.

[37] X. Duan, H. Sun, Y. Wang, J. Kang, S. Wang, N-doping-induced nonradical reaction on single-walled carbon nanotubes for catalytic phenol oxidation, ACS Catalysis 5(2) (2015) 553-559.

[38] S. Indrawirawan, H. Sun, X. Duan, S. Wang, Low temperature combustion synthesis of nitrogen-doped graphene for metal-free catalytic oxidation, Journal of Materials Chemistry A 3(7) (2015) 3432-3440.

[39] Y. Wang, H. Sun, H.M. Ang, M.O. Tadé, S. Wang, Facile synthesis of hierarchically structured magnetic $MnO_2/ZnFe_2O_4$ hybrid materials and their performance in heterogeneous activation of peroxymonosulfate, ACS Applied Materials & Interfaces 6(22) (2014) 19914-19923.

[40] G. Zhong, H. Wang, H. Yu, F. Peng, Nitrogen doped carbon nanotubes with encapsulated ferric carbide as excellent electrocatalyst for oxygen reduction reaction in acid and alkaline media, Journal of Power Sources 286 (2015) 495-503.

[41] T. Horikawa, N. Sakao, T. Sekida, J.i. Hayashi, D.D. Do, M. Katoh, Preparation of nitrogen-doped porous carbon by ammonia gas treatment and the effects of N-doping on water adsorption, Carbon 50(5) (2012) 1833-1842.

[42] S. Liu, W. Peng, H. Sun, S. Wang, Physical and chemical activation of reduced graphene oxide for enhanced adsorption and catalytic oxidation, Nanoscale 6(2) (2014) 766-771.

[43] W. Peng, S. Liu, H. Sun, Y. Yao, L. Zhi, S. Wang, Synthesis of porous reduced graphene oxide as metal-free carbon for adsorption and catalytic oxidation of organics in water, Journal of Materials Chemistry A 1(19) (2013) 5854-5859.
[44] O.S.G.P. Soares, R.P. Rocha, A.G. Gonçalves, J.L. Figueiredo, J.J.M. Órfão, M.F.R. Pereira, Easy method to prepare N-doped carbon nanotubes by ball milling, Carbon 91 (2015) 114-121.

Chapter 4 Ferric carbide nanocrystals encapsulated in nitrogen-doped carbon nanotubes as an outstanding environmental catalyst

Abstract

Nitrogen-doped carbon nanotubes encapsulated with iron carbide (Fe_3C) nanocrystals (Fe_3C@NCNT) were fabricated by a simple, direct pyrolysis method using melamine and ferric chloride as the C, N and Fe precursors. The surface morphology, structure and composition of the Fe_3C@NCNT materials were thoroughly investigated. The nanomaterials were employed as novel catalysts for peroxymonosulfate (PMS) activation, and an outstanding efficiency, a high stability and an excellent reusability were observed in catalytic oxidation of organics. The encapsulated Fe_3C nanoparticles played a key role in the emerging synergetic effect between the carbide and the protective graphitic layers. In addition, the quaternary N and the trace amount of iron on the CNT surface acted as the active sites. Various quenching experiments were carried out to elucidate the catalytic mechanism over Fe_3C@NCNT. It was unravelled that singlet oxygen, superoxide, sulfate and hydroxyl radicals worked together for the degradation of phenol solutions. The simple synthesis, low cost precursors, unique structure, excellent catalytic activity and stability of the novel iron-carbide-based composites would offer new strategic materials for environmental catalysis.

4.1 Introduction

The Century of Environment is the symbol of the 21st century.[1] The civilization and industrialization have discharged vast pollutants to water resources causing severe health and environmental implications.[2-6] Advanced oxidation processes (AOPs) over other physical processes such as adsorption, extraction and flocculation have been effectively applied for complete removal of such organic contaminants in wastewater. Metal-based materials, such as Co and Mn oxides [7-10], have become highly favorable to activate peroxymonosulfate (PMS) to produce sulfate radicals, which facilitated the emerging SR-AOPs (sulfate radical-based advanced oxidation processes). However, these metal-based catalysts are subject to the inevitable loss or leaching of metal ions in either homogeneous or heterogeneous reactions and thus cause secondary contamination.[11-14] Therefore, many efforts have been devoted to developing carbon-based catalysts (M-N_x/C, M = Co, Fe, Ni, etc.), metal-free carbon materials or N-doped carbon catalysts (N_xC) as alternatives to metal oxide catalysts.[15-17] Among them the best is the M-N_x/C catalyst where the active sites are believed to be surface nitrogen coordinated with metals.[15, 18] Even with extensive studies, these materials still suffer from either a low catalytic activity or a poor stability.[6, 8, 11, 19, 20] Therefore, it is very challenging to develop novel catalysts with a high activity, a good stability, low cost and environmental friendliness.

Fe-based materials have already been regarded as one of the most promising heterogeneous catalysts because Fe can be easily incorporated into the carbon framework by pyrolyzing ferric salt in an inert atmosphere and can catalyze the graphitization process at a lower

temperature. [21, 22] In addition, metal-based catalysts coated by a protective shell or matrix are proven to be of enhanced catalytic performance and stability. Recently, novel and efficient metal/metal carbide nanoparticles encapsulated in nanostructured carbon were developed, whose active sites were believed to be the graphitic carbon shells activated by the encapsulated nanoparticles.[23, 24] An interesting magnetic carbon encapsulated nano Fe^0/Fe_3C was synthesized by Wang et al. [25] *via* an *in situ* hydrothermal carbonization of glucose with melamine, accompanied by a self-reduction in N_2 atmosphere. Pronounced catalytic performance was evidenced by the complete removal of 20 ppm phenol within 10 min. They found that Fe_3C was conducive to its stability. In addition, Li et al. [24] discovered a novel catalyst consisting of iron carbide nanoparticles encapsulated by graphitic layers applied in oxygen reduction reaction (ORR). Bao et al. [23] prepared a pea-pod like carbon nanotubes with encapsulated Fe nanoparticles and used the materials as an ORR catalyst in acid media. Peng et al. [26] synthesized nitrogen-doped carbon nanotubes with encapsulated Fe_3C nanoparticles that showed good ORR nature in both acid and alkaline media. Yao et al. [27] fabricated magnetic metal (M= Fe, Co, Ni) nanocrystals encapsulated in nitrogen-doped carbon nanotubes using dicyandiamide as a C/N precursor, which exhibited varying activities toward Fenton-like reaction. These findings are noticeable because Fe_3C/Fe particles could *in situ* 'etch' into CNTs, and the resulting iron species encapsulated inside CNTs or graphene are particularly active for selective hydrogenation,[28] and oxygen reduction reaction.[29, 30] These important achievements inspired us to explore a new strategy for the controlled synthesis of novel carbon-supported iron-based catalysts for PMS activation with both a high catalytic activity and an excellent stability.

Carbon-based materials, for example, carbon nanotubes (CNTs) have been extensively studied in both fundamental research and practical applications because of their unique physico-chemical properties. Heteroatom doping with nitrogen or metals can further tune and improve the capabilities of CNTs. [31] Melamine, a green and cheap chemical with 67 wt% N content, has been employed as both a carburization reagent and nitridation reagent. [32, 33] Nallathambi et al. reported that the performance of Fe catalyst prepared from melamine is far superior to those from bipyridine, pyrazine and purine at the same N loading.[34] Single-walled NCNTs were synthesized by Duan et al. [35] via the pyrolysis of commercial SWCNTs and melamine, showing an extraordinarily high catalytic activity for PMS activation. However, a simple, low-cost, safe and scalable synthesis method of CNTs for the widespread and sustainable use of carbon materials in large-scale has been difficult to achieve.[28]

Generally, N-doped CNTs can be prepared through post-treatment of CNTs with ammonia, urea, or pyridine. However, few studies have directly synthesized N-doped CNTs from direct thermal carbonization of nitrogen-containing polymer precursors, such as polyacrylonitrile, polyaniline, polypyrrole, and melamine resin. [36, 37] The *in situ* approach may provide several advantages, such as an increase of the doping level and a uniform distribution of heteroatoms on CNTs for improving the catalytic activity. Furthermore, it is concluded that encapsulation of metal nanocrystals into N-doped CNTs to form a hybrid structure is an effective strategy to enhance the overall catalytic activity.[38, 39]

Herein, we report a new, one-pot and facile strategy for the controlled synthesis of N-doped carbon nanotubes with encapsulated Fe_3C through the direct pyrolysis of a mixture of melamine and iron chloride. Fe_3C and CNTs were formed *in situ* during the pyrolysis. Their morphologies, compositions, active sites and mechanism of catalytic degradation were systematically investigated. In addition, electron paramagnetic resonance (EPR) and classical radical quenching tests were used to probe PMS activation and mechanism of phenol oxidation. To our best knowledge, it reports for the first time that the well-designed Fe_3C-based CNTs composites have a great potential for an excellent catalytic activity and good stability for PMS reactions.

4.2 Experimental

Materials and Chemicals. Melamine (>99.0%), hexahydrate ferric chloride ($FeCl_3 \cdot 6H_2O$, >99.9%), potassium peroxymonosulfate ($2KHSO_5 \cdot 3KHSO_4 \cdot K_2SO_4$, Oxone), sodium azide ($NaN_3$), p-benzoquinone (PBQ), tert-butyl alcohol (TBA) and 5,5-dimethylpyrroline-oxide (DMPO, >99.0%) were purchased from Sigma-Aldrich. Phenol (>99.0%), acetone, ethanol and hydrochloric acid (32-37%) were obtained from Chem-Supply. High purity nitrogen gas (99.999%) was obtained from BOC. Ultrapure water was used in all of the experiments. All chemicals used herein were of analytic grade and used as received without any further purification.

Synthesis of Fe_3C@NCNT. Fe_3C@NCNT catalysts were fabricated via a facile thermal process using melamine as a C/N precursor.[6, 26, 40] In a typical procedure, 6 g melamine and 6 g $FeCl_3 \cdot 6H_2O$ were dissolved in 10 mL ethanol in a crucible with continuous stirring to form a clear

yellow solution. The resulting solution was then put in an oven at 80 ºC in air for around 48 h, to obtain a tawny solid. The dried powder was transferred to a quartz tube furnace to respectively anneal at 700, 800, or 900 ºC for 6 h under a nitrogen flow of 50 mL min^{-1}. After cooling down to room temperature, the as-obtained material was treated with 100 mL hydrochloric acid (32-37 wt%) with magnetic stirring for 6 h to remove any accessible iron species. The sample was then washed in succession with ultrapure water and acetone and dried at 60 ºC for 24 h to obtain the final material, named as Fe_3C@NCNT-X (X indicates the pyrolysis temperature). The obtained products were magnetic powders. Schematic representation for the synthesis route of Fe_3C@NCNT catalysts is illustrated in Figure 4.1 (a).

Characterization of materials. X-ray diffraction (XRD) patterns were performed on a Bruker D8-Advanced X-ray instrument using a Cu-Kα radiation with λ at 1.5418 Å. Scanning electron microscopy (SEM) was applied to investigate the morphology of the catalysts using a Zeiss Neon 40 EsB FIBSEM. Nitrogen sorption isotherms were acquired on a Tristar II 3020 after 4 h degassing of the samples at 100 ºC. The specific surface area and pore size distribution were evaluated by the Brunauer-Emmett-Teller (BET) equation and the Barrett-Joyner-Halenda (BJH) method, respectively. Chemical composition and states were determined by X-ray photoelectron spectroscopy (XPS) which was carried out on a Thermo Escalab 250 with Al-Kα X-ray. A Perkin-Elmer Diamond TGA/DTA thermal analyzer was utilized to evaluate thermogravimetric-differential thermal analysis (TG-DTA) via samples heating in an air flow of 100 mL min^{-1} and a heating rate of 10 ºC min^{-1}. Raman analysis was performed on an ISA dispersive Raman spectrometer with argon ion laser (514 nm).

Catalytic Oxidation of Phenol Solutions. The catalytic oxidation was carried out in a 250 mL conical flask with phenol solutions (20 ppm, 150 mL), the catalyst (0.2 g L^{-1}) and PMS (2.0 g L^{-1}) in a constant-temperature (25 ^{o}C) controlled water bath for the kinetic studies. During each interval, 1 mL phenol solution was withdrawn by a syringe, filtered by a 0.45 μm Millipore film, and injected into a vial, in which 0.5 mL of methanol as a quenching reagent was previously injected. The mixed solution was analyzed by a high performance liquid chromatograph (HPLC, Varian) with a C-18 column and a UV detector set at 270 nm. After each run, the used catalyst was collected by ultrasonic washing for 5 min and washed three times with ultrapure water, filtered and dried in an oven for reuse.

Mechanistic Studies of the Catalytic Processes. An EMS-plus EPR instrument from Bruker was employed to detect the free radicals captured by 5,5-dimethyl-1-pyrroline (DMPO, ＞ 99.0%) during PMS activation, operating under the following conditions: centre field, 3515 G; sweep width, 100 G; microwave frequency, 9.87 GHz; power setting, 18.75 mW; scan number, 3. The radical quantitative information was acquired from the Spin Fitting from Bruker Xenon Software Package.

4.3 Results and Discussions

The morphologies and structures of as-prepared Fe_3C@NCNT-700, Fe_3C@NCNT-800 and Fe_3C@NCNT-900 are shown in Figure 4.1 (b), (c) and (d). The characteristic morphologies of all the catalysts were dimensionally uniform and orderly arranged nanotubes with diameters of 200-300 nm for Fe_3C@NCNT-700 and Fe_3C@NCNT-800, but only 50-100 nm for Fe_3C@NCNT-900. [26, 28] However, CNTs with

nonuniform size with significant agglomeration were formed above 900 °C, which may be attributed to the breakdown of CNTs and decomposition of Fe_3C at a higher temperature.

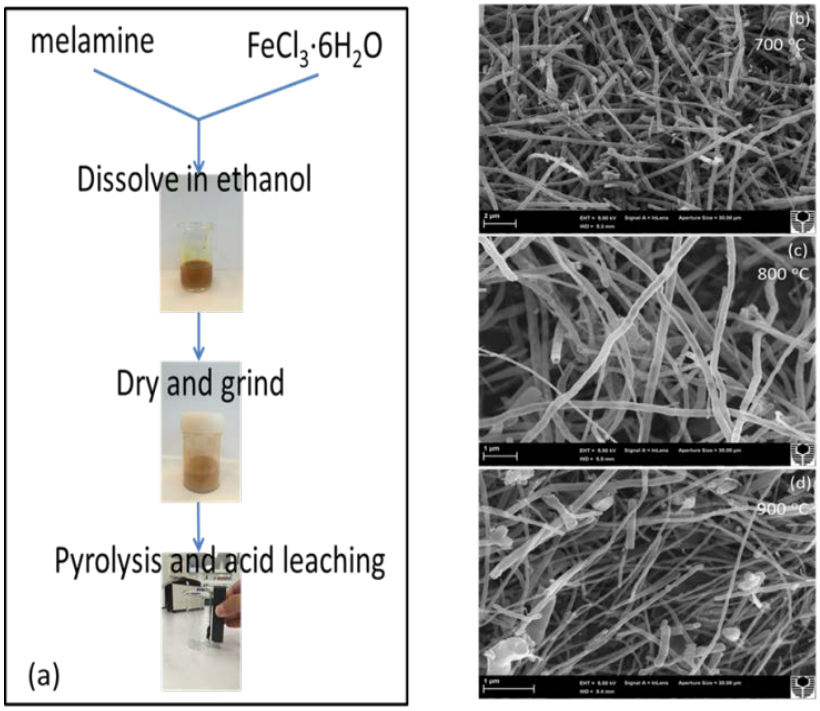

Figure 4.1 (a) Schematic illustration of the synthesis route of Fe_3C@NCNT. SEM images for Fe_3C@NCNT catalysts at (b) 700 °C, (c) 800 °C and (d) 900 °C.

As revealed by transmission electron microscopy (TEM) images (Figure 4.2), a large portion of pea-pod dark nanocrystals (identified as iron carbide by the XRD diffraction patterns, Figure 4.3) were encapsulated mainly inside the channels or at the tip of carbon nanotubes (sized in 40-50 nm for Fe_3C@NCNT-700 and Fe_3C@NCNT-900, 80-100 nm for Fe_3C@NCNT-800). HRTEM image of the Fe_3C nanoparticles in CNTs shows that most surface of Fe_3C nanoparticles were coated by multi-layered graphene. For a typical nanoparticle, the spacing of crystalline lattices in one direction was 0.31 nm, corresponding to the (111) crystal

planes of Fe_3C phase. The interlayer spacing of the coating graphene layer was 0.335 nm, in accordance with the experimental results for free-standing few-layer graphene.[26]

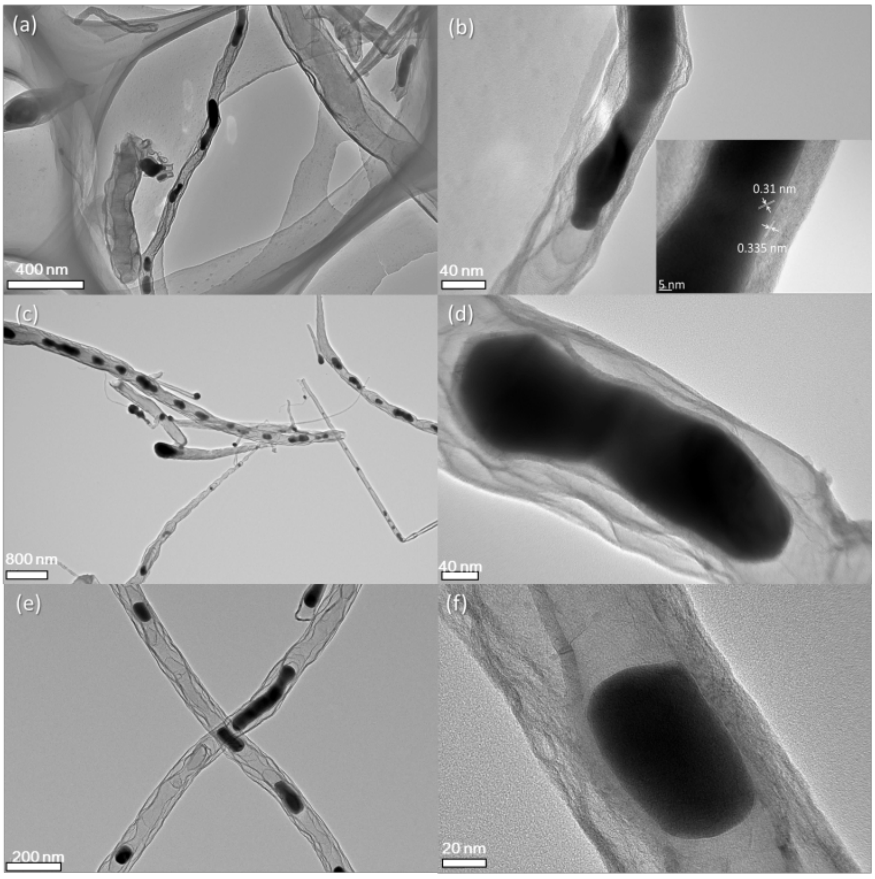

Figure 4.2 TEM images for Fe_3C@NCNT catalysts at 700 ^oC (a), (b), 800 ^oC (c), (d) and 900 ^oC (e), (f).

Because of the protection of the graphitic layers, the Fe_3C nanocrystals were quite inaccessible and chemically stable in hot acids, implying that the geometric confinement of Fe_3C@NCNT has been successfully achieved.[26-28, 41] Structure control has always been regarded as a difficult task for catalysts and materials prepared by pyrolysis. This is especially true for the synthesis and preparation of Fe_3C-based catalysts

by pyrolysis. As far as we know, few Fe_3C with uniform morphology and evenly dispersed nanoparticles has ever been reported.

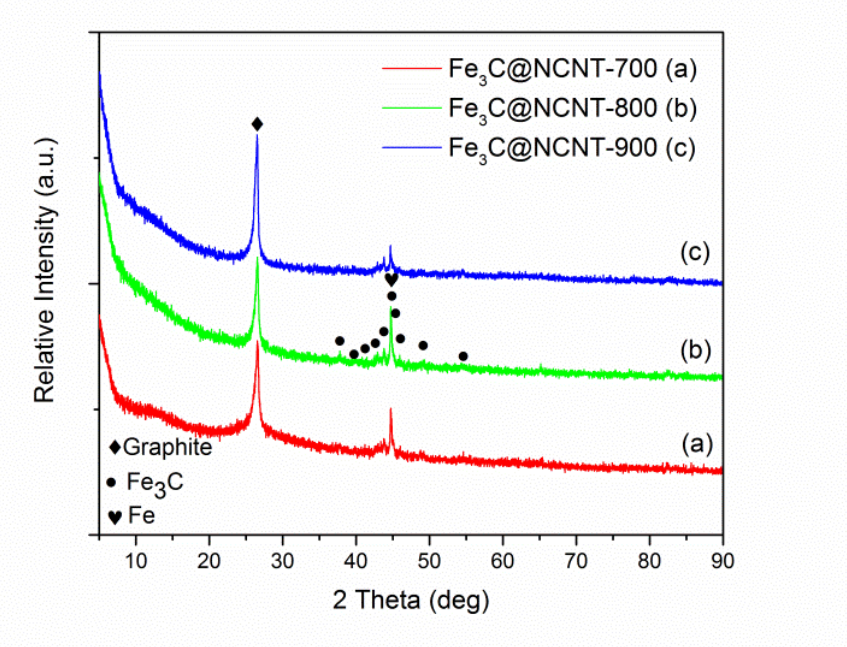

Figure 4.3 XRD patterns of Fe_3C@NCNT composites at varied pyrolysis temperatures.

X-ray diffraction (XRD) patterns of Fe_3C@NCNT obtained at different pyrolysis temperatures are shown in Figure 4.3. The diffraction peaks at 26.5° and 43.4° were observed at different calcined temperatures, corresponding to the (002) and (101) planes of graphitic carbon, respectively. [6] The diffraction peaks were very sharp and the intensity of diffraction peak at 26.5° increased with pyrolysis temperature, indicating that the degree of graphitization of Fe_3C@NCNT was very good and also had a strong dependence on pyrolysis temperature. Aside from this reflection, other diffraction peaks at 37-50° were typical diffraction peaks of Fe_3C, which cannot be found in NG [6] and were the major difference between Fe_3C@NCNT and NG. Diffraction peaks located at 37.8, 42.8, 43.9, 45.0, 45.8 and 49.2° were detected in

Fe_3C@NCNT, which could be assigned to the (021), (121), (210), (103), (211) and (113) crystalline planes of Fe_3C particles, respectively.[42] This confirmed that the nanoparticles encapsulated in the interior of nanotubes observed by the TEM, were dominantly Fe_3C when the temperature was above 700 ^oC. These diffraction peaks in Fe_3C@NCNT-800 were the highest and strongest. In addition, all the samples may contain traces of metallic iron due to the same characteristic peak as that of Fe_3C at 2θ of 44.6^o.[26, 33] The XRD results further confirmed that Fe_3C nanoparticles were encapsulated in graphitic layers which cannot be removed in hot acid solution and were well-preserved after the leaching process.

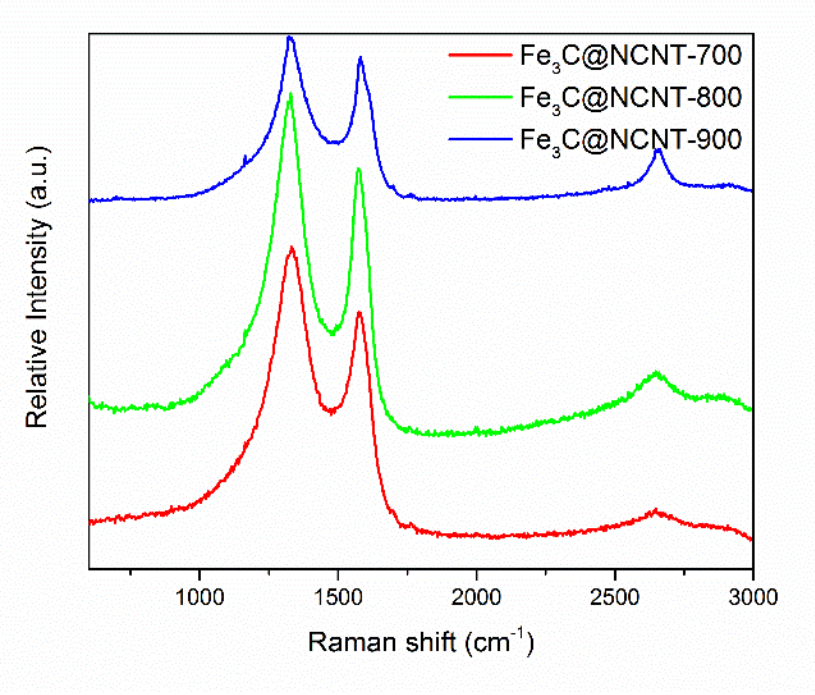

Figure 4.4 Raman spectra of Fe_3C@NCNT composites at varied pyrolysis temperature.

The degree of graphitization of the Fe_3C@NCNT samples was further investigated by Raman spectra and the results are shown in Figure 4.4. The G band (at 1350 cm^{-1}) shows the existence of sp^2-hybridized carbon

atoms, and the D band (at 1570 cm^{-1}) provides evidence of defects such as disorders, edges and boundaries of the graphene. I_D/I_G is the ratio of the integrated intensities of the D and G bands and it decreased with increasing pyrolysis temperature. As it can be seen from Figure 4.4, the intensity ratios of the D- and G-bands (I_D/I_G) for Fe_3C@NCNT-700, Fe_3C@NCNT-800 and Fe_3C@NCNT-900 were 1.20, 1.17 and 1.12, respectively, which demonstrated that the degree of graphitization increased with the pyrolysis temperature. An ordered graphitic structure can be formed easily at a higher temperature, but too high pyrolysis temperature could lead to irregular carbon nanostructures. The reason for this is that Fe_3C is temperature sensitive and metastable, and can break down into metallic Fe and free-C at a higher temperature, which may enter the CNT framework and thus change its crystal structure.[28]

Figure 4.5 displayed N_2 adsorption-desorption isotherms and the pore size distributions of the Fe_3C@NCNT samples. The isotherms in Figure 4.5 (a) showed that N_2 adsorption increased with pyrolysis temperature, due to the higher surface area and larger pore volume at a higher temperature. All the samples exhibited a typical IV isotherm with H3 type hysteresis loops. The hysteresis loops in P/P_0 = 0.4-0.9 were indicative of the mesoporous structures of Fe_3C@NCNT composites.[43] The specific surface areas of Fe_3C@NCNT-700, Fe_3C@NCNT-800 and Fe_3C@NCNT-900 were determined to be 40.1, 52.4 and 72.4 m^2/g, respectively. Table 4.1 shows that the BET surface area and pore volume increased with increasing pyrolysis temperature and pore size increased first but then decreased, reaching its peak at 800 ^oC. An increase in the BET area indicated that a high pyrolysis temperature could break CNT into smaller ones and thus resulted in the exposure of some Fe_3C nanoparticles, which might further increase active sites and enhance catalytic performance.

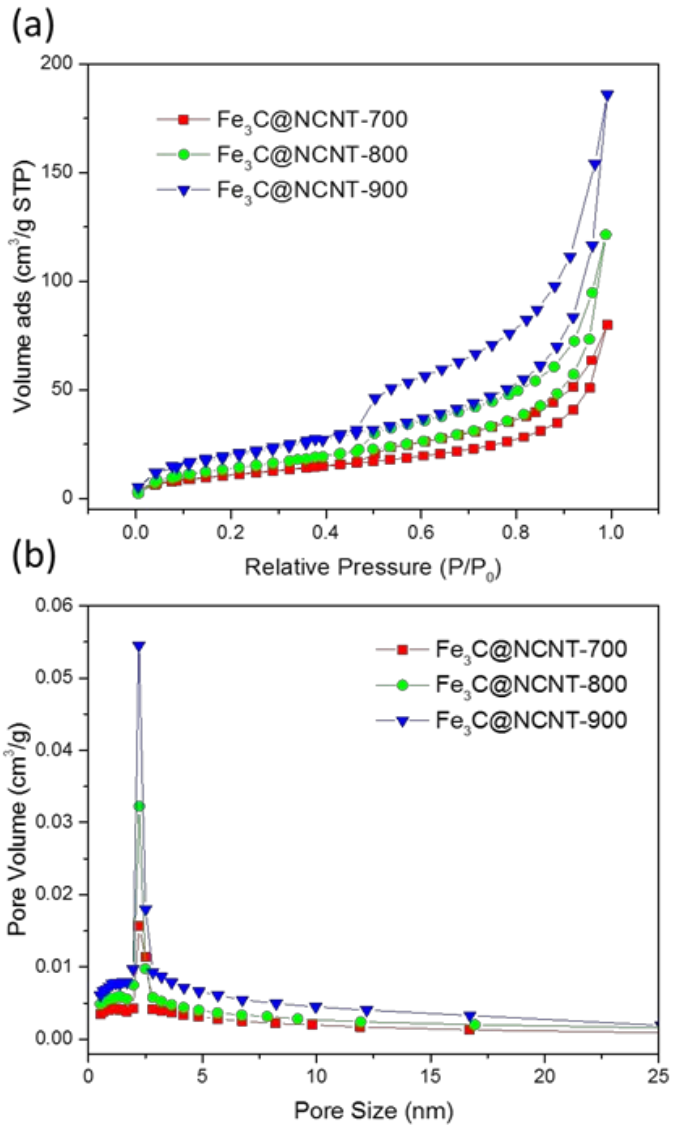

Figure 4.5 (a) Nitrogen sorption isotherms of samples, and (b) pore size distributions calculated from N_2 desorption isotherms for Fe_3C@NCNT-700, Fe_3C@NCNT-800 and Fe_3C@NCNT-900.

Figure 4.5 (b) displayed that all of the Fe_3C@NCNT presented a single mode of pore size. The pore size of Fe_3C@NCNT-700, Fe_3C@NCNT-800 and Fe_3C@NCNT-900 were centred at 6.1, 6.7 and 6.5 nm, which demonstrated that pyrolysis temperature exerted little effect on the pore size.[44]

Table 4.1 BET surface area and pore properties of Fe_3C@NCNT composites

	BET surface area, m^2/g	Pore volume, cm^3/g	Average pore size, nm
Fe_3C@NCNT-700	40.1	0.096	6.1
Fe_3C@NCNT-800	52.4	0.15	6.7
Fe_3C@NCNT-900	72.4	0.23	6.5

Figure 4.6 shows the representative TGA and DTA curves of Fe_3C@NCNT nanocomposites measured in air atmosphere from 25 to 1000 ^oC with a heating rate of 10 ^oC/min. The combustion temperature was found to be in the order: Fe_3C@NCNT-700 $<$ Fe_3C@NCNT-800 $<$ Fe_3C@NCNT-900.

The TGA plots of Fe_3C@NCNT composites showed a slight weight increase below 250 ^oC and then a mild weight loss from 250 to 450 ^oC, which can be assigned to the removal and destruction of the labile oxygenated functional groups on the carbon surface such as -OH and C=O in the forms of H_2O, CO and CO_2.[45] Then the weight decreased dramatically in the range from 450 to 700 ^oC being ascribed to the oxidation and decomposition of CNTs and the oxidation and transformation of Fe_3C into Fe_2O_3 between 360 and 550 ^oC. When the temperature reached 700 ^oC, the weight of the samples remained unchanged and almost no weight loss occurred beyond this temperature. A stable weight percentage of 24.25%, 29.30% and 17.54% (represents the weight of residual iron oxide yielding the iron contents of 16.98%, 20.51% and 12.27% by calculation) were achieved for Fe_3C@NCNT-

700, Fe_3C@NCNT-800 and Fe_3C@NCNT-900, respectively.[46] It was known that the weight loss rate of CNTs filled with ferromagnetic always becomes slower with increasing temperature because of the destruction of tube walls that provide protection of the inner filled metal, forming metal oxide subsequently. It is deduced that a point of inflection would exist in the TGA curve. However, the curves of Fe_3C@NCNT nanocomposites were relatively smooth, proving that the iron and iron carbide encapsulated inside were oxidized by air simultaneously with the tube walls.[47]

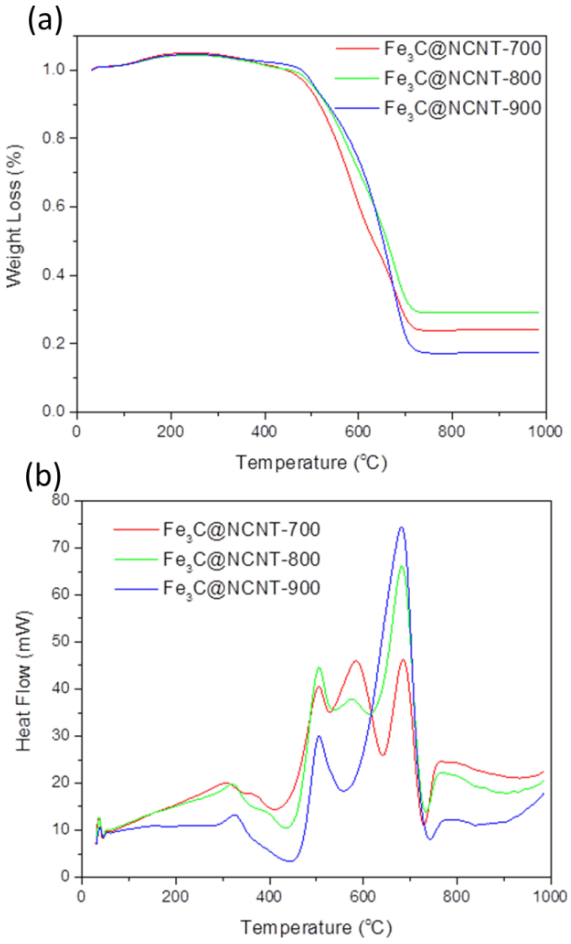

Figure 4.6 TGA and DTA curves of Fe_3C@NCNT composites.

Table 4.2 The content of iron ions detected by ICP.

	Fe_3C@NCNT-700	Fe_3C@NCNT-800	Fe_3C@NCNT-900
Iron ions (mg/L)	0.13	0.23	0.11

X-ray photoelectron spectra (XPS) studies were carried out to further investigate the surface nature of the Fe_3C@NCNT composites. Figure 4.7 (a) reveals that Fe_3C@NCNT catalysts were composed of C, O, N, and Fe, and no other impurity was observed. Although Fe was detected by ICP (Table 4.2), TEM and XRD, the XPS spectra revealed a quite low surface iron content (< 0.2%) on all the Fe_3C@NCNT composites, implying a complete leaching out of surface iron species during the acid treatment. This further proves that Fe_3C nanoparticles were entirely encapsulated by carbon layers in the catalysts and can thus be survived in the catalytic process. However, at a high temperature, carbon nanotubes may partially break up and crack (as shown in SEM) and thus the interior Fe_3C or Fe^0 may run out of the tubes. As a result, iron content analyzed by XPS in the Fe_3C@NCNT-900 was the highest among all the catalysts.

The total amount of N in the different catalysts was detected to be 3.69 at.%, 2.69 at.%, 1.82 at.% for Fe_3C@NCNT-700, Fe_3C@NCNT-800 and Fe_3C@NCNT-900, respectively. The decrease in total N content with increasing pyrolysis temperature might be ascribed to the decomposition of unstable nitrogen species at a high temperature. The N 1s spectra were deconvoluted into four peaks, assigned to pyridinic N (398.5-398.8 eV), pyrrolic N (399.9-400.2 eV), quaternary N (401.4-401.6 eV) and

pyridine-N-oxide (402-405 eV) [48], as shown in Figure 4.7 (b), (c) and (d).The content of quaternary N first increased dramatically from 700 to 800 ºC but then increased moderately from 800 to 900 ºC. The content of pyridinic N witnessed an inverse trend, first increased but then decreased with the increasing pyrolysis temperature due to the loss of unstable N at a higher temperature. Pyridinic N is generally regarded to have a connection with catalytic activity because of its reduction of energy barrier for adsorbing reactants on adjacent carbon atoms, and its acceleration of first-electron transfer limited by rate.[49, 50] However, recent research suggested that quaternary N in the graphene structure can cause electron to distribute non-uniformly, especially when two quaternary N atoms were doped into the same hexagon, leading to a dramatic improvement of catalytic activity of carbon surface.[28, 51]

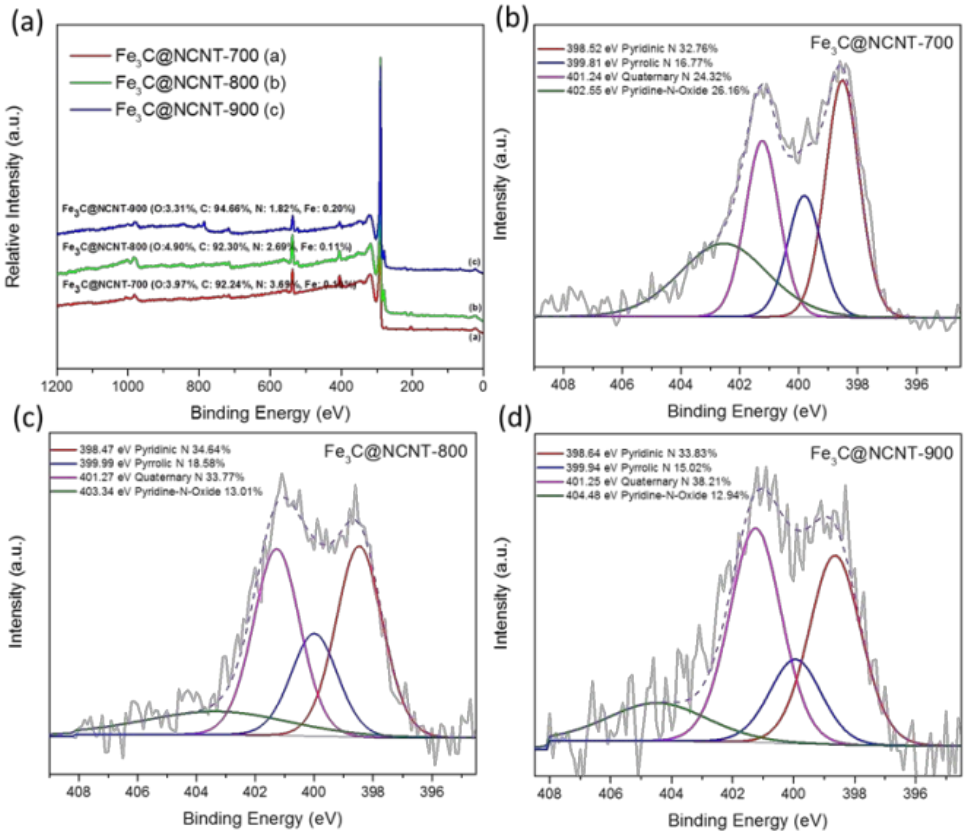

Figure 4.7 (a) XPS spectra of Fe_3C@NCNT composites at different temperatures and HR XPS N1s at (b) 700 ºC (c) 800 ºC and (d) 900 ºC.

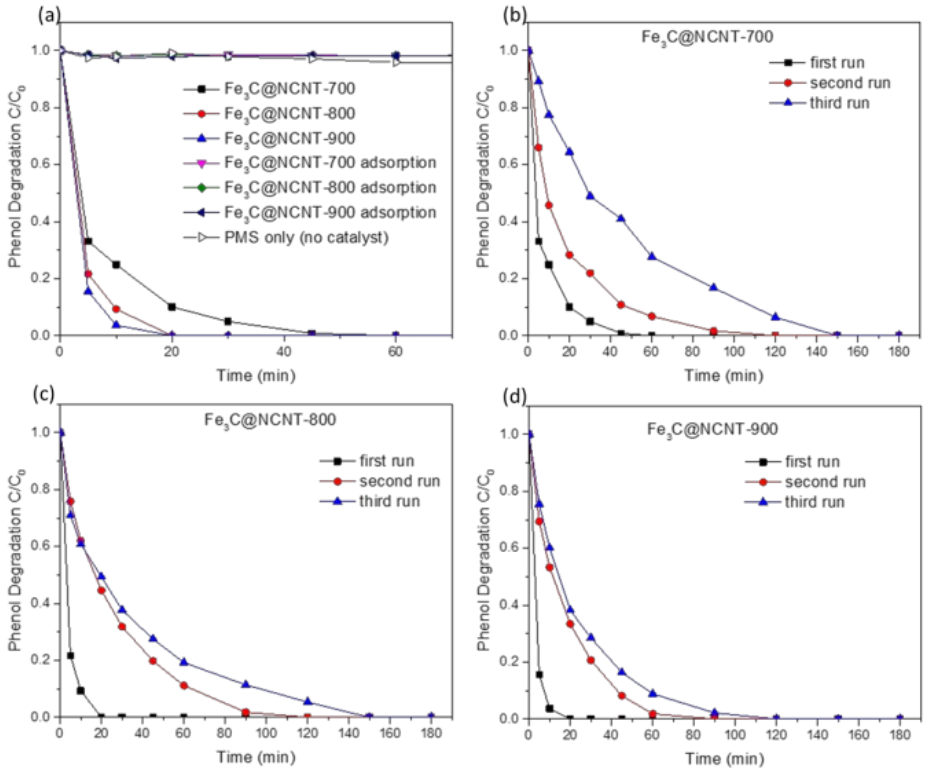

Figure 4.8 (a) Phenol removal in different conditions and stability of (b) Fe_3C@NCNT-700, (c) Fe_3C@NCNT-800 and (d) Fe_3C@NCNT-900. Reaction condition: phenol 20 ppm, catalyst loading 0.2 g/L, PMS 2 g/L, temperature 25 ^oC

Control experiments were carried out to evaluate adsorption, PMS self-oxidation and catalytic performance of Fe_3C@NCNT composites. Phenol removals in different conditions are shown in Figure 4.8 (a). In the presence of PMS without a catalyst, a negligible change (less than 6%) in phenol concentration was observed after 180 min, indicating that significant phenol oxidation could not be induced by PMS itself. A similar trend was found in the reaction of Fe_3C@NCNT catalysts adsorption. Less than 2% phenol was removed in 180 min, suggesting that phenol adsorption on Fe_3C@NCNT composites was negligible either. As shown in Figure 4.8 (a), Fe_3C@NCNT-700, Fe_3C@NCNT-

800 and Fe_3C@NCNT-900 can degrade 100% phenol in 45, 20 and 20 min, respectively. The efficiency was better than rGO [11], N-doped graphene[6, 52] and N-doped CNTs[14, 35], exceptionally better than some metal-based carbon materials [8, 44, 45], indicating that Fe_3C would be the active sites to accelerate this reaction. Fe_3C@NCNT-900 exhibited the best performance among all the Fe_3C@NCNT catalysts, implying that Fe_3C@NCNT-900 with wide and both opening ends CNTs was more accessible to enhance the phenol catalytic degradation reactions because phenol molecules and Fe_3C were in full contact in a relatively restricted area.[28]

It is known that the stability of the catalyst is of great importance in the practical application.[45] The stability and recyclability of Fe_3C@NCNT catalysts were evaluated by successive tests of phenol degradation under the same reaction conditions. For Fe_3C@NCNT-700, 100% phenol was degraded within 45, 120, 150 min for the first, second and third runs. For Fe_3C@NCNT-800, phenol removal could be completed in 20, 120, 150 min, respectively and Fe_3C@NCNT-900 would require 20, 90, 120 min, respectively. The stability results were exceptionally better than N-doped graphene [6, 52, 53] and N-doped CNT [14, 35], implying that the inner Fe_3C may play a role in the enhancement of catalyst stability. The stability of Fe_3@NCNT-900 was relatively better because carbon nanotubes and iron carbide were in close integration and active sites reduced relatively little after three successive reactions and Fe_3C in the third run were still enough to make the surrounding graphitic layers active, consequently activating the outer surface of carbon layer.[25]

In heterogeneous catalytic oxidation of phenol, reaction parameters such as catalyst loading and reaction temperature can affect phenol degradation rate. The effect of catalyst loading on phenol degradation

efficiency is shown in Figure 4.9 (a). Catalyst concentration exerted a significant influence on phenol degradation efficiency, which was dramatically enhanced with an increase in catalyst concentration. When catalyst concentration was 0.1 g/L, 98% and 99% phenol can be degraded in 180 min on Fe_3C@NCNT-700 and Fe_3C@NCNT-800, and 100% phenol can be degraded in 120 min on Fe_3C@NCNT-900. When catalyst concentration increased to 0.5 g/L, phenol was completely removed after 30, 5 and 5 min on Fe_3C@NCNT-700, Fe_3C@NCNT-800 and Fe_3C@NCNT-900, respectively. The improvement in efficiency was attributed to the increase in active sites of the reaction in the phenol solution and thereby generated more active radicals.

Figure 4.9 (b) revealed phenol degradation performance of Fe_3C@NCNT catalysts at different reaction temperatures. It can be seen that reaction temperature moderately affected oxidation efficiency and degradation rate for Fe_3C@NCNT-700. But for Fe_3C@NCNT-800 and Fe_3C@NCNT-900, the effect was relatively small. Specifically, at 15 ^oC, phenol degradation reached 100% in 90 min for Fe_3C@NCNT-700 while the time reduced to be 60 and 45 min when reaction temperature increased to 25 ^oC and 35 ^oC, respectively. The kinetics of phenol degradation was evaluated by the first-order kinetic model as listed below.

$$\ln(C/C_0) = -kt \qquad \text{(Eq. 4.1)}$$

where C and C_0 are the phenol concentrations at time (t) and t = 0, respectively and k is the reaction rate constant.[52]

The reaction rate constants (k) of phenol oxidation at 25 ºC on Fe_3C@NCNT-700, Fe_3C@NCNT-800 and Fe_3C@NCNT-900 were then calculated to be 0.097, 0.237 and 0.330 min^{-1}, respectively.

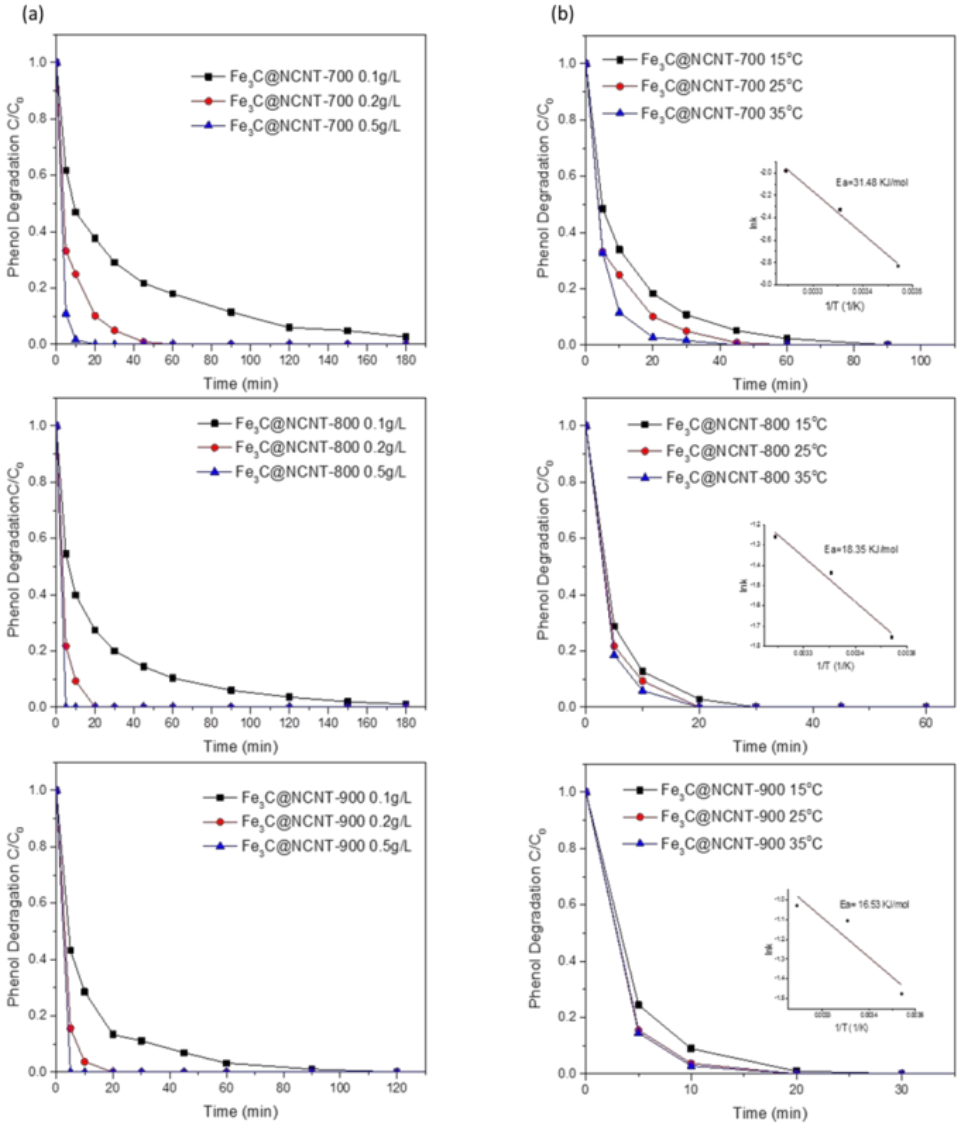

Figure 4.9 Effects of (a) catalyst loading, (b) reaction temperature on phenol degradation for different Fe_3C@NCNT catalysts. Reaction condition: phenol 20 ppm, PMS 2 g/L.

Based on the first-order kinetics, rate constants at varying temperatures were obtained and the relationship was found to follow the Arrhenius

equation. The activation energy was then obtained as 31.5 kJ/mol. For Fe_3C@NCNT-800 and Fe_3C@NCNT-900, degradation time decreased from 30 min to 20 min when the temperature increased from 15 to 35 °C. And the activation energies were 18.3 and 16.5 kJ/mol, respectively, much lower than that of N-doped graphene[6] and N-doped CNT.[35]

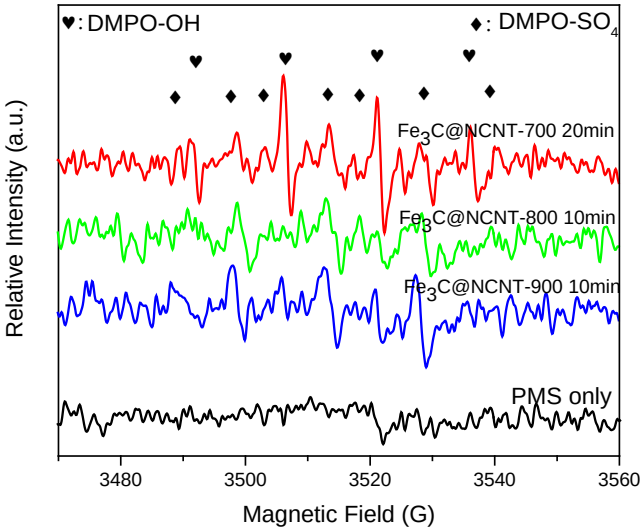

Figure 4.10 EPR spectra of PMS activation with Fe_3C@NCNT composites at different time.

The mechanisms of catalytic degradation of phenol on metal-based catalysts and carbon-based catalysts have recently been well investigated. Previous studies proved that these catalysts can activate PMS to produce sulfate and hydroxyl radicals.[7, 12, 35, 52, 54] As shown in Figure 4.10, Fe_3C@NCNT composites were able to effectively activate PMS to generate both $^{\bullet}OH$ and $SO_4^{\bullet-}$. Different radical quenching reactions were also performed to probe the radicals produced in Fe_3C@NCNT composites and the contribution of the reactive species to phenol degradation. The reactions referring to the electron transfer processes facilitated by Fe_3C@NCNT are shown below.

$$HSO_5^- + e^- \rightarrow OH^\bullet + SO_4^{2-}$$ (Eq. 4.2)

$$HSO_5^- + e^- \rightarrow OH^\bullet + SO_4^{\bullet-}$$ (Eq. 4.3)

$$HSO_5^- - e^- \rightarrow H^+ + SO_5^{\bullet-}$$ (Eq. 4.4)

$$OH^\bullet + SO_4^{2-} \rightarrow SO_4^{\bullet-} + OH^-$$ (Eq. 4.5)

$$SO_4^{\bullet-} + OH^- \rightarrow SO_4^{2-} + OH^\bullet$$ (Eq. 4.6)

Owing to the rapid reaction with both ˙OH and $SO_4^{\bullet-}$ radicals, ethanol was employed as an effective scavenger for both ˙OH and $SO_4^{\bullet-}$ radicals in the catalytic phenol degradation reactions. In most AOPs, the radicals are critical for the organic degradation process. Therefore, if the quenching agent of ethanol is present in solution, the degradation would be significantly reduced or prevented.[35] Control experiments were conducted to compare the catalytic performances with the addition of ethanol on Fe_3C@NCNT-700, Fe_3C@NCNT-800 and Fe_3C@NCNT-900. As shown in Figure 4.11 (a), (c) and (e), all of the three catalysts maintained excellent phenol degradation performance even with a high concentration of quenching reagent. Specifically, when ethanol was added at a molar ratio of 500:1 (ethanol : PMS), 100% phenol was degraded in 120, 45 and 45 min over Fe_3C@NCNT-700, Fe_3C@NCNT-800 and Fe_3C@NCNT-900, respectively. Even in complete ethanol solution, 100% phenol can also be degraded in 180, 90 and 60 min, respectively.

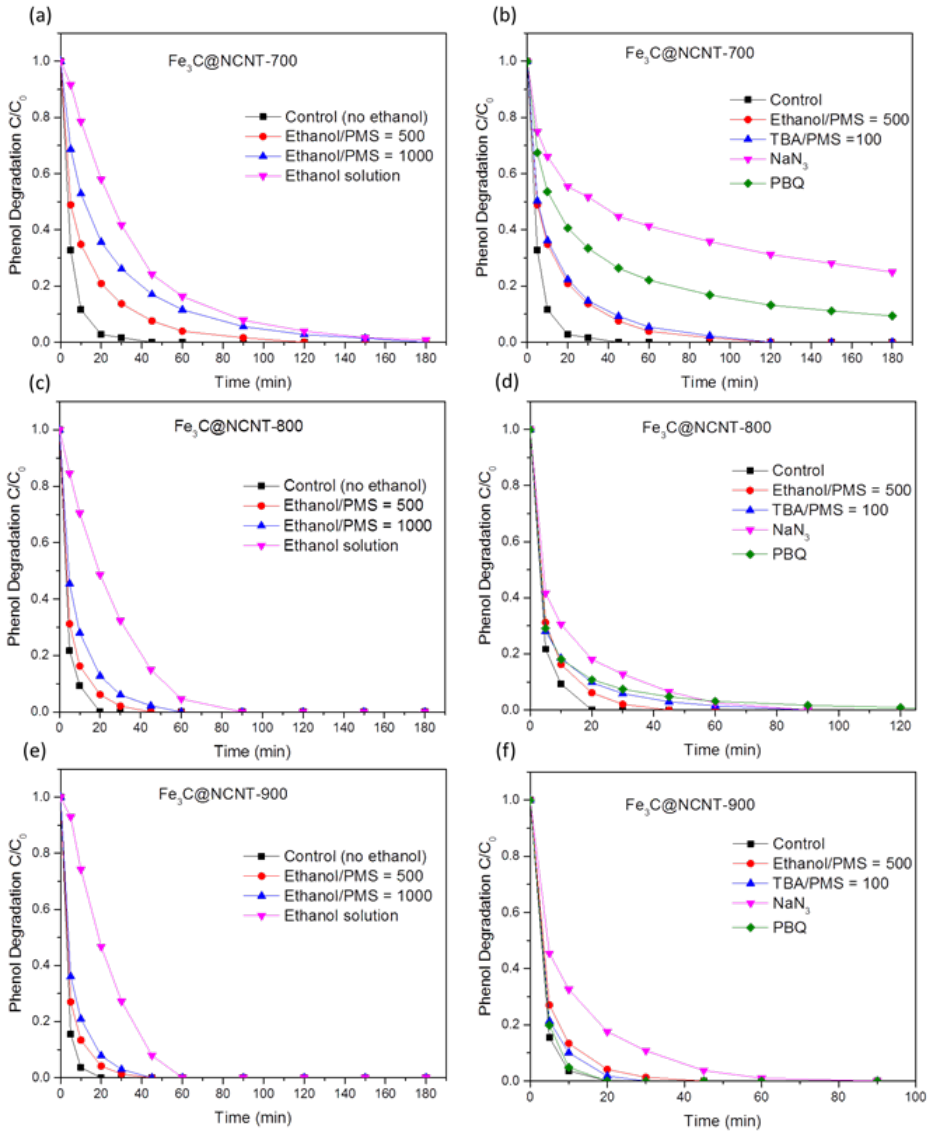

Figure 4.11 Ethanol effect of radical quenching on phenol degradation for (a) Fe_3C@NCNT-700, (c) Fe_3C@NCNT-800, and (e) Fe_3C@NCNT-900. Competitive radical tests for catalytic phenol degradation for (b) Fe_3C@NCNT-700, (d) Fe_3C@NCNT-800 and (f) Fe_3C@NCNT-900. Reaction condition: phenol 20 ppm, catalyst loading 0.2 g/L, PMS 2 g/L, temperature 25 ^oC.

Although degradation still occurs with the quenching agent, which indicates that radical process existed in this reaction, the results strongly suggested that generated $^{\bullet}OH$ and $SO_4^{\bullet-}$ radicals might play a relatively

small role in the phenol degradation and other radicals or non-radical process may play a more significant role. Due to the instantaneous reaction with hydroxyl radicals and the stagnated reaction with sulfate radicals, tert-butanol (TBA) was suggested to be an effective scavenger for $^{\bullet}OH$ in the catalytic oxidation process.[55] When TBA was added to the reaction solution at a molar ratio of 100:1 (TBA : PMS), 100% phenol was degraded in 120, 90 and 30 min on Fe_3C@NCNT-700, Fe_3C@NCNT-800 and Fe_3C@NCNT-900. The degradation efficiency was not significantly reduced or prevented by the addition of ethanol or TBA and thus we can conclude that both $^{\bullet}OH$ and $SO_4^{\bullet-}$ radicals were not the dominant reactive species for these catalytic oxidation process but $SO_4^{\bullet-}$ had a bigger contribution than $^{\bullet}OH$ in phenol degradation.

Previous studies demonstrated that singlet oxygen ($^1O_2$) was also generated from the catalytic oxidation process. Sodium azide (NaN_3) was an effective quenching agent for $^1O_2$ but it also reacts fast with $^{\bullet}OH$.[56-58] However, $^{\bullet}OH$ was proved not active for phenol decomposition in the above ethanol quenching experiment. In this process, 3 mM NaN_3 was added to the catalytic reaction solution. Although part of NaN_3 could be consumed by PMS, the remained NaN_3 was still sufficient to quench free radicals. It was found that phenol degradation efficiency dramatically decreased with the addition of NaN_3 and only 75% phenol can be degraded in 180 min for Fe_3C@NCNT-700 and 100% phenol can be degraded in almost 90 min on both Fe_3C@NCNT-800 and Fe_3C@NCNT-900. These results suggested that $^1O_2$ might be the major reactive species in phenol degradation.

The contribution of $^{\bullet}O_2^-$ in phenol degradation was determined by p-benzoquinone (PBQ), an effective quenching agent for $^{\bullet}O_2^-$.[59, 60] If 3

mM PBQ was put into the catalytic phenol solution, it was observed that 90.6% phenol was degraded in 180 min for Fe_3C@NCNT-700, 100% phenol was degraded in almost 180 min over Fe_3C@NCNT-800 and 100% phenol was degraded in 20 min over Fe_3C@NCNT-900. Phenol degradation efficiency was suppressed greatly by the addition of PBQ for Fe_3C@NCNT-700 and Fe_3C@NCNT-800, but did not change for Fe_3C@NCNT-900, revealing that $^{\bullet}O_2^-$ were responsible for phenol decomposition for the former two catalysts. This may be because of the breakup of CNTs at a high temperature led to the exposure of some Fe_3C nanoparticles and thus reduced the generation of $^{\bullet}O_2^-$. A proposed mechanism of PMS activation on Fe_3C@NCNT is illustrated in Scheme 4.1.

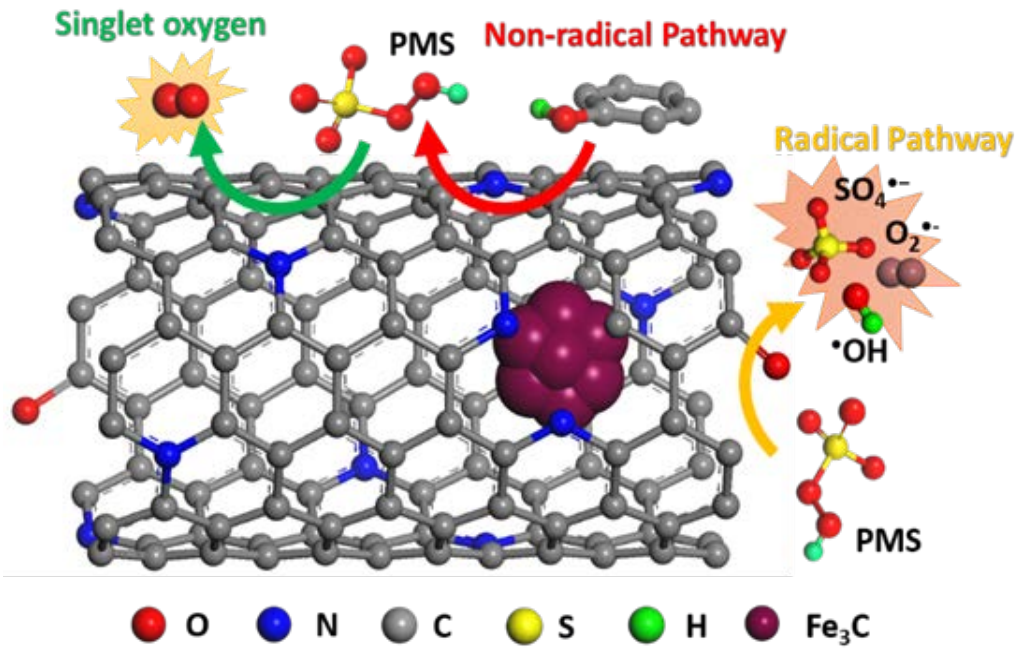

Scheme 4.1 Proposed mechanism of PMS activation on Fe_3C@NCNT.

Overall, on the above four scavenging tests, $^1O_2$ and $^{\bullet}O_2^-$ were recognized as the dominant reactive oxygen species generated in phenol catalytic degradation on Fe_3C@NCNT-700 and Fe_3C@NCNT-800

and $^1O_2$ exhibited a bigger contribution. However, for Fe_3C@NCNT-900, only $^1O_2$ was regarded as the major reactive oxygen species. For all of the three catalysts, both $^{\bullet}OH$ and $SO_4^{\bullet-}$ exert a very small impact on phenol degradation.[61] Therefore, in this investigation, the possible mechanism of the superior activity and excellent stability of Fe_3C@NCNT catalysts in the activation of PMS for phenol degradation would be explained by the combination of radical and nonradical processes, which were significantly promoted by quaternary and pyridinic N, synergetic effects between inner Fe_3C and outside carbon as well as trace amount of Fe on the surface.

4.4 Conclusions

In summary, nitrogen-doped carbon nanotubes with encapsulated Fe_3C nanoparticles (Fe_3C@NCNT) were successfully prepared through a simple and green pyrolysis process of melamine and iron chlorides. The characterization results showed that Fe_3C nanocrystals were mainly encapsulated in the interior of Fe_3C@NCNT composites. The as-prepared Fe_3C@NCNT catalysts exhibited both excellent catalytic performance and outstanding stability in phenol degradation. The quaternary and pyridinic N, synergetic effects between inner Fe_3C and outside carbon as well as trace amount of Fe on the surface may be the active sites to enhance catalytic degradation. Quenching experiments were used to observe the generated reactive radicals and $^1O_2$ and $^{\bullet}O_2^-$ were proven to be the major radicals in catalytic phenol degradation. The novel synthetic approach, unique structure and proposed mechanism will stimulate the development of active and durable metal-based carbon catalysts in the environmental science research.

References

[1] F. Perreault, A. Fonseca de Faria, M. Elimelech, Environmental applications of graphene-based nanomaterials, Chemical Society Reviews 44(16) (2015) 5861-5896.

[2] X.G. Duan, Z.M. Ao, L. Zhou, H.Q. Sun, G.X. Wang, S.B. Wang, Occurrence of radical and nonradical pathways from carbocatalysts for aqueous and nonaqueous catalytic oxidation, Applied Catalysis B-Environmental 188 (2016) 98-105.

[3] X.G. Duan, C. Su, L. Zhou, H.Q. Sun, A. Suvorova, T. Odedairo, Z.H. Zhu, Z.P. Shao, S.B. Wang, Surface controlled generation of reactive radicals from persulfate by carbocatalysis on nanodiamonds, Applied Catalysis B-Environmental 194 (2016) 7-15.

[4] J. Kang, X.G. Duan, L. Zhou, H.Q. Sun, M.O. Tade, S.B. Wang, Carbocatalytic activation of persulfate for removal of antibiotics in water solutions, Chemical Engineering Journal 288 (2016) 399-405.

[5] W.J. Tian, H.Y. Zhang, X.G. Duan, H.Q. Sun, M.O. Tade, H.M. Ang, S.B. Wang, Nitrogen- and sulfur-codoped hierarchically porous carbon for adsorptive and oxidative removal of pharmaceutical contaminants, ACS Applied Materials & Interfaces 8(11) (2016) 7184-7193.

[6] C. Wang, J. Kang, H.Q. Sun, H.M. Ang, M.O. Tade, S.B. Wang, One-pot synthesis of N-doped graphene for metal-free advanced oxidation processes, Carbon 102 (2016) 279-287.

[7] Y. Wang, S. Indrawirawan, X. Duan, H. Sun, H.M. Ang, M.O. Tadé, S. Wang, New insights into heterogeneous generation and evolution processes of sulfate radicals for phenol degradation over one-dimensional α-MnO_2 nanostructures, Chemical Engineering Journal 266 (2015) 12-20.

[8] Y. Wang, H. Sun, H.M. Ang, M.O. Tadé, S. Wang, Synthesis of magnetic core/shell carbon nanosphere supported manganese catalysts for oxidation of organics in water by peroxymonosulfate, Journal of Colloid and Interface Science 433 (2014) 68-75.

[9] Y. Wang, H. Sun, H.M. Ang, M.O. Tadé, S. Wang, 3D-hierarchically structured MnO_2 for catalytic oxidation of phenol solutions by activation of peroxymonosulfate: Structure dependence and mechanism, Applied Catalysis B: Environmental 164 (2015) 159-167.

[10] Y.J. Yao, Y.M. Cai, G.D. Wu, F.Y. Wei, X.Y. Li, H. Chen, S.B. Wang, Sulfate radicals induced from peroxymonosulfate by cobalt manganese oxides ($Co_xMn_{3-x}O_4$) for Fenton-like reaction in water, Journal of Hazardous Materials 296 (2015) 128-137.

[11] H. Sun, S. Liu, G. Zhou, H.M. Ang, M.O. Tadé, S. Wang, Reduced graphene oxide for catalytic oxidation of aqueous organic pollutants, ACS Applied Materials & Interfaces 4(10) (2012) 5466-5471.

[12] X. Duan, H. Sun, J. Kang, Y. Wang, S. Indrawirawan, S. Wang, Insights into heterogeneous catalysis of persulfate activation on dimensional-structured nanocarbons, ACS Catalysis 5(8) (2015) 4629-4636.

[13] H. Sun, Y. Wang, S. Liu, L. Ge, L. Wang, Z. Zhu, S. Wang, Facile synthesis of nitrogen doped reduced graphene oxide as a superior metal-free catalyst for oxidation, Chemical Communications 49(85) (2013) 9914-9916.

[14] H.Q. Sun, C. Kwan, A. Suvorova, H.M. Ang, M.O. Tade, S.B. Wang, Catalytic oxidation of organic pollutants on pristine and surface nitrogen-modified carbon nanotubes with sulfate radicals, Applied Catalysis B-Environmental 154 (2014) 134-141.

[15] M. Lefevre, E. Proietti, F. Jaouen, J.P. Dodelet, Iron-based catalysts with improved oxygen reduction activity in polymer electrolyte fuel cells, Science 324(5923) (2009) 71-74.
[16] Z. Chen, D. Higgins, A. Yu, L. Zhang, J. Zhang, A review on non-precious metal electrocatalysts for PEM fuel cells, Energy & Environmental Science 4(9) (2011) 3167-3192.
[17] Z.Y. Wu, X.X. Xu, B.C. Hu, H.W. Liang, Y. Lin, L.F. Chen, S.H. Yu, Iron carbide nanoparticles encapsulated in mesoporous Fe-N-doped carbon nanofibers for efficient electrocatalysis, Angewandte Chemie-International Edition 54(28) (2015) 8179-8183.
[18] Z.W. Chen, D. Higgins, A.P. Yu, L. Zhang, J.J. Zhang, A review on non-precious metal electrocatalysts for PEM fuel cells, Energy & Environmental Science 4(9) (2011) 3167-3192.
[19] X.G. Li, G. Liu, B.N. Popov, Activity and stability of non-precious metal catalysts for oxygen reduction in acid and alkaline electrolytes, Journal of Power Sources 195(19) (2010) 6373-6378.
[20] F. Jaouen, E. Proietti, M. Lefevre, R. Chenitz, J.P. Dodelet, G. Wu, H.T. Chung, C.M. Johnston, P. Zelenay, Recent advances in non-precious metal catalysis for oxygen-reduction reaction in polymer electrolyte fuel cells, Energy & Environmental Science 4(1) (2011) 114-130.
[21] T. Yang, G.Q. Han, Synthesis of a novel catalyst via pyrolyzing melamine with Fe precursor and its excellent electrocatalysis for oxygen reduction, Iernational Journal of Electrochemical Science 7(11) (2012) 10884-10893.
[22] H.J. Zhang, Q.Z. Jiang, L.L. Sun, X.X. Yuan, Z.P. Shao, Z.F. Ma, 3D non-precious metal-based electrocatalysts for the oxygen reduction reaction in acid media, International Journal of Hydrogen Energy 35(15) (2010) 8295-8302.

[23] D.H. Deng, L. Yu, X.Q. Chen, G.X. Wang, L. Jin, X.L. Pan, J. Deng, G.Q. Sun, X.H. Bao, Iron encapsulated within pod-like carbon nanotubes for oxygen reduction reaction, Angewandte Chemie-International Edition 52(1) (2013) 371-375.

[24] Y. Hu, J.O. Jensen, W. Zhang, L.N. Cleemann, W. Xing, N.J. Bjerrum, Q.F. Li, Hollow spheres of iron carbide nanoparticles encased in graphitic layers as oxygen reduction catalysts, Angewandte Chemie-International Edition 53(14) (2014) 3675-3679.

[25] Y. Wang, H. Sun, X. Duan, H.M. Ang, M.O. Tadé, S. Wang, A new magnetic nano zero-valent iron encapsulated in carbon spheres for oxidative degradation of phenol, Applied Catalysis B: Environmental 172–173 (2015) 73-81.

[26] G. Zhong, H. Wang, H. Yu, F. Peng, Nitrogen doped carbon nanotubes with encapsulated ferric carbide as excellent electrocatalyst for oxygen reduction reaction in acid and alkaline media, Journal of Power Sources 286 (2015) 495-503.

[27] Y.J. Yao, H. Chen, C. Lian, F.Y. Wei, D.W. Zhang, G.D. Wu, B.J. Chen, S.B. Wang, Fe, Co, Ni nanocrystals encapsulated in nitrogen-doped carbon nanotubes as Fenton-like catalysts for organic pollutant removal, Journal of Hazardous Materials 314 (2016) 129-139.

[28] J.J. Shi, Y.Y. Wang, W.C. Du, Z.Y. Hou, Synthesis of graphene encapsulated Fe_3C in carbon nanotubes from biomass and its catalysis application, Carbon 99 (2016) 330-337.

[29] M. Li, Y.P. Xiong, X.T. Liu, C. Han, Y.F. Zhang, X.J. Bo, L.P. Guo, Iron and nitrogen co-doped carbon nanotube@hollow carbon fibers derived from plant biomass as efficient catalysts for the oxygen reduction reaction, Journal of Materials Chemistry A 3(18) (2015) 9658-9667.

[30] W.X. Yang, X.J. Liu, X.Y. Yue, J.B. Jia, S.J. Guo, Bamboo-like carbon nanotube/Fe_3C nanoparticle hybrids and their highly efficient catalysis for oxygen reduction, Journal of the American Chemical Society 137(4) (2015) 1436-1439.

[31] W. Wei, H.W. Liang, K. Parvez, X.D. Zhuang, X.L. Feng, K. Mullen, Nitrogen-doped carbon nanosheets with size-defined mesopores as highly efficient metal-free catalyst for the oxygen reduction reaction, Angewandte Chemie-International Edition 53(6) (2014) 1570-1574.

[32] S. Trasobares, O. Stephan, C. Colliex, W.K. Hsu, H.W. Kroto, D.R.M. Walton, Compartmentalized CN_x nanotubes: Chemistry, morphology, and growth, Journal of Chemical Physics 116(20) (2002) 8966-8972.

[33] A.B. Wu, D.M. Liu, L.Z. Tong, L.X. Yu, H. Yang, Magnetic properties of nanocrystalline Fe/Fe_3C composites, Crystengcomm 13(3) (2011) 876-882.

[34] V. Nallathambi, N. Leonard, R. Kothandaraman, S.C. Barton, Nitrogen precursor effects in iron-nitrogen-carbon oxygen reduction catalysts, Electrochemical and Solid State Letters 14(6) (2011) B55-B58.

[35] X. Duan, H. Sun, Y. Wang, J. Kang, S. Wang, N-doping-induced nonradical reaction on single-walled carbon nanotubes for catalytic phenol oxidation, ACS Catalysis 5(2) (2015) 553-559.

[36] A.K. Schaper, H.Q. Hou, A. Greiner, F. Phillipp, The role of iron carbide in multiwalled carbon nanotube growth, Journal of Catalysis 222(1) (2004) 250-254.

[37] J.Y. Liang, C.C. Wang, S.Y. Lu, Glucose-derived nitrogen-doped hierarchical hollow nest-like carbon nanostructures from a novel template-free method as an outstanding electrode material for supercapacitors, Journal of Materials Chemistry A 3(48) (2015) 24453-24462.

[38] S.M. Zhang, H.Y. Zhang, Q. Liu, S.L. Chen, Fe-N doped carbon nanotube/graphene composite: facile synthesis and superior electrocatalytic activity, Journal of Materials Chemistry A 1(10) (2013) 3302-3308.

[39] H. Kim, W. Sigmund, Iron particles in carbon nanotubes, Carbon 43(8) (2005) 1743-1748.

[40] B. Zhang, J. Song, G. Yang, B. Han, Large-scale production of high-quality graphene using glucose and ferric chloride, Chemical Science 5(12) (2014) 4656-4660.

[41] Y. Yao, H. Chen, J. Qin, G. Wu, C. Lian, J. Zhang, S. Wang, Iron encapsulated in boron and nitrogen codoped carbon nanotubes as synergistic catalysts for Fenton-like reaction, Water Research 101 (2016) 281-291.

[42] M. Zhao, H.H. Song, Synthesis of carbon-encapsulated iron carbide/iron nanoparticles from phenolic-formaldehyde resin and ferric nitrate, Materials Chemistry and Physics 124(1) (2010) 861-864.

[43] Y.Z. Wang, Y. Liu, W. Liu, H.Y. Chen, G.X. Zhang, J.H. Wang, Morphological control of N-doped carbon nanotubes and their electrochemical properties, Materials Letters 154 (2015) 64-67.

[44] Y. Wang, H. Sun, H.M. Ang, M.O. Tadé, S. Wang, Facile synthesis of hierarchically structured magnetic $MnO_2/ZnFe_2O_4$ hybrid materials and their performance in heterogeneous activation of peroxymonosulfate, ACS Applied Materials & Interfaces 6(22) (2014) 19914-19923.

[45] Y. Wang, H. Sun, H.M. Ang, M.O. Tadé, S. Wang, Magnetic Fe_3O_4/carbon sphere/cobalt composites for catalytic oxidation of phenol solutions with sulfate radicals, Chemical Engineering Journal 245 (2014) 1-9.

[46] J. Zhang, R. Wang, E.Z. Liu, X.F. Gao, Z.H. Sun, F.S. Xiao, F. Girgsdies, D.S. Su, Spherical structures composed of multiwalled carbon

nanotubes: formation mechanism and catalytic performance, Angewandte Chemie-International Edition 51(30) (2012) 7581-7585.
[47] Y. Liu, X.Z. Wang, Y.F. Dong, Z.Y. Wang, Z.B. Zhao, J.S. Qiu, Nitrogen-doped graphene nanoribbons for high-performance lithium ion batteries, Journal of Materials Chemistry A 2(40) (2014) 16832-16835.
[48] S. Kundu, W. Xia, W. Busser, M. Becker, D.A. Schmidt, M. Havenith, M. Muhler, The formation of nitrogen-containing functional groups on carbon nanotube surfaces: a quantitative XPS and TPD study, Physical Chemistry Chemical Physics 12(17) (2010) 4351-4359.
[49] O. Soares, R.P. Rocha, A.G. Goncalves, J.L. Figueiredo, J.J.M. Orfao, M.F.R. Pereira, Easy method to prepare N-doped carbon nanotubes by ball milling, Carbon 91 (2015) 114-121.
[50] G. Wu, K.L. More, P. Xu, H.L. Wang, M. Ferrandon, A.J. Kropf, D.J. Myers, S.G. Ma, C.M. Johnston, P. Zelenay, A carbon-nanotube-supported graphene-rich non-precious metal oxygen reduction catalyst with enhanced performance durability, Chemical Communications 49(32) (2013) 3291-3293.
[51] M.L. Xiao, J.B. Zhu, L.G. Feng, C.P. Liu, W. Xing, Meso/Macroporous Nitrogen-doped carbon architectures with iron carbide encapsulated in graphitic layers as an efficient and robust catalyst for the oxygen reduction reaction in both acidic and alkaline solutions, Advanced Materials 27(15) (2015) 2521-2527.
[52] X. Duan, Z. Ao, H. Sun, S. Indrawirawan, Y. Wang, J. Kang, F. Liang, Z.H. Zhu, S. Wang, Nitrogen-doped graphene for generation and evolution of reactive radicals by metal-free catalysis, ACS Applied Materials & Interfaces 7(7) (2015) 4169-4178.
[53] X. Duan, K. O'Donnell, H. Sun, Y. Wang, S. Wang, Sulfur and nitrogen co-doped graphene for metal-free catalytic oxidation reactions, Small 11(25) (2015) 3036-3044.

[54] B. Jiang, D. Dai, Y. Yao, T. Xu, R. Li, R. Xie, L. Chen, W. Chen, The coupling of hemin with persistent free radicals induces a nonradical mechanism for oxidation of pollutants, Chemical Communications 52(61) (2016) 9566-9569.

[55] H. Zhao, Y.M. Dong, P.P. Jiang, G.L. Wang, J.J. Zhang, K. Li, C.Y. Feng, An alpha-MnO_2 nanotube used as a novel catalyst in ozonation: performance and the mechanism, New Journal of Chemistry 38(4) (2014) 1743-1750.

[56] A. Jawad, X.Y. Lu, Z.Q. Chen, G.C. Yin, Degradation of Chlorophenols by Supported Co-Mg-Al Layered Double Hydrotalcite with Bicarbonate Activated Hydrogen Peroxide, Journal of Physical Chemistry A 118(43) (2014) 10028-10035.

[57] J. Catalan, C. Diaz, L. Barrio, Analysis of mixed solvent effects on the properties of singlet oxygen ((1)Delta(g)), Chemical Physics 300(1-3) (2004) 33-39.

[58] R.A. Lundeen, C. Chu, M. Sander, K. McNeill, Photooxidation of the Antimicrobial, Nonribosomal Peptide Bacitracin A by Singlet Oxygen under Environmentally Relevant Conditions, Environmental Science & Technology (2016).

[59] M.Q. Yang, Y.H. Zhang, N. Zhang, Z.R. Tang, Y.J. Xu, Visible-Light-Driven Oxidation of Primary C-H Bonds over CdS with Dual Co-catalysts Graphene and TiO2, Scientific Reports 3 (2013).

[60] Y. Zhou, J. Jiang, Y. Gao, J. Ma, S.Y. Pang, J. Li, X.T. Lu, L.P. Yuan, Activation of Peroxymonosulfate by Benzoquinone: A Novel Nonradical Oxidation Process, Environmental Science & Technology 49(21) (2015) 12941-12950.

[61] Y.X. Wang, Y.B. Xie, H.Q. Sun, J.D. Xiao, H.B. Cao, S.B. Wang, Efficient catalytic ozonation over reduced graphene oxide for p-

hydroxylbenzoic acid (PHBA) destruction: active site and mechanism, Acs Applied Materials & Interfaces 8(15) (2016) 9710-9720.

Chapter 5 Morphological control of nitrogen-doped carbon nanostructures and their environmental application

Abstract

It is of great priority to design metal-free catalysts with excellent activity and good stability to be extensively applied in industry. Herein, a novel, facile and one-step synchronous carbonization and nitridation approach of nitrogen-doped mesoporous carbon nanostructures (NMCN) with different morphologies via one-step pyrolysis of a hybrid precursors (iron chloride, glucose and melamine) was reported, in which iron chloride served as a transition metal precursor, glucose as a carbon source and melamine as a nitridation agent. Detailed characterization techniques indicated that the morphologies and properties of catalysts depended strongly on the amount of nitrogen precursors. Different structures ranging from graphene to carbon nanotubes were observed in different materials, opening a straightforward and facile protocol to transform graphene into CNTs. NMCN-50 exhibited the largest specific surface area but NMCN-75 with the highest nitrogen content displayed some nanotubes. They were both highly active and stable for degradation of phenol via peroxymonosulfate activation. Kinetic investigations demonstrated that the first-order reaction kinetics was followed in the phenol degradation. Quenching experiments were implemented to probe the intrinsic mechanism of catalysts and demonstrated that a dominant non-radical processes together with a minimal radical processes coexisted in the phenol oxidation. The simple synthetic strategy, cheap precursors, excellent degradation efficiency and the proposed mechanism are likely to enlighten the development of green carbon-based catalysts in environmental remediation.

5.1 Introduction

An excessive growing of human society and rapid urbanization and industrialization have caused a range of environmental problems which exerted a heavy burden on the ecosystem, especially the negative impact on the safe and secured water for lives on the earth. Water pollution has become a public concern that requires ongoing evaluation and revision. With respect to wastewater treatment, a variety of effective methods such as physical adsorption, photocatalytic degradation, flocculation/coagulation, bioremediation, and chemical oxidation have been developed to remove the toxic contaminants in polluted waterbodies.[1-3]

In the past few decades, advanced oxidation processes (AOPs) have received great applauses because of the outstanding ability to oxidize stubborn organic compounds.[4, 5] However, hydroxyl radical-based AOPs suffer from the requirements for low pH and large quantity of chemical reagents. Recently, sulfate radical-based AOPs (SR-AOPs) have aroused public concern for removal of recalcitrant organics from wastewater because sulfate radicals have a stronger oxidative capacity (2.5-3.1 V), a better selectivity to target organics and a relatively long lifespan.[6-8] Electron transfer mechanism is present in its reaction with organic pollutants with 10^6-10^9 M^{-1} s^{-1} second-order rate constant. Sulfate radicals can be generated by the activation of persulfate (PS) or peroxymonosulfate (PMS) via UV, heat, transition metals and metal oxides, and metal-free catalysts.[9-12] Homogeneous and heterogeneous catalysis initiated by transition metals and their corresponding metal oxides have been applied for the effective activation of PMS to produce sulfate radicals to remove organic toxicants.[7, 13-16] However, metal-

based catalysts suffer from poor stability and inevitable metal ion leaching, which exerts a detrimental environmental impact and thus seriously restrains their practical applications.

In the past decades, carbon nanomaterials, such as graphene, graphene oxide, reduced graphene oxide and carbon nanotubes, etc. have been applied as favorable alternatives to metal-based catalysts without the problem of metal ion leaching due to their wide availability and unique physical and chemical properties including large theoretical surface area, chemical inertness to acidic and basic environments, distinctive electronic property, superb thermal conductivity, good recycling characteristics as well as unique carbon framework.[17-19]

Doping with heteroatoms, for example, N, S, P, have been demonstrated to modify surface chemistry of carbon materials.[20, 21] To be mentioned, the introduction of nitrogen atoms into a carbon skeleton can trigger the change of charge density on the atoms and enhance the polarity of carbon materials, and thus increase conductivity, wettability, and adsorption selectivity.[22] Simultaneously, the introduced nitrogen can increase the basicity and coordination properties of the carbon materials. And the amount of nitrogen present in the materials affects their performance in catalysis. Ubiquitous N-containing carbon materials are indispensable in a variety of state-of-the-art scientific applications such as water treatment, gas separation, catalyst supports, as well as electrodes for both electrochemical double layer capacitors and fuel cells.[23, 24] Nowadays, nitrogen-doped mesoporous carbon nanostructures (NMCN) have aroused great attentions due to the modification of surface structure, improvement of p-binding or π-binding ability and growth of active sites resulted from electron-rich

nitrogen atoms. Extensive researches have confirmed that doping nitrogen moderately into the carbon configuration can notably enhance the catalytic performance of nanocarbon structures applied in wastewater treatment, especially phenolic wastewater, because the functional groups with nitrogen improve the electronic conductivity enjoyed by carbon material itself.[25-30] Owing to the popularity of NMCN, a range of approaches have been developed to introduce N into carbon structures. On one hand, direct synthesis with nitrogen-containing precursors, such as melamine, N-heterocycles, and benzylamine can generate N-doped carbon materials.[31, 32] Melamine, due to tis high nitrogen content of 66.7%, is most commonly used as a nitrogen precursor. On the other hand, posttreatment of carbon exposed to N-containing compounds, for example, NH_3 at high temperatures can also obtain NMCN. N-doped carbon nanostructures synthesized by the former method often have more structural nitrogen and homogeneous incorporation of nitrogen combined with controlled bulk properties, and thereby is considered as the desirable methodology for the preparation of N-doped carbon.[33]

In this work, we report a novel and simple one-pot approach to controllably synthesize N-doped mesoporous carbon nanostructures with different morphologies from graphene to carbon nanotubes via direct pyrolysis of iron chloride, glucose and melamine. The obtained nitrogen-modified mesoporous carbon nanostructures were denoted as NMCN-X (X referring to the mass percentage of melamine to that of glucose). Various techniques were utilized to characterize the morphologies and structures of carbon nanomaterials and their catalytic performance were studied specifically by the degradation of phenolic wastewater.

5.2 Experimental

Materials and Chemical Reagents. D-glucose, melamine, potassium peroxymonosulfate ($2KHSO_5 \cdot 3KHSO_4 \cdot K_2SO_4$), hexahydrate ferric chloride ($FeCl_3 \cdot 6H_2O$), sodium azide (NaN_3), p-benzoquinone (PBQ), and tert-butyl alcohol (TBA) were brought from Sigma-Aldrich. Acetone and hydrochloric acid (35-37 wt%) were obtained from Chem-Supply. Phenol was obtained from Ajax Finechem. High purity nitrogen gas was from BOC. All these chemical reagents were of analytical grade and utilized as delivered with no further purification. Ultrapure water was employed in the whole process.

Synthesis of Nitrogen-doped Mesoporous Carbon Nanostructures. A typical process was shown as follows: 3g $FeCl_3 \cdot 6H_2O$, 3g D-glucose and X melamine (X means the mass percentage of melamine to that of glucose) were first mixed in 10 mL ultrapure water to obtain a uniform solution and put into an oven of 80 ^oC overnight to remove water. Then, a yellow solid was obtained and ground. Subsequently, the mixture was moved into a porcelain boat and put into the centre of tube furnace, and afterwards heated to 700 ^oC at a rate of 5 ^oC min^{-1} within a N_2 flow for 6 h. When falling to room temperature, the obtained combustion products was pulverized into powder and submerged in 35-37 wt% hydrochloric acid (HCl) solution to remove impurities for 6h. The product was washed in ultrapure water and acetone for several times until there is no chloride ion in the upper solution and dried overnight at 80 ^oC. Eventually, nitrogen-doped mesoporous carbon nanostructures with different amount of melamine (i.e., NMCN-25, NMCN-50, NMCN-75) were obtained. In addition, NMCN-25 ethanol, NMCN-50 ethanol, NMCN-75 ethanol were also prepared by the same processes but the precursors were dissolved in ethanol instead of water. By comparison,

NG was also prepared by the same procedures without the addition of melamine.

Characterization of Materials. X-ray diffraction (XRD) instrument of Bruker D8 Advance was used to characterize the crystalline structure of carbon materials using a Cu-Kα radiation withλ at 1.5418 Å. Raman spectra were obtained from an ISA dispersive Raman instrument with an argon ion laser at 514 nm. Information on surface compositions was acquired by X-ray photoelectron spectroscopy (XPS) on a Thermo Escalab 250 under radiation of Al-Kα X-ray. The specific surface areas as well as distributions of pore size, obtained on a Tristar II 3020, were calculated by the Brunauere-Emmette-Teller (BET) equation and the Barrette-Joynere-Halenda (BJH) method, respectively. Scanning electron microscopy (SEM) was utilized to characterize the surface morphologies of the samples by a Zeiss Neon 40 EsB FIBSEM. Thermal behavior of carbon materials was carried out by a Mettler-Toledo-Star thermal analyzer in air with a heating rate of 10 ^{o}C min^{-1} ranging from 35 to 1000 ^{o}C.

Catalytic Tests. The decomposition of phenol solution was implemented with a 250 mL glass bottle with certain concentrations of phenol solution, carbon catalysts and PMS in temperature-controlled water bath. 1 mL phenol solution, withdrawn by a syringe and filtered by a 0.45 mm Millipore film, was finally injected into a glass vial at each time interval. Subsequently, quenching agent of 0.5 mL methanol was added immediately. After shaking the vial vibrantly, the solution was analyzed by a Thermo-Fisher Scientific 3000 UHPLC system (ultra-high performance liquid chromatograph with a UV detector at 270 nm. An Acclaim RSLC C-18 column was utilized and a mixture of 30%

acetonitrile and 70% water was used as the mobile phase at a constant flow rate of 1 mL/min.

5.3 Results and Discussions

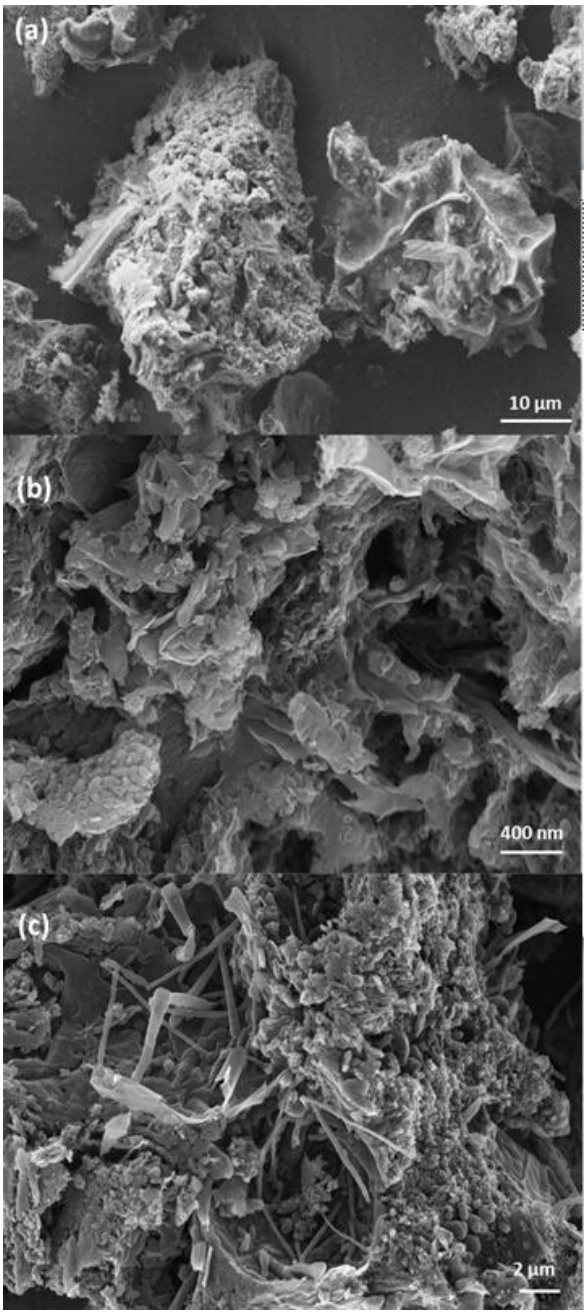

Figure 5.1 SEM images of (a) NMCN-25, (b) NMCN-50, (c) NMCN-75.

The morphologies and microstructures of different NMCNs were investigated by SEM. As illustrated in Figure 5.1, exfoliated and crinkled layers with partial aggregation were observed in NMCNs. The disruption and irregularity demonstrated that the incorporation of nitrogen into the framework was not only at the defective sites network but also into the interior. Some ultralong but nonuniform carbon nanotubes (CNTs) were occurred in NMCN-75, demonstrating that high content of nitrogen sources facilitate the transformation of graphene into CNTs, further improving the catalytic performance and in phenol degradation (as shown in Figure 5.7 (a)). It may open a straight and facile protocol to transfer graphene into CNTs.

Figure 5.2 displays XRD patterns of NMCN nanomaterials. Sharp and strong diffraction peaks at 26^{o} as well as broad and weak ones at 44^{o} were all observed in NMCN materials with water, which correspond to the (002) and (101) crystal planes of standard hexagonal graphite, respectively,[34] confirming the formation of graphitic structure and occurrence of pronounced graphitization during the carbonization.

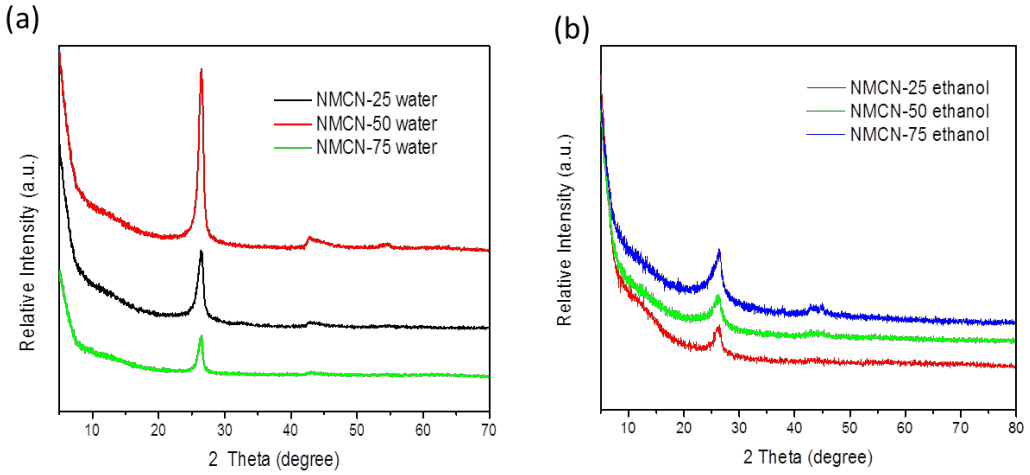

Figure 5.2 XRD patterns of NMCNs prepared in (a) water and (b) ethanol.

Same diffraction peaks were also observed in NMCN-25 ethanol, NMCN-50 ethanol, NMCN-75 ethanol but these peaks are weaker and broader than those of NMCNs synthesized with water, meaning that less pronounced graphitization occurred in ethanol and water can promote more graphitization of the catalysts during the process.

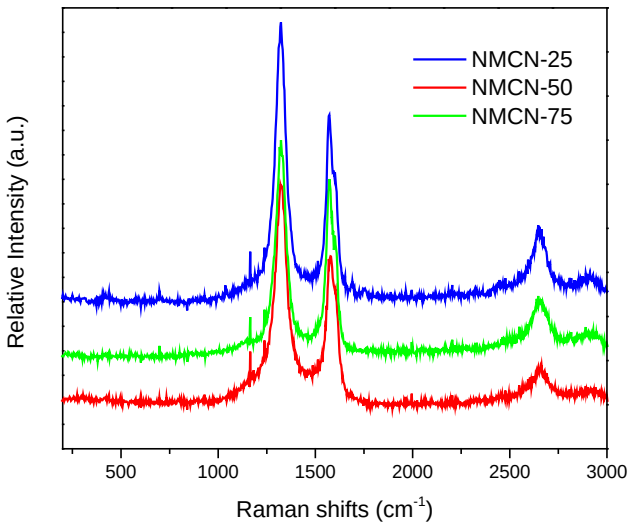

Figure 5.3 Raman spectra of NMCN-25, NMCN-50 and NMCN-75.

Raman spectroscopy is another cathedratic method for the in-depth study of graphitization degree, number of layers and doping condition of carbon nanostructures. G-band denotes the presence of sp^2-hybridized carbon atoms in carbon materials, D-band offers information on the existence of disordered carbon structure and 2D-band suggests the number of layers existed in graphene materials.[35]

Figure 5.3 depicts the Raman spectra of NMCN-25, NMCN-50 and NMCN-75. The distinctive D band at 1319 cm^{-1}, G band at1571 cm^{-1} and 2D band at 2646 cm^{-1} were all seen in Figure 5.3. I_D/I_G (the intensity ratio of D and G bands) is used to estimate the defect and disorder presented in carbon nanomaterials.[36] The I_D/I_G values of NMCN-25,

NMCN-50 and NMCN-75 were calculated to be 1.30, 1.43 and 1.16, respectively, demonstrating the graphitization degree increased first and then decreased with the amount of nitrogen sources. It could be inferred from Raman results that the most defective degrees were obtained in NMCN-50, which is most likely because nitrogen incorporation caused great interruption to the previous well-ordered honeycomb structures,[37] as illustrated by the largest amount of quaternary N in NMCN-50 from XPS results. The strong D band further showed that defect density could be greatly increased by the nitrogen doping.[38]

In addition, as seen from XPS results, most N dopants are at the location of the edges of carbon matrix and thus generate pyrrolic N and pyridinic N for NMCN-25 and NMCN-75, therefore, their graphitic structures are less distorted and the values of I_D/I_G are lower. Another reason for the smallest I_D/I_G of NMCN-75 is the formation of carbon nanotubes which limit the incorporation of nitrogen into the interior and thus generation of the most amount of pyridinic N.

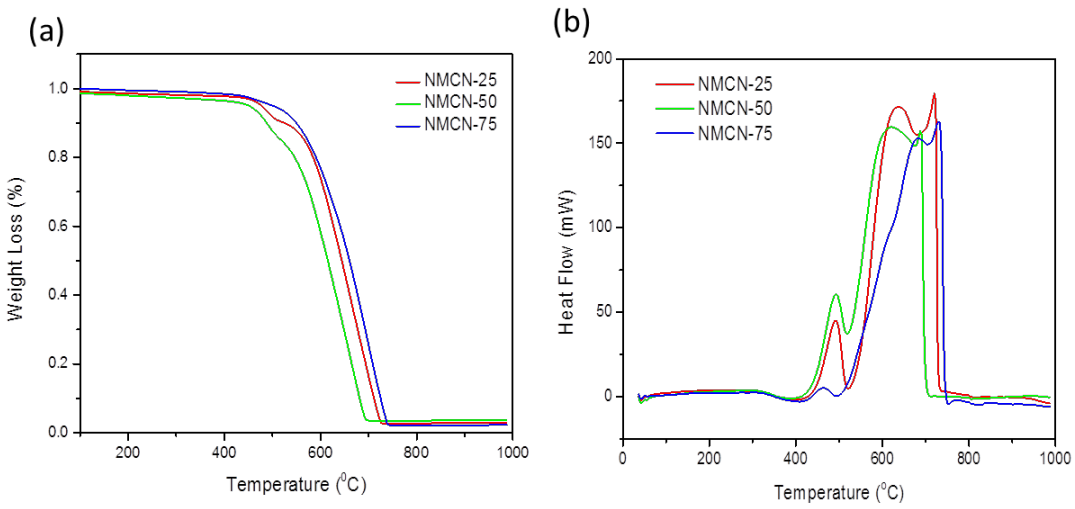

Figure 5.4 TGA (a) and DSC (b) curves of NMCN-25, NMCN-50 and NMCN-75.

The thermal behaviors of all the three samples were investigated by TGA-DSC with air atmosphere at a heating rate of 10 ^{o}C min^{-1} from 35 to 1000 ^{o}C. The curves are presented in Figure 5.4. Three regions are indicated by Figure 5.4 (a) about the process of NMCN weight loss. To start with, from 35 ^{o}C to approximately 300 ^{o}C, sample weight loss is slight as adsorbed water molecules evaporate. Afterwards, a minor loss in weight is emerged from 300 to 500 ^{o}C due to the emission of CO_2 and H_2O which generated by the decomposition of remaining oxygen functional groups, and the DSC curves also showed a characteristic step or peak at 492, 493, 462 ^{o}C for NMCN-25, NMCN-50 and NMCN-75, respectively. In the end, the temperature range from 500 to 730 ^{o}C witnesses a dramatic weight loss. The TGA and DSC curves demonstrate a characteristic step or strong exothermal peak at 636, 623, 684 ^{o}C for NMCN-25, NMCN-50 and NMCN-75, respectively, simply attributed to carbon combustion and breakdown. No further weigh loss of NMCN can be seen after 730 ^{o}C. The weight loss was determined to be stabilized at 2.8 %, 3.6 %, 2.3 % after 719, 687, 729 ^{o}C for NMCN-25, NMCN-50 and NMCN-75, respectively, indicating the complete combustion of carbon. In addition, thermal stability has an inverse dependence on the specific surface area. As shown in Figure 5.4 (b), the burn-off temperature of NMCN samples was in an order: NMCN-50 $<$ NMCN-25 $<$ NMCN-75.

The specific surface area and pore structures of the prepared carbon nanomaterials were studied by nitrogen sorption measurements. Figure 5.5 demonstrates N_2 adsorption/desorption isotherms as well as respective pore size distributions of NMCN-25, NMCN-50 and NMCN-75. All the samples exhibited the characteristic of type IV adsorption/desorption isotherm (classified by IUPAC) with a well-

defined hysteresis loop at the relative pressure ranging from 0.4 to 0.9, displaying the existence of mesoporous structures. NMCN-50 had a broader hysteresis loop than the other two samples, implying a more porous structure with larger surface area and pore volume. Table 5.1 specifically lists some textural parameters of the prepared carbon nanomaterials.

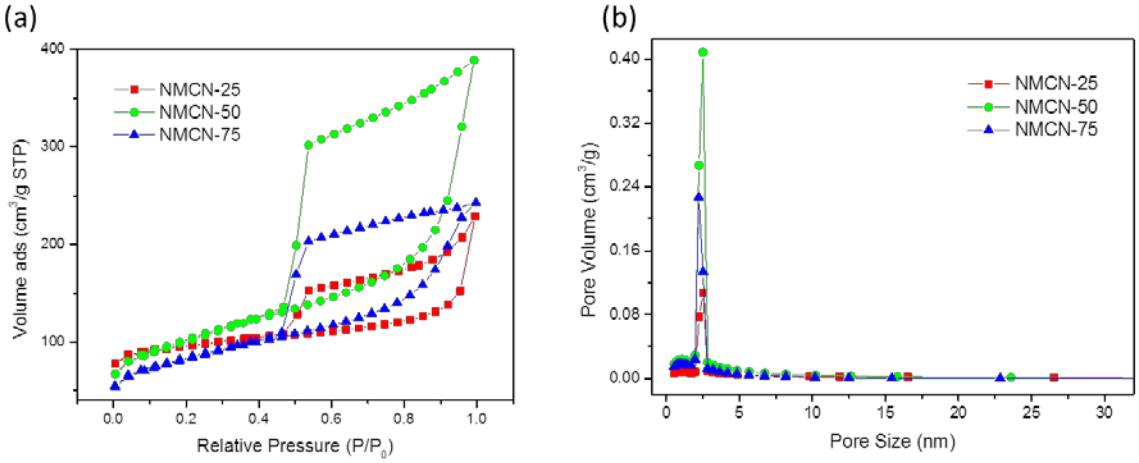

Figure 5.5 (a) N_2 adsorption/desorption isotherms and (b) pore size distributions of NMCN-25, NMCN-50 and NMCN-75.

The pore sizes of all samples are focused on 2-4 nm. The specific surface areas (SSA) are found to be 312.2, 348.1 and 284.3 m^2/g for NMCN-25, NMCN-50 and NMCN-75, respectively. NMCN-50 has the largest SSA, partially owing to the formation of high-quality graphene layers as shown in SEM. However, when the amount of melamine increased to 75% of that of glucose, SSA decreased accordingly, mainly because some carbon nanotubes were formed and the spaces between layered hierarchical structures decreased to induce lower exfoliation degree.

Table 5.1 Textural properties of NMCN-25, NMCN-50 and NMCN-75.

	BET surface area, m^2/g	Pore volume, cm^3/g	Average pore size, nm
NMCN-25	312.2	0.17	4.0
NMCN-50	348.1	0.35	2.7
NMCN-75	284.3	0.19	2.3

XPS was utilized to study the compositions of different elements on the surfaces of samples and relevant data and fitting results are illustrated in Figure 5.6. All the carbon nanostructures exhibit a very low ratio of oxygen, rather lower than that of rGO and N-rGO,[39, 40] indicating that this novel approach can generate high-quality carbon materials. Meanwhile, oxygen level increased with the amount of nitrogen precursors partially due to the introduction of more NO_x species. The nitrogen levels of NMCN-25, NMCN-50 and NMCN-75 were estimated to be 1.28%, 2.37% and 6.36%, exceptionally higher than those of nitrogen-doped single walled CNT[28], nitrogen-doped annealed nanodiamonds.[41]

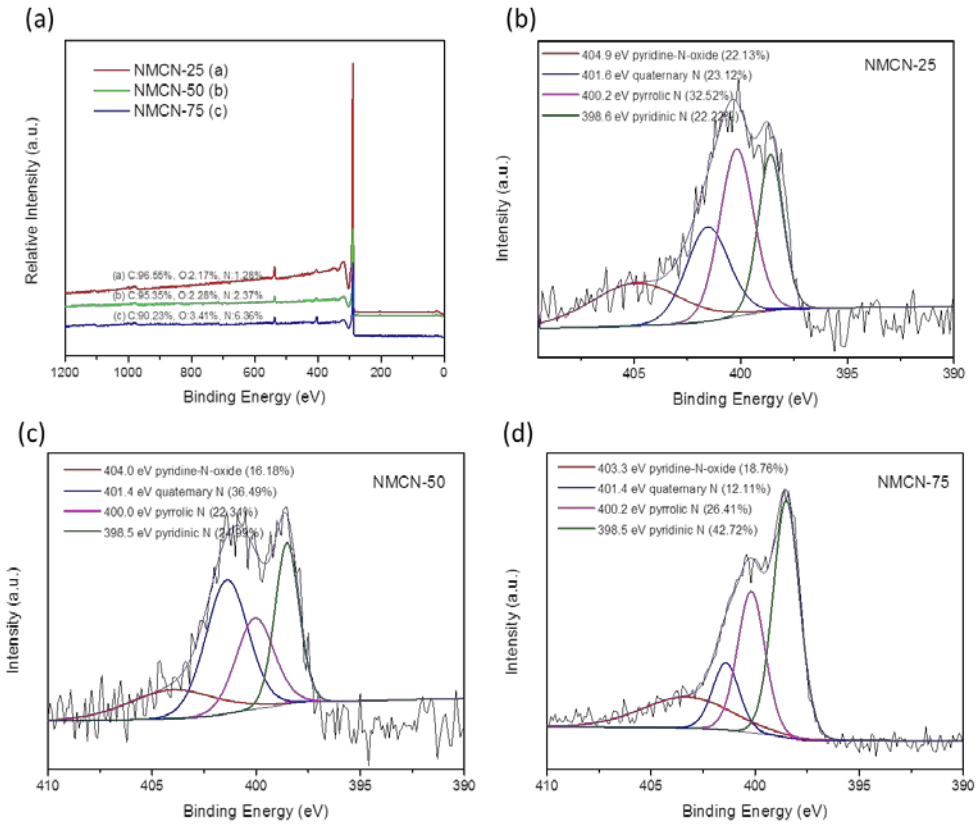

Figure 5.6 XPS surveys of NMCN-25, NMCN-50 and NMCN-75 (a); and N 1s scan of NMCN-25 (b), NMCN-50 (c) and NMCN-75 (d).

To be specific, pyridinic N is at the location of 398.3 eV, via the replacement of a carbon atom with a nitrogen atom on the edge or defect sites. In addition, peaks located at 399.7 eV and 401.4 eV are ascribed to pyrrolic and/or pyridone-N moieties and quaternary nitrogen, respectively. Meanwhile, pyridine-N-oxide at 403.0 eV was also found.[42, 43] More quaternary N were found in NMCN-50 but more pyridinic N were formed in NMCN-75, indicating that more nitrogen sources can help nitrogen incorporate into the interior of carbon materials, but excess nitrogen would exert a small impact on the formation of quaternary N. Another reason for the generation of pyridinic N instead of quaternary N in NMCN-75 may be partially due to the formation of carbon nanotubes, which limited the encapsulation of

nitrogen into the interior. Similar to previous studies, the pseudocapacitive interactions are primarily initiated by pyrrolic and pyridinic groups with negative charges, while quaternary N and pyridine-N-oxide with positive charges may be conducive to the electron transfer in the carbon configuration and thus improve conductivity of carbon nanomaterials. Therefore, more quaternary N and pyridine-N-oxide facilitate the catalytic performance to decompose phenolic compounds, as illustrated in the results of phenol degradation.

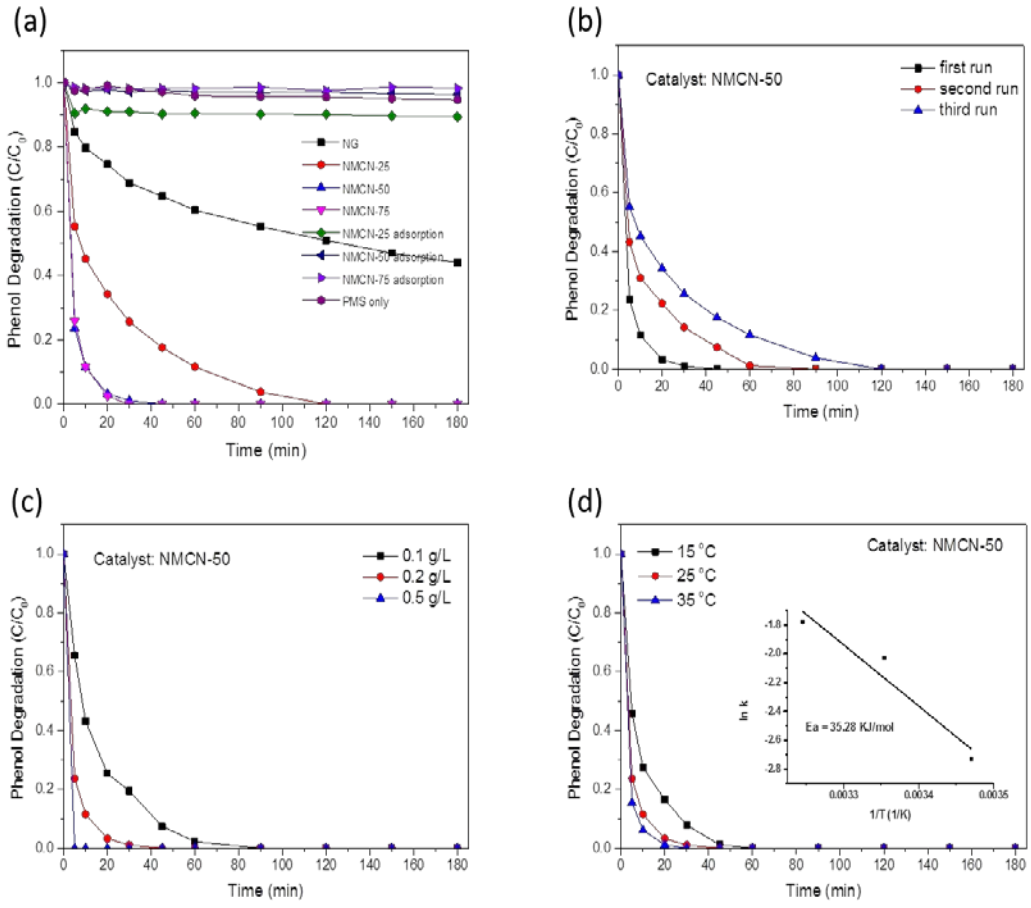

Figure 5.7 (a) catalytic oxidation of phenol under various carbon nanomaterials; (b) stability tests of NMCN-50 (catalyst: 0.2 g/L; PMS: 2 g/L; T: 25 ^{o}C); (c) effect of catalyst loading on the catalytic oxidation of phenol; (d) effect of reaction temperature on the catalytic oxidation of phenol.

Figure 5.7 displayed the catalytic degradation of phenol solutions by a range of carbon nanostructures via PMS activation. As shown in Figure 5.7 (a), without a catalyst, PMS can only degrade 6% phenol due to its weak ability to produce active radicals, indicating that ambient temperature cannot induce PMS activation to produce sulfate radicals. Similarly, with no PMS, only around 10, 4 and 2% phenol was adsorbed by NMCN-25, NMCN-50 and NMCN-75, respectively. NMCN-25, NMCN-50 and NMCN-75 had the ability to degrade 100% phenol in 120, 45 and 30 min, respectively, and NMCN-75 exhibited the best catalytic performance primarily owing to the synergistic effect of graphene and carbon nanotubes. These results were superior to some metal-based catalysts (Co_3O_4, MnO_2, CuO and Fe_3O_4), better than those of reduced graphene oxide,[40] pristine nanodiamond, single-walled carbon nanotubes (SWCNTs),[19] multi-walled carbon nanotubes (MWCNTs), CMK,[44] sulfur and nitrogen co-doped graphene[27], parallel to that of rGO-900.[19]

The outcomes of phenol degradation further concluded that nitrogen doping and SSA exerted vital impacts on the catalytic phenol removal. NMCN-50, with the largest SSA, can degrade 100% phenol in just 45 min and NMCN-75, with the most nitrogen doping, can degrade 100% phenol in only 30 min, implying that nitrogen doping is a decisive factor in the enhancement of phenol oxidation. The reason for this is that electronic structure of adjacent carbon atoms may be altered by the doped nitrogen and therefore electron transfer quickly to accelerate the catalytic reactions.

Despite post-treatment of acid leaching, metal impurities are often unfavorably introduced into the carbon materials in the synthesis of

carbon nanostructures, which will seriously affect the catalytic performance of carbon materials.[45, 46] However, Figure 5.6 (a) verified that no significant iron elements were found in all the carbon nanostructures. Meanwhile, the solution after phenol degradation presented no color, which demonstrated that there is no Fe^{2+} or Fe^{3+} in the solution, further proving that excellent catalytic activity was attributed to functional groups and active sites of carbon nanostructures in the PMS activation.

The following pseudo-first-order reaction was used to calculate the kinetic rates of carbon nanostructures,

$$\ln(C/C_0) = -kt \quad \text{(Eq. 5.1)}$$

In this equation, C_0 and C refer to the initial phenol concentration and that at different time, and k represents the reaction rate constant, which was calculated to be 0.065, 0.13 and 0.17 min^{-1} for NMCN-25, NMCN-50 and NMCN-75, respectively. With more nitrogen precursors, NMCN-50 and NMCN-75 presented higher activities than NMCN-25. However, the reaction rate of NMCN-75 is only a little bit faster than that of NMCN-50, suggesting that excess nitrogen sources have a small impact on the catalytic performance. Therefore, based on the above characterization results, we chose NMCN-50 as the typical catalyst to investigate the catalyst stability, impacts of catalyst loading and reaction temperature on the catalytic performance as well as the intrinsic mechanism.

Stability reactions were performed on NMCN-50 and are displayed in Figure 5.7 (b). Complete phenol removal were obtained at 45, 90 and

120 min for the first, second and third runs. However, 100% phenol was decomposed by N-doped CNT in 20 and 120 min in the first and second runs, respectively, but only 89% phenol for the third run.[28] In addition, the fresh sample can completely degrade phenol in 45 min, but took 180 min to remove only 58% and 31% phenol for the second and third times, respectively.[25] The intricate effects derived from surface chemistry and structure changes may result in the deactivation of nanomaterials. These effects include intermediates adsorption, alteration in pore structures, coverage of active sites on the surface, and reconstruction of dopants in the carbon framework.

The influence of catalyst loading exerted on phenol oxidation is shown in Figure 5.7 (c). Taking NMCN-50 as an example, complete phenol removal was obtained in just 5, 45 and 90 min for 0.5, 0.2 and 0.1 g/L loadings of NMCN-50, respectively. Due to the negligible adsorption of phenol on NMCN-50, more active sites from more catalyst usage for PMS activation may result in the superb increase in phenol degradation.
The influence of reaction temperature exerted on phenol removal by NMCN-50 is shown in Figure 5.7 (d). With elevated temperatures, the efficiency of phenol degradation increased moderately. Specifically, phenol was completely removed by NMCN-50 in 60, 45 and 30 min at 15, 25 and 35 ^{o}C, respectively. This may be attributed to the more reactive radicals created by electron transfer at elevated temperatures. The activation energy of NMCN-50 for phenol removal, on the basis of the first order kinetics and calculated by the Arrhenius equation, was estimated to be 35.3 kJ/mol, much lower than that of graphene (84.0 kJ/mol), annealed nanodiamonds (85.1 kJ/mol),[41] multi-walled carbon nanotubes (44.6 kJ/mol) and parallel to that of N-CNT (36.0 kJ/mol).[28]

Previous studies have investigated the mechanisms of catalytic oxidation of phenol by metal-based catalysts and metal-free carbon catalysts and found that hydroxyl and sulfate radicals are the major radicals generated to activate PMS to degrade phenol solutions.[25, 47-49] Recent reports have shown that PMS self-decomposition can generate singlet oxygen ($^1O_2$) with a rate constant k of approximately 0.2 M^{-1} s^{-1}.[50, 51] Meanwhile, PMS can also be activated by ketones and benzoquinone to generate $^1O_2$.[52]

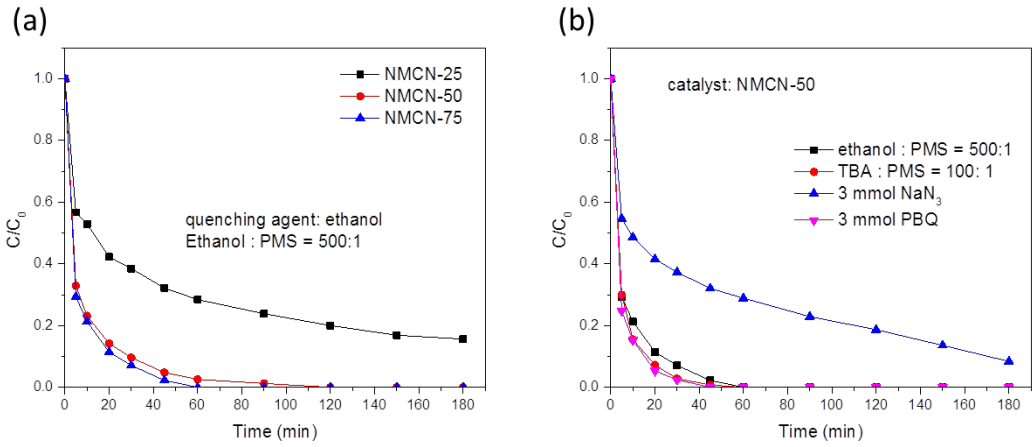

Figure 5.8 (a) Effects of radical quenching by ethanol on phenol degradation for NMCN-25, NMCN-50 and NMCN-75, and (b) Competitive radical tests of phenol degradation for NMCN-50. Reaction conditions: phenol 20 ppm, catalyst loading 0.2 g L^{-1}, PMS 2 g L^{-1}, temperature 25 °C.

To validate the effects of $^{\bullet}OH$ and $SO_4^{\bullet-}$ radicals and $^1O_2$, different radical quenching tests were performed. Ethanol was regarded as an effective quenching agent for $^{\bullet}OH$ and $SO4^{\bullet-}$ radicals. Phenol degradation would be greatly hindered if $^{\bullet}OH$ and $SO4^{\bullet-}$ are the dominant reactive species in the processes.[44] Control experiments on NMCN-25, NMCN-50 and NMCN-75 were conducted with addition of

ethanol at a molar ratio of ethanol : PMS = 500 : 1. As shown in Figure 5.8 (a), the catalytic performance of NMCN-25 was decreased but that of NMCN-50 and NMCN-75 were not greatly influenced compared to that without ethanol, indicating that $^{\bullet}OH$ and $SO_4^{\bullet-}$ were the major reactive species presented in the activation of PMS for NMCN-25 but not for NMCN-50 and NMCN-75. This further revealed that more nitrogen sources could change the mechanism from radical to non-radical processes. NMCN-50 was taken as the major catalyst to further investigate the radicals generated in the processes. *Tert*-butanol (TBA) was used as the scavenger of $^{\bullet}OH$ due to its stagnated reaction with $SO_4^{\bullet-}$ radicals. When the molar ratio of TBA to PMS is 100 : 1, degradation efficiency was not greatly reduced, further confirming that $^{\bullet}OH$ were not the dominant species and the process is not completely induced by radicals.[53]

Sodium azide (NaN_3) was selected to quench $^1O_2$ in the light of previous study.[54, 55] It is noticeable that $^1O_2$ could degrade phenol efficiently while minor reactivity was observed by ethanol and TBA. The addition of NaN_3 could prevent the effective degradation of phenol solution and only 92% phenol was removed in 180 min as illustrated in Figure 5.8 (b). Although $^{\bullet}OH$ and $SO_4^{\bullet-}$ radicals could also be scavenged by NaN_3, 3 mM NaN_3 exhibited a weaker ability to quench $^{\bullet}OH$ and $SO_4^{\bullet-}$ than that of ethanol, which is considered to be more effective in the prevention of phenol removal than NaN_3 if $^{\bullet}OH$ or $SO_4^{\bullet-}$ radicals are regarded as the dominant reactive species. On the contrary, $^1O_2$ was proved to contribute primarily to phenol degradation. As a result, the decrease in degradation efficiency from 100% phenol removal in just 45 min to 92% removal in 180 min with NaN_3 was ascribed to $^1O_2$ quenching. In addition, the

efficiency of phenol degradation was not suppressed by adding p-benzoquinone (PBQ), an effective scavenger for superoxide ($^{\bullet}O_2^-$).

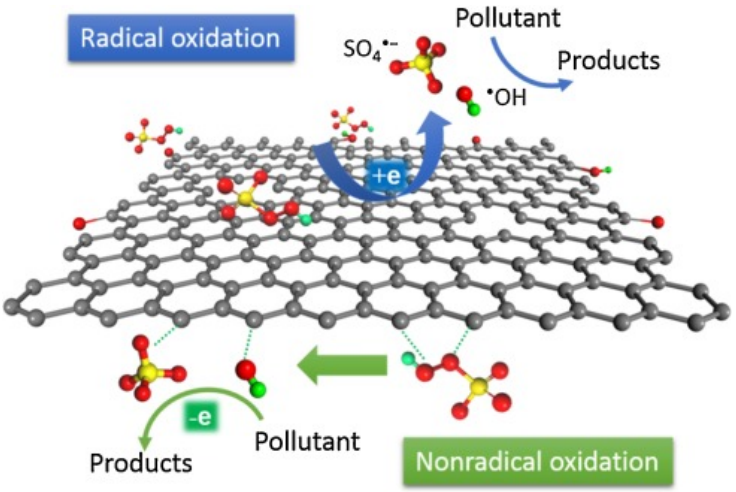

Scheme 5.1 The mechanism of PMS activation by NMCN-50.

In conclusion, although catalytic performance was a bit influenced by the introduction of ethanol and TBA, NaN_3 quenching exerted a more serious effect, demonstrating that $^1O_2$ was the major reactive oxygen species generated in phenol catalytic oxidation. The possible mechanism of the superb activity and outstanding stability of NMCN-50 in PMS activation for phenol degradation can be explained by a combination of radical and non-radical processes. The mechanism of PMS activation on NMCN-50 is illustrated in Scheme 5.1.[44]

5.5 Conclusions

A green and facile pyrolysis synthesis of iron chloride, melamine and glucose was applied to fabricate nitrogen-doped mesoporous carbon nanostructures with morphology modifications from graphene to carbon nanotube. The prepared materials have low oxygen content and high nitrogen content with large specific surface area. NMCN-50 and NMCN-

75 exhibited excellent performance in catalytic oxidation of PMS to degrade phenol solutions. The specific surface area as well as the amount of nitrogen precursors play a combined role in the enhancement of catalytic performance. However, excess nitrogen sources somehow prevent nitrogen from incorporating into the interior and thus decrease the defective sites, specific surface area and the amount of quaternary nitrogen, further limiting the improvement of catalytic performance. Quenching tests were employed to investigate the generated reactive species, and $^1O_2$ were demonstrated to be the dominant oxygen species in catalytic phenol oxidation. It was concluded that this catalyst follows major non-radical and minor radical processes to activate PMS to degrade phenol. This novel synthetic approach, excellent performance and stability and proposed mechanism will stimulate the development of green carbon-based materials in environmental remediation.

References

[1] X. Wang, Y. Qin, L. Zhu, H. Tang, Nitrogen-doped reduced graphene oxide as a bifunctional material for removing bisphenols: synergistic effect between adsorption and catalysis, Environmental science & technology 49(11) (2015) 6855-6864.

[2] V.J.P. Vilar, F.C. Moreira, A.C.C. Ferreira, M.A. Sousa, C. Gonçalves, M.F. Alpendurada, R.A.R. Boaventura, Biodegradability enhancement of a pesticide-containing bio-treated wastewater using a solar photo-Fenton treatment step followed by a biological oxidation process, Water research 46(15) (2012) 4599-4613.

[3] A.K. Verma, R.R. Dash, P. Bhunia, A review on chemical coagulation/flocculation technologies for removal of colour from textile

wastewaters, Journal of environmental management 93(1) (2012) 154-168.
[4] P.V. Nidheesh, R. Gandhimathi, S.T. Ramesh, Degradation of dyes from aqueous solution by Fenton processes: a review, Environmental Science and Pollution Research 20(4) (2013) 2099-2132.
[5] A.R. Ribeiro, O.C. Nunes, M.F.R. Pereira, A.M.T. Silva, An overview on the advanced oxidation processes applied for the treatment of water pollutants defined in the recently launched Directive 2013/39/EU, Environment international 75 (2015) 33-51.
[6] F. Ghanbari, M. Moradi, Application of peroxymonosulfate and its activation methods for degradation of environmental organic pollutants, Chemical Engineering Journal 310 (2017) 41-62.
[7] P. Hu, M. Long, Cobalt-catalyzed sulfate radical-based advanced oxidation: a review on heterogeneous catalysts and applications, Applied Catalysis B: Environmental 181 (2016) 103-117.
[8] W.-D. Oh, Z. Dong, T.-T. Lim, Generation of sulfate radical through heterogeneous catalysis for organic contaminants removal: Current development, challenges and prospects, Applied Catalysis B: Environmental 194 (2016) 169-201.
[9] M. Nie, Y. Yang, Z. Zhang, C. Yan, X. Wang, H. Li, W. Dong, Degradation of chloramphenicol by thermally activated persulfate in aqueous solution, Chemical Engineering Journal 246 (2014) 373-382.
[10] X. Chen, J. Chen, X. Qiao, D. Wang, X. Cai, Performance of nano-Co_3O_4/peroxymonosulfate system: kinetics and mechanism study using Acid Orange 7 as a model compound, Applied Catalysis B: Environmental 80(1) (2008) 116-121.
[11] Q. Liu, Z. Zheng, X. Yang, X. Luo, J. Zhang, B. Zheng, Effect of factors on decolorization of azo dye methyl orange by oxone/natural

sunlight in aqueous solution, Environmental Science and Pollution Research 19(2) (2012) 577-584.
[12] C. Liang, C.J. Bruell, M.C. Marley, K.L. Sperry, Persulfate oxidation for in situ remediation of TCE. I. Activated by ferrous ion with and without a persulfate-thiosulfate redox couple, Chemosphere 55(9) (2004) 1213-1223.
[13] G.P. Anipsitakis, D.D. Dionysiou, Degradation of organic contaminants in water with sulfate radicals generated by the conjunction of peroxymonosulfate with cobalt, Environmental science & technology 37(20) (2003) 4790-4797.
[14] G.P. Anipsitakis, D.D. Dionysiou, Radical generation by the interaction of transition metals with common oxidants, Environmental science & technology 38(13) (2004) 3705-3712.
[15] D.S. Mathew, R.-S. Juang, An overview of the structure and magnetism of spinel ferrite nanoparticles and their synthesis in microemulsions, Chemical Engineering Journal 129(1) (2007) 51-65.
[16] E. Saputra, S. Muhammad, H. Sun, H.-M. Ang, M.O. Tadé, S. Wang, Manganese oxides at different oxidation states for heterogeneous activation of peroxymonosulfate for phenol degradation in aqueous solutions, Applied Catalysis B: Environmental 142 (2013) 729-735.
[17] H.Q. Sun, C. Kwan, A. Suvorova, H.M. Ang, M.O. Tade, S.B. Wang, Catalytic oxidation of organic pollutants on pristine and surface nitrogen-modified carbon nanotubes with sulfate radicals, Applied Catalysis B-Environmental 154 (2014) 134-141.
[18] X. Duan, Z. Ao, D. Li, H. Sun, L. Zhou, A. Suvorova, M. Saunders, G. Wang, S. Wang, Surface-tailored nanodiamonds as excellent metal-free catalysts for organic oxidation, Carbon 103 (2016) 404-411.
[19] X. Duan, H. Sun, J. Kang, Y. Wang, S. Indrawirawan, S. Wang, Insights into Heterogeneous Catalysis of Persulfate Activation on

Dimensional-Structured Nanocarbons, ACS Catalysis 5(8) (2015) 4629-4636.
[20] B. Frank, J. Zhang, R. Blume, R. Schlögl, D.S. Su, Heteroatoms increase the selectivity in oxidative dehydrogenation reactions on nanocarbons, Angewandte Chemie International Edition 48(37) (2009) 6913-6917.
[21] Z. Yang, Z. Yao, G. Li, G. Fang, H. Nie, Z. Liu, X. Zhou, X.a. Chen, S. Huang, Sulfur-doped graphene as an efficient metal-free cathode catalyst for oxygen reduction, ACS nano 6(1) (2011) 205-211.
[22] D. Hulicova-Jurcakova, A.M. Puziy, O.I. Poddubnaya, F. Suárez-García, J.M.D. Tascón, G.Q. Lu, Highly stable performance of supercapacitors from phosphorus-enriched carbons, Journal of the American Chemical Society 131(14) (2009) 5026-5027.
[23] Y. Zhao, M. Liu, X. Deng, L. Miao, P.K. Tripathi, X. Ma, D. Zhu, Z. Xu, Z. Hao, L. Gan, Nitrogen-functionalized microporous carbon nanoparticles for high performance supercapacitor electrode, Electrochimica Acta 153 (2015) 448-455.
[24] Q. Xu, X. Yu, Q. Liang, Y. Bai, Z.-H. Huang, F. Kang, Nitrogen-doped hollow activated carbon nanofibers as high performance supercapacitor electrodes, Journal of Electroanalytical Chemistry 739 (2015) 84-88.
[25] X. Duan, Z. Ao, H. Sun, S. Indrawirawan, Y. Wang, J. Kang, F. Liang, Z.H. Zhu, S. Wang, Nitrogen-doped graphene for generation and evolution of reactive radicals by metal-free catalysis, ACS Applied Materials & Interfaces 7(7) (2015) 4169-4178.
[26] X. Duan, Z. Ao, H. Sun, L. Zhou, G. Wang, S. Wang, Insights into N-doping in single-walled carbon nanotubes for enhanced activation of superoxides: a mechanistic study, Chemical Communications 51(83) (2015) 15249-15252.

[27] X. Duan, K. O'Donnell, H. Sun, Y. Wang, S. Wang, Sulfur and nitrogen co-doped graphene for metal-free catalytic oxidation reactions, Small 11(25) (2015) 3036-3044.
[28] X. Duan, H. Sun, Y. Wang, J. Kang, S. Wang, N-doping-induced nonradical reaction on single-walled carbon nanotubes for catalytic phenol oxidation, Acs Catalysis 5(2) (2014) 553-559.
[29] X. Huang, Q. Wang, X.Y. Chen, Z.J. Zhang, N-doped nanoporous carbons for the supercapacitor application by the template carbonization of glucose: the systematic comparison of different nitridation agents, Journal of Electroanalytical Chemistry 748 (2015) 23-33.
[30] C. Wang, J. Kang, H. Sun, H.M. Ang, M.O. Tadé, S. Wang, One-pot synthesis of N-doped graphene for metal-free advanced oxidation processes, Carbon 102 (2016) 279-287.
[31] W. Li, D. Chen, Z. Li, Y. Shi, Y. Wan, G. Wang, Z. Jiang, D. Zhao, Nitrogen-containing carbon spheres with very large uniform mesopores: the superior electrode materials for EDLC in organic electrolyte, Carbon 45(9) (2007) 1757-1763.
[32] D. Hulicova, J. Yamashita, Y. Soneda, H. Hatori, M. Kodama, Supercapacitors prepared from melamine-based carbon, Chemistry of Materials 17(5) (2005) 1241-1247.
[33] Y. Shao, J. Sui, G. Yin, Y. Gao, Nitrogen-doped carbon nanostructures and their composites as catalytic materials for proton exchange membrane fuel cell, Applied Catalysis B: Environmental 79(1) (2008) 89-99.
[34] A. Zhao, J. Masa, W. Xia, A. Maljusch, M.-G. Willinger, G. Clavel, K. Xie, R. Schlögl, W. Schuhmann, M. Muhler, Spinel Mn-Co oxide in N-doped carbon nanotubes as a bifunctional electrocatalyst synthesized by oxidative cutting, Journal of the American Chemical Society 136(21) (2014) 7551-7554.

[35] L. Qu, Y. Liu, J.-B. Baek, L. Dai, Nitrogen-doped graphene as efficient metal-free electrocatalyst for oxygen reduction in fuel cells, ACS nano 4(3) (2010) 1321-1326.
[36] J. Long, X. Xie, J. Xu, Q. Gu, L. Chen, X. Wang, Nitrogen-doped graphene nanosheets as metal-free catalysts for aerobic selective oxidation of benzylic alcohols, Acs Catalysis 2(4) (2012) 622-631.
[37] Z.R. Ismagilov, A.E. Shalagina, O.Y. Podyacheva, A.V. Ischenko, L.S. Kibis, A.I. Boronin, Y.A. Chesalov, D.I. Kochubey, A.I. Romanenko, O.B. Anikeeva, Structure and electrical conductivity of nitrogen-doped carbon nanofibers, Carbon 47(8) (2009) 1922-1929.
[38] D.C. Higgins, M.A. Hoque, F. Hassan, J.-Y. Choi, B. Kim, Z. Chen, Oxygen reduction on graphene–carbon nanotube composites doped sequentially with nitrogen and sulfur, Acs Catalysis 4(8) (2014) 2734-2740.
[39] H. Sun, Y. Wang, S. Liu, L. Ge, L. Wang, Z. Zhu, S. Wang, Facile synthesis of nitrogen doped reduced graphene oxide as a superior metal-free catalyst for oxidation, Chemical Communications 49(85) (2013) 9914-9916.
[40] H. Sun, S. Liu, G. Zhou, H.M. Ang, M.O. Tadé, S. Wang, Reduced graphene oxide for catalytic oxidation of aqueous organic pollutants, ACS Applied Materials & Interfaces 4(10) (2012) 5466-5471.
[41] X. Duan, C. Su, L. Zhou, H. Sun, A. Suvorova, T. Odedairo, Z. Zhu, Z. Shao, S. Wang, Surface controlled generation of reactive radicals from persulfate by carbocatalysis on nanodiamonds, Applied Catalysis B: Environmental 194 (2016) 7-15.
[42] Z.-H. Sheng, L. Shao, J.-J. Chen, W.-J. Bao, F.-B. Wang, X.-H. Xia, Catalyst-free synthesis of nitrogen-doped graphene via thermal annealing graphite oxide with melamine and its excellent electrocatalysis, ACS nano 5(6) (2011) 4350-4358.

[43] X. Li, H. Wang, J.T. Robinson, H. Sanchez, G. Diankov, H. Dai, Simultaneous nitrogen doping and reduction of graphene oxide, Journal of the American Chemical Society 131(43) (2009) 15939-15944.

[44] X. Duan, Z. Ao, L. Zhou, H. Sun, G. Wang, S. Wang, Occurrence of radical and nonradical pathways from carbocatalysts for aqueous and nonaqueous catalytic oxidation, Applied Catalysis B: Environmental 188 (2016) 98-105.

[45] S. Wu, G. Wen, J. Wang, J. Rong, B. Zong, R. Schlögl, D.S. Su, Nitrobenzene reduction catalyzed by carbon: does the reaction really belong to carbocatalysis?, Catalysis Science & Technology 4(12) (2014) 4183-4187.

[46] S.L. Buchwald, C. Bolm, On the role of metal contaminants in catalyses with FeCl3, Angewandte Chemie International Edition 48(31) (2009) 5586-5587.

[47] J.E. Bennett, B.C. Gilbert, J.K. Stell, Mechanisms of peroxide decomposition. EPR studies of the one-electron oxidation of the peroxymonosulphate anion ($HOOSO_3^-$) and the reactions of $SO5^{\cdot-}$, Journal of the Chemical Society, Perkin Transactions 2 (8) (1991) 1105-1110.

[48] Y. Wang, H. Sun, X. Duan, H.M. Ang, M.O. Tadé, S. Wang, A new magnetic nano zero-valent iron encapsulated in carbon spheres for oxidative degradation of phenol, Applied Catalysis B: Environmental 172 (2015) 73-81.

[49] S. Indrawirawan, H. Sun, X. Duan, S. Wang, Low temperature combustion synthesis of nitrogen-doped graphene for metal-free catalytic oxidation, Journal of Materials Chemistry A 3(7) (2015) 3432-3440.

[50] D.F. Evans, M.W. Upton, Studies on singlet oxygen in aqueous solution. Part 3. The decomposition of peroxy-acids, Journal of the Chemical Society, Dalton Transactions (6) (1985) 1151-1153.

[51] D.L. Ball, J.O. Edwards, The kinetics and mechanism of the decomposition of Caro's acid. I, Journal of the American Chemical Society 78(6) (1956) 1125-1129.
[52] Y. Zhou, J. Jiang, Y. Gao, J. Ma, S.-Y. Pang, J. Li, X.-T. Lu, L.-P. Yuan, Activation of peroxymonosulfate by benzoquinone: a novel nonradical oxidation process, Environmental science & technology 49(21) (2015) 12941-12950.
[53] P. Liang, C. Zhang, X. Duan, H. Sun, S. Liu, M.O. Tade, S. Wang, An insight into metal organic framework derived N-doped graphene for the oxidative degradation of persistent contaminants: formation mechanism and generation of singlet oxygen from peroxymonosulfate, Environmental Science: Nano 4(2) (2017) 315-324.
[54] M.A.J. Rodgers, Solvent-induced deactivation of singlet oxygen: additivity relationships in nonaromatic solvents, Journal of the American Chemical Society 105(20) (1983) 6201-6205.
[55] C. Wang, J. Kang, P. Liang, H. Zhang, H. Sun, M.O. Tadé, S. Wang, Ferric carbide nanocrystals encapsulated in nitrogen-doped carbon nanotubes as an outstanding environmental catalyst, Environmental Science: Nano 4(1) (2017) 170-179.

Chapter 6 Co-based nanospheres supported on carbon sphere with a tunable oxidation layer in the applications of lithium ion battery and wastewater treatment

Abstract

Energy crisis and environmental pollution are two major concerns of the 21st century. It is of great priority to develop novel materials with maximum energy utilization and environmental friendliness. Here, Co-based nanospheres supported on a carbon substrate with a tunable oxidation layer are successfully synthesized by a controllable oxidation process. Fully oxidized carbon sphere (FC@CS) is used as the anode material in lithium ion batteries (LIBs), and the Co nanosized particles homogeneously anchored on the carbon exhibit superior LIBs performance with a large reversible capacity, excellent cyclic performance and good rate capability, highlighting the importance of the pomegranate-like structure and Co_3O_4 nanoparticles in the energy storage applications. In addition, partially oxidized carbon sphere (PC@CS) is employed as an excellent catalyst for efficient phenol removal by peroxymonosulfate (PMS) activation with both outstanding catalytic degradation performance and superb stability. Electron paramagnetic resonance (EPR) is performed to probe the generated reactive radicals and quenching experiments reveal that the catalytic mechanism is a radical process. To improve the usage efficiency of materials and reduce the cost, regeneration of inactive PC@CS after phenol degradation is carried out and applied for LIBs anode. This recycled material displays a comparable performance to FC@CS in the LIBs application, which not only removes the pollutants in the

wastewater but also reduces the production cost of LIBs. Due to the facile synthesis method, distinctive structure and dual applications in LIBs anode and wastewater treatment, these novel Co-based composites have great potential as new strategic materials for energy storage and environmental catalysis.

6.1 Introduction

Freshwater pollution and energy scarcity are critical issues for human beings in the 21st century. Although clean freshwater is the most basic natural resource for human beings to survive, rapid industrialization and urbanization, along with explosive population growth, have resulted in serious water pollution that is detrimental to the health of living organisms.[1, 2] Wastewater from processing industries contains many hazardous organics, such as phenolic compounds and dyes, which are highly toxic and recalcitrant to natural degradation and have caused serious issues to the environment.[3] In an effort to cope with water pollution, rapid and significant advances in wastewater treatment methods have been gained, such as photocatalysis, adsorption, separation processes and biodegradation.[4-7] In the past few decades, advanced oxidation processes (AOPs) have been developed into one of promising approaches to completely remove persistent organic pollutants in contaminated water.[8, 9] Fenton reaction, one of popular AOPs, has demonstrated to be effective for the efficient decomposition of many organic pollutants, but is subject to a series of shortcomings like a low pH range, metal leaching, difficulties in transportation and storage of H_2O_2 and large amount of sludge generation.[10, 11] Of late, sulfate radicals, an alternative to hydroxyl radicals, are generated from peroxymonosulfate (PMS) or persulfate (PS) to be applied for removing organic pollutants in aqueous solution due to their stronger redox potential than hydroxyl radicals, better selectivity, and no pH adjustment.[12, 13] It was found that sulfate radicals can be generated by activating PMS through UV radiation, heat, metal ions or oxides and metal-free materials.[14] Extensive investigations have been implemented to confirm that transition metals, especially cobalt ions or

oxides are highly effective in PMS activation to produce sulfate radicals to degrade organics in wastewater.[15-19] However, as a toxic heavy metal, the presence of cobalt in reaction solutions could be a serious threat to the health of both human beings and animals because it can trigger asthma, pneumonia and other lung problems.[20] Secondary contamination would be resulted from unsuitable recovery of the used catalyst in water and pose greater damages than pollutants. Generally, ultrafine particles cannot be successfully treated by conventional separation methods and high-speed centrifugation is thus required to inevitably enhance the cost of heterogeneous catalysis. However, magnetic separation can remove particles in wastewater with a simple use of an external magnetic field.[21] Therefore, for a feasible application, it is urgent to develop novel and recoverable catalysts that can be easily separated from solution with high activity and stability in heterogeneous PMS activation.[22]

Recently, rechargeable lithium ion batteries (LIBs) have potential applications ranging from portable electronic devices to electric vehicles, and are regarded as a promising choice for modern space and military facilities due to their high energy densities and long-term operation stability.[23-25] Therefore, in light of power density, safety and cycle life, these fields are the driving forces for the development of LIBs. For metal-free electrode materials, graphite is extensively applied as the anode material for LIBs. The lithiation potential, at a high rate in particular, is below 0.2 V versus Li/Li^+, approaching that of lithium stripping and having the possibility to cause safety issues. Additionally, the formation of a layer of solid-electrolyte interphase (SEI) with electronic insulation is unavoidably occurred on the surface of graphite below 1.0 V versus Li/Li^+. Also in the process of full lithium insertion

and extraction, a 9% volume variation is witnessed by the graphite anode.[26] For the inorganic metal oxide materials, Co_3O_4 was developed by Poizot et al into the anode in LIBs in 2000.[27] Due to conversion reaction mechanism, it is theoretically able to store more than 8 lithium per formula unit with a capacity as high as 890 mAh g^{-1}.[28] Different routes have been developed to produce Co_3O_4 nanostructures. However, one of major drawbacks for Co_3O_4 anode materials in the practical batteries is their poor capacity retention in the process of cycling and poor rate capability, which resulted from the slow kinetics of conversion reactions. Another key reason may be ascribed to the big variation in volume during lithium insertion/deinsertion. This results in material pulverization and electrical contact loss, which eventually causes the electrode failure. To address this issue, many researches have been reported on the design of porous or channel structures of advanced materials equipped with controlled nano/microstructures because of their superior properties than their bulk counterparts, or coating graphene or other carbon-based materials on the surface of Co_3O_4.[29-31] Co_3O_4 with different nanostructures, such as nanotubes, nanorods, nanosheets, nanocubes, nanoflowers and nanocages, have been studied extensively as the anode materials for lithium ion batteries.[32-36] For example, Wang et al. compared a variety of multi-shelled Co_3O_4 hollow particles with multi-shelled structures. The small diffusion lengths presented by the nanosheet building blocks as well as abundant void space exerted a synergetic effect, and thus led to an outstanding capacity and cyclic stability.[37] A feasible and controllable electrospinning approach was reported by Chen et al. to obtain Co_3O_4 nanotubes with diameters of 200-300 nm and interconnected nanoparticles of 20-40 nm. Compared to Co_3O_4 nanowire counterparts, this material exhibited a better cycle stability, higher specific capacity and improved rate capability.[38] Not

only the porous structures but also the quality of crystallinity and other factors exert a significant influence on the performance of LIBs. However, Lou compared the electrochemical performance of Co_3O_4 nanotubes with various crystallinities and concluded that the enhanced crystallinity resulted in a better cycling performance.[39] In spite of the successful preparation of Co_3O_4 nanoparticles with high capacity, its hollow structure or small size that plays a dominant role in the charge/discharge performance, has rarely been studied. Moreover, ordered mesoporous structure is considered as one of the most popular nanostructures for LIBs which consists of micrometer-sized particles with nanometer pores and similar size walls.[40, 41] Generally, ordered mesoporous structure can be prepared by two different template methods (soft or hard template method) with the so-called nanocasting process. Tian et al. prepared mesoporous Co_3O_4 nanotubes at varying calcination temperatures and optimized the charge/discharge performance.[42] Poizot et al. proposed that the best electrochemical performance was presented by a premium particle size for each metal oxide.[27] It can be suggested that the charge/discharge performance could be determined by several factors such as chemical compositions, morphology, crystallinity, specific surface area, and structural stability. Furthermore, the development of carbon composites (graphite, graphene or carbon nanotube) anchored with nanostructured Co_3O_4 particles can overcome the shortages of bulk Co_3O_4 electrode, by combining the respective merits of nanosized Co_3O_4 and carbon materials and thus enhance the performance of LIBs. Ultrafine Co_3O_4 nanoparticles in the homogeneous encapsulation of ultrathin porous graphitic carbon obtained a large specific surface area, excellent electronic conductivity, and superb mechanical flexibility. These outstanding properties are able to maintain the good stability of Co_3O_4 nanoparticles with a large capacity.[43]

Graphene anchored with Co_3O_4 nanoparticles were developed by Cheng et al. and displayed fantastic Li-battery performance with an excellent reversible capacity, superb cyclic performance, and large rate capability, which highlighted that nanoparticles anchored on graphene sheets can utilize electrochemically active Co_3O_4 nanoparticles as well as graphene to a maximum extent in energy storage for high-performance LIBs.[30] Consequently, the carbon- and cobalt- based composite materials can be considered as desirable anode materials to improve the performance of LIBs.

Although Co-based oxide materials, with or without carbon modification, have been investigated on the performance and reaction mechanism as LIBs anode, the exorbitant price of such an expensive metal is still a major barrier to its large-scale industrial production. Therefore, reducing the cost of Co-based electrode has become a new research hot spot. In this regard, one of promising approaches is the utilization of regeneration and activation processes to recycle the used Co-based materials as the anode of LIBs.

In this chapter, pomegranate-like structural Co spheres@carbon sphere composite materials were successfully prepared by a combination of hydrothermal method and high temperature oxidation. After different oxidation treatment, partially oxidized carbon sphere (PC@CS) and fully oxidized carbon sphere (FC@CS) were respectively used in the application of water treatment and anode of LIBs. In addition, PC@CS with good magnetism can be successfully separated from reaction solutions after phenol degradation to avoid secondary contamination caused by metal-based catalysts. Moreover, it can subsequently be used as the anode of LIBs through a regeneration process, and thereby

achieved the goal of highly efficient regeneration and multi-field recycling.

6.2 Experimental

Materials and Chemicals. Sucrose, hexahydrate cobalt nitrate ($Co(NO_3)_2$•$6H_2O$), potassium peroxymonosulfate ($2KHSO_5 \cdot 3KHSO_4 \cdot K_2SO_4$, Oxone), 5,5-dimethylpyrroline-oxide (DMPO, >99.0%) were purchased from Sigma-Aldrich. Phenol (>99.0%), acetone and ethanol were obtained from Chem-Supply. High purity nitrogen gas (99.999%) was obtained from BOC. Ultrapure water was used in all of the experiments. All chemicals used herein were of analytic grade and used as received without any further purification.

Materials Synthesis. The PC@CS and FC@CS precursors were prepared via a simple one-pot hydrothermal synthesis. One gram of sucrose and 0.3 g of $Co(NO_3)_2$•$6H_2O$ were ground in ultrapure water using a high-energy ball mill (Pulverisette 6, Fritsch, Germany) at 400 rpm for 0.5 h. After grinding, the obtained solution was transferred into a Teflon-lined stainless steel autoclave. The sealed autoclave was placed in an oven at 150 °C for 12 h and water-cooled down to the room temperature. The resultant black carbonaceous hydrogel monolith was heated under N_2 atmosphere to 600 °C for 6 h to form the carbon precursor with embedded metallic cobalt nanoparticles. Then, the precursor was treated in a muffle furnace at 350 °C for 0.5 h or 3 h to obtain PC@CS or FC@CS, respectively.

Materials Characterization. Field-emission scanning electron microscopy (Zeiss 1555 VP-FESEM) was used to characterize the

microscopic features of the samples. A FEI Titan G2 80–200 TEM/STEM with ChemiSTEM Technology operating at 200 kV was used to evaluate high angle annular dark field scanning transmission electron microscopy imaging and element mapping. Energy dispersive X-ray spectroscopy was employed to obtain the elemental mapping with the utilization of a Super-X detector on the Titan under a probe size of ≈1 nm along with a probe current of ≈0.4 nA. A Bruker D8 Advance X-Ray Diffractometer with Cu Kα radiation (λ = 1.5418 Å) was used to collect the XRD patterns of the products. The data were collected through a step-scan mode in a 2θ range of 10-90° at 0.02° per step. The Rietveld refinement was analyzed by TOPAS V5. Thermogravimetric analysis (TGA) was performed with a temperature ramp of 10 °C min^{-1} under an air flow. The specific surface area and pore size distribution of the samples were evaluated by the BET equation and the Barrett–Joyner–Halenda method on a TriStar II instrument, respectively. XPS was conducted on a ThermoEscalab 250 using an Al Kα X-ray source to detect the elemental composition of the carbon materials. The Raman spectra of the carbon materials were acquired from an ISA Raman spectrometer equipped with argon ion lasers at 514 nm to estimate the disorder degree of the carbon materials.

Electrochemical Measurements. The battery tests were carried out in a half-cell configuration. The working electrode consists of active materials, conductivity agent (Carbon black, Super P), and polymer binder (polyvinylidene fluoride, PVDF) with a weight ratio of 80:10:10. The active mass loading on the electrode is about 2.5 mg cm^{-2}. The electrolyte employed was a solution of 1 M $LiPF_6$ in a mixture of ethylene carbonate/dimethyl carbonate (EC/DMC) with 1:1 vol ratio. A microporous polypropylene film (Celgard 2400) was used as the

separator. For the galvanostatic charging-discharging tests, the electrodes were punched into discs with a diameter of about 1.4 cm. Lithium chip was used as both counter electrode and reference electrode. The coin type half cells were assembled in an argon-filled glove box and then tested using a computer-controlled battery test station (NEWARE BTS-5 V, 50 mA) between 0.01 and 3.00 V at different rates and under room temperature. A CHI 760a electrochemical workstation was used to record the CVs.

Catalytic Oxidation of Phenol Solutions. The decomposition of phenol solution was implemented with a 250 mL glass bottle with certain concentrations of phenol solution, carbon catalysts and PMS in a temperature-controlled water bath. One mL phenol solution, withdrawn by a syringe and filtered by a 0.45 mm Millipore film, was finally injected into a glass vial at each time interval. Subsequently, a quenching agent of 0.5 mL methanol was added immediately. After shaking the vial vibrantly, the solution was analyzed by a Thermo-Fisher Scientific 3000 UHPLC system (ultra-high performance liquid chromatograph with a UV detector at 270 nm. An Acclaim RSLC C-18 column was utilized and a mixture of 30% acetonitrile and 70% water was used as the mobile phase at a constant flow rate of 1 mL/min.

Mechanistic Studies of the Catalytic Processes. An EMS-plus EPR instrument from Bruker was employed to detect the free radicals captured by 5,5-dimethyl-1-pyrroline (DMPO, ＞ 99.0%) during PMS activation, operating under the following conditions: center field, 3515 G; sweep width, 100 G; microwave frequency, 9.87 GHz; power setting, 18.75 mW; scan number, 3. The radical quantitative information was acquired from the Spin Fitting from Bruker Xenon Software Package.

6.3 Results and discussion

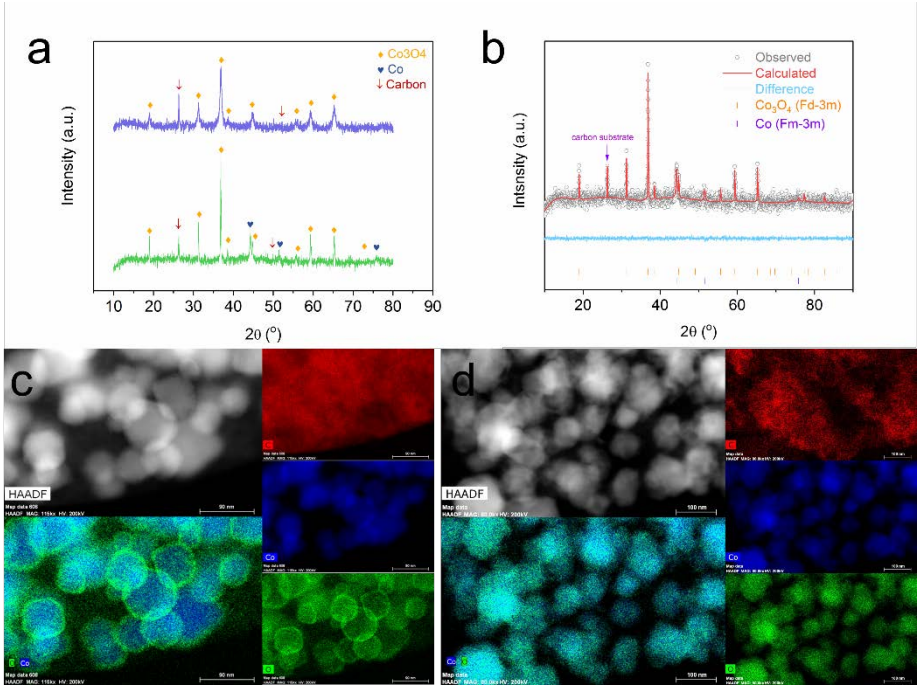

Figure 6.1 (a) XRD patterns of FC@CS and PC@CS; (b) Rietveld refinement of XRD data for PC@CS; STEM and EDS mapping of the elemental species on the composite of (c) PC@CS and (d) FC@CS.

It is well known that, due to its theoretical capacity during the lithium insertion/deinsertion conversion reaction, Co_3O_4 is an excellent anode material in the LIBs. However, the metal Co and CoO with lower valences are not ideal electrode materials in LIBs for their lower theoretical capacity.[44] However, as reductants, Co and CoO can be excellent catalysts for PMS activation to generate sulfate radicals in the treatment of wastewater containing phenolic compounds. During phenol degradation, the low valence Co-based materials can be oxidized to high valence Co-based oxides by PMS to purify wastewater. Two different types of cobalt nanospheres encapsulated in carbon spheres are tunably prepared by the combined methods of hydrothermal reaction and high-temperature oxidation. The crystal structures of fully oxidized cobalt

nanospheres encapsulated in carbon sphere (FC@CS) and partially oxidized cobalt nanospheres encapsulated in carbon sphere (PC@CS) are investigated by X-ray diffraction (XRD) and the results are presented in Figure 6.1 (a). The characteristic peaks of the FC@CS correspond excellently to those of face-centered Co_3O_4 with a space group of *Fd-3m* (JCPDS no. 65-3107), and the additional peak at 25.9^o comes from the carbon substrate. With respect to the XRD pattern of FC@CS, PC@CS displays some diffraction peaks in good agreement with metal Co with a space group of *Fm-3m*. Rietveld refinement fitting results of PC@CS are depicted in Figure 6.1 (b), which converge to lattice parameters of a=8.09 Å for Co_3O_4 and a=3.54 Å for Co with reliability factors of R_{wp}= 0.9872 and R_p=0.7637 with goodness of fit=0.001. The weight ratios of these two phases in PC@CS are 77.3% and 22.7% for Co_3O_4 and Co, respectively. The results are further verified by the high-angle annular dark field scanning transmission electron microscopy image (HAADF-STEM) and energy dispersive X-ray (EDX) elemental mappings. As shown in Figure 6.1 (c), the Co_3O_4 nanospheres are evenly distributed inside the carbon sphere substrate. The size of the carbon substrate is about 5 μm and the average size of Co_3O_4 nanospheres is 50-90 nm. However, Co nanospheres in the PC@CS exhibit a yolk-shell structure with an oxide layer of 5 nm thick, which completely covers the surface of metal Co nanospheres. It is indicated that the hydrothermal and calcination processes can simultaneously result in and improve sucrose carbonization at the conditions of high pressure and high temperature.

Figure 6.2 shows typical scanning electron microscopic images for PC@CS and FC@CS. It is demonstrated that both the PC@CS and FC@CS have the spherical shape with an average diameter of 6 μm.

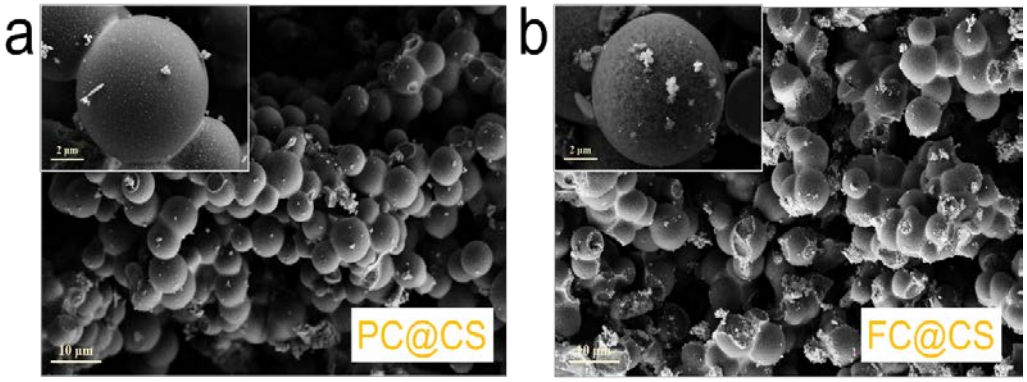

Figure 6.2 Representative SEM images of (a) PC@CS and (b) FC@CS.

Some nanosized Co-based particles can be viewed on the relatively tough surface of the carbon substrate with an average size of 6 μm, corresponding to the results of STEM-EDS. Compared to the rough surface of FC@CS, PC@CS shows a relatively smooth surface, which may be attributed to the generation of defect carbon from the burning of partial carbon substrate at high temperature for longer calcination time. This phenomenon can further be confirmed by the TGA, BET and Raman. The generation of the disordered defects of graphitic carbon can also be verified by nitrogen adsorption-desorption isotherms.

Figure 6.3 (a) and (b) display the nitrogen adsorption-desorption isotherms of PC@CS and FC@CS. Both samples display a typical IV isotherm with a H2-type hysteresis loop, elucidating the heterogeneous distribution of pore sizes and shapes. The Brunauer-Emmett-Teller (BET) surface areas of PC@CS and FC@CS were measured to be approximately 56.9 and 67.7 m^2 g^{-1}, respectively. Such large specific surface areas are vital for the enhancement in the active sites for both wastewater treatment and LIBs. Obviously, after the longer sintering time under air atmosphere, FC@CS displays a larger specific area,

demonstrating that more defect carbons are created during the oxidation process.

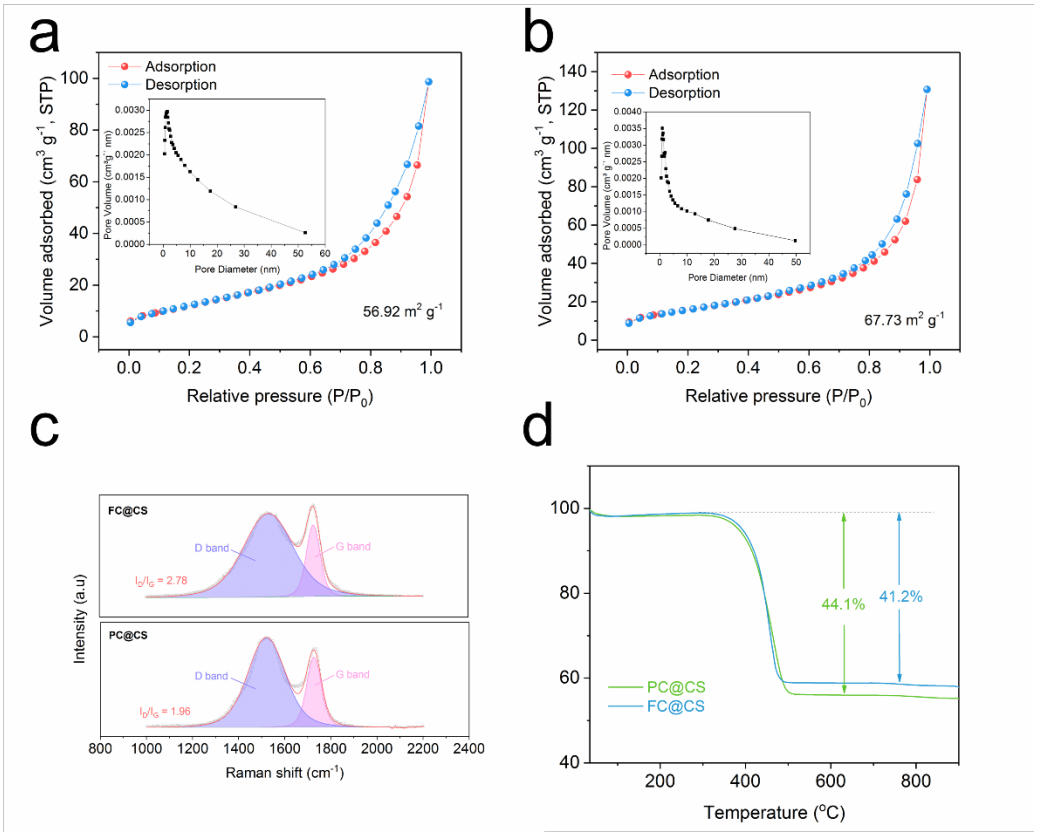

Figure 6.3 Nitrogen adsorption-desorption isotherm of (a) PC@CS and (b) FC@CS; (c) Raman spectra for these two composites with fitting peaks; (d) TGA plots for PC@CS and B) FC@CS.

Figure 6.3 (c) illustrates the Raman spectra of FC@CS and PC@CS. Distinctive D and G bands are observed in the Raman spectrum for these two samples. The D band gives evidence of defects on the structure, while the G band provides information on the vibration of sp^2 hybridized carbon. Thus, the intensity ratio of D peak to G peak is always used as an index to disclose the degree of graphitization or the extent of structural disorder. The obtained values of I_D/I_G for FC@CS and PC@CS are 2.78 and 1.96, respectively; manifesting well-crystallized graphitic structures are obtained for both the samples. Such high graphitization degrees

provide a good electronic conductive phase for the loaded Co-based nanospheres. The PC@CS displays a more intensive Raman peak and a lower I_D/I_G index value than those of FC@CS, suggesting that the defect carbon on the sphere surface can be created by the burn-off of carbon substrate for longer calcination under ambient air atmosphere. Thus, FC@CS exhibits a much lower degree of graphitic carbon and a relatively larger amount of disordered phase than that of PC@CS. In addition, it is also suggested that the calcination time is essential to the carbonization of the composite materials. The thermogravimetric curves of FC@CS and PC@CS are exhibited in Figure 6.3 (d). Two regions in the weight loss profiles are observed for FC@CS. The first weight loss of about 2% occurs up to 100 ^oC, corresponding to the elimination of water molecules intercalated and adsorbed on the surface or bulk of the sample. The second weight loss of 37.4% occurs between 320 ^oC and 500 ^oC, which may be attributed to the dehydration of Co_3O_4 and decomposition of carbonaceous materials. Above 600 ^oC, the weight loss continues, but is relatively small and thus can be ignored. The thermogravimetric curve of PC@CS displays a similar process with that of FC@CS, but demonstrating a bigger weight loss of 44.1% in the temperature range from 320 to 500 ^oC, which may be due to the partial burning of carbonaceous materials in the longer oxidation process at high temperature.

X-ray photoelectron spectroscopy (XPS) characterization was performed to study the valence of cobalt ion and chemical states of carbon in FC@CS and PC@CS. As it is well-known, the binding energy of element grows with its valence state.[45] Theoretically, the binding energy of Co is approximately at 778.2 eV for Co^0, 779.7 eV for Co^{2+} and 780.0 eV for Co^{3+}. Figure 6.4 displays the XPS spectra of Co 2p in

FC@CS and PC@CS samples. In FC@CS, the Co $2p_{3/2}$ XPS spectrum can be fitted into four peaks, that is, the peak of Co^{2+} at 779.3 eV, the peak of Co^{3+} at 780.7 eV and 782.1 eV and the satellite peak of $Co^{2+/3+}$ at 788.9 eV, corresponding to the signals of Co_3O_4. The fitting result indicates that the valence state of the Co element is 2+ and 3+ in the FC@CS with longer oxidation time. Based on the fitment of Co 2p XPS spectrum, the ratio of Co^{2+} : Co^{3+} is 35.2 : 64.8 in the FC@CS.

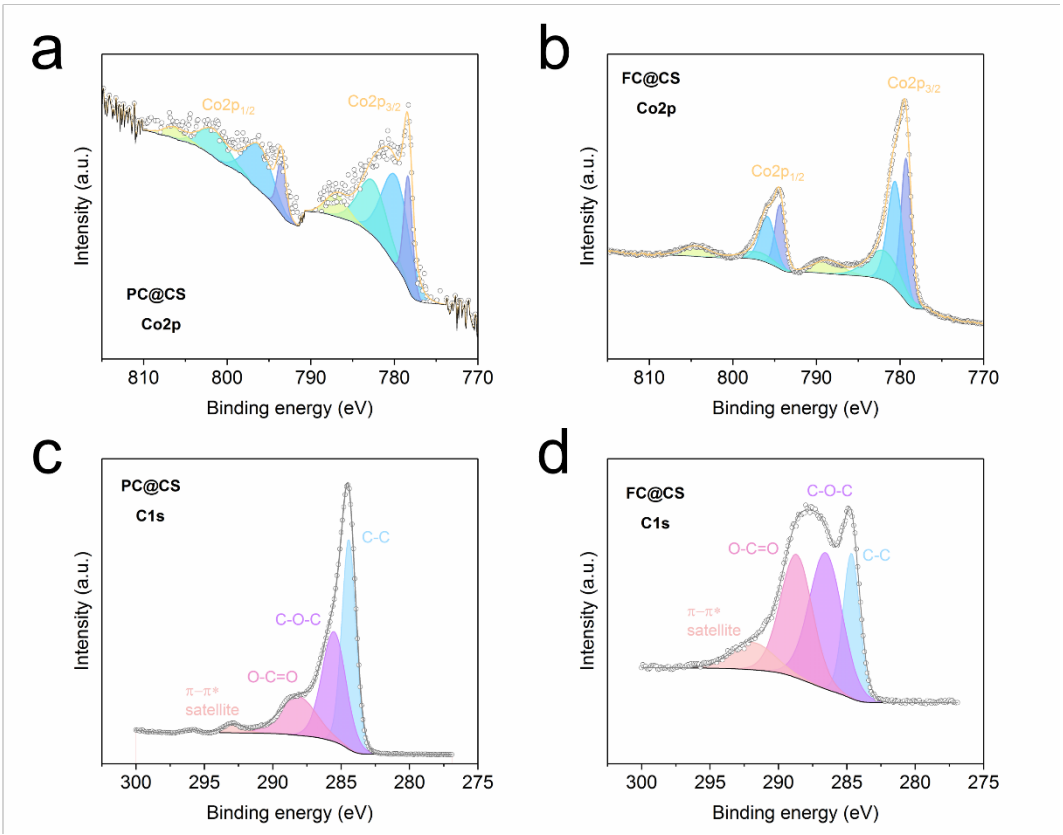

Figure 6.4 XPS analyses of Co 2p in (a) PC@CS and (b)FC@CS and C 1s regions of (c) PC@CS and (d)FC@CS.

In comparison, the Co 2p spectrum of PC@CS can also be fitted into four different peaks, namely, one metal Co peak at 778.3 eV, two primary and perspicuous peaks at 780.3 eV and 782.7 eV, in respective agreement to Co^{2+} and Co^{3+}, and a representative satellite line at about 787.2 eV. This result expounds that Co^0 was the exclusive valence state

in the partial oxidation sample. The ratio of the three types of Co ion with different valence (Co^0 : Co^{2+} : Co^{3+}) is 19.2 : 49.1 : 31.7 in PC@CS, exhibiting Co^0 is come from the core part of the core-shell structured PC@CS and all of the Co elements in the FC@CS are oxidized for longer treatment time. Moreover, as shown in Figure 6.4 (c), the C 1s XPS peaks centred at the binding energies of 284.4, 285.5 and 288.2 eV are allocated to the C-C, C-O-C and O-C=O, respectively. It can be clearly seen that most carbon atoms were sp^2-hybridized, and due to the short treatment of PC@CS in air at high temperature, the intensity of oxygenated functional groups (C-O-C and O-C=O) in the PC@CS was obviously decreased compared with that of FC@CS.

According to the above phase and component analysis of FC@CS and PC@CS, we can predict that FC@CS, owing to the high theoretical capacity, is more suitable for anode materials in lithium ion battery. However, the lower valence of Co in PC@CS sample are beneficial to PMS activation, which is because Co^{2+} and Co^0 ions with stronger reducibility can improve their reaction with PMS, and such an in-depth reaction will accelerate the degradation of phenol. In addition, owing to its magnetic properties, PC@CS can be easily separated using an external magnetic field, avoiding secondary contamination caused by the catalyst residues and thus indicating great potentials for practical applications.

Based on the high theoretical capacity of Co_3O_4, FC@CS is more suitable to be as an anode material in LIBs. In order to investigate the applicability of FC@CS composites in LIBs, the electrochemical properties in terms of Li insertion/extraction are investigated. The electrochemical properties of mechanical mixture of FC@CS composites

and commercial Co_3O_4 were investigated for comparison. Figure 6.5 (a) displays the representative cyclic voltammogram (CV) curves of FC@CS composites anode at room temperature from 0.01 to 3.00V at a scan rate of 0.1 mV s^{-1}. It can be clearly seen that the CV curve of the first cycle shows a great difference to those of subsequent cycles, especially for the discharge branch. The similar phenomenon also exists on other Co based anode and metal oxide anode materials.[30]

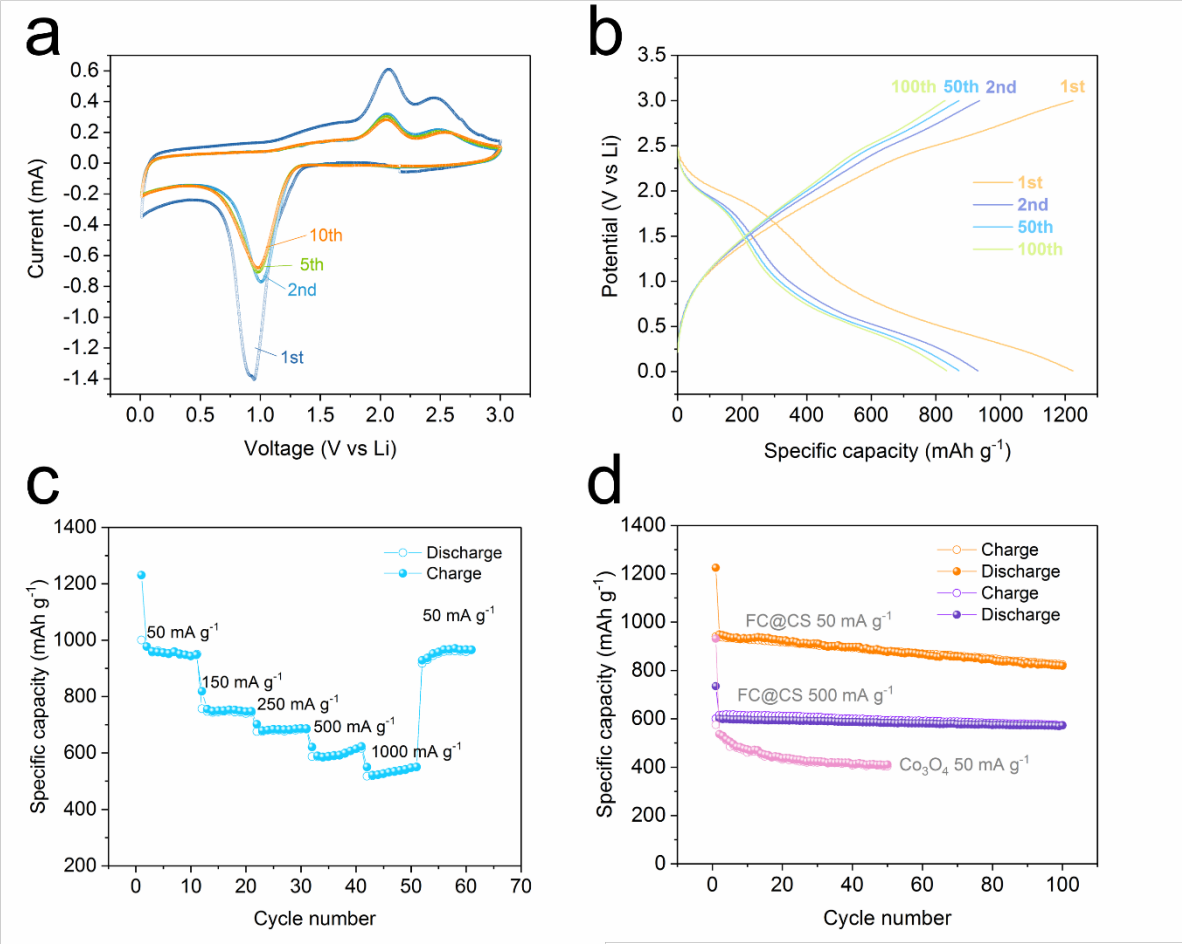

Figure 6.5 (a) Cyclic voltammograms of FC@CS composite at a scanning rate of 0.1 mV s^{-1}; (b) galvanostatic charge-discharge curves of FC@CS; (c) rate capability of FC@CS at various current densities between 50 and 1000 mA g^{-1}; (d) comparison of the cycling performance of FC@CS at current densities 50 and 500 mA g^{-1}, and commercial Co_3O_4.

In terms of the first discharge cycle, a broad peak is seen from 0.75 to 1.25 V in the first cathodic polarization process, which is attributed to initial insertion of lithium into crystal structure and $Co^{2+/3+}$ reduction to Co^0. Two anodic peaks are observed at 2.06 and 2.45 V, in correspondence to the reversible oxidation of Co^0 to $Co^{2+/3+}$. The following electrochemical reactions describe the formation of Co and Li_2O and the re-formation of Co_3O_4.

$$Co_3O_4 + 8Li^+ + 8e^- \leftrightarrow 4Li_2O + 3Co^0 \quad \text{(Eq. 6.1)}$$

$$8Li \leftrightarrow 8Li^+ + 8e^- \quad \text{(Eq. 6.2)}$$

$$Co_3O_4 + 8Li \leftrightarrow 4Li_2O + 3Co^0 \quad \text{(Eq. 6.3)}$$

Side reactions occurring on both electrode surfaces and interfaces are normally regarded as the position of special redox peaks in the first cycle. The peak intensity decreases apparently and significantly in the second cycle, indicating the occurrence of some irreversible reactions accompanied by the formation of a SEI film. Notably, the voltage-current curves almost overlap after the first cycle, indicating the formation of a stable SEI film on the surfaces and interfaces of pomegranate-like carbon shells in the first cycle. This can prevent the direct contact between encased Co_3O_4 nanoparticles and electrolyte and safeguard the structural integrity of inner Co_3O_4 during the subsequent charge-discharge cycles, which eventually results in a high Coulombic efficiency, good stability and noticeable reversibility of the sample. The decrease in the redox peak intensity implies that the capacity reduced during cycling.

Figure 6.5 (b) displays discharge-charge curves of FC@CS at various cycles measured at a current density of 50 mA g^{-1} with the potential ranging from 0.01 to 3.00 V (vs Li/Li^+). With increasing current density, the charge potential of FC@CS anode decreases but the discharge potential increases, demonstrating higher overpotential. In the first discharge process, an obvious plateau of nearly 2.0 V is obtained, which is replaced by a slope from 2.0 to 1.8 V in the following cycle in terms of the CV results. The as-prepared FC@CS sample has initial discharge and charge capacities of 1224.1 and 933.2 mAh g^{-1} at 50 mA g^{-1}, respectively. The irreversible capacity is believed to be arisen from the consumption of lithium ions during the formation of SEI film, incomplete re-oxidation of Co metal and the irreversible lithium insertion and extraction from graphite lattice. After 50 cycles, the reversible capacity is still as high as 871.4 mAh g^{-1}. Moreover, FC@CS anode material still retains a high reversible capacity of 828.9 mAh g^{-1} after 100 cycles. The rate capacity of the anode materials is also a decisive factor for electrochemical performance. Figure 6.5 (c) shows the rate capability of FC@CS from the current density of 50 mA g^{-1} to 1000 mA g^{-1}. FC@CS composite demonstrates a superior performance, particularly at the current density of 1000 mA g^{-1}, the specific capacity of FC@CS composite still retains 533.6 mAh g^{-1}, which is 43.6% of the initial capacity. The excellent rate capability could be attributed to the nanosized Co_3O_4 particles and low resistance resulted from the carbon shell.[30]

To highlight the superiority of FC@CS composite in the application of anode materials for LIBs, the cycle performance of the composite electrode was measured at a current density of 50 mA g^{-1} and 500 mA g^{-1}. The commercial Co_3O_4 composite was also investigated under the

same condition for comparison. As displayed in Figure 6.5 (d), an exceptionally better cyclic retention is presented by FC@CS composite electrode than that of commercial Co_3O_4. FC@CS displays a high reversible capacity of 871 mAh g^{-1} after 50 cycles and 828 mAh g^{-1} even after 100 cycles, about 93.2% and 88.6% of the initial capacity, respectively. In addition, their Coulombic efficiency increases instantly from 76.8% at the first cycle to approximately 100% after 2 cycles and maintains approximately 100% after 100 cycles, demonstrating the successful lithium insertion/extraction in association with efficient transport of ions and electrons in the electrodes. For the commercial Co_3O_4 with larger average diameter of about 500-1000 nm, their capacity decreases quickly for the first few cycles. The close interaction of graphene substrates with Co_3O_4 nanoparticles directly grown on them are the mainly responsible for the high capacity, good rate capability and excellent cycling stability of FC@CS hybrid. These superb properties make Co_3O_4 electrochemically active due to the effective and rapid conduction of charge carries from Co_3O_4 nanoparticle to current collector back and forth via three-dimensional graphite network with high conduction. For FC@CS hybrid materials, the expansion of Co_3O_4 nanoparticles upon lithiation can be achieved with no break of the carbon shell due to its carbon shell and porous carbon structure. In addition, as it is known to all, reversible conversion reaction between the lithium ion and Co_3O_4 achieves high lithium storage capacity of Co_3O_4 and the dispersion of Co nanocrystal in the Li_2O matrix, which are beneficial for the carbon shell to restrain the formed Co nanocrystal from decomposing the outer SEI. This in turn enables a stable SEI to grow on the carbon shell surface and inhibit the continuing rupture and reformation of SEI. Their capacity maintains excellently after the formation of the stable SEI and therefore the anode of FC@CS composites exhibits exceptionally

excellent cycling performance. However, pure commercial Co_3O_4 sample will cause SEI rupture because in the processes of lithium extraction, volume expansion and contraction generate great mechanical strain, giving rise to the cyclical exposure of the electrode surface to the electrolyte. This will further lead to the successive formation of very thick SEI films and consecutive consumption of electrolyte. In addition, low Coulombic efficiency, greater resistance to ionic transportation, and bad electronic conductivity of the electrode can be resulted from the cyclical rupture and SEI growth. Consequently, the pure commercial Co_3O_4 does not exhibit a stable cycle performance for the long-term charge-discharge process.

In the wastewater treatment, the mechanism of phenol decomposition is based on the reaction between Co-based catalyst as a reductant and PMS as an oxidant. From this point of view, Co at low valence state is more reactive than those at high state. Therefore, we employ partially oxidized PC@CS as a catalyst to degrade phenol solution by activation of PMS. Figure 6.6 (a) indicates that without a solid catalyst, PMS itself can hardly induce phenol oxidation. Meanwhile, only about 11% phenol was removed by the adsorption of PC@CS without PMS. Complete phenol removal was achieved on PC@CS in only 10 min, exhibiting a better catalytic performance than Co_3O_4-graphene (100% phenol degradation in 30 min),[46] nanoscaled zerovalent iron encapsulated in carbon spheres (100% phenol decomposition in 15 min)[47] and exceptionally better than some other metal-based materials such as MnO_2 (15% phenol degradation in 180 min),[48] Fe_3O_4 (10% phenol degradation in 180 min),[49] Co_3O_4 prepared by thermal decomposition of cobalt nitrate (24% phenol degradation in 180 min),[50] MnO_2 supported Co_3O_4 (100% phenol degradation in 120 min),[51] magnetic core/shell

nanosphere supported manganese catalyst (100% phenol degradation in 120 min).[52]

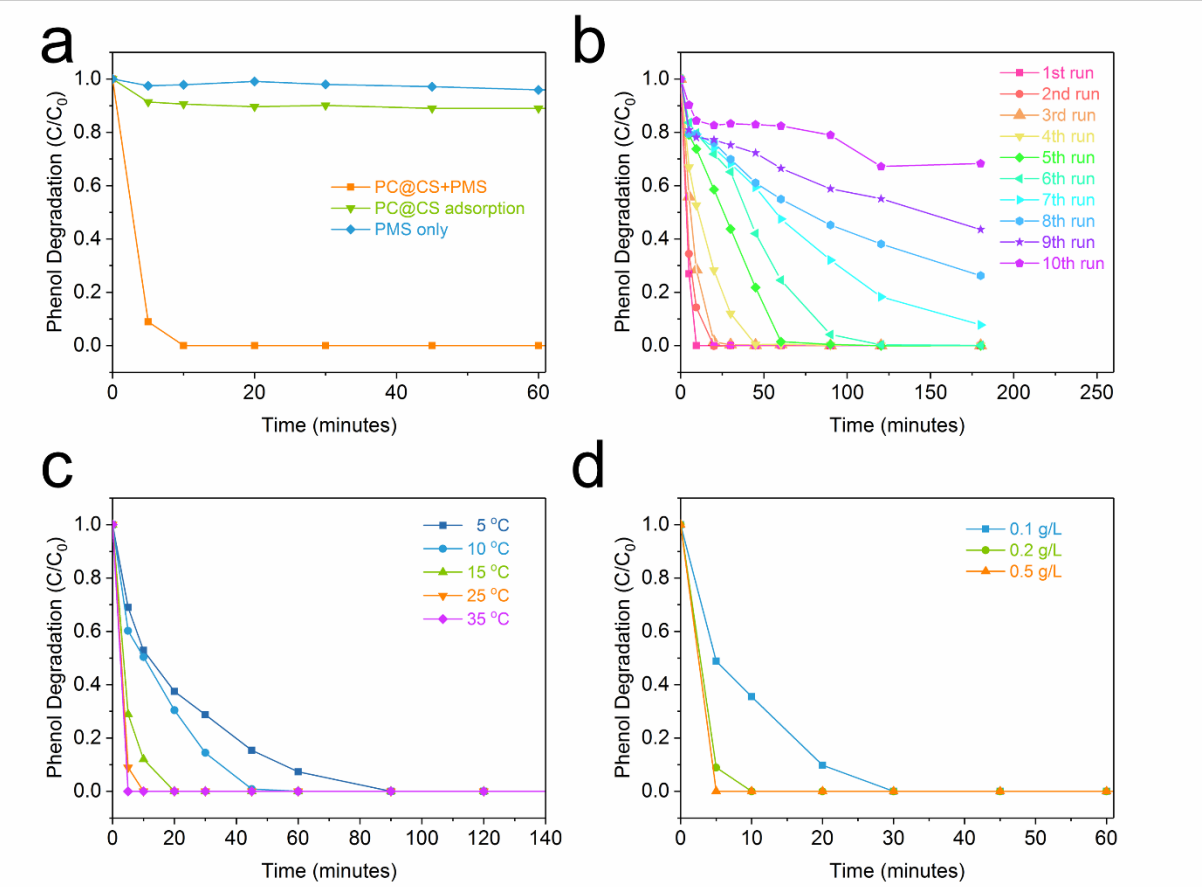

Figure 6.6 (a) Phenol degradation of PC@CS under various reaction conditions; (b) Stability and recyclability studies of PC@CS; (Condtions: phenol 50 ppm, catalyst 0.2 g/L, PMS 2 g/L, temperature 25 ^{o}C) (c) The effect of temperature on phenol removal; (Conditions: phenol 50 ppm, catalyst 0.2 g/L, PMS 2 g/L) (d) The effect of catalyst loading on phenol removal (Conditions: phenol 50 ppm, PMS 2 g/L, temperature 25 ^{o}C).

The results strongly suggested that the encapsulated partially oxidized Co_3O_4 and Co^0 and the outside carbon spheres may result in a synergistic effect that stimulates higher phenol removal efficiency of PC@CS.[53]

SEM, TEM and Raman characterizations show strong attachment of Co^0 encapsulated Co_3O_4 on carbon sphere and carbon defects. The distinctive core-shell structure and inner Co^0 would activate the outside carbon sphere and alter the electronic structure of nearby carbon atoms, and accelerate the electron transfer for the catalytic processes accordingly.[54] Compared to base Co_3O_4 catalyst, the outside carbon sphere provides an environment to obstruct aggregation of Co^0 encapsulated Co_3O_4 and prevents the loss of activity. The improved activity of PC@CS to degrade phenol may be in connection with the strong interaction (Co-O-C) between Co^0 encapsulated Co_3O_4 and carbon sphere and excellent dispersion of Co^0 encapsulated Co_3O_4 particles in the hybrids.[55] The Co-O-C sites will facilitate OH formation on Co_3O_4 and stimulate $HSO_5^{\bullet-}$ activation for the generation of sulfate radicals.[56] A pseudo-first-order reaction was applied to estimate the kinetic rates of PC@CS, as shown below:

$$\ln(C/C_0) = -kt \qquad \text{(Eq. 6.4)}$$

where C_0 and C represent phenol concentrations at initial and different time, t symbolizes the reaction time and k indicates the reaction rate constant.

The reaction rate constant (k) of phenol oxidation on PC@CS was evaluated to be 0.423 min^{-1}, much faster than NG-700 (0.319 min^{-1}), rGO-700 (0.004 min^{-1}), GNs (0.00138 min^{-1}), Mn/N_2-MCS (0.0418 min^{-1}), superior to the popular metal-based catalyst of crystalline Co_3O_4 (0.0173 min^{-1}) with more than 24 times enhancement.

Practical applications rely heavily on the stability of a catalyst. The stability and reusability were evaluated on PC@CS by successive tests under the same conditions and the results are shown in Figure 6.6 (b). Phenol removal at 100% was attained in 20 and 30 min for the second and third runs, respectively, compared to complete decomposition of phenol in 10 min for the fresh catalyst. Even after the 10^{th} run, PC@CS could still degrade approximately 30% phenol in 180 min. In a similar study, the activity of nanoscaled zerovalent iron encapsulated in carbon spheres rapidly decreased after the second and third runs, providing 31.7% and 13.4% phenol removal, respectively,[49] while the fresh sample completely degraded phenol in just 15 min. The excellent stability may be due to the inner stability and close integration of Co_3O_4 and Co^0 with supported carbon spheres, which led to little conversion of Co^0 into Co^{2+}/Co^{3+} in the reaction. The encapsulated Co^0 did not consume much after successive reactions and were still sufficient enough to activate the surrounding carbon sphere shell to degrade phenol in the following runs. However, the gradual decreases in phenol degradation were observed on PC@CS, which is mainly attributed to the attachment of intermediates generated in the reaction on the surface of the catalyst, leading to a reduction in the active sites and surface area of the catalyst.

The effect of solution temperature on phenol degradation by FC@CS is displayed in Figure 6.6 (c). Phenol degradation efficiency, as observed, is significantly increased by elevated temperatures. To be specific, complete phenol removal was attained in 90 min, 45 min, 20 min, 10 min and 5 min at 5 ^oC, 10 ^oC, 15 ^oC, 25 ^oC and 35 ^oC, respectively. It is generally believed that elevated temperature can stimulate phenol adsorption and facilitate electron transfer to generate more reactive radicals. The activation energy of PC@CS for phenol oxidation was calculated to be 33.0 kJ/mol, much lower than other Co-based materials

in the references.[57] Therefore, in light of excellent activity and low activation energy, PC@CS is regarded as a promising catalytic material for oxidation processes.

Figure 6.6 (d) reveals the influence of catalyst loading on phenol removal. At 0.1 g/L, complete phenol removal can be achieved in 30 min, which can dramatically be reduced to 10 and 5 min with 0.2 and 0.5 g/L loadings, respectively. Because of the minor influence of PC@CS adsorption, the enhancement of catalytic efficiency was ascribed to more active sites provided by more catalyst to activate PMS.

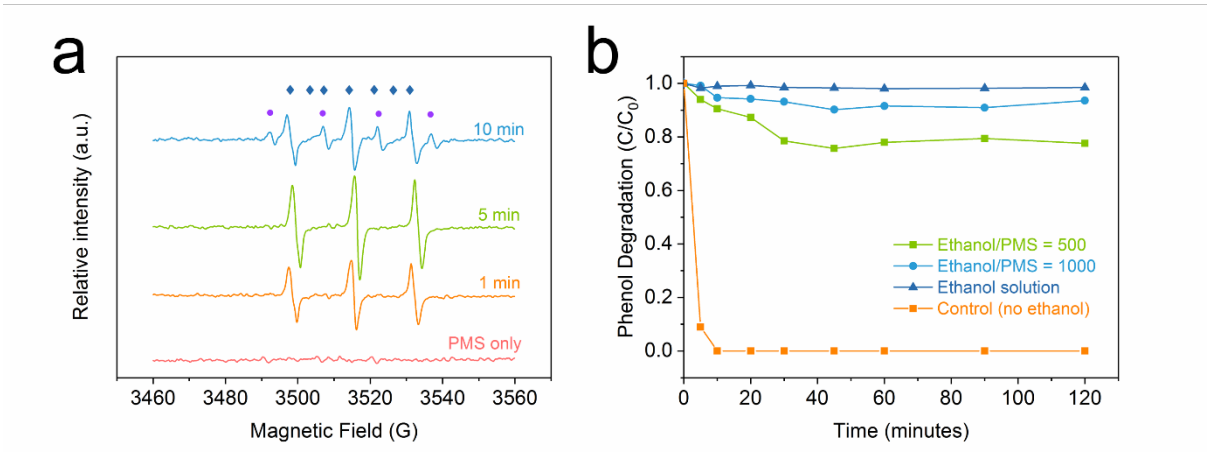

Figure 6.7 (a) EPR spectra of DMPO adducts under different conditions (●: DMPO-OH; ◆: DMPO-SO_4); (b) Quenching tests of PC@CS on phenol degradation (Conditions: phenol 50 ppm, catalyst loading 0.2 g/L, PMS 2g/L, temperature 25 ºC).

Many investigations have demonstrated that either homogeneous or heterogeneous activation can generate both hydroxyl radicals (•OH) and sulfate radicals ($SO_4^{\bullet-}$).[58, 59] Electron paramagnetic resonance (EPR) with 5,5-dimethylpyrroline-oxide (DMPO) as a radical spin trapping agent was utilized as a powerful tool to evaluate the generation of

reactive radicals and probe the dominant radicals from PMS activation on PC@CS for phenol oxidation process.

Figure 6.7 (a) demonstrates that PMS itself can barely generate active radicals with no catalyst but PC@CS can initiate PMS activation efficiently to generate both $SO_4^{\bullet-}$ and $^{\bullet}OH$. Many $SO_4^{\bullet-}$ were produced quickly in the first 1 min, and subsequently its amount increased continuously after 5 min. However, in 10 min, its amount dropped, which may be ascribed to the consumption by phenol degradation. Conversely, the amount of $^{\bullet}OH$ increased in 10 min, which is resulted from the accumulation of PMS and the transformation from $SO_4^{\bullet-}$.

To further investigate the generation of radicals responsible for phenol degradation, classical quenching experiments with ethanol as a radical scavenger were carried out. It is reported that ethanol is able to react rapidly with both hydroxyl and sulfate radicals in the activation process, which are vital for the degradation of organic pollutants in most AOPs. As a result, if ethanol is present in reaction solution, phenol degradation would be substantially reduced or prevented.[13, 60] Figure 6.7 (b) shows the effect of ethanol on the catalytic decomposition of phenol by PC@CS. Based on the above studies, 50 ppm phenol is completely removed in just 10 min at standard reaction conditions. However, the efficiency reduced dramatically at a molar ratio of 500:1 (ethanol : PMS). Specifically, only around 23% of phenol was removed in 180 min. In addition, it can be seen that the efficiency decreased significantly with increasing amount of ethanol in the solution and phenol cannot be removed when the solution was completely replaced by ethanol. This indicates that ethanol quenched the generated radicals rapidly before they reacted with phenol molecules. Therefore, it can be deduced that both $SO_4^{\bullet-}$ and $^{\bullet}OH$ play a dominant role in the phenol oxidation process activated by PC@CS, which can be defined as a radical-based process.

The mechanisms of PMS activation on PC@CS for phenol removal might be proposed as follows.[61]

$$Co^{2+} + HSO_5^- \rightarrow Co^{3+} + SO_4^{\bullet -} + OH^- \quad \text{(Eq. 6.5)}$$

$$Co^{2+} + HSO_5^- \rightarrow Co^{3+} + SO_4^{2-} + OH^{\bullet} \quad \text{(Eq. 6.6)}$$

$$Co^{3+} + HSO_5^- \rightarrow Co^{2+} + SO_5^{\bullet -} + H^+ \quad \text{(Eq. 6.7)}$$

$$SO_4^{\bullet -} + \text{OH}^{\bullet} + \text{phenol} \rightarrow [\ldots many\ steps \ldots] \rightarrow CO_2 + H_2O \quad \text{(Eq. 6.8)}$$

From the thermodynamic point, the reaction is circulatory until the complete consumption of PMS at enough time because Co^{3+} can be reversibly transferred to Co^{2+}.[62]

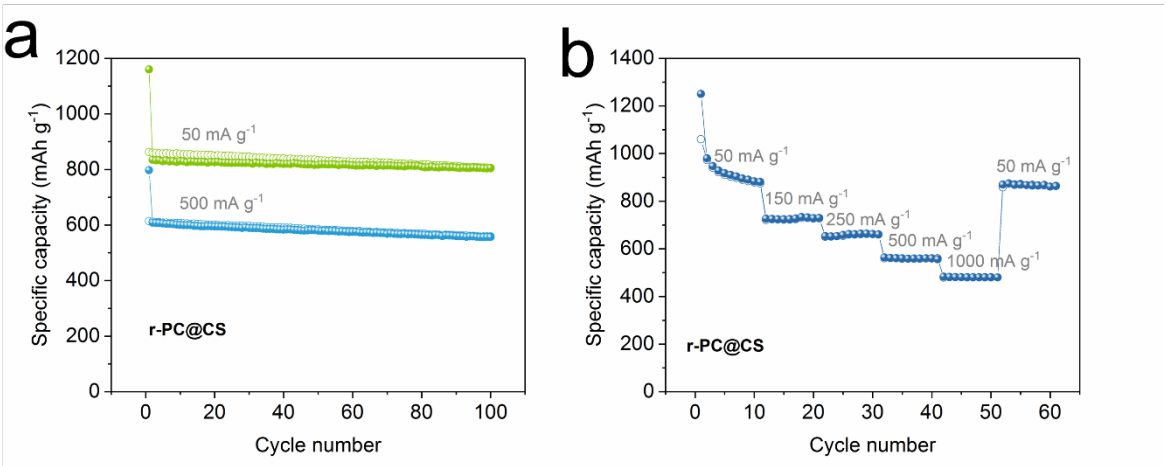

Figure 6.8 (a) Comparison of the cycling performance of r-PC@CS at current densities 50 and 500 mA g^{-1}; (b) Rate capability of r-PC@CS at various current densities between 50 and 1000 mA g^{-1}.

Cobalt is considered as a metal with growing demand in the technology, health and energy industries of the modern society in the future.

Specifically, Co is a primary component in various novel rechargeable batteries such as electric cars, mobile phones, and laptop computers. Plenty of LIBs contain up to 60% Co. However, cobalt can only be produced in a limited number of countries and the increasing cobalt prices will be maintained as cobalt consumers react to increasing Co demand, producer country risk and depleting mine grades in near future. Therefore, considering cost reductions, positive impacts on the environment, the conservation of natural resources and energy savings, the recycling of Co-based materials is obviously beneficial for the application of lithium ion battery. After phenol degradation, PC@CS material is completely collected by a magnet to prevent the secondary contamination. Subsequently, the used catalyst is regenerated in a tube furnace for calcination at 600 ^{o}C under hydrogen atmosphere and then cooling down to 300 ^{o}C and switch to air atmosphere to calcination for 2 h to remove the absorbed intermediates in the process of phenol decomposition. Because PC@CS undergoes an oxidizing reaction with PMS as well as a regeneration process in the air, all of the metal Co can be converted to Co_3O_4, which is a suitable anode material with high theoretical capacity for the lithium ion battery. Figure 6.8 (a) exhibits the lithium storage performance and cycling stability of regenerative PC@CS catalyst after phenol degradation (r-PC@CS) at a galvanostatic charge/discharge current of 50 mAh g^{-1} and 500 mAh g^{-1} between 0.01 V and 3.0 V (vs Li^{+}/Li). Figure 6.8 (a) indicates that r-PC@CS displays similar discharge and charge capacity with FC@CS. At the current density of 50 mAh g^{-1}, r-PC@CS displays an initial discharge capacity of 1160.9 mAh g^{-1} and an initial Coulombic efficiency of 74.2%. At the 50th cycle, the discharge capacity can still maintain a value of 98.1%. For the discharge capacity at 500 mA g^{-1}, r-PC@CS demonstrates a discharge capacity of 797.4 mAh g^{-1} and a charge capacity of 613.9 mAh g^{-1} on the

first cycle, corresponding to a Coulombic efficiency of 76.9%. From the 2nd cycle to 100th cycle, the capacity reduces gradually and slightly. After 50 cycles, the discharge capacity can be kept at a value of 556.6 mAh g^{-1} until the 100th cycle. In terms of the rate capability tests displayed in Figure 6.8 (b), the average specific capacities of r-PC@CS composite after regeneration are 880.8, 727.6, 661.6, and 559.5 mAh g^{-1} at the current densities of 50, 150, 250, and 500 mA g^{-1}, respectively. Even at a very large current density of 1000 mA g^{-1}, specific capacity is still as high as 480.6 mAh g^{-1}, which is nearly 1.5 times higher than the theoretical capacity of commercial graphite, displaying superb rate capability of r-PC@CS.

6.4 Conclusion

In summary, the pomegranate-like structural PC@CS and FC@CS composites are developed by the combination of a hydrothermal method and a controllable oxidation process. Different compositions and characteristics are presented by PC@CS and FC@CS composites. FC@CS is used as the anode of LIBs due to its high theoretical capacity and stable structure during the Li ion insertion/extraction. It exhibits a large reversible capacity of 933.2 mAh g^{-1} at 50 mA g^{-1} and 533.6 mAh g^{-1} at 1000 mA g^{-1}, excellent cyclic performance at both high and low current density, high Coulombic efficiency and good rate capability. On the other hand, PC@CS is employed as an excellent metal-based catalyst in phenol degradation with no secondary contamination. Not only outstanding catalytic performance but also superb stability is displayed by PC@CS. EPR spectra and quenching tests suggest that both $SO_4^{\bullet-}$ and $^{\bullet}OH$ were generated and played a vital role in phenol removal. After the degradation of phenol, the inactive PC@CS was regenerated in

hydrogen and air atmospheres at high temperature, and applied to LIBs anode, which exhibits a comparable capacitance and 100 cycles stability at at 50 mA g^{-1} and 500 mA g^{-1}, a good rate capacity at various current densities between 50 and 1000 mA g^{-1}. These results reach the aim of materials recycle in environmental protection and reduce the production cost of LIBs.

References

[1] A.K. Kivaisi, The potential for constructed wetlands for wastewater treatment and reuse in developing countries: a review, Ecol. Eng. 16(4) (2001) 545-560.

[2] S.S. Schiffman, J.M. Walker, P. Dalton, T.S. Lorig, J.H. Raymer, D. Shusterman, C.M. Williams, Potential health effects of odor from animal operations, wastewater treatment, and recycling of byproducts, J Agromedicine 7(1) (2000) 7-81.

[3] E. Saputra, S. Muhammad, H. Sun, H.-M. Ang, M.O. Tadé, S. Wang, A comparative study of spinel structured Mn_3O_4, Co_3O_4 and Fe_3O_4 nanoparticles in catalytic oxidation of phenolic contaminants in aqueous solutions, J. Colloid Interface Sci. 407(Supplement C) (2013) 467-473.

[4] X. Xiao, M. Lu, J. Nan, X. Zuo, W. Zhang, S. Liu, S. Wang, Rapid microwave synthesis of I-doped $Bi_4O_5Br_2$ with significantly enhanced visible-light photocatalysis for degradation of multiple parabens, Appl. Catal., B 218(Supplement C) (2017) 398-408.

[5] S. Wang, Y. Peng, Natural zeolites as effective adsorbents in water and wastewater treatment, Chem. Eng. J. 156(1) (2010) 11-24.

[6] C. Chiemchaisri, K. Yamamoto, Performance of membrane separation bioreactor at various temperatures for domestic wastewater treatment, J. Membr. Sci. 87(1) (1994) 119-129.

[7] A. Joss, S. Zabczynski, A. Göbel, B. Hoffmann, D. Löffler, C.S. McArdell, T.A. Ternes, A. Thomsen, H. Siegrist, Biological degradation of pharmaceuticals in municipal wastewater treatment: Proposing a classification scheme, Water Res. 40(8) (2006) 1686-1696.
[8] N.N. Mahamuni, Y.G. Adewuyi, Advanced oxidation processes (AOPs) involving ultrasound for waste water treatment: A review with emphasis on cost estimation, Ultrason. Sonochem. 17(6) (2010) 990-1003.
[9] L. Prieto-Rodríguez, I. Oller, N. Klamerth, A. Agüera, E.M. Rodríguez, S. Malato, Application of solar AOPs and ozonation for elimination of micropollutants in municipal wastewater treatment plant effluents, Water Res. 47(4) (2013) 1521-1528.
[10] P. Villegas- Guzman, S. Giannakis, S. Rtimi, D. Grandjean, M. Bensimon, L.F. de Alencastro, R. Torres-Palma, C. Pulgarin, A green solar photo-Fenton process for the elimination of bacteria and micropollutants in municipal wastewater treatment using mineral iron and natural organic acids, Appl. Catal., B 219(Supplement C) (2017) 538-549.
[11] A. Babuponnusami, K. Muthukumar, A review on Fenton and improvements to the Fenton process for wastewater treatment, J. Environ. Chem. Eng. 2(1) (2014) 557-572.
[12] C. Wang, J. Kang, P. Liang, H. Zhang, H. Sun, M.O. Tade, S. Wang, Ferric carbide nanocrystals encapsulated in nitrogen-doped carbon nanotubes as an outstanding environmental catalyst, Environ. Sci. Nano 4(1) (2017) 170-179.
[13] C. Wang, J. Kang, H. Sun, H.M. Ang, M.O. Tadé, S. Wang, One-pot synthesis of N-doped graphene for metal-free advanced oxidation processes, Carbon 102(Supplement C) (2016) 279-287.

[14] F. Ghanbari, M. Moradi, Application of peroxymonosulfate and its activation methods for degradation of environmental organic pollutants: Review, Chem. Eng. J. 310(Part 1) (2017) 41-62.
[15] Y. Yao, H. Chen, C. Lian, F. Wei, D. Zhang, G. Wu, B. Chen, S. Wang, Fe, Co, Ni nanocrystals encapsulated in nitrogen-doped carbon nanotubes as Fenton-like catalysts for organic pollutant removal, J. Hazard. Mater. 314(Supplement C) (2016) 129-139.
[16] E. Saputra, S. Muhammad, H. Sun, H.M. Ang, M.O. Tadé, S. Wang, Red mud and fly ash supported Co catalysts for phenol oxidation, Catal. Today 190(1) (2012) 68-72.
[17] P. Shukla, H. Sun, S. Wang, H.M. Ang, M.O. Tadé, Co-SBA-15 for heterogeneous oxidation of phenol with sulfate radical for wastewater treatment, Catal. Today 175(1) (2011) 380-385.
[18] G.P. Anipsitakis, D.D. Dionysiou, Degradation of organic contaminants in water with sulfate radicals generated by the conjunction of peroxymonosulfate with cobalt, Environ. Sci. Technol. 37(20) (2003) 4790-4797.
[19] K.H. Chan, W. Chu, Degradation of atrazine by cobalt-mediated activation of peroxymonosulfate: Different cobalt counteranions in homogenous process and cobalt oxide catalysts in photolytic heterogeneous process, Water Res. 43(9) (2009) 2513-2521.
[20] A. Başoğlu, S. Parlayan, M. Ocak, H. Alp, H. Kantekin, M. Özdemir, Ü. Ocak, Selective recognition of Cobalt (II) ion by a new cryptand compound with $N_2O_2S_2$ donor atom possessing 2-hydroxy-1-naphthylidene schiff base moiety, Journal J Fluoresc 19(4) (2009) 655-662.
[21] Y. Yao, C. Xu, S. Miao, H. Sun, S. Wang, One-pot hydrothermal synthesis of $Co(OH)_2$ nanoflakes on graphene sheets and their fast

catalytic oxidation of phenol in liquid phase, J. Colloid Interface Sci. 402(Supplement C) (2013) 230-236.
[22] Q. Yang, H. Choi, S.R. Al-Abed, D.D. Dionysiou, Iron–cobalt mixed oxide nanocatalysts: Heterogeneous peroxymonosulfate activation, cobalt leaching, and ferromagnetic properties for environmental applications, Appl. Catal., B 88(3) (2009) 462-469.
[23] S. Chen, L. Shen, P.A. van Aken, J. Maier, Y. Yu, Lithium-ion batteries: Dual-functionalized double carbon shells coated silicon nanoparticles for high performance lithium-ion batteries, Adv. Mater. 29(21) (2017) n/a-n/a.
[24] S. Choi, T.-w. Kwon, A. Coskun, J.W. Choi, Highly elastic binders integrating polyrotaxanes for silicon microparticle anodes in lithium ion batteries, Science 357(6348) (2017) 279.
[25] W. Li, A. Dolocan, P. Oh, H. Celio, S. Park, J. Cho, A. Manthiram, Dynamic behaviour of interphases and its implication on high-energy-density cathode materials in lithium-ion batteries, Nat. Commun. 8 (2017) 14589.
[26] L. Zhao, Y.-S. Hu, H. Li, Z. Wang, L. Chen, Porous $Li_4Ti_5O_{12}$ coated with N-doped carbon from ionic liquids for Li-ion batteries, Adv. Mater. 23(11) (2011) 1385-1388.
[27] P. Poizot, S. Laruelle, S. Grugeon, L. Dupont, J.M. Tarascon, Nano-sized transition-metal oxides as negative-electrode materials for lithium-ion batteries, Nature 407(6803) (2000) 496-499.
[28] S. Sun, X. Zhao, M. Yang, L. Wu, Z. Wen, X. Shen, Hierarchically ordered mesoporous Co_3O_4 materials for high performance Li-ion batteries, Sci. Rep. 6 (2016) 19564.
[29] F. Hao, Z. Zhang, L. Yin, Co_3O_4/carbon aerogel hybrids as anode materials for lithium-ion batteries with enhanced electrochemical properties, ACS Appl. Mater. Interfaces 5(17) (2013) 8337-8344.

[30] Z.-S. Wu, W. Ren, L. Wen, L. Gao, J. Zhao, Z. Chen, G. Zhou, F. Li, H.-M. Cheng, Graphene anchored with Co_3O_4 nanoparticles as anode of lithium ion batteries with enhanced reversible capacity and cyclic performance, ACS Nano 4(6) (2010) 3187-3194.
[31] N.S. Marzuki, N.U. Taib, M.F. Hassan, N.H. Idris, Enhanced lithium storage in Co_3O_4/carbon anode for Li-ion batteries, Electrochim. Acta 182(Supplement C) (2015) 452-457.
[32] N. Du, H. Zhang, B.D. Chen, J.B. Wu, X.Y. Ma, Z.H. Liu, Y.Q. Zhang, D.R. Yang, X.H. Huang, J.P. Tu, Porous Co_3O_4 nanotubes derived from $Co_4(CO)_{12}$ clusters on carbon nanotube templates: A highly efficient material for Li-battery applications, Adv. Mater. 19(24) (2007) 4505-4509.
[33] X. Wang, X.-L. Wu, Y.-G. Guo, Y. Zhong, X. Cao, Y. Ma, J. Yao, Synthesis and lithium storage properties of Co_3O_4 nanosheet-assembled multishelled hollow spheres, Adv. Funct. Mater. 20(10) (2010) 1680-1686.
[34] N. Yan, L. Hu, Y. Li, Y. Wang, H. Zhong, X. Hu, X. Kong, Q. Chen, Co_3O_4 nanocages for high-performance anode material in lithium-ion batteries, J. Phys. Chem. C 116(12) (2012) 7227-7235.
[35] J. Xu, J. Wu, L. Luo, X. Chen, H. Qin, V. Dravid, S. Mi, C. Jia, Co_3O_4 nanocubes homogeneously assembled on few-layer graphene for high energy density lithium-ion batteries, J. Power Sources 274(Supplement C) (2015) 816-822.
[36] J.S. Chen, T. Zhu, Q.H. Hu, J. Gao, F. Su, S.Z. Qiao, X.W. Lou, Shape-controlled synthesis of cobalt-based nanocubes, nanodiscs, and nanoflowers and their comparative lithium-storage properties, ACS Appl. Mater. Interfaces 2(12) (2010) 3628-3635.
[37] X. Wang, X.-L. Wu, Y.-G. Guo, Y. Zhong, X. Cao, Y. Ma, J. Yao, Synthesis and Lithium Storage Properties of Co3O4 Nanosheet-

Assembled Multishelled Hollow Spheres, Advanced Functional Materials 20(10) (2010) 1680-1686.
[38] M. Chen, X. Xia, J. Yin, Q. Chen, Construction of Co_3O_4 nanotubes as high-performance anode material for lithium ion batteries, Electrochim. Acta 160(Supplement C) (2015) 15-21.
[39] X.W. Lou, D. Deng, J.Y. Lee, J. Feng, L.A. Archer, Self-supported formation of needlelike Co_3O_4 nanotubes and their application as lithium-ion battery electrodes, Adv. Mater. 20(2) (2008) 258-262.
[40] G. Wang, H. Liu, J. Horvat, B. Wang, S. Qiao, J. Park, H. Ahn, Highly ordered mesoporous cobalt oxide nanostructures: Synthesis, characterisation, magnetic properties, and applications for electrochemical energy devices, Chem. Eur. J. 16(36) (2010) 11020-11027.
[41] Y. Li, L. Zou, J. Li, K. Guo, X. Dong, X. Li, X. Xue, H. Zhang, H. Yang, Synthesis of ordered mesoporous $NiCo_2O_4$ via hard template and its application as bifunctional electrocatalyst for Li-O_2 batteries, Electrochim. Acta 129(Supplement C) (2014) 14-20.
[42] L. Tian, H. Zou, J. Fu, X. Yang, Y. Wang, H. Guo, X. Fu, C. Liang, M. Wu, P.K. Shen, Q. Gao, Topotactic conversion route to mesoporous quasi-single-crystalline Co_3O_4 nanobelts with optimizable electrochemical performance, Adv. Funct. Mater. 20(4) (2010) 617-623.
[43] X. Leng, S. Wei, Z. Jiang, J. Lian, G. Wang, Q. Jiang, Carbon-encapsulated Co_3O_4 nanoparticles as anode materials with super lithium storage performance, Sci. Rep. 5 (2015) 16629.
[44] J.M. Tarascon, M. Armand, Issues and challenges facing rechargeable lithium batteries, Nature 414(6861) (2001) 359-367.
[45] Q. Chen, H. Wang, S. Perero, Q. Wang, Q. Chen, Structural, optical and magnetic properties of Fe_3O_4 sputtered TeO_2–PbO–B_2O_3 and PbO–

Bi_2O_3–B_2O_3 glasses for sensing applications, J. Non-Cryst. Solids 408(Supplement C) (2015) 43-50.
[46] Y. Yao, Z. Yang, H. Sun, S. Wang, Hydrothermal synthesis of Co_3O_4–graphene for heterogeneous activation of peroxymonosulfate for decomposition of phenol, Ind. Eng. Chem. Res. 51(46) (2012) 14958-14965.
[47] H. Sun, G. Zhou, S. Liu, H.M. Ang, M.O. Tadé, S. Wang, Nano-Fe^0 Encapsulated in Microcarbon Spheres: Synthesis, Characterization, and Environmental Applications, ACS Appl. Mater. Interfaces 4(11) (2012) 6235-6241.
[48] E. Saputra, S. Muhammad, H. Sun, H.-M. Ang, M.O. Tadé, S. Wang, Manganese oxides at different oxidation states for heterogeneous activation of peroxymonosulfate for phenol degradation in aqueous solutions, Appl. Catal., B 142(Supplement C) (2013) 729-735.
[49] H. Sun, G. Zhou, S. Liu, H.M. Ang, M.O. Tadé, S. Wang, Nano-Fe0 Encapsulated in Microcarbon Spheres: Synthesis, Characterization, and Environmental Applications, ACS Applied Materials & Interfaces 4(11) (2012) 6235-6241.
[50] Y. Wang, L. Zhou, X. Duan, H. Sun, E.L. Tin, W. Jin, S. Wang, Photochemical degradation of phenol solutions on Co_3O_4 nanorods with sulfate radicals, Catal. Today 258(Part 2) (2015) 576-584.
[51] H. Liang, H. Sun, A. Patel, P. Shukla, Z.H. Zhu, S. Wang, Excellent performance of mesoporous Co_3O_4/MnO_2 nanoparticles in heterogeneous activation of peroxymonosulfate for phenol degradation in aqueous solutions, Appl. Catal., B 127(Supplement C) (2012) 330-335.
[52] Y. Wang, H. Sun, H.M. Ang, M.O. Tadé, S. Wang, Synthesis of magnetic core/shell carbon nanosphere supported manganese catalysts for oxidation of organics in water by peroxymonosulfate, J. Colloid Interface Sci. 433(Supplement C) (2014) 68-75.

[53] Y. Yao, Z. Yang, H. Sun, S. Wang, Hydrothermal Synthesis of Co3O4–Graphene for Heterogeneous Activation of Peroxymonosulfate for Decomposition of Phenol, Industrial & Engineering Chemistry Research 51(46) (2012) 14958-14965.
[54] Z. Ji, X. Shen, G. Zhu, H. Zhou, A. Yuan, Reduced graphene oxide/nickel nanocomposites: facile synthesis, magnetic and catalytic properties, J. Mater. Chem. 22(8) (2012) 3471-3477.
[55] Q. Zhang, C. Tian, A. Wu, T. Tan, L. Sun, L. Wang, H. Fu, A facile one-pot route for the controllable growth of small sized and well-dispersed ZnO particles on GO-derived graphene, J. Mater. Chem. 22(23) (2012) 11778-11784.
[56] G.P. Anipsitakis, D.D. Dionysiou, M.A. Gonzalez, Cobalt-mediated activation of peroxymonosulfate and sulfate radical attack on phenolic compounds. Implications of chloride ions, Environ. Sci. Technol. 40(3) (2006) 1000-1007.
[57] H. Sun, H. Tian, Y. Hardjono, C.E. Buckley, S. Wang, Preparation of cobalt/carbon-xerogel for heterogeneous oxidation of phenol, Catal. Today 186(1) (2012) 63-68.
[58] E. Saputra, S. Muhammad, H. Sun, H.-M. Ang, M.O. Tadé, S. Wang, Manganese oxides at different oxidation states for heterogeneous activation of peroxymonosulfate for phenol degradation in aqueous solutions, Applied Catalysis B: Environmental 142(Supplement C) (2013) 729-735.
[59] G.P. Anipsitakis, D.D. Dionysiou, Degradation of Organic Contaminants in Water with Sulfate Radicals Generated by the Conjunction of Peroxymonosulfate with Cobalt, Environmental Science & Technology 37(20) (2003) 4790-4797.
[60] P. Liang, C. Zhang, X. Duan, H. Sun, S. Liu, M.O. Tade, S. Wang, N-doped graphene from metal–organic frameworks for catalytic

oxidation of p-hydroxylbenzoic acid: N-functionality and mechanism, ACS Sustainable Chem. Eng. 5(3) (2017) 2693-2701.
[61] G.P. Anipsitakis, D.D. Dionysiou, M.A. Gonzalez, Cobalt-Mediated Activation of Peroxymonosulfate and Sulfate Radical Attack on Phenolic Compounds. Implications of Chloride Ions, Environmental Science & Technology 40(3) (2006) 1000-1007.
[62] W. Guo, S. Su, C. Yi, Z. Ma, Degradation of antibiotics amoxicillin by Co_3O_4-catalyzed peroxymonosulfate system, Environ. Prog. Sustainable Energy 32(2) (2013) 193-197.

Every reasonable effort has been made to acknowledge the owners of copyright material. I would be pleased to hear from any copyright owner who has been omitted or incorrectly acknowledged.

Chapter 7 Conclusions and Perspectives

7.1 Conclusions

In this thesis, nitrogen-doped carbon nanomaterials and Co-based nanospheres have successfully prepared via green and simple methods and demonstrated outstanding performances toward heterogeneous activation of peroxymonosulfate (PMS) for phenol degradation. The main objectives described in the first chapter have been achieved satisfactorily with comprehensive research. Nitrogen-doped graphene, nitrogen-doped carbon nanotubes with encapsulated iron carbide and nitrogen-doped mesoporous carbon nanostructures have been synthesized via direct pyrolysis of iron chloride and different nitridation agents. Pomegranate-like structural Co sphere @carbon sphere composite materials have been prepared by a one-step hydrothermal method. All of these catalysts were characterized by various techniques and tested for catalytic oxidation of phenol solutions by PMS activation to generate hydroxyl radicals, sulfate radicals and singlet oxygen. In addition, Co sphere@carbon sphere with different degrees of oxidation treatment were also used in the application of anode of lithium ion battery. Nitrogen-doping can significantly promote the catalytic activity of carbon materials for PMS activation. Electron paramagnetic resonance (EPR) proved that both hydroxyl and sulfate radicals were produced and responsible for the degradation of organic pollutants during the PMS activation processes. In addition, non-radical oxidation pathway was discovered upon ferric carbide nanocrystals encapsulated in nitrogen-doped carbon nanotubes for aqueous oxidation with PMS. The comprehensive mechanism studies of PMS activation with carbocatalysis are illuminated with different quenching experiments.

7.1.1 One pot synthesis of N-doped graphene for metal-free advanced oxidation processes

- A green and feasible synthesis was developed to fabricate nitrogen-doped graphene with both structural and compositional modifications. This approach can produce both high-quality and a quantity of graphene without involving strong oxidants and acids.
- The prepared N-doped graphene has a low oxygen content but relatively high nitrogen content.
- N-doped graphene presented an excellent performance in catalytic activation of PMS for phenol oxidation, and was superior to rGO from Hummers' method.
- Kinetic studies indicated that catalyst loading will influence the degradation efficiency, whereas the temperature showed a marginal effect.
- EPR spectra suggested that both $SO_4^{\bullet-}$ and •OH were generated during the activation and oxidation processes and played essential roles in phenol removal.

7.1.2 Ferric carbide nanocrystals encapsulated in nitrogen-doped carbon nanotubes as an outstanding environmental catalyst

- Nitrogen-doped carbon nanotubes with encapsulated Fe_3C nanoparticles (Fe_3C@NCNT) were successfully prepared through a simple and green pyrolysis process of melamine and iron chlorides.
- The characterization results showed that Fe_3C nanocrystals were mainly encapsulated in the interior of Fe_3C@NCNT composites.
- The as-prepared Fe_3C@NCNT catalysts exhibited both excellent catalytic performance and outstanding stability in phenol degradation. The quaternary and pyridinic N, synergetic effects

between inner Fe_3C and outside carbon as well as trace amount of Fe on the surface may be the active sites to enhance catalytic degradation.

- Quenching experiments were used to observe the generated reactive radicals and $^1O_2$ and $^{\bullet}O_2^-$ were proven to be the major radicals in catalytic phenol degradation.

7.1.3 Morphological control of nitrogen-doped carbon nanostructures and their environmental application

- A green and facile pyrolysis synthesis of iron chloride, melamine and glucose was applied to fabricate nitrogen-doped mesoporous carbon nanostructures with morphology modifications from graphene to carbon nanotube.
- The prepared materials have low oxygen content and high nitrogen content with large specific surface area.
- NMCN-50 and NMCN-75 exhibited excellent performance in catalytic oxidation of PMS to degrade phenol solutions.
- The specific surface area as well as the amount of nitrogen precursors play a combined role in the enhancement of catalytic performance. However, excess nitrogen sources somehow prevent nitrogen from incorporating into the interior and thus decrease the defective sites, specific surface area and the amount of quaternary nitrogen, further limiting the improvement of catalytic performance.
- Quenching tests were employed to investigate the generated reactive species, and $^1O_2$ were demonstrated to be the dominant oxygen species in catalytic phenol oxidation. It was concluded that this catalyst follows major non-radical and minor radical processes to activate PMS to degrade phenol.

7.1.4 Co-based nanospheres supported on carbon sphere with a tunable oxidation layer in the applications of lithium ion battery and wastewater treatment

- The pomegranate-like structural PC@CS and FC@CS composites are developed by the combination of a hydrothermal method and a controllable oxidation process.
- Different compositions and characteristics are presented by PC@CS and FC@CS composites.
- FC@CS is used as the anode of LIBs due to its high theoretical capacity and stable structure during the Li ion insertion/extraction. It exhibits a large reversible capacity of 933.2 mAh g^{-1} at 50 mA g^{-1} and 533.6 mAh g^{-1} at 1000 mA g^{-1}, excellent cyclic performance at both high and low current density, high Coulombic efficiency and good rate capability.
- PC@CS is employed as an excellent metal-based catalyst in phenol degradation with no secondary contamination. Not only outstanding catalytic performance but also superb stability is displayed by PC@CS.
- EPR spectra and quenching tests suggest that both $SO_4^{\bullet-}$ and $^{\bullet}OH$ were generated and played a vital role in phenol removal.
- After the degradation of phenol, the inactive PC@CS was regenerated in hydrogen and air atmospheres at high temperature, and applied to LIBs anode, which exhibits a comparable capacitance and 100 cycles stability at at 50 mA g^{-1} and 500 mA g^{-1}, a good rate capacity at various current densities between 50 and 1000 mA g^{-1}.

7.2 Perspectives and suggestions for future research

Due to deficient understanding of the rich surface chemistry of nanocarbons, their possible application in industrial catalysts has been considered questionable. Therefore, it is of vital significance to carry out controlled synthesis in terms of not only the type of materials and nanoarchitecture but especially uniform characteristics, including type and density of defects.

Meanwhile, the reaction conditions and dosage of PMS and carbocatalysts need to be adjusted and optimized in the real wastewater applications. The total cost of mineralization effectiveness, recovery and post-treatment of the deactivated catalysts should be taken into considerations.

The reactivity of nancarbons is largely associated with the presence of defects and edge sites, doping heteroatoms, and the interaction between these sites. The systematic studies of the relationship between the nature of the active sites in nanocarbons and their catalytic reactivity are still limited.

Inherent problem of PMS is still remained which is related to sulfate ion release as the main by-product. This issue is exacerbated by two other salts (K_2SO_4, $KHSO_4$) which are applied along with PMS in Oxone salt structure. Here the solution might be the application of a subsequent process (ion exchange, membrane, etc.) after PMS-based processes with high PMS dosages for sulfate removal. In addition, optimization of PMS dosage is a suitable strategy to avoid excessive PMS thereby reducing the amounts of sulfate within the effluent.

The application discussed in the thesis is the catalytic oxidation of phenol solutions. Catalytic oxidation by strong oxidants such as PMS, PDS or H_2O_2 activation should be done using different variety of organic pollutants, such as 2,4,6-trichlorophenol (TCP), sulfachloropyridazine (SCP) and p-hydroxybenzoic acid (PHBA). A further detailed understanding of the surface properties of defects and other functional sites in nanocarbons and the possibility of their tailored tuning will open the door to new development area for oxygen reduction reaction and advanced electrodes, as well as in selective oxidation and hydrogenation reactions.

The heterogeneous activation of PMS by carbon materials is an intricate process. In addition to $^{\bullet}OH$ and $SO_4^{\bullet-}$, other reactive species may also contribute to the catalytic performance of phenol degradation. Meanwhile, their respective contributions to the phenol removal are not quantified. Therefore, the combination of EPR, various quenching experiments and theoretical modelling are needed to understand the reaction mechanism and the reasons for the remarkable catalytic activity.

Appendix

Title: Application of peroxymonosulfate and its activation methods for degradation of environmental organic pollutants: Review

Author: Farshid Ghanbari,Mahsa Moradi

Publication: Chemical Engineering Journal

Publisher: Elsevier

Date: 15 February 2017

Order Completed

Thank you for your order.

This Agreement between Curtin University -- Chen Wang ("You") and Elsevier ("Elsevier") consists of your license details and the terms and conditions provided by Elsevier and Copyright Clearance Center.

Your confirmation email will contain your order number for future reference.

printable details

License Number	4284510082149
License date	Feb 08, 2018
Licensed Content Publisher	Elsevier
Licensed Content Publication	Chemical Engineering Journal
Licensed Content Title	Application of peroxymonosulfate and its activation methods for degradation of environmental organic pollutants: Review
Licensed Content Author	Farshid Ghanbari,Mahsa Moradi
Licensed Content Date	Feb 15, 2017
Licensed Content Volume	310
Licensed Content Issue	n/a
Licensed Content Pages	22
Type of Use	reuse in a thesis/dissertation
Portion	figures/tables/illustrations
Number of figures/tables/illustrations	2
Format	both print and electronic
Are you the author of this Elsevier article?	No
Will you be translating?	No
Original figure numbers	Figure 3 & Figure 5
Title of your thesis/dissertation	The Synthesis and Application of Novel Nanostructured Carbon Materials
Expected completion date	Oct 2017
Estimated size (number of pages)	200
Attachment	
Requestor Location	Curtin University B601 Chemical Engineering Lab, 3 Turner Avenue, Bentley, WA,6102 Perth, 6102 Australia Attn: Curtin University
Publisher Tax ID	GB 494 6272 12
Total	0.00 AUD

ORDER MORE CLOSE WINDOW

Title:	Generation of sulfate radical through heterogeneous catalysis for organic contaminants removal: Current development, challenges and prospects
Author:	Wen-Da Oh,Zhili Dong,Teik-Thye Lim
Publication:	Applied Catalysis B: Environmental
Publisher:	Elsevier
Date:	5 October 2016

Order Completed

Thank you for your order.

This Agreement between Curtin University -- Chen Wang ("You") and Elsevier ("Elsevier") consists of your license details and the terms and conditions provided by Elsevier and Copyright Clearance Center.

Your confirmation email will contain your order number for future reference.

printable details

License Number	4284510248401
License date	Feb 08, 2018
Licensed Content Publisher	Elsevier
Licensed Content Publication	Applied Catalysis B: Environmental
Licensed Content Title	Generation of sulfate radical through heterogeneous catalysis for organic contaminants removal: Current development, challenges and prospects
Licensed Content Author	Wen-Da Oh,Zhili Dong,Teik-Thye Lim
Licensed Content Date	Oct 5, 2016
Licensed Content Volume	194
Licensed Content Issue	n/a
Licensed Content Pages	33
Type of Use	reuse in a thesis/dissertation
Portion	figures/tables/illustrations
Number of figures/tables/illustrations	1
Format	both print and electronic
Are you the author of this Elsevier article?	No
Will you be translating?	No
Original figure numbers	Figure 1
Title of your thesis/dissertation	The Synthesis and Application of Novel Nanostructured Carbon Materials
Expected completion date	Oct 2017
Estimated size (number of pages)	200
Attachment	
Requestor Location	Curtin University B601 Chemical Engineering Lab, 3 Turner Avenue, Bentley, WA,6102 Perth, 6102 Australia Attn: Curtin University
Publisher Tax ID	GB 494 6272 12
Total	0.00 AUD

ORDER MORE CLOSE WINDOW

Title: Reduced Graphene Oxide for Catalytic Oxidation of Aqueous Organic Pollutants

Author: Hongqi Sun, Shizhen Liu, Guanliang Zhou, et al

Publication: Applied Materials

Publisher: American Chemical Society

Date: Oct 1, 2012

PERMISSION/LICENSE IS GRANTED FOR YOUR ORDER AT NO CHARGE

This type of permission/license, instead of the standard Terms & Conditions, is sent to you because no fee is being charged for your order. Please note the following:

- Permission is granted for your request in both print and electronic formats, and translations.
- If figures and/or tables were requested, they may be adapted or used in part.
- Please print this page for your records and send a copy of it to your publisher/graduate school.
- Appropriate credit for the requested material should be given as follows: "Reprinted (adapted) with permission from (COMPLETE REFERENCE CITATION). Copyright (YEAR) American Chemical Society." Insert appropriate information in place of the capitalized words.
- One-time permission is granted only for the use specified in your request. No additional uses are granted (such as derivative works or other editions). For any other uses, please submit a new request.

If credit is given to another source for the material you requested, permission must be obtained from that source.

Title: N-Doping-Induced Nonradical Reaction on Single-Walled Carbon Nanotubes for Catalytic Phenol Oxidation

Author: Xiaoguang Duan, Hongqi Sun, Yuxian Wang, et al

Publication: ACS Catalysis

Publisher: American Chemical Society

Date: Feb 1, 2015

PERMISSION/LICENSE IS GRANTED FOR YOUR ORDER AT NO CHARGE

This type of permission/license, instead of the standard Terms & Conditions, is sent to you because no fee is being charged for your order. Please note the following:

- Permission is granted for your request in both print and electronic formats, and translations.
- If figures and/or tables were requested, they may be adapted or used in part.
- Please print this page for your records and send a copy of it to your publisher/graduate school.
- Appropriate credit for the requested material should be given as follows: "Reprinted (adapted) with permission from (COMPLETE REFERENCE CITATION). Copyright (YEAR) American Chemical Society." Insert appropriate information in place of the capitalized words.
- One-time permission is granted only for the use specified in your request. No additional uses are granted (such as derivative works or other editions). For any other uses, please submit a new request.

If credit is given to another source for the material you requested, permission must be obtained from that source.

Title: Nanocarbons for the Development of Advanced Catalysts

Author: Dang Sheng Su, Siglinda Perathoner, Gabriele Centi

Publication: Chemical Reviews

Publisher: American Chemical Society

Date: Aug 1, 2013

PERMISSION/LICENSE IS GRANTED FOR YOUR ORDER AT NO CHARGE

This type of permission/license, instead of the standard Terms & Conditions, is sent to you because no fee is being charged for your order. Please note the following:

- Permission is granted for your request in both print and electronic formats, and translations.
- If figures and/or tables were requested, they may be adapted or used in part.
- Please print this page for your records and send a copy of it to your publisher/graduate school.
- Appropriate credit for the requested material should be given as follows: "Reprinted (adapted) with permission from (COMPLETE REFERENCE CITATION). Copyright (YEAR) American Chemical Society." Insert appropriate information in place of the capitalized words.
- One-time permission is granted only for the use specified in your request. No additional uses are granted (such as derivative works or other editions). For any other uses, please submit a new request.

If credit is given to another source for the material you requested, permission must be obtained from that source.

Title: Environmental applications of graphene-based nanomaterials

Author: François Perreault,Andreia Fonseca de Faria,Menachem Elimelech

Publication: Chemical Society Reviews

Publisher: Royal Society of Chemistry

Date: Mar 26, 2015

Order Completed

Thank you for your order.

This Agreement between Curtin University -- Chen Wang ("You") and Royal Society of Chemistry ("Royal Society of Chemistry") consists of your license details and the terms and conditions provided by Royal Society of Chemistry and Copyright Clearance Center.

Your confirmation email will contain your order number for future reference.

printable details

License Number	4284520153006
License date	Feb 08, 2018
Licensed Content Publisher	Royal Society of Chemistry
Licensed Content Publication	Chemical Society Reviews
Licensed Content Title	Environmental applications of graphene-based nanomaterials
Licensed Content Author	François Perreault,Andreia Fonseca de Faria,Menachem Elimelech
Licensed Content Date	Mar 26, 2015
Licensed Content Volume	44
Licensed Content Issue	16
Type of Use	Thesis/Dissertation
Requestor type	academic/educational
Portion	figures/tables/images
Number of figures/tables/images	1
Distribution quantity	10000
Format	print and electronic
Will you be translating?	no
Order reference number	
Title of the thesis/dissertation	The Synthesis and Application of Novel Nanostructured Carbon Materials
Expected completion date	Oct 2017
Estimated size	200
Attachment	
Requestor Location	Curtin University B601 Chemical Engineering Lab, 3 Turner Avenue, Bentley, WA,6102 Perth, 6102 Australia Attn: Curtin University
Billing Type	Invoice
Billing address	Curtin University B601 Chemical Engineering Lab, 3 Turner Avenue, Bentley, WA,6102

Perth, Australia 6102
Attn: Curtin University

Total 0.00 USD

ORDER MORE CLOSE WINDOW

Title: Carbocatalysis by Graphene-Based Materials

Author: Sergio Navalon, Amarajothi Dhakshinamoorthy, Mercedes Alvaro, et al

Publication: Chemical Reviews

Publisher: American Chemical Society

Date: Jun 1, 2014

PERMISSION/LICENSE IS GRANTED FOR YOUR ORDER AT NO CHARGE

This type of permission/license, instead of the standard Terms & Conditions, is sent to you because no fee is being charged for your order. Please note the following:

- Permission is granted for your request in both print and electronic formats, and translations.
- If figures and/or tables were requested, they may be adapted or used in part.
- Please print this page for your records and send a copy of it to your publisher/graduate school.
- Appropriate credit for the requested material should be given as follows: "Reprinted (adapted) with permission from (COMPLETE REFERENCE CITATION). Copyright (YEAR) American Chemical Society." Insert appropriate information in place of the capitalized words.
- One-time permission is granted only for the use specified in your request. No additional uses are granted (such as derivative works or other editions). For any other uses, please submit a new request.

If credit is given to another source for the material you requested, permission must be obtained from that source.

Title: One-pot synthesis of N-doped graphene for metal-free advanced oxidation processes

Author: Chen Wang,Jian Kang,Hongqi Sun,H.M. Ang,Moses O. Tadé,Shaobin Wang

Publication: Carbon

Publisher: Elsevier

Date: June 2016

Title:	Occurrence of radical and nonradical pathways from carbocatalysts for aqueous and nonaqueous catalytic oxidation
Author:	Xiaoguang Duan,Zhimin Ao,Li Zhou,Hongqi Sun,Guoxiu Wang,Shaobin Wang
Publication:	Applied Catalysis B: Environmental
Publisher:	Elsevier
Date:	5 July 2016

Order Completed

Thank you for your order.

This Agreement between Curtin University -- Chen Wang ("You") and Elsevier ("Elsevier") consists of your license details and the terms and conditions provided by Elsevier and Copyright Clearance Center.

Your confirmation email will contain your order number for future reference.

printable details

License Number	4284530005827
License date	Feb 08, 2018
Licensed Content Publisher	Elsevier
Licensed Content Publication	Applied Catalysis B: Environmental
Licensed Content Title	Occurrence of radical and nonradical pathways from carbocatalysts for aqueous and nonaqueous catalytic oxidation
Licensed Content Author	Xiaoguang Duan,Zhimin Ao,Li Zhou,Hongqi Sun,Guoxiu Wang,Shaobin Wang
Licensed Content Date	Jul 5, 2016
Licensed Content Volume	188
Licensed Content Issue	n/a
Licensed Content Pages	8
Type of Use	reuse in a thesis/dissertation
Portion	figures/tables/illustrations
Number of figures/tables/illustrations	1
Format	both print and electronic
Are you the author of this Elsevier article?	No
Will you be translating?	No
Original figure numbers	scheme 1
Title of your thesis/dissertation	The Synthesis and Application of Novel Nanostructured Carbon Materials
Expected completion date	Oct 2017
Estimated size (number of pages)	200
Attachment	
Requestor Location	Curtin University B601 Chemical Engineering Lab, 3 Turner Avenue, Bentley, WA,6102 Perth, 6102 Australia Attn: Curtin University
Publisher Tax ID	GB 494 6272 12
Total	0.00 USD

ORDER MORE CLOSE WINDOW